OÉ Gaillimh
NUI Galway

Building envelope thermal bridging heat loss assessment using infrared thermography

Małgorzata O'Grady

Supervisor: Dr. Annette Harte

Co-supervisor: Dr. Agnieszka Lechowska

Thesis submitted to the National University of Ireland Galway as fulfilment for the requirements for the Degree of Doctor of Philosophy

Civil Engineering, National University of Ireland Galway, April 2018

Abstract

Reduction of greenhouse gas emissions and energy use is necessary to stop the progress of climate warming, which may have a serious impact on the human environment and the ecosystem. To achieve this reduction, it is essential that energy usage in buildings is limited, as they have been identified as the world's largest energy consumer. In the European Union, buildings-related energy accounts for 40 % of total consumption and the thermal quality of the existing European building stock is below acceptable standards. Thermal upgrading of the building stock gives significant potential for overall energy reduction and is a key concern in current European Union policy. Putting this policy into practice involves, among others, implementation of thermal assessments of existing buildings. Performing such an assessment before and after building retrofitting allows determination of the actual energy reduction achieved, and monitoring of the overall thermal quality of the building stock.

In general, the retrofitting process starts with the building envelope as this is one of the major factors determining the energy demand of a building. To assess the thermal quality of the building envelope, the heat losses, via its plain components such as walls and via thermal bridging appearing on the connection of these components, must be quantified. In this project, a non-destructive method for thermal evaluation of thermal bridging located in existing building envelopes, using quantitative infrared thermography technique (ITT), has been developed. This is a significant contribution to state of the art. With this method, the heat loss is expressed by thermal bridging heat flow rate q_{TB} and linear thermal transmittance Ψ-value. The approach employs the surface energy balance principle on a building component surface containing a thermal bridge. Consistent with this principle, the amount of energy transferred to the surface is equal to the amount of energy leaving the surface. The energy leaving the surface is evaluated from surface temperatures recorded during a thermographic survey using an infrared camera. This approach eliminates the necessity for knowledge of the internal structure and materials of the building, which is often unavailable for older buildings.

As part of the development and validation of the methodology, an experimental program was designed in consultation with an industrial partner to ensure that realistic test cases of thermal bridging in buildings were considered. The methodology for the use of the indoor and the outdoor ITT was validated in a hot box device where environmental conditions were strictly monitored. Furthermore, in order to verify the suitability of the methodology to thermal assessment of existing buildings, in-situ testing was carried out. The methodology included the establishment of procedures for undertaking the thermographic survey to enhance the accuracy of the data gathered. The analysis of the data from the thermographic survey was implemented in a Microsoft Excel-based tool for convenient thermal bridging heat loss calculations based on indoor or outdoor measurements.

The developed methodology has the potential to be implemented into the overall thermal assessment of existing buildings. Based on a thermal assessment involving in-situ measurements such as proposed in this project, a building retrofit strategy can be planned. Repeating the assessment after building retrofitting will quantify the actual improvement in thermal performance.

List of publications

Journal Articles:

- Małgorzata O'Grady, Agnieszka A. Lechowska, Annette M. Harte, Infrared thermography technique as an in-situ method of assessing heat loss through thermal bridging, Energy and Buildings, 2017, 135:20-32.

- Małgorzata O'Grady, Agnieszka A. Lechowska, Annette M. Harte, Quantification of heat losses through building envelope thermal bridges influenced by wind velocity using the outdoor infrared thermography technique, Applied Energy, 2017, 208:1038-1052.

- Małgorzata O'Grady, Agnieszka A. Lechowska, Annette M. Harte, Application of infrared thermography technique to the thermal assessment of multiple thermal bridges and windows, Energy and Buildings, 2018, 168: 347-362.

Conference Proceedings:

- Małgorzata O'Grady, Agnieszka A. Lechowska, Prof. Jacek Schnotale, Annette M. Harte, Assessment of thermal bridging heat loss by means of the infrared thermography technique. In Proceedings of the 9th International Cold Climate Conference, Kiruna – Sweden, 12-15 March 2018.

Acknowledgments

First of all, I would like to express my gratitude to my supervisor, Dr. Annette Harte for her guidance, assistance, and support during my PhD, the most ambitious and difficult project in my career. Her determination and constant encouragement throughout the whole project, especially during the papers publication process was what I needed to complete the research, including three publications in exceptional quality journals. I appreciate her patience and understanding during times when I was not at my best. Her strength helped me get to the place I am now.

Many thanks to my co-supervisor, Dr. Agnieszka Lechowska from Cracow University of Technology CUT for her help and expertise whenever I needed. Her optimistic and reassuring approach always had a calming effect on me and made things easier. Sharing stories about her own PhD project allowed me to see my situation from a different, safer perspective.

I would like to thank many members of NUIG staff that I had the privilege to meet over the past few years. I send thanks to Prof. Padraic O'Donoghue and Dr. Marcus Keane for advice and supportive comments during Graduate Research Committee meetings and unofficial chats. Many thanks for all the good words, help and guidance that I experienced on a daily basis from Prof. Peter McHugh, Dr. Bryan McCabe, Dr. Magdalena Hajdukiewicz, Dr. Mark Healy, Dr. Jamie Goggins, Dr. Mike Hartnette, Dr. Stephen Nash, Dr. Suhaib Salawdeh, Dr. Xinmin Zhan, Bríd Flaherty, Aodh Dalton, Maja Drapiewska, Gerard Hynes, Peter Fahy, William Kelly, Maura McDonagh, Mary O'Brien and Colm Walsh.

I would like to thank a number of institutions for providing technical and financial support for my research. Many thanks to the NUIG College of Engineering and Informatics for granting a Postgraduate Scholarship to me. Thanks to Cracow University of Technology for giving me the opportunity to carry out the experimental work in their laboratory, in particular to the Head of the Institute Prof. Jacek Schnotale and to the technician Mariusz Rusiecki for assistance during the testing, and for sharing their knowledge. I extend my appreciation to SIP Energy Ltd, especially John Moylan for supplying test specimens and to Enterprise Ireland for financial support

through Innovation Voucher IV-2014-4203. I send special gratitude to Patryk and Chris from Kierbud Ltd. for invaluable support and assistance in setting up my experimental work.

I would like to thank the postgraduates and post-doctoral researchers that accompanied me on the way to PhD for their humour and for cheering me up when I needed it, Caitríona, Conan, Karol, Karlo, Luka, Des, Sameer, Daniel, David, Sinéad, Tarek, Fatima, Collette, Kelly, Ronan, Hose and John. Many thanks to my dear friends around the world that have been always for me, Ania, Anna, Ewa, Kat, Ola, Magda, Jacek, Kasia, Milena, Agnieszka, Krzys, Asia, Joanna, Patrycja, Piotr, Basia, Iza, Renia, Marcin, Pawel.

Special enormous gratitude goes to my dearest husband Joe for his endless support, for reminding me that I am worthy (also without a PhD) and for constantly believing that the victory day would come to me, to my beloved Mia for distracting and relaxing my tired brain and for waiting, sometimes long hours, for me, to my sorely missed best granny in the World Maria for upbringing me and not spoiling me, to my dear parents, my sister and my nieces for their confidence in me that I would always accomplish anything I decide, to dear Butch for his non-judgemental attitude and great company. Thanks for all your love.

I also send my appreciation to my in-laws, relatives, neighbours, and acquaintance for keeping their fingers crossed for me.

Table of Contents

Abstract ……...I
List of Publications ……...III
Acknowledgments ……IV
Table of Contents ……VI
Declarations ……X
Nomenclature ……XI

1. Introduction ……1
1.1. Background ……..1
1.2. Building envelope energy efficiency ……2
1.3. Policy related to energy performance ……...3
1.3.1. Review of global policy in relation to building energy performance ……..4
1.3.2. Review of European Union policy in relation to building energy performance ……6
1.3.3. Review of Irish policy in relation to building energy performance ……9
1.3.4. Summary of building energy-related policy ……...15
1.4. Thermal Evaluation of the existing building envelope ……16
1.5. Motivation and Research objectives ……...17
1.6. Structure of dissertation ……..19
1.7. References ……..20

2. Literature review ……..23
2.1. Introduction ……23
2.2. Building Physics principles and standard approaches to heat transfer evaluation…… 24
2.2.1. Heat transfer modes: conduction, convection, and radiation ……24
2.2.2. Thermal evaluation of building envelope ……...32
2.3. Overview of building envelope thermal performance assessment methods …39
2.3.1. Analytical and numerical approaches to building envelope assessment …40
2.3.2. Experimental approaches to building envelope assessment ……..43
2.3.2.1. Heat Flow Meter ……44
2.3.2.2. Hot Box method ……46
2.3.2.3. Infrared Thermography Technique ……51
2.3.2.3.1. History outline and operational principles ……..51
2.3.2.3.2. Evaluation of *U*-value by means of ITT ……..…58
2.3.2.3.3. Evaluation of thermal bridging by means of ITT ……...62
2.3.2.3.4. Summary of ITT applications ……..…64
2.4. Summary and conclusions ……..….65

2.5. References ……..68

3. Infrared thermography technique as an in-situ method of assessing heat loss through thermal bridging ……75

3.1. Paper overview ……...75
3.2. Abstract ……..76
3.3. Introduction.…….....77
3.3.1. Methods of assessing the *U*-value ……78
3.3.2. Methods of assessing the thermal bridge heat loss ……...81
3.3.3. Summary ……...84
3.4. Methodology for quantifying the heat flow rate through a thermal bridge q_{TB} and Ψ-value by means of ITT …… 85
3.5. Testing and validation the methodology ……...92
3.5.1. Experimental set up ……..92
3.5.2. Geometries and description of the specimens ……..93
3.5.3. Calorimetric Hot Box device, tests and results ……95
3.6. Thermographic survey ……100
3.7. Measurement results ……101
3.7.1. Surface temperatures ……...102
3.7.2. Comparison of the heat flow rate through the specimen $\dot{Q}_{sp}$ and the overall heat transfer coefficient *U*-value ……105
3.7.3. Comparison of thermal bridge heat flow rate q_{TB} and linear thermal transmittance Ψ-value ……106
3.8. Summary and conclusions ……...109
3.9. Acknowledgments ……...110
3.10. References ……...111

4. Quantification of heat losses through building envelope thermal bridges influenced by wind velocity using infrared thermography technique ……..117

4.1. Paper overview ……117
4.2. Abstract ……119
4.3. Introduction ……..119
4.4. Different approaches to accounting for wind effects on a building external surface ……..124
4.5. Experimental study ……..128
4.5.1. Experimental set up ……129
4.5.2. Geometries and description of the specimens ……....130
4.5.3. Hot Box testing ……..…..131
4.5.4. ITT testing ……...133
4.6. Outdoor ITT methodology ……...…136
4.6.1. Evaluating heat transfer coefficients using heat transfer theory ……..137
4.6.2. Determination of heat transfer coefficients for test specimens ……139

4.6.3. Evaluating heat transfer coefficients using Jürges' equation ……..141
4.7. Experimental results and discussion ……142
4.7.1. Surface temperatures measured by the outdoor ITT …… .142
4.7.2. Thermal bridge heat loss expressed by linear thermal transmittance Ψ-value ……...145
4.8. Comparison of measured and standard Ψ-value ……..……..…149
4.8.1. Standard Ψ-value obtained from finite element software ……..……..149
4.8.2. Comparison of designed and measured Ψ-value ……..……151
4.9. Adjustment of Ψ-value measured at different wind velocities to the standard values ……..…152
4.10. Conclusions ……..…….158
4.11. Acknowledgments ...……160
4.12. References ……..……...160

5. Application of infrared thermography to the thermal assessment of multiple thermal bridges and windows ……..…...165
5.1. Article overview ……...……165
5.2. Abstract ……..……...166
5.3. Introduction ……..…167
5.4. Experimental study ……..172
5.4.1. Experimental procedure ……173
5.4.2. Test specimen description ……173
5.4.3. Hot Box measurements ……176
5.4.4. Thermographic survey ……..180
5.5. Application of ITT methodology to quantifying the heat loss through multiple thermal bridges and through window elements ……181
5.6. Numerical studies ……186
5.6.1. Two-dimensional heat transfer finite element models in Abaqus Standard……...187
5.6.2. Three-dimensional numerical simulations in Ansys Fluent ……189
5.6.2.1 Mesh and model settings ……192
5.6.3. Three-dimensional heat transfer finite element models in Abaqus Standard……...193
5.7. Results and discussion ……194
5.7.1. Linear parallel thermal bridges ……..194
5.7.1.1. Surface temperature distributions ……194
5.7.1.2. Thermal bridge heat flow rate q_{TB} and linear thermal transmittance Ψ-value ……..198
5.7.1.3. Influence of the distance between parallel thermal bridges on Ψ-value …….....200
5.7.2. Window system thermal bridges ……...201
5.7.2.1. Surface temperature distributions ……...202

5.7.2.2. Comparison of window thermal bridging heat low rate $\dot{Q}_{TB}$ and window thermal transmittance *M*-value ……..205
5.8. Summary and conclusions ……..…..206
5.9. Acknowledgments ……..…..209
5.10. References ……209

6. Application of the infrared thermography technique of assessing heat loss through thermal bridging in a real existing building ……...215
6.1. Introduction ……215
6.2. Experimental set up ……216
6.3. In situ measurements ……..216
6.4. Numerical simulations ……....219
6.5. Results and discussion ……223
6.5.1. Results simulated with standard boundary conditions ……..223
6.5.2. Comparison of measured and numerical results ……224
6.5.2.1. Surface temperature comparison ……..…224
6.5.2.2. Thermal bridge heat flow rate q_{TB} and Ψ-value comparison ……225
6.6. Summary and conclusions ……..226
6.7. References ……...227

7. Conclusions and Recommendations …….……..229
7.1. Conclusions ……...229
7.2. Recommendation for the future work …….…….. 234
7.3. References ……236

Appendices ……..239
A. Excerpt from analysis using indoor ITT of Specimen 1, Chapter 3 …….241
B. Excerpt from analysis using outdoor ITT and Nusselt number of Specimen 1, Chapter 4 ……....245
C. Excerpt from analysis using outdoor ITT and Jürges approximation of Specimen 1, Chapter 4 ……...…249

Declarations

This thesis or any part thereof, has not been, or currently being submitted for any degree at any other university.

Małgorzata O'Grady

The work reported herein is a result of my own investigation, except where acknowledged and referenced.

Małgorzata O'Grady

Nomenclature

A	area of the specimen, m^2
α	thermal diffusivity, m^2/s
β	expansion coefficient, 1/K
ε	surface emissivity, -
Φ	heat power, W
g	acceleration due to gravity, m/s^2
h	heat transfer coefficient, W/m^2K
H	height, m
ITT	Infrared thermography technique
Ju	Jürges, -
l	length, m
k	thermal conductivity of air, W/m^2K
ν	kinematic viscosity, m^2/s
Nu	Nusselt number, -
M	window thermal transmittance, W/K
$\dot{m}$	mass flow rate, kg/s
Pr	Prandtl number, -
q	heat flow rate per unit height, W/m
$\dot{q}$	surface heat flux, W/m^2
$\dot{Q}$	heat flow rate, W
Ra	Rayleigh number
RD	relative percentage deviation, %
ρ	density, kg/m^3
σ	Stefan-Boltzmann constant, W/m^2K^4
T	temperature, ^oC

u	uncertainty, the unit depends on the measurement
Φ	heat power, W
Ψ	linear thermal transmittance, W/mK
w	air velocity, m/s

Subscripts

adj	adjusted
c	convective
ch	characteristic
b	baffle
e	cold side, external conditions
edge	edge zone between the specimen and the surrounding panel
i	warm side, indoor conditions
in	input to the hot box
meas	measured
min	minimum
n	environmental
p	panel
plain	component without thermal bridge
r	radiative
s	surface
S	standard
S1	sensor 1
S2	sensor 2
sp	specimen
sur	surrounding

TB	thermal bridge
tot	total
u	uniform
x	pixel

Chapter 1

Introduction

1.1. Background

Warming of the global climate system has been observed since the 1950s. The temperature of the atmosphere and the oceans has increased and the volumes of snow and ice have decreased. This has been instigated by increasing anthropogenic greenhouse gas emissions caused by population growth and economic growth. Prolonged emission of greenhouse gases will increase global warming over time. It is likely that this may have a severe and irreversible influence on the human and natural environment. This can be avoided only by extensive emissions reductions over the next few decades which is a global priority [1]. Reduction of energy use related to buildings must receive special focus, as buildings are associated with one-third of global final energy consumption and greenhouse gas emissions. This makes the building sector the world's largest energy consumer [2]. In order to achieve total global energy savings, the energy usage related to buildings must be reduced. This has led to the development of building energy policy frameworks, which are being implemented at global, European and national levels.

In the European Union, building-related energy accounts for 40% of the total energy use [3]. Therefore, European Union Directives have imposed requirements on Member States to limit building-related energy use. One of the main requirements is the introduction of stricter national building energy regulations. Consequently, new buildings are constructed to a high thermal standard. On the other hand, the existing

building stock in European Union countries is relatively old and currently, about 75 % buildings are energy inefficient [4]. More than 40 % of buildings were constructed before 1960 and 90 % before 1990. It is expected that the majority of them will be still occupied in 2050. It is estimated that up to 110 million buildings need retrofitting to meet minimum requirements related to thermal performance [5]. However, only 0.4 % - 1.2 % of existing buildings, depending on Member State, are retrofitted annually [4]. Thermal upgrading of the existing building stock provides a considerable opportunity to achieve overall energy and greenhouse gas emissions reductions. Therefore, the focus of most current European legislation is to push forward retrofitting of existing buildings.

One of the decisive factors in ensuring building energy efficiency is the building envelope thermal quality. As the building envelope provides the thermal barrier between the indoor and outdoor environments, any improvement in its thermal standard reduces a building's overall energy demand. One of the challenges in upgrading the thermal performance of existing buildings to current standards is a lack of information on the internal structure and current material characteristics of the building façade. Therefore, the thermal standard of the existing building envelopes must be assessed in-situ by taking measurements to determine the actual thermal state of the building envelope components.

The thermal assessment of a building envelope can be helpful in the retrofitting planning stage, especially for owners of multiple properties, for instance City Councils. Such assessments can identify which buildings most need improvement, allowing them to be prioritised. The assessment will give an indication of the level of retrofitting needed, thus allowing a retrofit strategy to be planned. To quantify the thermal improvement achieved, measurement should also be carried out after retrofitting.

1.2. Building envelope energy efficiency

The energy efficiency of a building envelope is generally examined by considering the plain components such as walls or roof together with regions of thermal bridging (Fig.

1.1). For plain components, the surface temperature distribution is uniform. The heat losses via plain building components are conventionally expressed by the thermal transmittance (*U*-value). The *U*-value is the heat transmitted per unit area divided by the temperature difference between the inside and outside of the component. A thermal bridge is a region of building envelope with different geometry and/or a thermal conductivity higher than the surrounding plain component. Thermal bridging is associated with higher heat losses than the plain components. These heat losses are usually expressed by the linear thermal transmittance (Ψ-value). This Ψ-value is the heat loss per unit length of the thermal bridge divided by the temperature difference across the component. For precise building envelope thermal assessment, it is important to account for heat losses through both plain components and thermal bridging. National building regulations define minimum acceptable building envelope thermal performance by specifying minimum values of thermal transmittance.

Fig. 1.1. Heat losses via building envelope.

1.3. Policy related to energy building performance

Improvement of the thermal quality of buildings requires adequate policy that defines an acceptable energy efficiency standard for buildings. Therefore, over the last numbers of years, policy on the global, European and national levels has been changing to ensure that the buildings are becoming more energy efficient. Table 1.1.

summarises the relevant policy and legislative instruments on these three levels. These are discussed in detail over next three sub-sections.

Table 1.1. Global, European and Irish policy.

Policy		
Global	European	Irish
Transition to Sustainable Buildings [2]	Energy Efficiency Directive 2012 [9] with its amendment [10]	White Papers 2009 [17] and 2015 [18]
Energy Performance Certification of Buildings [6] Modernizing Building Energy Codes [7]	Directive 2010/31/EU on Energy Performance of Buildings [3] and its amendment [4]	Introducing Sustainable Authority of Ireland, Introducing Building Certification System, Building Regulations Part L 2017 [27]
	European Energy Efficiency Plan 2011 [13]	4th National Energy Efficiency Action Plans [30] Long Term Renovation Strategy [31]

1.3.1. Review of global policy in relation to building energy performance

The International Energy Agency (IEA), in their 2013 report Transition to Sustainable Buildings [2], presented strategies and opportunities to significantly reduce global building-related energy use and greenhouse gas emissions by 2050 using a combination of technology and intelligent policy. A wide range of materials and technologies, such as space and water heating, lighting and domestic and business appliances and equipment, is used in buildings. Over the next number of years, these technologies should be continually replaced by more cost-effective and energy efficient technologies and combined with renewable energy sources. Implementation of a policy promoting such technologies is essential to achieve long-term changes in the building sector. Several recommendations for policy makers are presented by the

IEA that will result in an immediate acceleration of building energy efficiency improvements.

The IEA has also issued a Policy Pathway series, designed for policy makers in all counties, to provide guidance on implementation of energy efficiency policies. This series includes Energy Performance Certification of Buildings [6] that is a key policy instrument in the reduction of the building energy consumption. An energy performance certification system evaluates building energy efficiency. The system stores data on buildings and thus helps governments in assessing the progress in energy efficiency improvement on the national level. It also increases citizens' awareness of energy consumption and its impact on the environment and buildings' running costs. Introducing an effective certification system requires validation of assessment procedures, potential assessors training, and an adequate administrative system. IEA member countries are at different stages of implementing or improving building energy certification schemes.

A continuation of the Policy Pathway series, Modernizing Building Energy Codes [7], explains how codes can be effective instruments in the process of making buildings more energy efficient. Recent history shows that making stricter mandatory codes in terms of energy conservation resulted in a reduction of annual energy consumption per dwelling from 22% (e.g. in Germany and Netherlands) to 6% (in Southern European countries). IEA member countries use two different approaches when designing building energy codes, namely prescriptive and performance approaches. In the prescriptive approach, minimum requirements for each building component are set, such as *U*-value for a wall but the interactions between the components are not accounted for. In codes using the performance approach, energy requirements are set for a building's overall energy consumption. The IEA promotes this second approach as it treats a building as one integral system. It accelerates energy optimization of the whole building design by taking into account interactions between all building components. It also supports the development of efficient technologies and designs. Another IEA recommendation is to include, in building energy codes, requirements to provide a proportion of the energy from renewable energy sources and energy efficiency measures. Training and constant support should be provided for all stakeholders of the construction process to ensure the advanced building energy codes

and their applications are understood. Governments should secure human and financial resources to effectively implement building energy codes. It is also governments' responsibility to monitor the building compliance with these codes and any non-compliance should be openly addressed. Imposing more strict requirements in updated codes should aim to bring buildings toward the nearly zero-energy buildings (NZEBs). A nearly zero-energy building is one that has a very high energy performance. The nearly zero or very low amount of energy required should be covered to a very significant extent by energy from renewable sources [3].

The implementation of energy efficiency policies entails incremental energy efficiency investment in buildings. The IEA in their 2016 Energy Efficiency Market Report [8] showed that global investment in building energy efficient products and services was USD 388 billion in 2015. This represents 8 % of total building construction spending and this share has been rising. The major proportion of this investment relates to building envelope energy efficiency, mostly windows and insulation, and amounted to USD 237 billion in 2015. Between 2000 and 2015, a significant reduction in energy consumption per meter square has been achieved in both non-residential (by 37 %) and residential buildings (by 26 %).

1.3.2. Review of European Union policy in relation to building energy performance

Under the EU Energy Efficiency Directive 2012/27/EU (EED 2012) [9], all member countries are required to use energy more efficiently at all stages, from production to consumption. To ensure that a 20 % reduction of primary energy consumption by 2020 will be reached, this directive sets up obligations for all Member States. Some examples are to request their public sectors to purchase only energy efficient buildings, products and services and to retrofit annually at least 3 % of buildings owned and used by government. In November 2016, the European Commission proposed an amendment to this Directive [10], including a new binding energy savings target of 30 % by 2030. EED 2012 [9] and its proposed amendment [10] obligates Member States to submit National Energy Efficiency Action Plans (NEEAPs) every 3 years, including a Long Term Renovation Strategy (LTRS). This strategy overviews the national

building stock, stimulates renovations and estimates energy savings that can be achieved as the result. The requirement by each Member State to produce an LTRS indicates the importance of the building stock improvement in achieving the overall energy reduction.

According to EU Directive 2010/31/EU on the Energy Performance of Buildings (EPBD 2010) [3] (recast of EU Directive 2002/91/EC [11]), buildings account for 40% of the total energy consumption in the European Union and that usage is growing. The EPBD 2010 focuses on improvements in energy performance of both new and existing buildings that should be cost-effective and adjusted to the local climate.

Summing up the Directive it:

- gives a framework for calculating the building energy performance and requires each Member State to develop its own methodology, in accordance with national norms and standards
- underlines that it is the responsibility of each Member State to set minimum standards on the energy performance of new buildings and existing buildings
- obliges the Member States to ensure that all new buildings and buildings for sale and rent have an energy performance certificate provided by the owner
- lays down the requirements of the regular inspection of boilers and of air-conditioning systems in buildings
- sets requirements on national plans for increasing the number of nearly zero-energy buildings.

In all Member States countries, all newly-constructed buildings shall be nearly zero energy buildings by the end of 2020 and after 31 December 2018 all new buildings occupied and owned by public authorities shall be nearly zero energy buildings.

The European Commission, in 2016, carried out an evaluation of the EPDB 2010 [12] and concluded that changes introduced in Member States countries, such as strict building energy codes and building energy performance certification systems, work effectively especially when considering newly constructed buildings. At the same time, the majority of existing buildings (about 75 %) are still energy inefficient. Implementing the requirements of EPDB 2010 has resulted in an energy saving of 48.9

Million Tonnes of Oil Equivalent (Mtoe) in the building sector. Nevertheless, this saving can be significantly increased if the retrofitting of existing building stock is fast-tracked. Another conclusion of the evaluation [12] is that, at the national level, building compliance with minimum standard requirements and the independent control of this compliance should be improved.

Based on the evaluation [12], it is proposed to amend EPDB 2010 [4]. Its main focus will be to speed up retrofitting of existing buildings. This proposal includes strategies for complex building renovation, developing a plan for financial support and developing a plan to decarbonize by 2050. In Europe, the construction industry accounts for 18 million direct jobs and increasing the volume of renovation work should result in a significant increase in this number. Another positive effect of building stock renovation is an improvement in the quality of the indoor environment, thus improving occupants' health and wellbeing. Finally, it could significantly reduce the number of households living in energy poverty. Acceleration of building retrofitting will directly contribute to reaching the target, set out in the proposed EED 2012 amendment [10] of a 30% energy savings by 2030.

The European Energy Efficiency Plan 2011 [13] also emphasizes the importance of prioritizing the retrofitting process in public and private buildings to improve the energy performance of both the building components and appliances used in buildings. As two-thirds of the energy used in buildings relate to space heating (Fig. 1.2), limiting this energy is key in reducing the overall energy consumption. This can be achieved by upgrading the heating system and/or by improving the insulation of the building envelope that will reduce heat losses. Understandably, improvement of the building envelope thermal performance should take precedence over the heating system upgrade to conserve energy that is already generated.

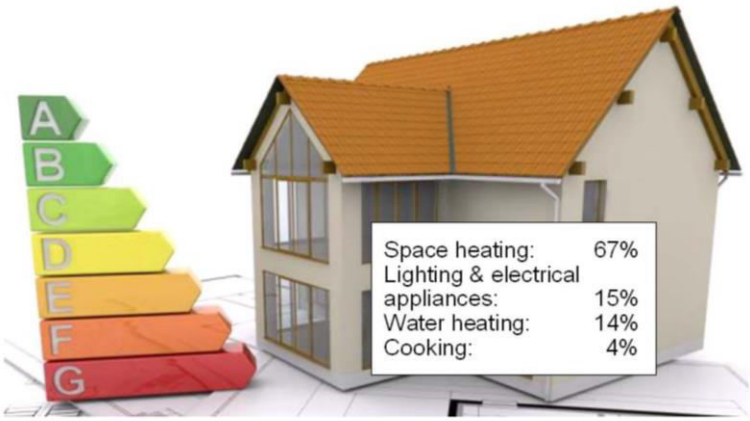

Fig. 1.2. Energy consumption at an existing residential building [13].

In relation to greenhouse gas (GHG) emissions, the EU Commission initially set a target of GHG reduction of 20 % by 2020, when compared to 1990 levels [14]. This goal was updated in 2014 to 40 % cuts in emissions by 2030 [15]. The long-term goal of EU is the reduction of GHG emissions by 80-95%, when compared to 1990 levels, by 2050 [16]. The Energy Roadmap 2050 [16] states that to achieve these targets, development of low-carbon technologies and grid infrastructure are necessary. These are to be accompanied with increasing use of both renewable energy and energy efficiency measures throughout all sectors.

As European policy drives policy in each EU Member State, the next section focuses on Irish energy policy and its implementation in order to meet the European targets.

1.3.3. Review of Irish policy in relation to building energy performance

In response to EU requirements related to energy saving, the Irish Government has introduced a series of measures aimed at ensuring compliance at the national level. These measures include:

- Issuing of a series of White Papers
- Establishment of the Sustainability Authority of Ireland (SEAI)

- Updating of the Irish Buildings Regulations
- Implementation of National Energy Efficiency Action Plans (NEEAPs) including a Long Term Renovation Strategy (LTRS).

The Sustainable Energy White Paper, Delivering a Sustainable Energy Future for Ireland [17], was published in 2009. In this document, a strategy for Ireland to achieve the EU targets within the timeframe 2007-2020 was set out. In terms of energy efficiency, the goal for Ireland is to achieve an improvement of 20% by 2020, across the whole Irish economy. This document was followed in 2015 by another White Paper, Irelands Transition to a Low Carbon Energy Future 2015-2030 [18], that updated the Irish energy policy to align with changes in the EU requirements. It presents a vision of a low carbon Ireland, with a reduction in GHG emissions of between 85 % - 90 % by 2050 compared to 1990 levels, which is in alignment with EU Energy Roadmap 2050 [16]. These emissions should fall to zero by 2100 or earlier. To achieve these goals, several actions are required. One of them is changing the behaviour of citizens, industry, and Government by extending their awareness of this issue. The main focus is on generating more electricity from renewable sources and applying energy efficient solutions across the whole economy. The Irish Government committed to supporting research into new technologies that lead to energy and GHG emission reductions.

The SEAI was established as a body responsible for implementing sustainable energy structures, technologies and practice in Ireland. It has an advisory role to Government and organizes a number of programmes, which aim to reduce energy consumption in Ireland. SEAI's key objective is to help homes, business, communities, and industries to be more energy efficient. SEAI, among other activities, advises homeowners, investors, and contractors on how to construct highly energy-efficient buildings and how to renovate existing buildings through their website and publications [19,20]. It also contributes to the development of passive houses in Ireland [21] and encourages homeowners to retrofit their homes to reach passive house standard.

SEAI administers, on behalf of Department of Communications, Climate Action and Environment, the Better Energy Programme that covers several different

grant schemes which support investors/homeowners in building energy improvement. One of the most popular schemes is the Better Energy Homes (BEH) [22] dedicated to homeowners of houses built before 2016. Under this scheme, homeowners can apply for grants to upgrade the building envelope thermal performance by using internal, external or cavity insulation and to upgrade the heating system. To determine how much the BEH scheme contributes to energy saving, SEAI compared the average energy consumption of 210 houses before (in 2010) and after (in 2018) using the BEH grants. According to the impact report [23], householders who carry out energy-efficiency home improvements reduced their annual energy costs by up to 21 %.

SEAI developed and coordinate the building energy rating (BER) certification system as a tool to assess the energy efficiency of buildings. The energy certification scheme came into force in January 2007 for new residential buildings and in July 2008 for new non-residential buildings. From the beginning of 2009, all existing public buildings with an area of over 1000 m^2 and existing residential buildings for sale or rent required BER certification. The BER certificate uses a scale from *A1* (the most efficient) to *G* (the least efficient). Each letter indicates the amount of energy in kWh per m^2 of building area per year needed to provide a suitable indoor air temperature and hot water for the users. The BER certificate also shows the building greenhouse gas emission level. The certificate is accompanied by recommendations regarding possible cost-effective and energy performance improvements. A database of BER certificates enables statistical analysis of energy efficiency improvement at a national level. The Irish BER certification system has been recognized by the IEA [6] as a positive example and guideline for countries aiming to implement building energy certification.

Up to 2016, over 350,000 households have upgraded their homes using SEAI grants. However, over 1 million existing houses still need retrofitting to make them energy efficient [24]. To find a way to encourage citizens to retrofit their homes, SEAI carried out a survey to understand the approach in the residential sector to energy efficiency. The survey revealed that, for the majority of home occupants (70%), insufficient funds is the main barrier to home improvement. Most house owners base their decision to investing in energy efficient measures not only on cost and energy savings but also on the impact of the investment on their comfort.

To improve the thermal standard of Irish buildings and to meet EU obligations, Ireland updated the Building Regulations related to Conservation of Fuel and Energy in Dwellings in 2011 and 2017. The previous Building Regulations Part L Technical Guidance Document (TGD) 2007 [25] was replaced by Building Regulations Part L TGD 2011 [26] and then amended in 2017 [27] to include a definition of NZEB. These updated versions are much stricter in comparison to the 2007 regulations, in order to optimise the energy efficiency of dwellings and minimise CO_2 emissions. For new dwellings, the 2017 regulations require the primary energy consumption and related CO_2 emissions to be limited insofar as reasonably practicable. This should be calculated using the Dwelling Energy Assessment Procedure (DEAP) methodology published by SEAI, while taking into account all factors contributing to energy use and associated GHG emissions. A reasonable proportion of the energy consumption should be provided from renewable sources. Further requirements relate to new and existing dwellings when upgraded. These are installing energy efficient heating systems with the effective control system, maximising heat gain through the fabric (glazing) and limiting heat losses via building envelope fabrics and pipes or ducts. In relation to the building envelope, according to the updated Building Regulations Part L TGD 2011 with the 2017 Amendment [27], each building element has to achieve an area-weighted *U*-value lower or equal to the values presented in Table 1.2. As can be seen in this table, the maximum values required in the 2017 regulations are significantly lower than in 2007. In addition to providing the *U*-values presented in Table 1.2, limiting of air permeability and of heat loss through thermal bridging is required. Two methods of accounting for this heat loss are acceptable by the Building Regulations Part L TGD 2011 with the 2017 Amendment [27]. The first method is by using a multiplier Y applied to the total exposed area A_{exp} of building envelope and the second one is by summing up Ψ-values multiplied by the thermal bridges' lengths. The regulations [27] give a choice of deriving values of Ψ from numerical analysis, measurements or using tabulated values are given in these regulations. For buildings other than dwellings, the Building Regulations Part L TGD 2008 [28] are still to be followed. They are currently under review in order to upgrade their requirements by 50% to 60% over 2008 standards.

Table 1.2. The requirements for area-weighted average elemental *U*-value.

Fabric element	Area-weighted average elemental *U*-value required in 2017 [27]	Area-weighted average elemental *U*-value required in 2007 [25]
Pitched Roof – insulation at ceiling	0.16	0.16
Pitched Roof – insulation on slope	0.16	0.20
Flat roof	0.20	0.22
Walls	0.21	0.25
Ground floors – no underfloor heating	0.21	0.25
Ground floor with underfloor heating	0.15	-
External doors, windows, rooflights	1.60	2.00

To provide guidance for the public, the National Standards Authority of Ireland published Standard Recommendation S.R. 54:2014 Code of practice for energy efficient retrofitting of dwelling [29]. In this document, different construction solutions such as internal, cavity and external wall insulation and their impact on the overall building performance are presented.

As mentioned previously, in accordance to EED 2012 [9] and its proposed Amendment [10], Ireland issues National Energy Efficiency Action Plans (NEEAPs) every 3 years. The most recent, the 4th NEEAP [30], launched in 2017, summarises Ireland's progress in achieving its 2020 energy efficiency goals. It states that just under 12% of the 20% target was achieved by the end of 2016 (Fig. 1.3). Based on the current measures and findings, it was estimated that by 2020 only 16.23% of the 20% target will be achieved. Therefore, the key objective of the 4th NEEAP [30] is to accelerate the progress in improving energy efficiency in Ireland and fill the 3.77 % shortfall. It was recognized that the Better Energy Programme has a very positive impact on buildings energy efficiency. However, in general, it has been found that homeowners grant-aided by the Better Energy Programme have limited the upgrade to a single building element, such as walls, instead of improving the entire building envelope components and the heating system thereby limiting the effectiveness of the thermal upgrading. To improve the overall efficiency and effectiveness of the thermal

retrofitting, the Department of Communications, Climate Action and Environment are collaborating with SEAI to provide grant aid for deep retrofitting.

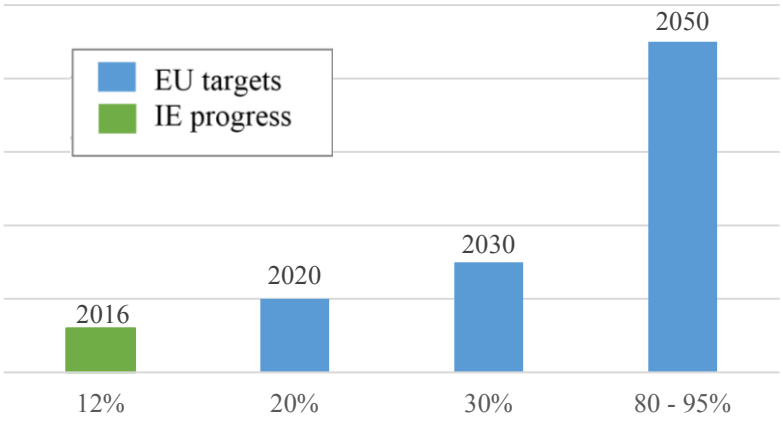

Fig. 1.3. EU energy efficiency improvement targets and Irish progress towards 2020 target.

As there is significant potential for energy savings in existing buildings, all European Member States are requested to prepare an LTRS [9]. Ireland issued the LTRS in 2017 [31] to maximise Ireland's progress towards 2020 and post-2020 goals. In relation to residential sectors, two new measures are being tested under pilot programs, from 2017 to 2020. First, the Deep Retrofit Programme supports deeper and more complex retrofitting strategies. Using this scheme, measures such as roof and wall insulation, windows and external door replacement, air tightness and mechanical ventilation installation can be upgraded to achieve a high energy efficiency standard. This upgrading can be supplemented with heating system improvement and installation of solar water heating. Second, the Warmth and Wellbeing Scheme aims to improve homes of older people and children suffering from chronic respiratory conditions. The LTRS includes a plan to make the BER documentation more understandable and helpful for homeowners, by including information about possible improvement measures and their likely costs. Minimum standards of energy efficiency in rented accommodations will be introduced from 2020. For existing buildings under renovation, a requirement of achieving energy efficiency equivalent to *B3* BER rating

will be imposed. It is likely that this requirement will be applied from the 1st of January 2019.

SEAI estimates that, in order to meet the 2020 targets, approximately 75,000 Irish buildings must be annually retrofitted to upgrade their thermal performance [32]. This is very challenging and requires immediate, well-organized actions.

In relation to greenhouse gas emissions, Ireland agreed on a target of a 20% GHG reduction when compared to 2005 level. However, in 2015, the Environmental Protection Agency (EPA) recorded an increase of 3.7 % in GHG emissions in comparison to 2014 emissions [33]. EPA projections [32] show that Ireland will fail to achieve the 2020 goal. GHGs are expected to be reduced by only 4 % - 6 % by 2020 and by 1 % - 3 % by 2030.

Achieving the energy efficiency improvement goal by Ireland is also very challenging because, as presented in this section, up to the year 2016 Ireland had only achieved an energy use reduction of 12 % whereas the EU goal is a 20 % energy reduction by 2020. Reduction in energy consumption related to buildings can be significantly increased only by retrofitting the existing building stock. The retrofitting should start with the improvement of building envelope thermal quality to conserve the energy generated by space heating. To evaluate the thermal upgrading, accurate building envelope thermal performance assessment before and after retrofitting is necessary.

1.3.4. Summary of building energy-related policy

The IEA has identified two key policy instruments that promote improvements in building energy efficiency on a global scale. They are the energy performance certification of buildings, and the introduction of strict building energy codes that force investors to build to a high thermal standard. Similarly, the European Union aims to motivate Member States to improve building thermal efficiency by the introduction of the directive EPBD 2010 [3].This directive obliges Members States to take specific actions, such as launching building energy certification systems and updating the building energy requirements. These actions have resulted in significant

improvements of the thermal standard of new buildings. However, as identified by the European Commission in 2016, an untapped potential of energy savings lies in the existing building stock. Throughout EU countries, about 75 % of existing buildings are still energy inefficient. It is necessary to focus on improving these existing buildings energy performance in order to achieve the EU target of 20 % energy saving compared to projections by 2020. Retrofitting of existing buildings is the key goal of the Proposal of amending EPDB[4].

1.4. Thermal evaluation of the existing building envelope

Improving the thermal quality of the existing building envelope is necessary as it is one of the most important factors determining the overall energy demand of a building. The building envelope consists of plain components and thermal bridging that may significantly increase overall heat losses. All these heat losses must be quantified to define the thermal quality of the building envelope. The current BER procedure in Ireland is based on approximate *U*-values and Ψ-values. This approach is suitable for new buildings where building documentation is available. On the other hand, for existing buildings information about the internal structure of the building envelope is often unknown. In this case, a thermal assessment method involving measurements of the actual heat losses must be undertaken.

Current approaches to in-situ measurement of thermal quality are primarily based on use of the heat flow meter (HFM) or the infrared-thermography technique (ITT). The HFM device measures the heat flow only through a small area of the building envelope and is, therefore, more suitable for measuring the uniform heat flow through the plain part of the envelope (*U*-value). In the ITT approach, a thermal image of the indoor or outdoor surface of the building envelope is recorded, which gives the full temperature distribution on the recorded surface. Modern high-resolution infrared cameras can give detailed information on the temperature distribution making this approach suitable not only for the plain part of the building envelope but also the thermal bridging, which can result in steep temperature gradients.

In practice, the ITT approach has primarily been used as a qualitative tool to identify areas of thermal bridging. However, there is significant potential to use this technology

as a quantitative tool for building thermal assessment. Most of the research to date has focussed on the use of ITT for *U*-value assessment.
Significantly less work has been done on the use of this technology for thermal bridging assessment.

1.5. Motivation and Research objectives

Limiting greenhouse gas emissions and energy use is essential to avoid further climate warming that may have a critical impact on the human environment and the ecosystem. As buildings are the world's largest energy consumer [2], limiting energy usage related to buildings is necessary in the process of overall greenhouse gas emissions and reduction of energy consumption. As a result, binding targets related to reduction in energy usage have been introduced across European member states. To help achieve these targets, stricter building regulations related to energy efficiency of buildings have been introduced. Currently, the greatest potential lies with the retrofitting of the existing building stock. To design appropriate retrofitting strategies, it is necessary to have accurate, non-invasive and efficient tools for in-situ assessment of the building envelope.

The primary aim of this research is to develop a methodology for building envelope heat loss assessment based solely on the use of the qualitative ITT. As access to the interior surface of a building is not always possible, methodologies for both indoor and outdoor assessment will be created. As the heat loss from the exterior surface of a building is highly dependent on the external environmental conditions, especially wind, the approach used will need to account for environmental conditions. The application of ITT requires steady state conditions to be present while measurements are being made. While these conditions can be achieved in a controlled laboratory setting, this is unlikely to occur in practice and therefore the application of the developed methodology in quasi-steady state conditions on an existing building will be investigated and recommendations for on-site application of the methodology will be developed. To ensure that the experiment programme reflect real thermal bridging appearing in building envelope, consultation with industry partners was undertaken.

Achieving the aims of the project will involve the following objectives:

- Develop, under laboratory conditions, an ITT methodology for quantification of thermal bridging performance based on indoor thermographic measurements. It is intended that the methodology will include evaluation of the heat loss via plain building components surrounding a thermal bridge using the same thermogram. Investigate the influence of the approach to determining surface convective and radiative heat transfer coefficients on the accuracy of the methodology. Validate the methodology using measurements in a hot box device.

- Using a combination of experimental and finite element modelling techniques, develop a methodology to quantify heat loss assessment based on the outdoor ITT. Quantify the influence of one of the main environmental factors, the wind velocity, on the thermal bridging heat losses. Develop an adjustment procedure to convert Ψ-value measurements at any wind velocity to the Ψ-value corresponding to the standard wind velocity of 4 m/s.

- Use the developed quantitative ITT methodology to investigate interaction effects in the case of multiple thermal bridges. In real buildings, the heat flow through a thermal bridge is impacted by heat flow through neighbouring thermal bridges. The heat flow through thermal bridging will be over-estimated if these interaction effects are not considered. Multiple thermal bridging can result in steep thermal gradients on the surface of the building. The ability of the ITT approach to accurately capture this behaviour is investigated. In the case of windows installed in the building envelope, due to the multiple thermal interactions, the individual thermal bridging effects cannot be separated using the ITT approach. For windows, a new way of characterizing the whole window thermal performance, based on a proposed M-value is presented.

- Perform an on-site study to test the methodology in the real building under the quasi-steady-state conditions. Develop recommendations for the on-site application of the methodology.

1.6. Structure of dissertation

This thesis is presented as a series of papers. It comprises three published journal papers that are presented sequentially in thesis chapters 3 – 5 followed by a further chapter with content that is yet to be published. Each publication contributes to meeting the project objectives.

Chapter 2 reviews the literature relevant to the research. Fundamental principles of heat transfer through a building envelope are presented. This is followed by presentation and evaluation of the state-of-the-art in building envelope thermal assessment. This includes analytical, numerical and experimental assessments. The latter is further discussed by presenting HFM, the hot box, and ITT. Current research findings related to the application of ITT for building heat loss assessment are reviewed with a view to informing the approach developed in the current work.

Chapter 3 describes the development of a methodology for in-situ thermal bridging assessment using the indoor thermography technique. The basis of the method is the application of the surface energy balance principle to the internal face of a building component containing a thermal bridge. According to this principle, the energy transferred to the surface is equal to the energy transferred from the surface and these can be evaluated from the surface temperatures. The methodology is applied to test specimens containing different types of thermal bridging, and the results are validated against measurements from testing in a calibrated hot box.

In Chapter 4, the development of a methodology for thermal bridging assessment based on outdoor thermography is presented. As external environmental conditions significantly impact on the heat transfer losses from external building surfaces, this chapter includes quantification of the wind velocity impact on the thermal bridging heat loss. Using experimental measurements and numerical analyses, a thermal bridging adjustment factor is developed, which allows the Ψ-value measured at any wind velocity to be converted to the Ψ-value measured at standard wind velocity which is 4 m/s and compared to the design Ψ-value.

In Chapter 5, the application of the ITT methodology to multiple thermal bridging assessment is described. Where two or more thermal bridges are situated

close to each other, the degree of the interaction between them will influence the Ψ-value. To avoid overestimation when assessing multiple thermal bridging, this interaction must be accounted for. The application of the ITT to complex thermal bridging assessment situations, such as window systems installed in a building wall, is presented. A practical approach for this case is the assessment of all heat losses associated with the window, including the installation Ψ-value, together as an additional heat loss via building component. This is expressed by a proposed window thermal transmittance or M-value.

Chapter 6 describes the testing of the methodology for indoor ITT assessment on an existing building under real environmental conditions. Under these conditions, it is not possible to maintain steady state conditions and so site implementation of the methodology must be carried out under quasi-steady state conditions. The implications of this for on-site assessment are discussed.

Chapter 7 contains a summary of the research and main conclusions based on the outcome of the project. It also gives recommendations for further research in this area.

1.7 References

[1] Climate Change 2014 Synthesis Report, Intergovernmental Panel on Climate Change, 2014.

[2] Transition to Sustainable Buildings: Strategies and Opportunities to 2050, International Energy Agency, Paris 2013.

[3] Directive 2010/31/EU of the European Parliament and of the Council on the Energy Performance of Buildings, 2010.

[4] Proposal for a Directive of the European Parliament and of the Council amending Directive 2010/31/EU on the Energy Performance of Buildings, 2016.

[5] Boosting Building Renovation: What potential and value for Europe?, Policy

Department A at the request of the Committee on Industry, Research and Energy of the European Parliament, 2016.

[6] Energy Performance Certification of Buildings - A Policy Tool to Improve Energy Efficiency, International Energy Agency, 2010.

[7] Modernising Building Energy Codes to secure our Global Energy Future: Policy Pathway, International Energy Agency, 2013.

[8] Energy Efficiency Market Report 2016, International Energy Agency, Paris 2016.

[9] Directive 2012/27/EU of the European Parliament and of the Council on Energy Efficiency, 2012.

[10] Proposal for a Directive of the European Parliament and of the Council amending Directive 2012/27/EU on Energy Efficiency, 2016.

[11] Directive 2002/91/EC of the European Parliament and of the Council on the Energy Performance of Buildings, 2003.

[12] Evaluation of Directive 2010/31/EU of the European Parliament and of the Council on the Energy Performance of Buildings, European Commission, 2016.

[13] Energy Efficiency Plan 2011, European Commission, 2011.

[14] 20 20 by 2020 Europe's climate change opportunity, Commission of the European Communities, 2008.

[15] A policy framework for climate and energy in the period from 2020 to 2030, European Commision, 2014.

[16] Energy Roadmap 2050, European Commission, 2015.

[17] Delivering a sustainable energy future for Ireland, Government White Paper, Department of Communications, Marine and Natural Resources, 2007.

[18] Ireland's Transition to a Low Carbon Energy Future 2015 - 2030, Department of Communications, Energy and Natural Resources, 2015.

[19] Insulating your home, Sustainable Energy Authority of Ireland, 2005.

[20] Efficient home heating guide, Sustainable Energy Authority of Ireland, 2013.

[21] Passive homes, Sustainable Energy Authority of Ireland, 2008.

[22] Better Energy Homeowner Grants, Sustainable Energy Authority of Ireland, 2015.

[23] Better Energy Warmer Homes Scheme, Impact Report - Billing Analysis, 2014.

[24] Behavioural insights on energy efficiency in the residential sector, Sustainable Energy Authority of Ireland, 2017.

[25] Building Regulations Conservation of Fuel and Energy - Dwellings, Technical Guidance Document Part L 2007.

[26] Building Regulation Conservation of Fuel and Energy - Dwellings, Technical Guidance Document Part L 2011.

[27] Building Regulation Conservation of Fuel and Energy - Dwellings, Technical Guidance Document Part L 2011 with Amendment 2017.

[28] Building Regulation Conservation of Fuel and Energy - Building other than dwellings, Technical Guidance Document Part L 2008.

[29] Standard Recommendation, Code of practice for the energy efficiency retrofit of dwellings, National Standard Authority of Ireland, 2014.

[30] National Energy Efficiency Action Plan for Ireland 2017 - 2020, Department of Communication, Climate Action and Environment, 2017.

[31] Ireland Long Term Renovation Strategy 2017-2020 Department of Communication, Climate Action and Environment, 2017.

[32] Ireland's Energy Targets, Sustainable Energy Authority of Ireland, 2016.

[33] Ireland's Final Greenhouse Gas Emissions in 2015, Environmental Protection Agency, 2016.

Chapter 2

Literature review

2.1. Introduction

In order to achieve European targets related to energy savings in buildings, it is necessary to accelerate the thermal retrofitting of the existing building stock. The thermal quality of a building mainly depends on the quality of its building envelope. In terms of conserving energy within a building, the envelope must be properly insulated including regions of thermal bridging. In this chapter, the principles of building physics governing heat flow are presented to demonstrate the how the heat is lost via building components. In order to determine the quality of a building envelope and design an appropriate retrofitting strategy, it is necessary to perform building thermal assessment. Post-retrofitting assessment is also important to assess the efficacy of the implemented strategy. In general, three types of assessment methods are available, namely, analytical, numerical and experimental. Each of these approaches is discussed. For many existing buildings, the internal wall structure and condition are unknown, and so in-situ measurement is the only feasible option. The available options for in-situ measurement are limited mainly to using heat flow meters or using IR thermography. The state-of-the-art with regard to these methods is described and limitations of current approaches are identified.

2.2. Building physics principles and standard approaches to heat transfer evaluation

In this section, the building physics' fundamental principles governing how heat is transferred via a building envelope are presented. The equations describing heat transfer allow for evaluation of the heat losses via plain components and thermal bridging. Most commonly the evaluation is carried out following procedures from standards and Building Regulations, as described in this section.

2.2.1. Heat transfer modes: conduction, convection, and radiation [1]

The heat loss associated with a building envelope is directly dictated by the indoor and outdoor temperature difference, environmental conditions (such as wind speed or solar radiation) and the thermal quality of the building envelope. Fig. 2.1 shows a scenario where the indoor air temperature T_i is higher than the external air temperature T_e resulting in a difference in temperatures between the indoor T_{si} and external surfaces T_{se} of the building envelope component.

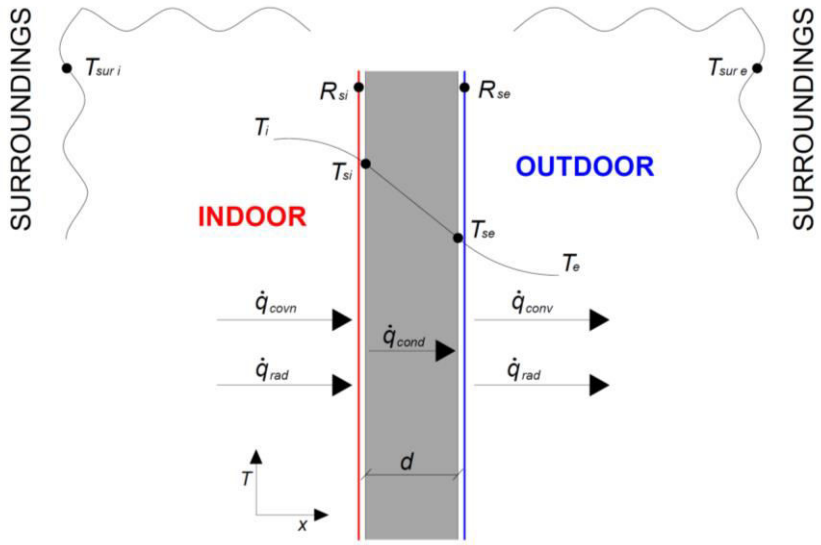

Fig. 2.1. Heat loss through a building envelope component, adapted from [1].

As illustrated in Fig. 2.1, heat loss via the building envelope is complex and heat is transferred in three modes, namely, conduction, convection, and radiation [1]. They are designated by heat fluxes $\dot{q}_{cond}$, $\dot{q}_{conv}$ and $\dot{q}_{rad}$, respectively and represent the rate of heat transfer per unit area.

When there is a temperature difference within a component, the heat is transferred by conduction. This involves the transfer of energy from the more energetic parts of the component to the less energetic parts of the object. In other words, the heat flows from the region of higher temperature (T_{si}) to the region of lower temperature (T_{se}).

Conductive heat flux is described by Fourier's Law. Equation (2.1) describes Fourier's Law applied to three-dimensional problems in Cartesian coordinates *x, y,* and *z*. The heat flux $\dot{q}_{cond}$ is the heat transfer rate per unit area perpendicular to the direction of transfer and it is proportional to the temperature gradient.

$$\dot{q}_{cond} = k_x \frac{dT}{dx} + k_y \frac{dT}{dy} + k_z \frac{dT}{dz} \qquad (2.1)$$

where
k_x, k_y, k_z are the thermal conductivities in the *x, y, z* directions. For an isotropic material, the thermal conductivity *k* is independent of direction. The thermal conductivity is a property describing a material's ability to conduct heat.

For plain building component such as a wall, the conductive heat transfer is commonly treated as one-dimensional flow through the thickness of the wall element. In that case, Fourier's Law can be simplified to Equation (2.2).

$$\dot{q}_{cond\,x} = k \frac{dT}{dx} \qquad (2.2)$$

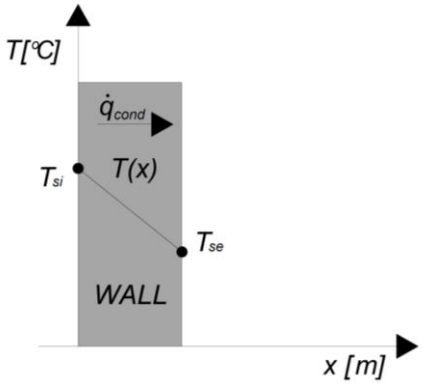

Fig. 2.2. One-dimensional conductive heat transfer, adapted from [1].

In one-dimensional steady-state conditions where the temperature is distributed in a linear fashion, the conductive heat flux can be expressed by Equation (2.3) and illustrated in Fig. 2.2.

$$\dot{q}_{cond} = k \frac{T_{si} - T_{se}}{d} \tag{2.3}$$

where

d is the width of the element

Each material resists conductive heat transfer, and this is described by its conductive thermal resistance R_{cond} (Equation (2.4)). The greater the thermal resistance of the material the better its insulating properties so less heat loss occurs.

$$R_{cond} = \frac{T_{si} - T_{se}}{\dot{q}_{cond}} \tag{2.4}$$

For homogeneous building components, R_{cond} can be also written as Equation (2.5). It can be clearly seen that its value depends on the thermal conductivity of the component k and its thickness d. When a component consists of several layers in series the conductive thermal resistance is equal to the sum of the resistances of all layers (Equation (2.6)).

$$R_{cond} = \frac{d}{k} \tag{2.5}$$

$$R_{cond} = \sum_{i=1}^{n} \frac{d_i}{k_i} \tag{2.6}$$

where

n is the number of layers

Between the building envelope surface and the surrounding air, heat transfer occurs in a convective mode. Two modes of convection can be distinguished, namely free and forced convection. Free convection is induced by changes in air density near the surface that result in air movement. This mode usually appears at the indoor surface of the building envelope. Forced convection is induced by wind in the natural environment or by artificial sources such pumps or fans. It usually appears at the external surface of the building envelope that is exposed to wind. In both modes, the convective heat flux can be described by Newton's law of cooling and is proportional to the difference between the surface and the fluid temperature (Equation (2.7)).

$$\dot{q}_{conv} = h_c(T_s - T_{air}) \tag{2.7}$$

where h_c is the surface convective heat transfer coefficient (or convection coefficient).

According to the well-established heat transfer theory, the most precise way of calculating the convective heat transfer coefficient is by using the Nusselt number *Nu* (Equation (2.8)) [1].

$$h_c = \frac{Nu\, k}{l_{ch}} \tag{2.8}$$

where l_{ch} is the characteristic length in the direction over which h_c applies.

The *Nu* is evaluated differently for the indoor and the external convection coefficients, h_{ci} and h_{ce} respectively, as they represent different convective conditions. In the indoor environment, where free convection occurs, the h_{ci} depends mostly on factors such as the surface geometry and coarseness, and the fluid thermodynamic

properties [1]. For the indoor surface of a building element, represented by a wall, the Churchill-Chu correlation for a vertical plate under natural convection can be used (Equation (2.9)).

$$Nu = \left\{ 0.825 + \frac{0.387Ra^{1/6}}{\left[1+\left(\frac{0.492}{Pr}\right)^{9/16}\right]^{8/27}} \right\}^2 \quad (2.9)$$

where *Pr* is the Prandtl number representing the ratio of kinematic viscosity to thermal diffusivity and the *Ra* is the Rayleigh number defining a ratio of buoyancy and viscous forces that can be calculated from Equation (2.10)

$$Ra = \frac{g\beta(T_i - T_s)l_{ch}^3}{\nu\alpha} \quad (2.10)$$

where
g is acceleration due to gravity, m/s^2
β is expansion coefficient, 1/K
ν is kinematic viscosity, m^2/s
α is thermal diffusivity, m^2/s

The external surface of a building component is usually exposed to a forced convective mode, where wind velocity significantly influences the h_{ce}. Within this convective mode, two types of flow can occur, laminar and turbulent. As they occur over the surface, they are called boundary layer flows. They are characterized by Reynolds number, which is expressed as the ratio of the inertia to viscous forces:

$$Re = \frac{w\, l_{ch}}{\nu} \quad (2.11)$$

Flow caused by wind over a flat surface is first spread from the edge in a laminar mode and then, at a certain distance from the edge, converts into turbulent flow. Conventionally, the conversion from laminar to turbulent flow occurs at the distance from the edge where the Reynolds number is equal to 5 x 10^5. The transition

from laminar to turbulent flow is influenced by roughness of the surface and/or disturbances of the flow and still can occur at a different distance. The Nusselt number in forced convection depends on the Reynolds (*Re*) and Prandtl (*Pr*) numbers, however, the relationship is different for laminar and for turbulent flow. For a building component surface, correlations for parallel flow over the surface of a flat plate can be applied. They are expressed, depending on the flow type, by Equations (2.12) – (2.14). Although these correlations were developed for parallel flow, they can be also used for flow in a direction other than parallel to external building component surface. This was experimentally found by Rowley and Eckley [2], who noticed that the convection coefficient only slightly decreased when the angle between the surface and the wind stream was increased from 15° to 90°.

Equations (2.12), (2.13) and (2.14) are used for the Nusselt number evaluation for laminar flow, mixed flow and turbulent flow, respectively. The mixed flow conditions (Equations (2.13)) often occur in the real outdoor environments where no obstacles of the flow along the surface building component are present. However, the flow near a building is often disturbed, for instance by a tree branch, an electric wire or by the surface roughness. In this case, the flow is fully turbulent over the whole length [2] and the Nusselt number should be evaluated using Equation (2.14).

$$Nu = 0.664 Re^{1/2} Pr^{1/3} \qquad (2.12)$$

$$Nu = (0.037 Re^{4/5} - 871) Pr^{1/3} \qquad (2.13)$$

$$Nu = 0.037 Re^{4/5} Pr^{1/3} \qquad (2.14)$$

All air properties used in Equations (2.8) – (2.14) are evaluated at a film temperature, which is the arithmetic mean of the surface temperature and the air temperature.

The thermal resistance for heat transfer in convection, or convective surface resistance, is expressed by Equation (2.15).

$$R_{conv} = \frac{T_s - T_{air}}{\dot{q}_{conv}} \quad (2.15)$$

which gives:

$$R_{conv} = \frac{1}{h_c} \quad (2.16)$$

The third mode of heat transfer associated with the building envelope is thermal radiation that describes the energy *E* emitted by a surface when its temperature is different to the temperature of the surroundings. A material that is a perfect emitter is known as a blackbody and no other material can, at a certain temperature, emit more energy. Using the Stefan-Boltzmann law, the emissive power of a blackbody at a certain temperature can be found. It is proportional to its absolute temperature to the fourth power (Equation (2.17)).

$$E_b = \sigma T_s^4 \quad (2.17)$$

where
σ is the Stefan-Boltzmann constant and is equal to 5.67 x 10^{-8} W/(m^2K^4)
T_s is the absolute temperature of the surface.

A real surface will emit less energy than a blackbody and this can be found using Equation (2.18)

$$E = \varepsilon \sigma T_s^4 \quad (2.18)$$

where the emissivity ε defines the efficiency of surface emissivity relative to a blackbody.

The surface also absorbs radiation from its surroundings. The rate at which radiation is incident on a unit area of a surface is termed the irradiation *G*. All or a portion of the irradiation can be absorbed by the surface depending on the surface

absorptivity α. A building surface at temperature T_s is surrounded by other surfaces at surrounding temperature T_{sur} where $T_s \neq T_{sur}$. In this case, the irradiation can be approximated by the emission of a blackbody, with $\varepsilon = 1$, at T_{sur} ($G = \sigma T_{sur}^4$). With the assumption that the surface is diffuse-grey where $\alpha = \varepsilon$, the net radiative heat flux leaving the surface can be calculated using Equations (2.19) – (2.21).

$$\dot{q}_{rad} = E - G \tag{2.19}$$

$$\dot{q}_{rad} = \varepsilon\sigma T_s^4 - \alpha\sigma T_{sur}^4 \tag{2.20}$$

$$\dot{q}_{rad} = \varepsilon\sigma(T_s^4 - T_{sur}^4) \tag{2.21}$$

Conventionally, the radiation leaving the surface is described by Equation (2.22) and the radiative heat transfer coefficient h_r by Equation (2.23).

$$\dot{q}_{rad} = h_r(T_s - T_{sur}) \tag{2.22}$$

$$h_r = \varepsilon\sigma(T_s + T_{sur})(T_s^2 + T_{sur}^2) \tag{2.23}$$

The thermal resistance for heat transfer in radiative mode can be expressed by Equation (2.24).

$$R_{rad} = \frac{T_s - T_{sur}}{\dot{q}_{rad}} \tag{2.24}$$

which gives:

$$R_{rad} = \frac{1}{h_e} \tag{2.25}$$

Conductive, convective and radiative heat fluxes are quantified in order to evaluate the heat loss associated with the building envelope as described in the next section.

2.2.1. Thermal evaluation of building envelope

As mentioned earlier, a building envelope consists of plain components such as walls, roof and floor, and regions of thermal bridging. Thermal bridging is a part of building envelope with different thermal conductivity or geometry. To assess the total heat losses through the building envelope, heat losses via both plain components and thermal bridging should be quantified. The total heat loss via the external envelope is expressed by the heat transmission coefficient H (Equation (2.26)). The first term in the equation is the sum of heat losses via the plain building components, expressed by the thermal transmittance or U-value, and the second part is a sum of heat losses via thermal bridging, described by the transmission heat loss coefficient H_{TB}.

$$H = \sum (A_j * U_j) + \sum H_{TB} \qquad (2.26)$$

where A_j is the area of component j and U_j is the thermal transmittance of component j. The European Standard EN ISO 6946 [3] provides an analytical method for U-value calculation for a building component comprising one or several homogeneous or inhomogeneous layers. Using this method, thermal resistances are added, in accordance with Equation (2.27). R_{si} represents indoor surface resistance including indoor radiative and convective resistances whereas R_{se} is the external surface resistance including external radiative and convective resistances. R_{si} and R_{se} describe indoor and external boundary conditions, respectively (Fig. 2.3). The U-value is equal to the inverse of total resistance R_{tot} and represents a rate of heat transfer through a building element per unit area (Equation (2.28)).

$$R_{tot} = R_{si} + \sum_{i=1}^{n} R_{cond\,i} + R_{se} \tag{2.27}$$

$$U = \frac{1}{R_{tot}} \tag{2.28}$$

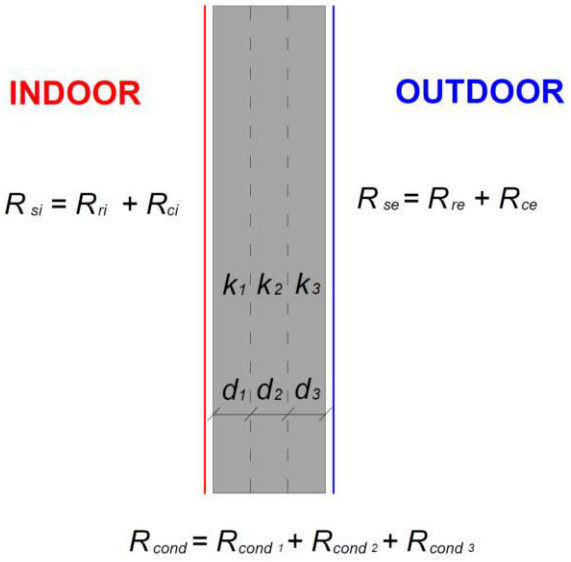

Fig. 2.3. Conductive and surface resistances.

The boundary conditions can be expressed by surface resistances or by surface radiative and convective coefficients. According to EN ISO 6946 [3], in the absence of specific information about the boundary conditions, conventional surface resistances are to be used (Table 2.1). These values were calculated for a surface emissivity of 0.9 and the external surface resistances values were evaluated assuming a wind velocity of 4 m/s. These resistances depend on the direction of heat flow and apply to surfaces in contact with air.

Table 2.1. Surface resistances in accordance to EN ISO 6946 [3].

Surface resistance (m^2K/W)	Direction of heat flow		
	Upwards	Horizontal	Downwards
R_{si} internal surface	0.10	0.13	0.17
R_{se} external surface	0.04	0.04	0.04

In case of using surface heat transfer coefficients to characterize the boundary conditions, the standard EN ISO 6946 [3] gives an approximate approach for the h_c and the h_r evaluation.

According to this standard, the h_r is calculated according to Equation (2.29).

$$h_r = \varepsilon h_{r0} \qquad (2.29)$$

The h_{r0} is a black body radiative coefficient and its values are given in this standard, depending on the mean temperature of the surface and its surroundings.

According to the same standard EN ISO 6946 [3], the convection coefficient at the internal surface component h_{ci} depends on the heat flow direction as presented in Table 2.2.

Table 2.2. Indoor convection coefficient h_{ci} according to EN ISO 6946 [3]

h_{ci} (W/m^2K)	Type of heat flow
5.0	upward
2.5	horizontal
0.7	downward

On the other hand, according to EN ISO 6946 [3], the convection coefficient at the external surfaces h_{ce} depends only on the wind velocity w and can be approximated using Equation (2.30).

$$h_{ce} = 4 + 4w \qquad (2.30)$$

Approximate boundary conditions expressed as thermal resistances (Table 2.1) or as radiative (Equation (2.29)) and convective coefficients on indoor (Table 2.2) and outdoor (Equation (2.30)) surfaces are conventionally used for heat transfer analytical and numerical simulations or for calculations from in-situ measurements.

In regard to thermal bridging, in accordance with ISO 14683 [4], two types of thermal bridges can be distinguished namely, point and linear thermal bridges. A point thermal bridge occurs where three building components meet. Its heat loss is described by the point thermal transmittance χ, which is the heat flow rate in the steady state divided by the temperature difference between the environments on either side of the thermal bridge. A linear thermal bridge is characterized by a uniform cross-section along one of the three orthogonal axes. The heat loss associated with linear thermal bridging is expressed as the linear thermal transmittance or Ψ-value, which is the heat flow in the steady state per unit length divided by the temperature difference between the environments on either side of the thermal bridge. Table 2.3 shows examples of thermal bridges. The left column presents digital images of thermal bridges occurring on internal building surfaces. The right column presents infrared images of the red outlined section. Samples (a) – (c) present linear thermal bridges and sample (d) a point thermal bridge. They are characterized by surface temperatures lower than the surrounding plain components.

Table 2.3. Examples of thermal bridges.

Digital images	Infrared images
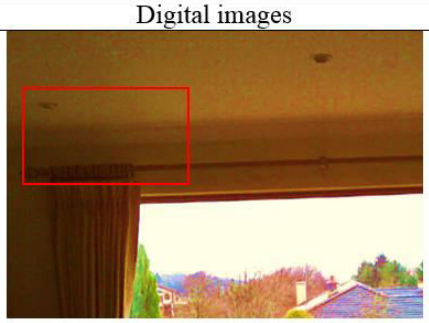	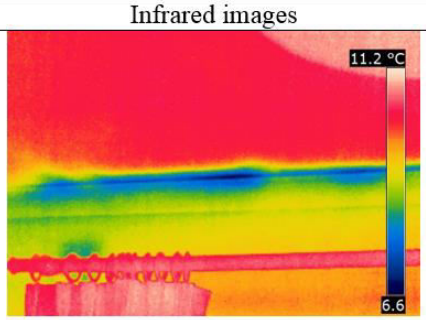
(a) thermal bridge at the wall/ceiling connection	
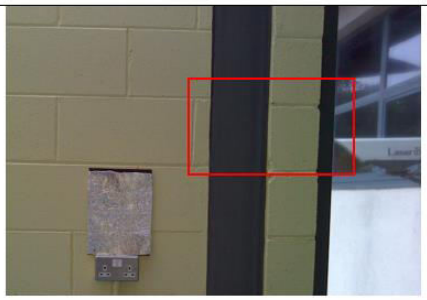	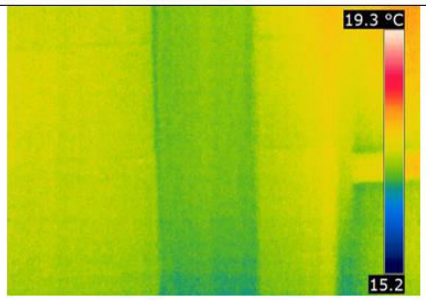
(b) thermal bridge created by a steel column	
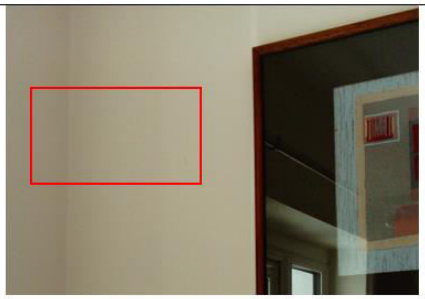	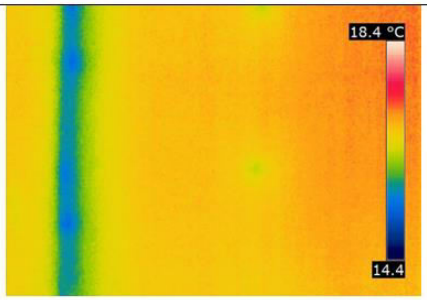
(c) thermal bridge at the corner of two walls	
	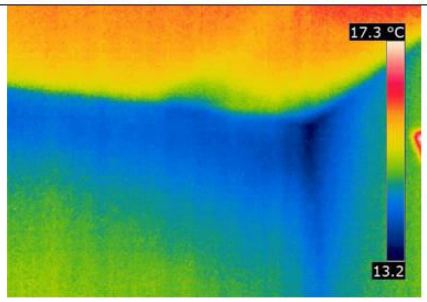
(d) a point thermal bridge at the wall/wall/ceiling connection	

Thermal bridging heat loss is not included in the *U*-value of the plain element and must be added when calculating the total heat loss through the fabric of a building.

The transmission heat loss coefficient associated with linear thermal bridges, H_{TB}, describes the total thermal bridging heat loss in a building. According to the Irish Building Regulations Part L 2011 [5], this can be determined in two ways. First is by using a multiplier Y applied to the total exposed area A_{exp} (Equation (2.31)):

$$H_{TB} = Y * A_{exp} \quad (2.31)$$

If all thermal bridging junctions in a building are equivalent to those set out in 'Limiting Thermal Bridging and Air Infiltration – Acceptable Construction Details' [6] then Y is equal to 0.08. In other cases, Y is assumed to be 0.15. The second way of determining H_{TB} is by summing the products of the linear thermal transmittance Ψ and the length for each thermal bridge (Equation (2.32)). The values of Ψ can be taken from the appendix of the Building Regulations Part L 2011 [5] and they can be also obtained from numerical modelling or measurements.

$$H_{TB} = \sum(l * \Psi) \quad (2.32)$$

The heat losses associated with point thermal bridges are very small and are, therefore, conventionally neglected when evaluating thermal bridging heat loss.

The International Standard ISO 14683 [4] also describes methods for determination of the Ψ-value including numerical calculations (typical accuracy ± 5%), thermal bridges catalogues (typical accuracy ± 20%), manual calculations (typical accuracy ± 20%) and default values (typical accuracy 0% - 50%) given in the standard.

Standard ISO 10211 [7] sets out guidelines for obtaining the Ψ-value from numerical calculations. The principle is that the construction details are known. In general, numerical models of a component containing a thermal bridge should include at least 1m of plain component surrounding the thermal bridge, as illustrated in Fig. 2.4 or finish at the thermal bridge symmetry plane. The linear thermal transmittance separating two environments is given by Equation (2.33).

$$\Psi = L_{2D} - \sum_{j=1}^{Nj} U_j \, l_j \qquad (2.33)$$

where

L_{2D} is a thermal coupling coefficient obtained from a 2-D calculation of the component separating the two environments being considered.

U_j is the thermal transmittance of the plain component j

l_j is the length of the 2-D geometrical model over which the value U_j applies.

N_j is the number of 1-D components.

Fig. 2.4 presents an example of a geometry of a wall containing a thermal bridge created by a column made from material with higher thermal conductivity than the wall in which it is embedded. The blue arrows represent L_{2D} which is two-dimensional heat flow caused by the thermal bridge presence.

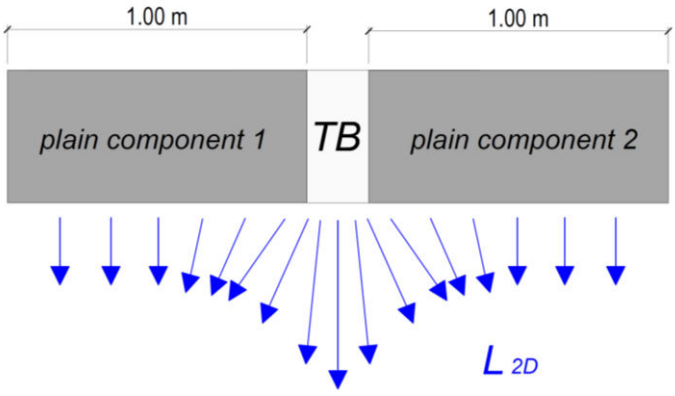

Fig. 2.4. Thermal coupling coefficient of a wall containing a thermal bridge created by a column.

Berggren and Wall [8] carried out a survey among building engineers, architects and contractors in Sweden to find out the level of knowledge and understanding of the impact of thermal bridges and the calculation methods for accounting for their impact. The survey showed that the state of knowledge is not satisfactory. The authors pointed out that clear guidelines on how to apply the international codes and training should be provided. The study also revealed that when

a building envelope is thermally improved, the percentage effect of thermal bridges increases so that accurate characterisation of their impact is paramount.

Fundamental principles of building physics presented in this section illustrate heat transfer principles. Following these principles, the heat loss associated with plain building components (described by U-values) and linear thermal bridges (described by Ψ-values) can be calculated. This evaluation can be performed using different methods that are presented in the next section.

2.3. Overview of building envelope thermal performance assessment methods

This section presents available methods of building envelope thermal assessment. In general, three types of assessment can be distinguished, namely analytical, numerical and experimental. Thermal evaluation of a plain building component can easily be performed analytically as it refers to a one-dimensional heat transfer problem. A thermal quality of a plain component is characterized by U-value calculated from Equation (2.28). The presence of thermal bridging in the building envelope causes two- or three-dimensional heat transfer that is difficult to handle analytically, so as described in Section 2.2.1, a simplified approach is given in the standards. This approach is not very precise so, to improve the accuracy, numerical or experimental approaches are required. Numerical approaches are widely used and are mostly based on finite element (FE) steady or unsteady heat transfer analysis or on computational fluid dynamics (CFD) modelling. The experimental approach involves in-situ measurements taken with devices such as heat flow meters (HFM), hot box or infrared cameras. Each of these methods is now discussed in further detail.

2.3.1. Numerical approach to building envelope assessment

The numerical approach provides an efficient solution for complex heat transfer problems, and therefore, is widely used for thermal bridging assessments of building envelopes. Two most common numerical methods are the FE and CFD approaches. For the FE method, the domain of interest is discretised with a suitable level of refinement, and FE equations are derived, which are then solved subject to specified boundary conditions. Most commonly, CFD codes adopt are based on a finite volume approach. The domain is discretized into cells and the solution is found for each volume surrounding each node.

In a FE model, for the purpose of quantification the heat transfer within the building envelope, the boundary conditions are defined by air temperatures, convective heat transfer coefficient and surfaces emissivity on both sides of the model. Using CFD simulation for building envelope evaluation, the boundary conditions can be defined similarly as in the FE simulations. However, in the case of CFD simulation, expressing the convection and radiation by coefficients can be avoided. Instead, air with prescribed behaviour and properties, surrounding the building component can be included in the simulation.

Troppová et al. [9] used FE software ANSYS Workbench to evaluate Ψ-value of thermal bridges in a prefabricated wooden house. The models were prepared in accordance with EN ISO 10211 [7]. Numerically predicted Ψ-values were compared with tabulated values given in EN ISO 14683 [4]. Fig. 2.5 shows the heat flux distribution through a simulated prefabricated timber panel where the green colour on the timber studs represents increased heat flux, thus indicating thermal bridging. The values derived from simulations were found to be significantly lower than the tabulated values, showing that the tabulated values overestimate the thermal bridging heat loss.

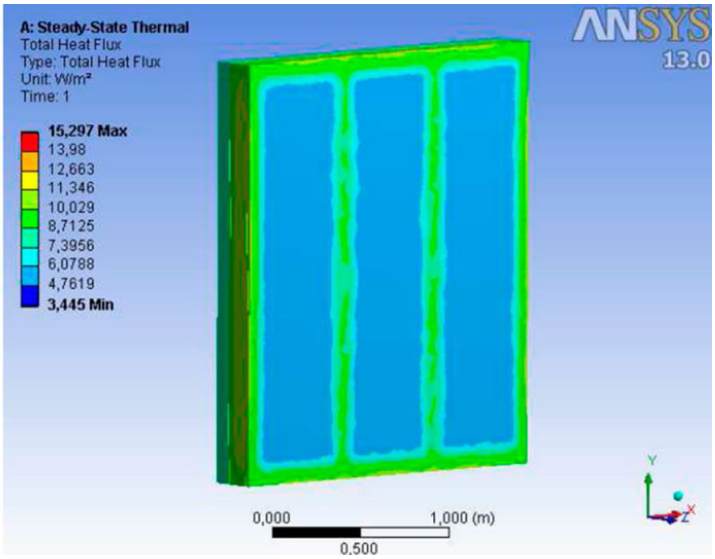

Fig. 2.5. Heat flux field of a prefabricated timber panel [9].

Viot et al. [10] also performed FE simulations for thermal bridging in wood-frame construction. Part of the meshed geometry is shown in Fig. 2.6. They used the commercial software COMSOL Multiphysics to create models in steady-state and dynamic conditions. They demonstrated that rounding the Ψ-value to two decimal places instead to three decimal places led to significant errors. Evaluating Ψ-value of one timber stud and then multiplying it by the number of studs instead of including the whole wall in the numerical model was identified as another source of errors. They demonstrated that these two sources of errors caused a maximum discrepancy of 40% for a wall with 7 timber studs. They also suggested out that the correct way of thermal bridging heat loss evaluation is by unsteady 3D model.

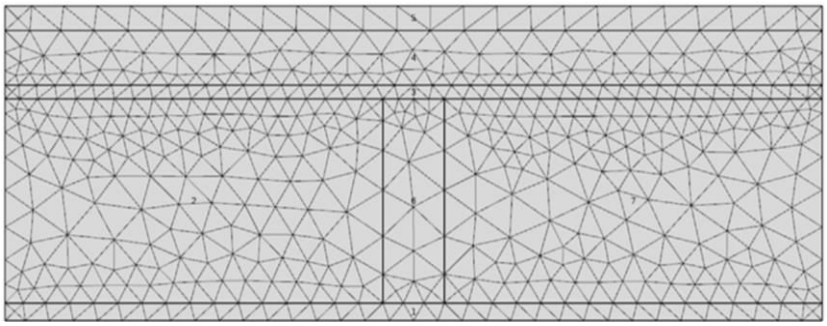

Fig. 2.6. Meshed geometry of a part wood-frame wall [10].

Other researchers used CFD to calculate the heat transfer associated with thermal bridges. Asdrubali et al. [11] carried out CFD analysis using the commercial code FLUENT for the analysis of thermal bridge heat loss between a window frame and window glazing. The temperature distribution obtained from the analysis is presented in Fig. 2.7. Thermal performance of this thermal bridge was also tested using the ITT methodology (described in more detail in section 2.3.2.3.3.) and HFMs. Good agreement was found between these three methods.

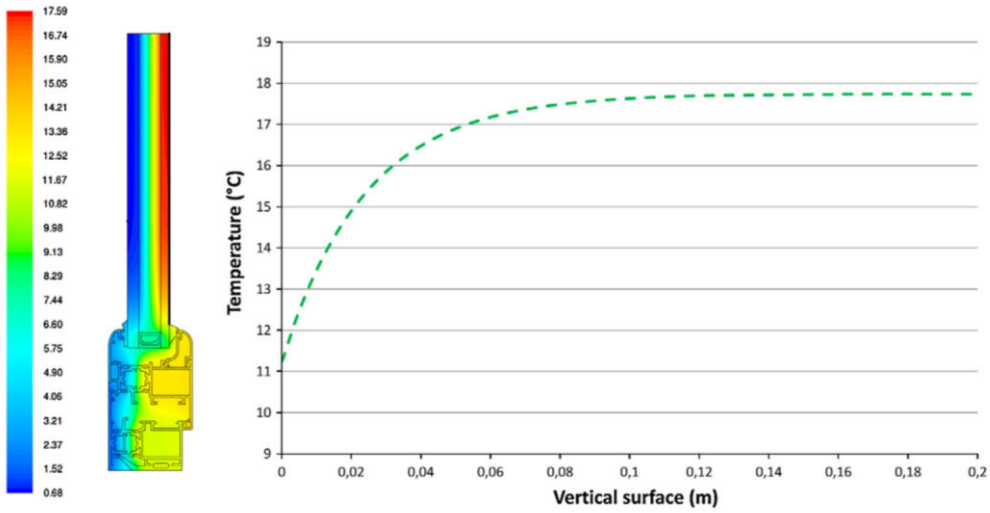

Fig. 2.7. Temperature distribution obtained from CFD analysis [11].

Also, Martin et al. [12] used FLUENT for evaluation of thermal bridging impact. They carried out a dynamic simulation of a building wall sample, with and without thermal bridging created by a concrete column. A wall sample with the same geometry and properties was experimentally tested in a guarded hot box. They found only 2 % difference between measured and simulated results for the plain wall and 8 % for the wall containing a thermal bridge.

As the development of FE and CFD models for complex geometry may be time-consuming and also require significant computational power, Ascione et al. [13] developed a simplified procedure for calculating heat loss associated with thermal bridging using the conduction transfer function method. The advantage of this method is that it needs significantly less computational power and is less time consuming than

FE or CFD methods. Comparison of the results obtained using the proposed method and the CFD method showed good agreement with a maximum deviation of 4.5 %.

Other numerical approaches, for instance, the finite difference (FD) method, may be used for thermal bridging evaluation. Capozzoli et al. [14] used the FD simulation code TRISCO to model a number of different common junctions in the building envelope, in accordance with EN ISO 10211 [7]. The models of thirty-six thermal bridges in a masonry structure with a different type of insulation were used for a sensitivity analysis to identify the significance of different variables on the Ψ-value. The authors found out that the thickness of the insulation layer is the most important variable that influences the Ψ-value in almost all cases with continuous insulation. On the other hand, in cases with non-continuous insulation, the thermal conductivity of the masonry is the most significant variable that determinates the Ψ-value.

Numerical simulations are widely used to calculate heat losses associated with thermal bridges. However, this approach is limited to building elements with known geometric and parameters. Because of this, numerical methods are useful at the building design stage to predict heat loss caused by thermal bridging. For existing buildings, the internal structure is very often unknown. Also, numerical analysis is based on ideal conditions and material properties and do not take into account possible workmanship errors. These conditions may not mirror the actual thermal performance of building components. For constructed buildings, with unknown structure, the thermal evaluation should be based on in-situ measurements. As they take into account the actual material conditions, they should quantify the actual heat losses.

2.3.2. Experimental approaches to building envelope assessment

Experimental approaches to building envelope thermal assessment are an alternative to analytical or numerical approaches, where the internal structure of a building is not known. This is very often the case with existing buildings. Experimentally measured building envelope thermal quality should reflect possible workmanship mistakes and

material aging. Three experimental assessment methods are presented in the following sub-sections: the heat flow meter, hot box, and infrared thermography technique.

2.3.2.1. Heat Flow Meter

The only standardized method for in-situ measurement of building envelope thermal properties is the HFM. According to ISO 9869 [15], this tool is suitable for measuring the thermal resistance *R*, conductivity *k* and thermal transmittance *U*-value of a plain building element. Use of the HFM requires personnel with experience and knowledge in building physics and measurement techniques. The HFM comprises thermal resistive plates with temperature sensors that are mounted on the surveyed building component. To accurately choose the location for the HFM and avoid any disturbances such the vicinity of thermal bridges, is recommended to first investigate the building component using the qualitative infrared thermography technique (ITT), in accordance with ISO 13187 [16]. The test duration must be at least 72 hours if the air temperature around the HFM is stable, otherwise, the test duration should be more than 7 days. The surface heat flux $\dot{q}$ and the measured internal and external surface temperatures (T_{si}, T_{se}) are recorded usually at intervals of 0.5 – 1.0 hour. Using these data, thermal resistance, thermal conductivity or *U*-value can be calculated.

This method was used by Building Research Establishment Limited (BRE) [17] to predict the as-built thermal performance of construction elements. This project aimed to compare thermal transmittance of building elements measured on site to values calculated in accordance with ISO 6946 [3]. The *U*-value of 29 building walls, including block cavity walls and timber and steel frame walls, were measured by using HFMs fixed to the element for several days. The investigation revealed that the *U*-value of a constructed wall is generally about 20 % higher than that predicted using ISO 6946 [3]. HFMs have been also used by Byrne et al. [18] to investigate the in-situ thermal behaviour of building components before and after retrofitting. The thermal behaviour of the building envelope was monitored over three stages. The first stage started when the indoor and outdoor temperature were the same and then the heating was turned on to its full power until a quasi-steady state had been reached. In the second stage, the heating remained constant for a few days and, in the third stage, the

heating was switched off to allow the building to cool down. The HFMs were placed on the north facing wall and on the ceiling below the attic space. The measurements showed that by insulating walls and ceiling, the average indoor temperature increases by 3.66°C with the same heating input. It was demonstrated that after retrofitting, during the cooling stage the heat stored in the building envelope flows back to the inner space. Because of this, the total heat loss via retrofitted walls, over 12 days, was reduced by 60.8 % for the same heat energy input. Byrne et al. [18] concluded that in all their study cases, the theoretically calculated resistances are overestimated: the ceiling resistance by 75% and wall resistance by 60%. These theoretically calculated values overestimated the reduction of the heat loss after retrofitting by 50 % via ceilings and by 20 % via walls. Also, Asdrubali et al. [19] used HFMs to evaluate the thermal transmittance of six green building walls. After comparing the measurements with calculated values, a discrepancy of between -14 % and +43 % was found. The authors stated that these differences may be caused by poor workmanship, overestimation of the material properties and weather conditions. The HFM was also by Evangelisti et al. [20] to measure the *U*-value of three different existing building walls and compare them to the theoretical values, calculated in accordance to ISO 6946 [3]. It was found that the measured *U*-values were smaller than calculated for the hollow brick wall by 153 % and for tuff block walls by 17 %. On the other hand, for a wall constructed of hollow bricks and concrete, the measured *U*-value was greater than the calculated, with a maximum deviation of 53 %. Some researchers have used the HFM as a validation technique for numerical simulations. For instance, using this technique, Ascione et al. [21] validated their simplified numerical code for quick thermal bridges' heat loss assessment for the case of a thermal bridge in a real building corner. One HFM was mounted on the plain part of the wall (1 m away from the corner) and ten heat flux sensors were placed in the corner and at different distances from the corner. The difference between the measured and simulated heat fluxes varied between -12% and +6%, representing good agreement. Zalewski et al. [22] also used HFMs to experimentally quantify the heat loss caused by thermal bridging in a prefabricated building wall. The full-scale wall specimen was placed between two climatic chambers, mirroring the indoor and outdoor environments. One HFM was placed on the thermal bridge and two on the plain part of the wall. The heat flux measured in the plain part of the wall and on the thermal bridge were compared. The

result shows that the presence of thermal bridging increases the *U*-value up to 27%. These experimental measurements validated the numerical predictions made using thermal analysis software TRISCO. In the above-mentioned studies [17-22], the qualitative ITT was used as a supporting technique to correctly position the heat flow meters.

The HFM is a widely used technique for evaluating the thermal performance of plain building components. As presented in this section, many researchers have applied it to measure the *U*-value and to compare it to the theoretically calculated values [17-19]. Because the HFM only covers a small area of the building component, it is conventionally used to characterize the thermal performance of a plain component, which has uniform properties. For thermal bridging heat loss assessment, HFMs were also used [21,22] but, a large number of devices is required to accurately capture the temperature gradient in the vicinity of the thermal bridge. The qualitative ITT is often used in parallel with the HFM to help select a location for attaching the HTM. The key disadvantage of the HFM method is the time required to undertake a test (minimum of 72 hours).

2.3.2.2. Hot Box method

A hot box is a device that can be used to measure thermal properties, such as the thermal resistance *R* and thermal transmittance *U*-value, of a specimen, representing a building envelope component. The humidity and the temperature, as well as wind velocity, can be designed and controlled for each test. The European standard EN ISO 8990 [23] lays down the principles for the hot box design. It also outlines the procedure for obtaining a steady state for thermal properties' determination. The box walls are built of a high thermal resistance material to keep the heat losses through the box walls as low as possible. The hot box consists of two climatic chambers. The metering box replicates indoor environmental conditions and the cold box outdoor conditions. Between them, a tested specimen is installed. There are two types of hot box, namely guarded and calibrated hot boxes.

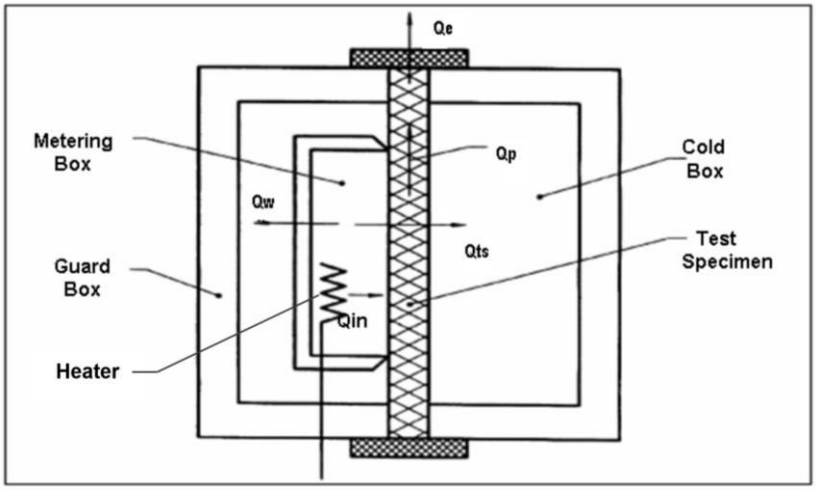

Fig. 2.8. Guarded hot box, source [23]

In a guarded hot box, shown in Fig. 2.8, the metering box is surrounded by a guard box to reduce the losses through the metering box walls to a minimum. After mounting the specimen between the chambers, air temperatures in both the guard and the metering boxes are kept at the same level. Also, the air temperature in the cold box is kept steady. Once the steady-state is reached, the heat rate through the specimen will be equal to the heat input to the metering box. To calculate the thermal properties of the tested specimen, the air and surface temperatures in the steady state and the power input provided to maintain the steady state are measured. The power input to the electric heater installed in the metering box is determined from the product of the voltage measured by a voltmeter and the current measured by an ampere meter. The guarded hot box allows testing of non-homogenous specimens giving a total heat flow through the tested specimen. The minimum size of the metered area is 3 times specimen thickness or 1 m x 1 m, whichever is greater.

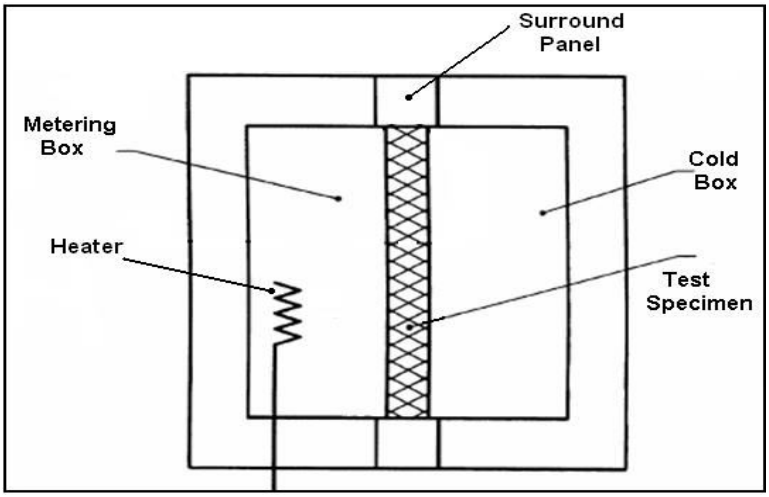

Fig. 2.9. Calibrated hot box, source [23]

A calibrated hot box consists of two chambers that are kept at constant temperatures, namely, the environmental box, also called the cold box, and the metering box on the warm side, as shown in Fig. 2.9. The main difference between the calibrated and the guarded hot boxes is the absence of a guard box in the calibrated hot box. Because of this, the heat losses via metering box walls are greater in calibrated hot box than in the guarded one. However, the advantage of calibrated hot box is that two approaches for thermal evaluation of the specimen can be used. In the first one, similarly to the guarded hot box, the power input required to maintain a steady state is determined. In the second approach, the heat flux through the specimen is evaluated using HFMs attached to the specimen surface. It should be borne in mind that these measurements relate only to a small area covered by the HFM. To thermally characterize inhomogeneous specimens, several sensors must be attached to areas representing different parts of the specimen. The minimum size of the specimen tested in this type of the hot box is 1.50 m x 1.50 m [23].

The hot box method has been widely used to investigate the thermal behaviour of building elements. For example, the guarded hot box method was also used to assess the influence of convective flow in a wall with different cavity depths (40mm, 60mm, 78 and 100mm) on the overall wall heat transfer by Aviram et al. [24]. A 1.2 m x 1.2 m cavity wall with block and brick leaves was constructed between the hot and cold chambers. It was noted that flow changed from turbulent to laminar when the cavity

depth reduced from 78 mm to 40 mm and that the thermal resistance of the air in the cavity increased with reducing cavity depth. It was also noted that the thermal conductivity of the mortar can be up to seven times greater than that of the surrounding block wall. The guarded hot box device, but with removable chambers, was also used by Nussbaumer et al. [25] to determine the thermal performance of vacuum-insulation panels (VIPs) applied to concrete building walls. First, the *U*-value of a non-insulated 180 mm thick reinforced concrete wall was measured by the hot box and evaluated numerically. Afterward, insulation boards, consisting of 40 mm thick VIPs and a 20mm EPS layer, were glued onto the cold side of the wall and two layers of plaster were applied and the-measurements were repeated. A thermal improvement of over 95 % was observed using this type of insulation. This 60 mm thick insulation is equivalent to 212 mm thick traditional insulation. During the experiment, within one minute of removing the cold box, a qualitative ITT survey was performed. The infrared image (IR image) showed higher temperatures where the VIPs were damaged and on the junction between the specimen and on joints between panels. The IR image did not show the influence of the reinforcing bars on the surface temperatures. Numerical analysis showed good agreement with the experimental values. The hot box is also an approved method for determination of thermal transmittance of windows and doors (EN ISO 12567-1 [26]) and windows frames (EN 12412-2 [27]). Lechowska et al. [28] used a guarded hot box to study the thermal performance of a novel polyvinylchloride (PVC) window frame. In the hot box, a standard PVC frame available on the market was tested, followed by two improved options. The measurements revealed that insertion of polyurethane foam into the air gaps reduces the frame thermal transmittance by 27 %. A similar effect (28 % reduction) was measured after application of the low-emissivity coating on the PVC surface in the air gaps. Good agreement was found between numerical analysis and the hot box measurements.

Asdrubali and Baldinelli [29] compared the testing procedure and the accuracy of the calibrated hot box measurements obtained in accordance to three different standards: ISO 8990 [23], ASTM C1363-05 [30] and GOST 26602.1-99 [31]. They tested these three approaches on aluminum windows and obtained similar *U*-values, 2.19 W/m^{2}K, 2.15 W/m^{2}K and 2.12 W/m^{2}K, respectively. The ISO and ASTM standard procedures are very similar in terms of calibration of the hot box before

testing and calculation of uncertainties. Therefore, similar *U*-value uncertainties were obtained, +/-0.15 W/m^{2}K for ISO and +/-0.16 W/m^{2}K for the ASTM approach. According to these standards, the *U*-value is calculated based on the amount of power required to maintain a steady state in the hot box. On the other hand, the GOST standard does not require a calibration procedure and the uncertainty calculation relates only to the thermocouples, the HFMs and specimen dimensions. As a result, the calculated uncertainty is significantly lower amounting to only +/-0.06 W/m^{2}K. According to the GOST standard, the evaluation of the *U*-value of an inhomogeneous specimen starts with dividing the surface specimen into sections with homogeneous properties. HFMs and thermocouples are attached to each section. Based on these measurements, the *U*-value is calculated. The authors concluded that characterizing each part of the inhomogeneous specimen gives specific information about each part of the specimen, which is an advantage of this approach. The authors concluded that this approach should be used while performing testing in accordance with ISO or ASTM standards. Zalewski et al. [22] used the calibrated hot box in an experiment where the impact of thermal bridges on the overall *U*-value of a prefabricated steel framework used for building walls was quantified by HFMs [22]. In this experiment, three HFMs were used: one attached to the middle of the thermal bridge and two outside the thermal bridge zone of influence. Comparing of the heat fluxes measured at these three positions, the thermal bridge impact on the whole steel framework could be defined. However, using this approach the linear thermal transmittance was not quantified. This type of hot box was also used by Baldinelli [32] to measure the thermal resistances of low-e panels. The results were compared to the thermal resistances measured with HFMs, with a guarded hot plate and calculated theoretically according to ISO 6946 [3]. The thermal resistances calculated theoretically showed good agreement with measured values.

Summing up, the hot box is a useful measurement technique for the determination of thermal quality of building envelope components. Using the hot box according to the standard [23,26,27] requires that testing is carried out under steady-state conditions. This is not feasible in field conditions. Due to the significant size of the hot box device, testing of specimens representing the actual building envelope sections is possible, which is its significant advantage. Using this method, the

environmental conditions on both sides of the specimen can be controlled. This gives an opportunity for testing at different air temperatures, air velocities, and humidity levels so that influence of these parameters on the thermal performance of the specimen can be investigated. However, besides all these advantages of the hot box, this method is not suitable for a thermal assessment of a real building.

2.3.2.3. Infrared Thermography Technique (ITT)

The infrared thermography technique (ITT) can be used for both qualitative and quantitative measurements of building envelope thermal performance in real conditions. The use infrared thermography for qualitative measurements to identify anomalies in the external envelope, such as missing or defective insulation, thermal bridges, air leakages, water infiltration and excessive moisture in building components, is widespread. On the other hand, the potential of the ITT quantitative measurements, allowing quantification of the heat losses, has not been fully realized yet.

2.3.2.3.1. History outline and operational principles

Infrared rays were discovered by Willian Herschel in 1800 [33]. In his experiment, he split the sun's heat radiation through a glass prism and measured the temperature of each colour. He noticed that the temperature of colours increases from the violet part to the red part. Moreover, he discovered that the temperature just beyond the red is the higher of any of the colours even in the absence of exposure to visible sunlight. This way he discovered a non-visible source of light. He also proved that the invisible rays can be refracted, absorbed, transmitted and reflected the same way as visible rays. He named the newly discovered rays infrared rays, which from Latin means below red. Fig. 2.10 presents different wavelength ranges corresponding to the different types of rays. The wavelength of infrared rays spans from 0.7 μm to about 100 μm [1].

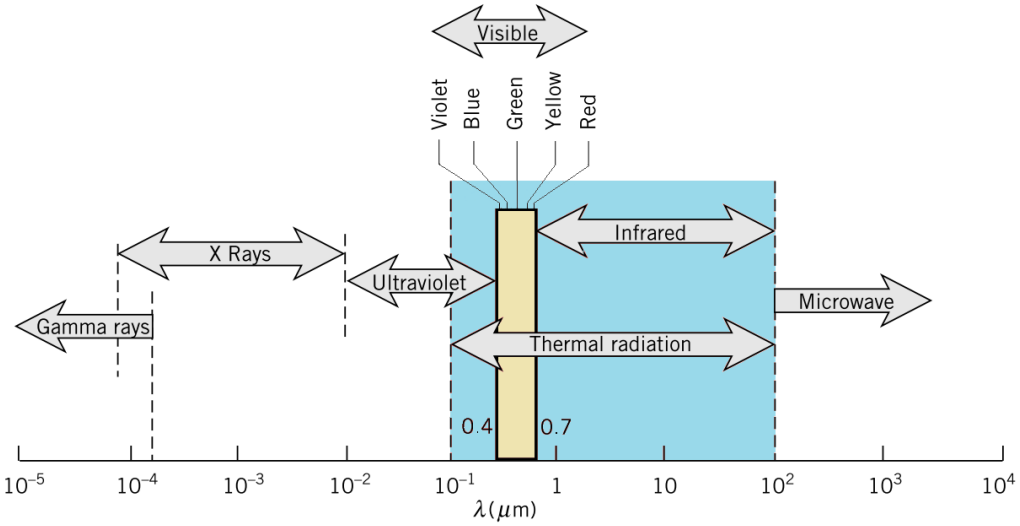

Fig. 2.10. The spectrum of electromagnetic radiation, adapted from [1].

Each object, at temperatures higher than absolute zero, radiates energy. Its intensity depends on the object temperature and on its ability to radiate. A blackbody is a perfect emitter that, at a given temperature, emits energy over a range of wavelengths, as defined by Planck in the spectral distribution of energy radiated by a blackbody, presented in Fig. 2.11. The blackbody curves link the spectral emissive power, which is the rate of radiant energy emitted by a surface per unit area per unit wavelength, to the wavelength for different temperatures. As can be seen in this figure, at any wavelength, the energy radiated by a blackbody increases with increasing temperature. The total emissive power of a blackbody at a given temperature can be found by summing the power emitted at each wavelength. This total emissive power is proportional to its absolute temperature to the fourth power, according to the Stefan-Boltzmann law. The dashed line across the curves connects the points at which the blackbody radiates the maximum amount of energy at any wavelength at any given temperature and is defined by Wien's displacement law. According to this law, the maximum emissive power is displaced to shorter wavelengths with increasing temperature [1,34]. As indicated in Fig. 2.11, only the spectral emissive power peak for solar radiation (5800 K) is within visible spectral range. The peaks for objects at other temperatures cannot be seen with the naked eye as they are in the infrared spectrum. Therefore, the development of the infrared thermography technique has

been of fundamental importance in the ability to measure the emissive power of objects at various temperatures.

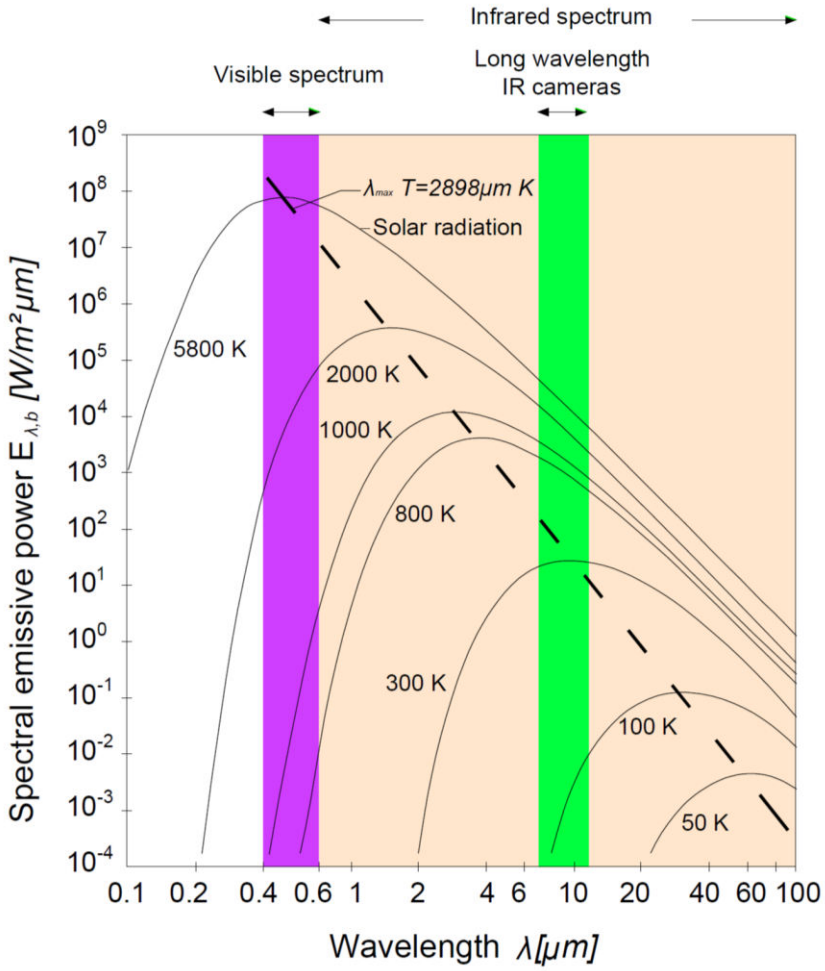

Fig. 2.11. Spectral distribution of energy radiated from blackbody at various temperature (Planck spectral distribution), adapted from [1].

Different types of IR cameras are available depending on the wavelength of interest. These include short wavelength cameras for detection in the spectral range of 0.9-1.7 microns, which is very close to the visible light spectrum, mid-wavelength cameras in the spectral range of 2-5 microns and long wavelength cameras in the range of 7-12 microns. The last type is the most common and the most suitable for building applications where the objects of interest stay in the region of 300 K (marked in green in Fig. 2.11). The way the IR camera works is that it detects the intensity of

infrared radiation emitted by objects of interest. The detected radiation passes through the lens to the detector which, based on the information recorded by a matrix of detectors, converts it into an electronic signal. An IR camera with resolution 240 x 320 has 76 800 detectors, one for each pixel. The signal may be different for each pixel, depending on the intensity of the infrared radiation registered by the camera. The signal is then processed into temperature with an assigned colour that can be seen on the thermogram.

For a thermographic analysis, only the heat power emitted by the object is of interest. A real body emits a fraction of energy emitted by a blackbody. The emissivity ε is a measure of how efficiently the surface emits energy in comparison to a blackbody. To enable the IR camera to correctly measure the power emitted by the object, it is necessary to specify the value of ε of the surface considered. In accordance with ISO 18434-1 [35], the emissivity can be obtained using the reference emissivity material method or the contact method. Using the reference emissivity material method, a material with known emissivity, for instance, black tape is placed on the examined surface. With the camera set with the known tape emissivity, its surface temperature is measured. Since the surface temperature of the uncovered surface beside the tape is the same, its emissivity is adjusted until the camera indicates the same temperature. The contact method requires independent surface temperature measurement of a spot. In the IR camera, the emissivity is adjusted until the same temperature is reached. As illustrated in Fig. 2.12, the power reflected by the object and the power transmitted by the atmosphere is also detected by the IR camera. The reflected power is excluded from the thermogram by determining the reflected temperature T_{ref}. This temperature should be or measured with the IR camera in-situ according to ISO 18434-1 [35]. This procedure involves obtaining the average surface temperature of a piece of aluminum foil with the emissivity set to 1.0 and has been implemented previously by a number of researchers [11,36]. The power transmitted by the atmosphere can be accounted for by specifying the atmospheric temperature T_{atm} and the distance between the object and the camera.

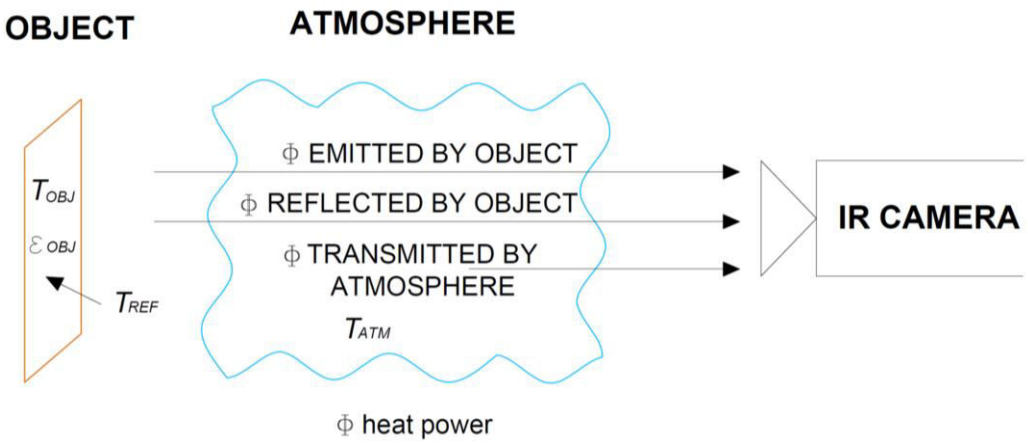

Fig. 2.12. The process of acquiring an IR image.

The ITT has been applied in different disciplines. In applications for building energy conservation, it has been used both as a qualitative and a quantitative tool. The qualitative ITT is well established and is used to visualize excessive heat losses via the building envelope. These can be caused by missing insulation, air leakage, construction failures or thermal bridging. With the qualitative ITT, these problems can be easily located [37]. However, using this approach the amount of heat being lost is not specified. Using the quantitative approach, the surface temperatures on the thermogram are used to quantify the heat loss via the building components captured on the thermogram. This approach has been developed using both, the indoor and the outdoor thermograms and each approach has different advantages and limitations. The main limitation using the indoor ITT is getting clear access to the building component surface of interest as it may be covered by furniture, radiators or other fittings. An indoor thermographic survey may be also disturbing for the inhabitants and difficult to arrange. On the other hand, the indoor thermography is not directly influenced by meteorological conditions, which is the main limitation of the outdoor ITT.

For both indoor and the outdoor thermographic surveys, a minimum difference between the indoor and outdoor air temperatures has to be achieved and maintained. A few recommendations can be found in the literature. According to infrared camera manufacturer FLIR manual [38] and Fokaides and Kalogirou [36], this difference should be not smaller than 10 ºC. Other manufacturers such as Tesco [39] recommend 15 ºC. A similar minimum temperature difference (10 ºC - 15 ºC) is recommended by

Albatici and Tonelli [40]. A study of Lehman et al. [41] investigated how long the external air temperature disturbances influence the wall surface temperatures. This study shows that the disturbance of surface temperatures of all investigated wall surfaces, caused by an air temperature difference not higher than 8°C, cease immediately after the outdoor air temperature becomes stable.

As mentioned earlier, the outdoor ITT is impacted by the weather conditions such as precipitation, irradiation, and wind and this makes it very challenging. Over the past number of years, a number of studies have focused on identifying the most suitable weather conditions on the outdoor ITT. Rain [42] and solar irradiation [16,42] strongly impact on the surface temperature and, therefore, they should be always avoided when using the outdoor ITT. EN ISO 13187 [16] recommends no precipitation at least 12 hours before the thermographic survey.

Lehman et al. [41] simulated the influence of solar irradiation on six different buildings walls: a brick wall before and after retrofitting, cavity wall, concrete wall and timber frame wall. Simulations showed that solar irradiation increases wall surface temperatures at different rates, depending on their thermal mass. These increases in surface temperatures cease within different time periods, for different walls, after sunset. The external insulated wall needed less than 1 hour, the cavity wall 5 hours, while the solid, non-insulated brick wall needed between 5 and 25 hours to dissipate the sun's influence on the exterior surface temperature. The longest period necessary for the sun's influence to disappear was recorded for the concrete wall with internal insulation and lasted between 33 and 45 hours. This study [41] gives clear instructions on the waiting periods required before undertaking an outdoor ITT survey of an element previously exposed to direct sunshine. Albatici et al. [42] recommended early mornings, two hours before sunrise, as the best times for a thermographic survey. At this time, the influence of possible solar irradiation is minimized. Moreover, a fully overcast sky is recommended by Lehman et al. [41] and Albatici et al. [42] for a thermographic survey. This is important in order to achieve a sky temperature similar to the air temperature and thus minimize radiative heat losses from the building element to the sky. Albatici et al. [42] state that the necessary period of overcast weather before undertaking a survey is 12 hours. Lehman et al. [41] remark that light

structure walls cool down more quickly while exposed to low sky temperature than heavy structure walls.

Wind speed significantly influences the exterior surface temperatures of a building element. Many researchers have aimed to define the wind speed limit for the accurate outdoor thermographic surveys. According to Balaras et al. [37], an external survey should be avoided while the wind speed is higher than 5 m/s. Albatici et al. [42] stated that local wind speed near the façade during measurement must be less than 0.5m/s and that the hourly average of free stream wind in the building boundaries within 24 hours must be lower than 5m/s. Pulsating wind up to 2 m/s is suggested by Lehman et al. [41] as having an insignificant effect on the thermography. Surface temperature disturbances caused by wind decay within a few hours. This decay is faster on wall surfaces with external insulation than on other wall surfaces.

Over last numbers of years, different researchers have applied both qualitative and quantitative ITT to the thermal evaluation of building envelopes. They were based on the indoor and/or the outdoor thermographic survey. In general, the quantitative use of the ITT is based on the phenomenon of surface energy balance, which states that the rate at which the energy is transferred to the surface $\dot{E}_{in}$ is equal to the rate at which energy is transferred from the surface $\dot{E}_{out}$ (Equation (2.34)) [1].

$$\dot{E}_{in} - \dot{E}_{out} = 0 \qquad (2.34)$$

For the external surface of a building wall, presented in Fig. 2.13, $\dot{E}_{in}$ is represented by the conductive heat flux $\dot{q}_{cond}$ and $\dot{E}_{out}$ by radiative $\dot{q}_{rad}$ and convective heat flux $\dot{q}_{conv}$ and the surface balance can be written as Equation (2.35).

$$\dot{q}_{cond} - \dot{q}_{rad} - \dot{q}_{conv} = 0 \qquad (2.35)$$

This means the heat loss via a building component can be calculated by summing the radiative and convective heat flow rate and this can be done using the surface temperatures.

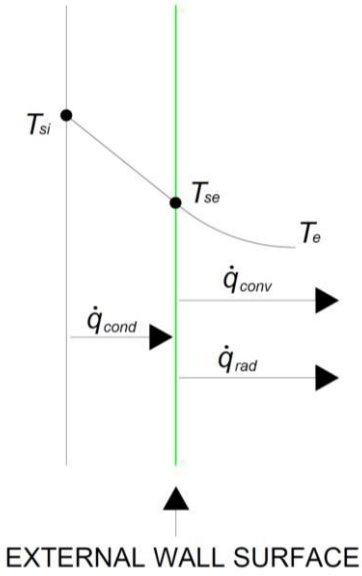

Fig. 2.13. Energy balance applied at an external building wall surface, adapted from [1].

2.3.2.3.2. Evaluation of *U*-value by means of ITT

An example of the quantitative use of ITT is obtaining the thermal transmittance *U*-value from data recorded during the thermographic survey. Albatici and Tonelli [40] used the outdoor ITT measurements to obtain thermal transmittance, using Equation (2.36).

$$U = \frac{5.67\varepsilon\left(\frac{T_{se}}{100}\right)^4 - \left(\frac{T_e}{100}\right)^4 + 3.8054w(T_{se} - T_e)}{T_i - T_e} \qquad (2.36)$$

The methodology was tested on three case studies. A difference of about + 30 % was found out when comparing the *U*-value obtained from the ITT and theoretical calculated values. The ITT result for the first case was validated by HFM, where a difference of -21% was recorded. It should be noted that an error of 13% is associated with HFM measurements. This includes correction for thermal storage effects, calibration of the HFM, in-situ use, the accuracy of the temperature difference and repeatability of the system [15]. Comparing both methods, the advantage of the ITT

method is its speed – only one day is needed to collect data for the whole building. It is a non-destructive method and this is usually important for dwellings. The ITT survey considers all the surface area, not just a point on the surface, which is the case when using HFM. The IR camera reading is strongly influenced by the ambient conditions. Therefore, for further validation of the methodology, Albatici et al. [42] set up an experimental building with five different light-weight and heavy external walls. They acquired data for over 3 years, taking a series of IR images from outside the building, for each of the walls. *U*-values of the same walls were also measured using HFMs and calculated theoretically. The ITT results showed much better agreement with HFM and with theoretically calculated values for heavy walls than for lightweight walls. The *U*-values of light-weight walls using the ITT indicated absolute deviations of around 30 – 40 % compared to other methods. On the other hand, for the heavy walls, the ITT results showed absolute deviations of 8 – 20% when comparing to the *U*-values obtained from HFM, and around 20% when compared to the theoretically calculated *U*-values. The authors suggested that the ITT methodology is more suitable for heavy walls whereas for light-weight and well-insulated walls it needs further development.

Dall'O' et al. [43] also used the outdoor ITT for in-situ thermal transmittance evaluation, according to Equation (2.37).

$$U = \frac{h_{ce}(T_s - T_e)}{(T_i - T_e)} \qquad (2.37)$$

where the external convective coefficient h_{ce} is calculated in accordance to Jürges equation (Equation (2.38)) and w is the wind velocity.

$$h_e = 5.8 + 3.8054w \qquad (2.38)$$

They tested fourteen heavy and light structure walls of existing buildings using the outdoor ITT. They compared *U*-values obtained from the ITT to the theoretically calculated *U*-value and found a deviation of between -40% and +60% for building heavy structure walls situated in a suburban area and exposed to a wind speed of 1

m/s. A much greater deviation, of between -70% and +105%, was found for externally insulated walls where the wind speed was zero. Therefore, the authors concluded that the methodology is not suitable for these types of walls. However, different studies showed better agreement between ITT results and other methods for externally insulated walls. For instance, Albatici et al. [42] obtained absolute deviations of around 30 – 40 %. This shows that the ITT methodology should not be excluded for this type of walls.

Also, Fokaides and Kalogirou [36] measured the *U*-value of building envelope components by means of the indoor ITT and compared them to *U*-values calculated theoretically in accordance to EN ISO 6946 [3]. The surface temperatures measured by the IR camera were validated by comparing with measurements from surface-mounted thermocouples. The authors concluded that thermography is suitable for *U*-value determination. In this study, *U*-value was calculated using Equation (2.39).

$$U = [4\varepsilon\sigma T_W^3 (T_s - T_{ref}) + h_{ci} (T_s - T_i)] / (T_i - T_e) \quad (2.39)$$

where h_{ci} is the indoor convective coefficient and was derived from ISO 6946 [3]. During the experiment, the thermal transmittance of the external envelope components such as walls, glazing, and roofs of five dwellings in Cyprus was evaluated based on the indoor surface temperatures. Steady-state conditions were obtained using cooling/heating systems for at least 3 hours prior to taking measurements. The surface temperatures were measured every 20 min for 3 hours and the *U*-value was an average of 10 measurements for each building element. Surface temperatures of the same elements were also measured with thermocouples. These temperature measurements were recorded every second for 3 hours and, based on this data, the *U*-values were calculated. The deviation in the *U*-values calculated from surface temperatures measured with the ITT and with the thermocouple from the theoretical *U*-values calculated in accordance with the EN ISO 6946 [3] standard varied by 10 – 20%, with greater deviation for roof and glazing. According to the authors, this deviation may have been due to solar exposure.

Nardi et al. [44] compared the methodologies for assessing the *U*-value by means of the outdoor ITT, developed by Albatici and Tonelli [40] and Dall'O' et al. [43] and for indoor ITT developed by Fokaites and Kalogirou [36] and by Madding [45]. The tested component was a concrete, externally insulated wall placed in the hot box with movable chambers. For the experimental setup, only the hot chamber was attached to the specimen, whereas the laboratory acted as the cold chamber. This setup allowed performance of ITT from a distance of 5 m. No wind was induced in the laboratory, so the testing was carried out with negligible wind speed. The results were compared to the theoretically calculated *U*-value and to the *U*-values obtained from HFM. When considering the *U*-values obtained using methodologies for outdoor ITT with the *U*-values obtained from the HFM, percentage differences of +15% for the Albatici and Tonelli [40] method and +26% for the Dall'O' et al. [43] method were found. Larger discrepancies were noticed with the theoretically calculated *U*-value of +27% and +39%, respectively. By using the indoor ITT methodology developed by Fokaites and Kalogirou [36] and by Madding [45] the same *U*-value was obtained. Both were different by -8% from the *U*-value measured by HFM and by +2% from the theoretically calculated U-value. In both methodologies, the convective heat transfer coefficient for natural convection was derived from EN ISO 6946 and this may be a reason for obtaining the same *U*-values. The significantly larger percentage deviations for *U*-values obtained by Albatici and Tonelli [40] and by Dall'O' et al. [43] methods could be a result of inappropriate application of methodologies that were developed for forced convection conditions but tested under natural convection conditions. Better agreement may have found if testing was carried out under forced convection.

Tejedor et al. [46] recently proposed a method for determining the in-situ *U*-value using indoor ITT. Using Equation (2.40) they calculated the radiative surface heat flux $\dot{q}_r$ based on Stefan-Bolzmann's law and the convective surface heat flux $\dot{q}_c$ with indoor convective coefficient h_{ci} evaluated using the Nusselt number.

$$U = \frac{(\dot{q}_r + \dot{q}_c)}{(T_i - T_e)} \qquad (2.40)$$

Using surface temperatures recorded during an indoor thermographic survey, they evaluated the *U*-value of two walls of existing buildings, one non-insulated and the other externally insulated. They used the same surface temperatures to calculate *U*-values of the same walls using standard h_{ci} derived from EN ISO 6949 [3] of 2.5 W/m^{2}K and h_{ci} derived from EN ISO 9869 [47], of 3.0 W/m^{2}K. These measured *U*-values obtained using three different approaches to determining h_{ci} were then compared to the theoretically calculated *U*-values, according to EN ISO 6949 [3], using tabulated material thermal properties from EN ISO 10456 [48]. The highest absolute deviation from the theoretical values, between 14.05 % and 42.87 %, was found for *U*-values calculated using h_{ci} in accordance with EN ISO 9869 [47]. The *U*-values obtained using h_{ci} from EN ISO 6949 [3] deviated between 3.06 % and 30.47 % from the theoretical values. The lowest deviation (0.44 % - 3.97 %) was recorded for the results calculated using h_{ci} evaluated using the Nusselt number. This demonstrates that precise evaluation of h_{ci} instead using standard h_{ci} values significantly improves the results and this approach may be useful for evaluation of both, non-insulated and externally insulated walls. As mentioned previously, for the latter type of wall, high discrepancies were found between *U*-values evaluated using the outdoor ITT and standard h_{ce} from EN ISO 6949 [3] when compared to the theoretical values [42,43].

2.3.2.3.3. Evaluation of thermal bridging by means of ITT

The ITT has been also applied by a limited number of researchers to thermal bridging evaluation. Benkő [49] defined an energy saving factor *ES* as the ratio of the heat losses through a building component with and without a thermal bridge. *ES* is calculated using Equation (2.41), based on the surface temperatures recorded by means of the outdoor ITT.

$$ES = \frac{\dot{Q}_J}{\dot{Q}_{si}} = \frac{h_j A_j (T_j - T_e)}{h_{si} A_{si} (T_{si} - T_e)} = a \frac{(T_{avr} - T_e)}{(T_{min} - T_e)} \qquad (2.41)$$

where

$\dot{Q}_J$ is the heat flow rate for a component with a thermal bridge,

$\dot{Q}_{si}$ is the heat flow rate for a plain component,

a is the area factor, which is the ratio of the area of thermal bridge A_j to the area of a plain component A_{si}.

For the calculations, two surface temperatures were used. The first was the uniform temperature T_{si} measured on the building surface and the second temperature was measured on the thermal bridge T_j, created by a joint between slabs. The convective coefficient h was assumed to be constant in the thermal bridging region and away from thermal bridging impact. T_j is the average temperature caused by the thermal bridge T_{avg} and T_{si} is the minimum temperature T_{min} on the surface not impacted by the thermal bridge. Using this energy saving factor, it is possible to calculate the energy saving if the thermal bridge is eliminated from the structure.

Asdrubali et al. [11] introduced a thermal incidence factor for the thermal bridge, I_{tb}, that indicates the increase of the heat loss due to the thermal bridging and is defined by Equation (2.42). Their approach is more precise than Benkő's as the calculations use the measured temperatures at each pixel.

$$I_{tb} = \frac{\sum_{p=1}^{N}(T_i - T_{pixel\_is})}{N(T_i - T_{1D\_is})} \qquad (2.42)$$

The T_{pixel_is} are the surface temperatures disturbed by thermal bridge whereas T_{1D_is} represents the surface temperature not impacted by the thermal bridge. They validated the methodology with HFM measurements in laboratory conditions on a thermal bridge between window glazing and a window frame. The I_{tb} obtained using the ITT methodology was 7.4 % different to that obtained by HFM and 4.6 % different from numerical simulations. To obtain the *U*-value of a component including thermal bridging impact U_{tb} (Equation (2.43)), they evaluated the *U*-value of the building component not influenced by thermal bridging U_{1D} from HFM measurements. On the other hand, Bianchi et al. [50] who tested this methodology on a full-scale building, calculated U_{1D} theoretically.

$$U_{tb=}U_{1D} * I_{tb} \quad (2.43)$$

As the number of pixels may affect the accuracy of the I_{tb}, Baldinelli et al. [51] and Asdrubali et al. [52] recently proposed a mathematical algorithm for the IR image reconstruction. An appliance of this algorithm resulted in an increase of the original IR image resolution. The I_{tb} and Ψ-values calculated from reconstructed IR image had improved levels of accurate.

2.3.2.3.4. Summary of ITT applications

In this section, the principles of operating the IR camera and an application of the ITT for the thermal assessment of building components have been presented. A significant advantage of this method for assessment of existing structures is the fact that it is non-destructive. A number of researchers have used this technique for *U*-value evaluation using both outdoor [40,42,43] and indoor [36,46] thermography. As presented in this section, Dall'O' et al. [43] and Albatici et al. [42] recorded high deviations between the *U*-values measured by means of the outdoor ITT and theoretically calculated *U*-values for externally insulated walls. On the other hand, for *U*-values of the same type of walls, Tejedor et al. [46] found good agreement between the indoor ITT measurements and theoretical calculations. It can be concluded that the Tejedor approach is a good alternative for externally insulated walls assessment. Another factor which contributed to the accuracy of their method the use of the Nusselt number in the calculation of the convective coefficient.

In terms of thermal bridging heat loss evaluation, an approach combining the ITT and HFM measurements or calculation has been developed. Using the ITT, the increase of heat loss due to the presence of thermal bridging has been measured. This was expressed as a proportion of the heat flow rate through a building component with and without a thermal bridge. To fully quantify the thermal bridging heat loss, the *U*-value of plain building component was measured by HFM or calculated theoretically.

Two factors expressing heat flow rate with and without thermal bridge have been developed. The first one, an energy saving factor *ES* [49], was developed for the outdoor thermography and the other, an incidence factor [11] for the thermal bridge I_{tb}, for the use with indoor ITT. An enhanced approach to determining the I_{tb} factor has been recently proposed based on a mathematical algorithm that increases the IR image resolution, thus making it more precise [51,52]. Using I_{tb}, the *U*-value affected by the thermal bridge and Ψ-value can be calculated. These calculations, however, are based on the *U*-value of the plain component measured by the HFM or calculated theoretically. Using HFM is usually time-consuming and the theoretical calculations maybe not feasible for cases where the building envelope structure is not known.

2.4. Summary and conclusions

Thermal assessment of a building envelope is necessary to define the degree of retrofitting needed to ensure that a high thermal standard of the building envelope is achieved. Over the years, different types of assessments have been developed. An analytical approach is usually undertaken for one-dimensional heat transfer to evaluate *U*-value of a plain building component. For solving more complex problems of multi-dimensional heat transfer involving a presence of thermal bridges, the numerical approach is widely used. However, the necessity of knowing the building structure makes analytical and numerical assessments usually feasible only at the building design stage. For many existing buildings, experimental assessment involving measurements tools is needed. The HFM is a tool approved by ISO 9869 [15] for measuring the thermal resistance *R*, conductivity *k,* and thermal transmittance *U*-value. Because it covers a relatively small area of a building surface, it is suitable for plain building components' assessment. Researchers have used this tool also for thermal bridging assessment, however, it that case, a large number of HFMs is needed. As the use of this tool is well-established and standardized, it is often used as a validation method for ITT measurements. However, the practicality of this approach is limited as it is time-consuming. Another experimental standardized approach, the hot box, has been used for thermal assessments of both plain building components and components containing thermal bridging. With this approach, the assessment

environmental conditions can be controlled making this approach ideal for validation of other approaches under laboratory conditions. Still, it is not an in-situ measurement that has the potential to be used for existing building assessment.

A measurement tool that is portable, non-invasive, quick and relatively easy to use is an IR camera. It has been widely used as a qualitative tool to define surfaces with an excessive heat loss. However, to quantify these heat losses, quantitative use of the IR camera must be employed. This approach is not standardized for building applications. Researchers have applied the quantitative ITT for *U*-value assessment of building components. For this purpose, they have used both indoor and outdoor ITT. Both have their advantages and disadvantages and they can be used interchangeably. It was found that for particular cases, such as an externally insulated wall, indoor ITT worked more accurately than the outdoor ITT. It should be kept in mind that a building envelope consists of plain components and thermal bridging that may significantly increase the overall heat losses. However, the level of knowledge and understanding of the impact of thermal bridges and the calculation methods for accounting for their impact is not satisfactory [8].

Significantly fewer research projects have been undertaken on the application of ITT to the assessment of thermal bridging than to the assessment of plain building components. The increase of heat loss caused by thermal bridging by means of ITT has been examined. This increase was expressed as a proportion of the heat flow rate via a building component with and without a thermal bridge. The first proportion factor was based on a single temperature measured on a thermal bridge and a single temperature measured on a plain component and was developed for outdoor conditions [49]. A more precise factor was introduced for indoor conditions by Asdrubali et al. [11] who took into account the entire temperature distribution affected by thermal bridging. For full quantification of the heat loss associated with thermal bridging, the *U*-value of a plain building component was either measured by HFM or calculated theoretically. Using two combined measurement methods may it inconvenient. HFM assessment is usually time-consuming, and performing theoretical calculations is not feasible for cases where the building envelope structure is unknown. In Asdrubali's [11] approach, it was assumed that the surface heat transfer coefficients along the thermal bridging and the plain component surfaces are equal. This assumption is

contrary to a well-established building physics theory, presented in section 2.2.1. of this chapter, according to which the indoor convective coefficient is correlated with surface temperature, thus its value is different at the surface of thermal bridging than on the plain surface.

In this section, the state-of-the-art research on ITT application for building thermal bridging assessment has been presented. So far, the heat loss associated with thermal bridging is described as a factor expressing a proportion of heat losses via building component with and without thermal bridge. Evaluation of this factor is based on assumption that the surface heat transfer coefficient along the thermal bridging and the plain component surfaces is constant [11,49]. Using a proportion factor evaluated from ITT measurements and *U*-value obtained from HFM measurements [11] or from theoretical calculation [50], Ψ-value is calculated. Based on the most current approaches, this research aims to develop a methodology for assessment of thermal bridging performance in the existing building envelope. The key point of the methodology is the fact that it is based on measurements entirely, so it is suitable for buildings with unknown internal structure. Using only one measurement tool for heat loss evaluation, the ITT, makes the methodology relatively quick. This research investigates how the evaluation of the heat transfer coefficients correlated with surface temperatures impacts on the accuracy of the methodology. As discussed in this chapter, both indoor and outdoor ITT have their limitations. The main limitation for the indoor ITT is linked to building access, and for the outdoor ITT to environmental conditions that influence the IR camera reading. This research, therefore, includes development of the thermal bridging assessment methodology by means of indoor and outdoor ITT. These can be used alternatively, depending which conditions, indoor or outdoor, are more conducive for a thermographic survey. As wind velocity significantly influences the exposed surface temperatures and thus heat losses, this project plans to quantify the impact of the wind velocity on the Ψ-value. As outlined in section 2.2.2. of this chapter, conventionally, the boundary conditions for evaluation of building envelope heat losses at design stage are linked to wind velocity 4 m/s. It is not feasible to carry out the thermographic survey at this particular wind velocity. Therefore, this project includes the development of an adjustment procedure that will enable measurements of Ψ-value taken at any wind velocity to be converted to the

equivalent Ψ-value at the standard wind velocity of 4 m/s. In a real building, thermal bridges are often located close to each other. In this case, they interact with each other thereby influencing the Ψ-values. To avoid overestimation when assessing multiple thermal bridging, this interaction must be accounted for. A practical approach to multiple thermal bridging assessment will be proposed including complex thermal bridging assessment such as occurs with windows installed in a building wall. The outcome of this research will provide a methodology for thermal bridging assessment in the existing building that is convenient, accurate and easy-to-use. As this methodology is based on measurements only, it will be especially useful during thermal assessment of existing buildings.

2.5. References

[1] M.J. Moran, H.N. Shapiro, B.R. Munson, D.P. Dewitt, Introduction to Thermal Systems Engineering: Thermodynamics, Fluid Mechanics and Heat Transfer, Hohn Wiley & Sons, Inc., 2003.

[2] E. Sartori, Convection coefficient equations for forced air flow over flat surfaces, Sol. Energy 80 (9) (2006) 1063–1071.

[3] EN ISO 6946 Building components and building elements - thermal resistance and thermal transmittance - calculation method, 2017.

[4] ISO 14683 Thermal bridges in buildings construction - linear thermal transmittance - simplified methods and default values, 2007.

[5] Building Regulation Conservation of Fuel and Energy Technical, Guidance Document Part L 2011 with Amendment 2017.

[6] Limiting Thermal Bridging and Air Infiltration. Acceptable Construction Details, Environment, Heritage and Local Government, 2011.

[7] EN ISO 10211 Thermal bridges in building construction - Heat flows and surface temperatures - Detailed calculations, 2017.

[8] B. Berggren, M. Wall, Calculation of thermal bridges in (Nordic) building envelopes - Risk of performance failure due to inconsistent use of methodology, Energy Build 65 (2013) 331–339.

[9] E. Troppová, J. Klepárník, J. Tippner, Thermal bridges in a prefabricated wooden house: comparison between evaluation methods, Wood Mater. Sci. Eng. 11 (5) (2016) 305–311.

[10] H. Viot, A. Sempey, M. Pauly, L. Mora, Comparison of different methods for calculating thermal bridges: Application to wood-frame buildings, Build. Environ. 93 (2015) 339–348.

[11] F. Asdrubali, G. Baldinelli, F. Bianchi, A quantitative methodology to evaluate thermal bridges in buildings, Appl. Energy 97 (2012) 365-373.

[12] K. Martin, A. Campos-Celador, C. Escudero, I. Gómez, J. M. Sala, Analysis of a thermal bridge in a guarded hot box testing facility, Energy Build. 50 (2012) 139–149.

[13] F. Ascione, N. Bianco, R. Francesca, D. Masi, F. De Rossi, G. Peter, Simplified state space representation for evaluating thermal bridges in building: Modelling, application and validation of a methodology, Appl. Therm. Eng. 61 (2) (2013) 344–354.

[14] A. Capozzoli, A. Gorrino, V. Corrado, A building thermal bridges sensitivity analysis, Appl. Energy 107 (2013) 229–243.

[15] ISO 9869 Thermal Insulation - Building elements - In-situ measurement of thermal resistance and thermal transmittance, 1994.

[16] EN 13187 Thermal performance of buildings-qualitative detection of thermal irregularities in building envelopes - infrared method, 1999.

[17] Field investigations of the thermal performance of construction elements as built, BRE East Kilbride, 2001.

[18] A. Byrne, G. Byrne, A. Davies, A.J. Robinson, Transient and quasi-steady thermal behaviour of a building envelope due to retrofitted cavity wall and

ceiling insulation, Energy Build. 61 (2013) 356–365.

[19] F. Asdrubali, C. Buratti, F. Cotana, G. Baldinelli, M. Goretti, E. Moretti, C. Baldassarri, E. Belloni, F. Bianchi, A. Rotili, M. Vergoni, D. Palladino, D. Bevilacqua, Evaluation of Green Buildings' Overall Performance through in Situ Monitoring and Simulations, Energies 6 (2013) 6525–6547.

[20] L. Evangelisti, C. Guattari, P. Gori, R. De Lieto Vollaro, In situ thermal transmittance measurements for investigating differences between wall models and actual building performance, Sustainability 7 (8) (2015) 10388–10398.

[21] F. Ascione, N. Bianco, R.F. De Masi, G.M. Mauro, M. Musto, and G.P. Vanoli, Experimental validation of a numerical code by thin film heat flux sensors for the resolution of thermal bridges in dynamic conditions, Appl. Energy 124 (2014) 213–222.

[22] L. Zalewski, S. Lassue, D. Rousse, K. Boukhalfa, Experimental and numerical characterization of thermal bridges in prefabricated building walls, Energy Convers. Manag. 51 (12) (2010) 2869–2877.

[23] EN ISO 8990 Thermal insulation - Determination of steady-state thermal transmission properties - Calibrated and guarded hot box, 1997.

[24] D.P. Aviram, A.N. Fried, J.J. Roberts, Thermal properties of a variable cavity wall, Build. Environ. 36 (2001) 1057–1072.

[25] T. Nussbaumer, K.G. Wakili, C. Tanner, Experimental and numerical investigation of the thermal performance of a protected vacuum-insulation system applied to a concrete wall, Appl. Energy 83 (8) (2006) 841–855.

[26] EN ISO 12567-1 Thermal performance of windows and doors - Determination of thermal transmittance by the hot-box method - Part 1: Complete windows and doors, 2010.

[27] EN 12412-2 Thermal performance of windows, doors and shutters - determination of thermal transmittance by hot box method - Part 2: Frames, 2003.

[28] A.A. Lechowska, J.A. Schnotale, G. Baldinelli, Window frame thermal transmittance improvements without frame geometry variations: An experimentally validated CFD analysis, Energy Build. 145 (2017) 188–199.

[29] F. Asdrubali, G. Baldinelli, Thermal transmittance measurements with the hot box method: Calibration, experimental procedures, and uncertainty analyses of three different approaches, Energy Build. 43 (7) (2011) 1618–1626.

[30] ASTM C1363-05 Standard Test Method for Thermal performance of Building Materials and Envelope Assemblies by Means of a Hot Box Apparatus, 2005.

[31] GOST 26602.1-99, Windows and doors. Methods of determination of resistance of thermal transmission, 1999.

[32] G. Baldinelli, A methodology for experimental evaluations of low-e barriers thermal properties: Field tests and comparison with theoretical models, Build. Environ. 45 (4) 1016–1024, 2010.

[33] Tigran Khanzadyan, Looking at the Universe through Infrared Spectacles. [Online]. Available: https://www.slideshare.net/TigranKhanzadyan/gac-talk090131. accessed 1.10.2017.

[34] R. P. Madding, Science Behind Thermography, In Proceedings of Conference Thermosense V, Detroit, USA, 1983, pp. 2–9.

[35] ISO 18434-1 Condition monitoring and diagnostics of machines. Thermography Part 1: General procedure, 2008.

[36] P.A. Fokaides, S.A. Kalogirou, Application of infrared thermography for the determination of the overall heat transfer coefficient (*U*-Value) in building envelopes, Appl. Energy 88 (12) (2011) 4358–4365.

[37] C.A. Balaras, A.A. Argiriou, Infrared thermography for building diagnostics, Energy Build. 34 (2) 171–183, 2002.

[38] Flir User's manual for IR cameras FLIR Bxxx series FLIR Txxx series, 2011.

[39] Tesco, Kieszonkowy przewodnik Termografia, 2009.

[40] R. Albatici, A.M. Tonelli, Infrared thermovision technique for the assessment of thermal transmittance value of opaque building elements on site, Energy Build. 42 (11) (2010) 2177–2183.

[41] B. Lehmann, K. Ghazi Wakili, T. Frank, B. Vera Collado, C. Tanner, Effects of individual climatic parameters on the infrared thermography of buildings, Appl. Energy 110 (2013) 29–43.

[42] R. Albatici, A.M. Tonelli, M. Chiogna, A comprehensive experimental approach for the validation of quantitative infrared thermography in the evaluation of building thermal transmittance, Appl. Energy 141 (2015) 218–228, 2015.

[43] G. Dall'O', L. Sarto, A. Panza, Infrared screening of Residential Buildings for Energy Audit Purposes : Results of a Field Test, Energies 6 (2013) 3859–3878.

[44] I. Nardi, D. Paoletti, D. Ambrosini, T. De Rubeis, S. Sfarra, U-value assessment by infrared thermography: A comparison of different calculation methods in a Guarded Hot Box, Energy Build. 122 (2016) 211–221.

[45] R. Madding, Finding R-Values of Stud Frame Constructed Houses with IR Thermography, in Proceedings of Conference InfraMation, Reno, USA, 2008.

[46] B. Tejedor, M. Casals, M. Gangolells, X. Roca, Quantitative internal infrared thermography for determining in-situ thermal behaviour of façades, Energy Build. 151 (2017) 187–197.

[47] ISO 9869 Thermal insulation - Building elements - In-situ measurement of thermal resistance and thermal transmittance, 1994.

[48] EN ISO 10456 Building materials and products - Hygrothermal properties - Tabulated design values and procedures for determining declared and design thermal values, 2012.

[49] I. Benkő, Quantitative analysis of thermal bridges of structures through infrared thermograms, In Proceedings of International Conference on Quantitative Infrared Thermography Qirt, Dubrovnik, Croatia, 2002, pp. 203–208.

[50] F. Bianchi, A. Pisello, G. Baldinelli, F. Asdrubali, Infrared Thermography Assessment of Thermal Bridges in Building Envelope: Experimental Validation in a Test Room Setup, Sustainability 6 (10) (2014) 7107–7120, 2014.

[51] G. Baldinelli, F. Bianchi, A. Rotili, D. Costarelli, M. Seracini, G. Vinti, F. Asdrubali, L. Evangelisti, A model for the improvement of thermal bridges quantitative assessment by infrared thermography, Appl. Energy 211 (2018) 854–864.

[52] F. Asdrubali, G. Baldinelli, F. Bianchi, D. Costarelli, A. Rotili, M. Seracini, G. Vinti, Detection of thermal bridges from thermographic images by means of image processing approximation algorithms, Appl. Math. Comput. 317 (2018) 160–171.

Chapter 3

Infrared thermography technique as an in-situ method of assessing heat loss through thermal bridging

3.1. Paper overview

This chapter describes a new approach to thermal bridging evaluation by means of the ITT. In the proposed methodology, the surface energy balance principle is applied to the internal face of a building component containing a thermal bridge. Consistent with this principle, the amount of energy transferred to the surface is identical to the amount of energy leaving the surface. The energy leaving the surface can be calculated from the surface temperatures, measured with an infrared (IR) camera. With modern IR high-resolution cameras, detailed information on the surface temperature distribution is available from which the thermal bridging heat flow rate q_{TB} and Ψ-value can be evaluated. According to the methodology proposed here, this evaluation is based on the temperatures from a line of pixels across the thermal bridge derived from the thermogram. Precise calculation of the surface heat transfer coefficients for the full range of surface temperatures on the IR line is carried out. Testing of the methodology is undertaken in a controlled laboratory environment using a hot box device under steady state environmental conditions. The test results showed that this approach to surface coefficient calculation increased the accuracy of the methodology in comparison to evaluation using a constant coefficient related to a plain part of a

building component. In the proposed method, the heat loss evaluation requires only one measurement tool, an IR camera, that making the methodology relatively straightforward to implement on site.

The content of this chapter has been published in Energy and Building journal: *M. O'Grady, A.A. Lechowska, A.M. Harte, Infrared thermography technique as an in-situ method of assessing heat loss through thermal bridging, Energy and Buildings, 2017,135:20-32.* In this joint publication, Małgorzata O'Grady, supervised by Dr. Annette Harte, designed the experiment, performed the testing, analysed the test results and developed the methodology for indoor ITT assessment. Dr. Agnieszka Lechowska facilitated the testing.

3.2. Abstract

A key aspect in assessing the thermal standard of building envelopes is the quantification of the heat loss through thermal bridging, which can be expressed in terms of the linear thermal transmittance Ψ. Values of Ψ may be obtained from tabulated values for standard building details, from numerical modelling or from measurement. Where the internal structure of the building envelope is unknown, which is very often the case, measurement is the only option. This study shows how the infrared thermography technique (ITT) can be used as a non-invasive and easy-to-use method to provide quantitative measures of the actual thermal bridging performance. The novelty of this approach includes evaluation of the actual heat flow rate caused by thermal bridge q_{TB} and Ψ-value by means of the ITT solely, without any supporting methods. Another important aspect of the methodology is that it accounts for the correlation between the surface temperature and the convective and radiative heat transfer coefficients. Values for these coefficients are assessed for the whole range of the surface temperatures recorded on the thermogram resulting in improve accuracy. The q_{TB} and Ψ-value calculated using the presented methodology fully mirrors the real thermal performance of the thermal bridge. The methodology has been tested under laboratory conditions in a steady state in a hot box with excellent agreement.

3.3. Introduction

Today the importance of saving energy and limiting the greenhouse effect cannot be underestimated. Responding to the increasing cost of energy and growing environmental concerns, the Commission of the European Communities, in their Energy Efficiency Action Plan [1], set a target for 2020 of saving 20% of primary energy consumption compared to projections. Ireland's response was the Government Sustainable Energy White Paper 'Delivering a Sustainable Energy Future for Ireland' [2] with an indicative target of 30% reduction in energy demand by 2020. In 2014, The European Commission set higher targets for energy use reduction by setting energy saving goals of 25 – 40% for 2030 [3].

To meet this target, two parallel actions should take place: developing and using renewable energy, and significant limiting of energy consumption in all sectors. Special focus should be given to limiting energy used by buildings, as this accounts for 40% of the total energy used in the European Union [4]. There are a number of aspects that can make a building energy efficient, such as the shape of the building, positioning of the building at an orientation that maximises passive solar heating, and the installation of highly efficient heating and a domestic hot water system fully or partly contributed to by energy from renewable sources. All these factors have to be addressed while constructing or retrofitting a building, but the starting point to achieve an energy efficient building should be the limiting of heat loss via the external envelope of the building. That includes its plain components such as wall or roof and the thermal bridging that appears where the geometry or thermal conductivity of the building envelope components changes.

The heat loss through a plain building component can be expressed by the thermal transmittance or *U*-value. The *U*-value [W/m^2K] is defined as the rate at which thermal energy is transmitted through a unit area per unit temperature difference between the environments on either sides. The *U*-value can be calculated theoretically using the European Standard EN ISO 6946 [5] or based on measurements. Simultaneously to the heat loss via the plain parts of the building envelope, heat loss via thermal bridging takes place also. It is crucial to limit thermal bridging as much as possible to avoid additional heat loss, local condensation problems and mould growth.

The value describing the heat loss associated with thermal bridging is the linear thermal transmittance or Ψ-value [W/mK], which according to the European Standard ISO 14683 [6] is the heat flow rate per unit length in the steady state divided by the temperature difference between the environments on either sides of the thermal bridge. Standard EN ISO 10211 [7] explains how to numerically model a building element containing a thermal bridge for calculation of the total heat flow. The principle is that the environmental conditions and the construction details are known; however, that condition cannot be met in many existing structures.

3.3.1. Methods of assessing the *U*-value

To date, the only method that is approved by standard ISO 9869 [8] as a method to be used on site for measuring the heat flow through the plain element of a building envelope, and thus the *U*-value, is the heat flow meter (HFM) method. This method was used during a study carried out by the Scottish Building Research Establishment (BRE) [9], which showed that the predicted *U*-value based on ISO 6946 [5] is typically underestimated by 20%. Asdrubali et al. [10], [11] used the HFM for part of the evaluation of green buildings overall performance. The *U*-values of six walls were measured and the difference in the *U*-value determined using the HFM measurements varied between -14% and +43% of the theoretically calculated values. Also, Evangelisti at al. [12] compared the *U*-value obtained from the HFM and calculated theoretically in accordance to ISO 6946 [5] with percentage difference between -50% and +153%. Byrne et al. [13] found that the theoretically calculated thermal resistances (which is a reciprocal of *U*-value) of walls were overestimated by 60% and of ceilings by 75% while compared to HFM results. Desogus et al. [14] compared the thermal resistance obtained using the HFM with a destructive method where, using a drill, a sample of an external building wall was acquired, the thickness of its layers were measured and, using the conductivities from manufacturers or standards [15][16], the thermal resistance was calculated. Authors stated that because the differences between the results were very small, they can be defined as compatible and both could be used for in-situ thermal resistance evaluation.

Another method, approved by the standard EN ISO 8990 [17], that allows testing of the thermal properties of external building elements, but in laboratory conditions, is the hot box method. The hot box device consists of two climatic chambers where atmospheric conditions can be controlled and the tested element is placed between them. This device has been widely used to test the thermal properties of building materials, for example by Nussbaumer at al. [18], who determined the thermal performance of vacuum-insulation panels (VIPs) applied to concrete building walls. Numerical analysis showed good agreement with the experimental values. Aviram et al. [19] used the hot box to observe the convective flow in cavity walls with different cavity widths and noted that the thermal resistance of the air in the cavity increases with the reduction of the cavity depth. Also in the hot box device, the thermal transmittance of multi-layer glazing with ultrathin internal glass partitions was measured by Lechowska et al. [20] with very good agreement with results from CFD simulations.

Researchers in some of the above mentioned studies [10-13] used the Infrared Thermography Technique (ITT) as a qualitative tool to define the correct locations for HFM sensors as it is important to attach the HFM sensors in a place without any defects or inhomogeneities that may lead to incorrect results. The ITT was also used in [18], where the infrared image was taken within 1 minute of opening the hot box to minimise wall surface temperature changes. The IR image showed higher temperature where the VIPs were damaged, on the junction between the specimen and surrounding panel, and on joints between panels.

Besides its well-established use to provide qualitative data, summarized in EN 13187 [21], the ITT has potential as a quantitative in-situ tool for measuring the heat loss through the building external envelope. By means of the ITT, Albatici and Tonelli [22] evaluated the *U*-value and found a difference of about + 30 % compared to the theoretical values. To comprehensively validate the methodology, Albatici and Tonelli carried out thermographic surveys in an experimental building consisting of five different light-weight and heavy external walls for over 3 years [23]. The *U*-values calculated for heavy walls using the ITT showed absolute deviations of 8 – 20% in comparison to the *U*-values obtained from HFM, and around 20% in comparison to the theoretically calculated *U*-values. The *U*-values of light-weight walls using the

ITT had absolute deviations of around 30 – 40 % compared to other methods. The authors concluded that measurement of light-weight and well-insulated walls needed further development. Because IR camera readings are influenced by many factors, Nardi et al. [24] tested the methodology developed by Albatici and Tonelli [22,23] in a controlled environment provided by the hot box apparatus. The *U*-value of a large specimen representing a plain concrete wall insulated with EPS was calculated theoretically, obtained from the measured mean heat flux by the HFM, and finally obtained with the ITT. The difference between results from the ITT varied between 3.2% and 12.9% compared to results from HFM and between 3.4 – 7.1% compared to the theoretical values. The authors deemed these differences as acceptable for an in-situ method. The same authors in a further study [25] obtained the *U*-value of walls of three different existing buildings under real environmental conditions. Good agreement between the *U*-value obtained by HFM and the ITT was found for walls of a historical stone building (2.6%) and of a concrete structure (1.3%), whereas, for a light-weight wall made of cement-wood brick and insulated internally, a discrepancy of 47.6% was recorded. This variance may be caused by external wall surface temperature fluctuations during the HFM measurements. Comparing the theoretical *U*-values and those obtained from the ITT, the difference was 9.5% for the stone building, 4.4% for the light-weight wall and 46.2% for the concrete structure. The authors considered the theoretical *U*-value in the last case as not reliable as the structure of this wall was complex, which may explain the large discrepancy. Fokaites and Kalogirou [26] also used the ITT to estimate the *U*-value of masonry walls, roofs and glazing of five dwellings with results of 10-20% higher than the theoretical prediction. Tanner et al. [27] proposed a standardization of the methodology in order to obtain a *U*-value by means of the ITT. Performing the ITT under favourable environmental conditions, the uncertainty of the surface temperature and the *U*-value were defined as 0.5K and 0.21 W/m²K, respectively. This means that the measurements for walls with a high *U*-value of 1.2 W/m^{2}K would have a 17% uncertainty whereas for walls with a *U*-value of 0.29 W/m^{2}K the uncertainty is 70%.

3.3.2. Methods of assessing the thermal bridge heat loss

Researchers have used different approaches to evaluate the heat loss caused by thermal bridging. Zalewski [28] focused on characterization of thermal bridges in prefabricated building walls. The ITT was used from the cold side of the wall to satisfactorily locate the thermal bridges. To quantify the heat loss caused by thermal bridging, three HFMs were installed, one on the thermal bridge and two on the plain part of the wall. Then the measured heat flux on the plain part of the wall was compared to that on the thermal bridge for three cases. Results show that thermal bridging increases the *U*-value by 13.5 – 26.2 %. The experiment validated the numerical predictions made using thermal analysis software. Similarly, ITT was used by Ascione et al. [29,30] as a supporting technique to visualize the location of the thermal bridge in order to optimally position a set of heat flow meters and thin flux sensors around it. The heat flux measurements were used as a reference to verify the reliability of a proposed simplified numerical code to effectively and quickly assess the heat loss through thermal bridges. The difference between the measured and predicted heat losses varied between -12% and +6%. Heinrich and Dahlem [31] compared the surface temperature distribution along a thermal bridge (I-beam in lightweight construction wall) collected using an IR image to that obtained using the finite element method. They found that the zone of influence of the thermal bridge was smaller in the numerical model than that measured using the ITT. Wróbel and Kisielewicz [32] developed a numerical model of a thermal bridge and calibrated the model using the ITT measurements. The calibrated model was then used to determinate the lowest surface temperature caused by the thermal bridge for a range of temperature conditions. Taylor et al. [33] used the ITT to assess the severity of thermal bridging at the construction stage. One of the earliest researchers to base the assessment of heat loss through thermal bridging on the information gathered on the IR image of a building façade was Benkő [34]. Using the outdoor thermography of a building slab, the surface uniform temperature T_{si} on the part of the building envelope that was not disturbed by thermal bridge (joint) and the surface temperature on the thermal bridge T_j were recorded. Using those two temperatures, Benkő introduced an energy saving factor *ES* as the ratio of the heat losses through a building component with and without a thermal bridge:

$$ES = \frac{\dot{Q}_J}{\dot{Q}_{si}} = \frac{h_j A_j (T_j - T_{env})}{h_{si} A_{si} (T_{si} - T_{env})} \quad (3.1)$$

where the numerator relates to the "real" heat flow rate influenced by thermal bridge and the denominator to the "perfect" part of the slab not influenced by thermal bridge. Assuming the heat transfer coefficients *h* are the same at the thermal bridge and away from thermal bridge, defining T_j as the average temperature T_{avg} caused by a thermal bridge and T_{si} as the minimum temperature T_{min} on the surface not influenced by thermal bridge and introducing the area factor $a=A_j/A_{si,}$ where A_j is the area of thermal bridge and A_{si} is the area of the slab excluding the thermal bridge, the energy saving factor was then expressed as in Equation (3.2).

$$ES = a \frac{(T_{avg} - T_{env})}{(T_{min} - T_{env})} \quad (3.2)$$

The greater the influence of the thermal bridge the higher the value of *ES.* This factor indicates the potential of energy saving that can be achieved if the thermal bridge is eliminated, however, it does not show the actual heat loss caused by the thermal bridge.

Likewise, Asdrubali et al. [35] expressed the heat loss associated with thermal bridging as a ratio that reflects the increase of heat loss in the presence of a thermal bridge by means of the ITT. The methodology for evaluating this ratio, the incidence factor I_{tb}, was validated on a thermal bridge between window glazing and the window frame. The window was placed between an environmentally controlled space and the laboratory. The I_{tb} was expressed by Equation (3.3):

$$I_{tb} = \frac{Q_{tb}}{Q_{1D}} = \frac{h_{tb\_i} A_{pixel} \sum_{p=1}^{N} (T_i - T_{pixel\_is})}{h_{1D_i} A_{1D} (T_i - T_{1D\_is})} \quad (3.3)$$

where numerator relates to heat flow rate influenced by thermal bridge and denominator to part of the component not influenced by thermal bridge. This formulation is more precise than the Benkő approach as the calculations account for the temperature in each pixel. Like Benkő [34], Asdrubali et al. [35] considered the laminar coefficient *h* the same in the entire captured area so the expression for I_{tb} is simplified to:

$$I_{tb} = \frac{\sum_{p=1}^{N}(T_i - T_{pixel\_is})}{N(T_i - T_{1D\_is})} \quad (3.4)$$

where *N* is the number of pixels.

The I_{tb} obtained from the ITT under laboratory conditions for a thermal bridge between a window frame and glazing was 7.4% different from that obtained from the HFM and 4.6% different from the value calculated from numerical analysis. The I_{tb} obtained by means of the ITT can be multiplied by the *U*-value of building component not influenced by thermal bridge U_{1D}, to obtain the *U*-value of a component including thermal bridging U_{tb} (Equation 3.5):

$$U_{tb} = U_{1D} * I_{tb} \quad (3.5)$$

While applying the methodology to in-situ thermal bridges, U_{1D} was evaluated by means of HFM.

Bianchi et al. [36] validated this methodology in a full-scale building, exposed to real environmental conditions that were monitored and recorded. The internal structure of the building envelope was known which allowed U_{1D} calculation for all plain elements instead of using the HFM. Determination of U_{1D} was possible because the internal structure of the building envelope was known.

The following expression for calculating Ψ –value from I_{tb} calculation was presented:

$$\Psi = (I_{tb} - 1)\, U_{1D}(l_{tb} - l_{1D}) \qquad (3.6)$$

where l_{tb} and l_{1D} apply to the length of the thermal bridge and the length of the plain component, respectively.

3.3.3. Summary

As presented above, researchers have successfully quantified the heat loss through plain building envelope elements by means of the ITT. The assessment of the heat loss via thermal bridging has been implemented using a combination of the ITT and HFM measurements or calculation. Using the ITT, the increase in the heat flow rate caused by thermal bridge has been expressed as a proportion of the heat flow rate with and without the thermal bridge. To fully quantify the heat loss caused by thermal bridges, the *U*-value of the plain element was provided either by the HFM or calculations. In many existing building envelopes, the thickness and conductivity of individual layers are not known and therefore the calculation method cannot be used. The other alternative, the HFM is time-consuming and requires significant expertise to operate.

This paper presents a methodology for quantifying the heat flow rate through a thermal bridge and the linear thermal transmittance by means of the ITT solely. This means that the current methodology is not supported by other measurements methods or tabulated values. Another important feature of the current methodology, not implemented in previous studies, includes accounting for the variation in the convective and radiative heat transfer coefficients where surface temperatures are disturbed by the thermal bridge. These coefficients are precisely calculated based on the thermogram pixel surface temperatures, together with in-situ measurement of the emissivity and air properties. The validity of the presented methodology is assessed by undertaking comparative measurements on elements containing thermal bridges in a controlled environment in a calibrated hot-box.

3.4. Methodology for quantifying the heat flow rate through a thermal bridge q_{TB} and the Ψ-value by means of ITT

A thermal bridge is a part of a building envelope with different thermal conductivity, thickness of fabric or geometry. In a building envelope, two types of thermal bridging take place. The first type is a point thermal bridge, which appears for example in building corners, where three building elements meet. The second type is a linear thermal bridge characterized by a uniform cross-section along one of the three orthogonal axes [6]. A common linear thermal bridge occurs when a structural element such as a post or a beam is located in the building envelope. In this study, this type of thermal bridge is investigated. As previously mentioned, the heat loss associated with thermal bridging may be expressed as the linear thermal transmittance or Ψ-value. EN ISO 14683 [6] gives possible methods for the determination of the Ψ-value such as numerical calculations (typical accuracy ± 5%), thermal bridges catalogues (typical accuracy ± 20%), manual calculations (typical accuracy ± 20%) and default values given in the standard (typical accuracy 0% - 50%).

As mentioned above, there is no standardised method for determining the linear thermal transmittance based on measurements from the external envelope of an existing building. This paper presents a methodology to determine the actual heat flow rate caused by the thermal bridge in a building. This thermal bridge heat flow rate, q_{TB}, is the additional heat loss through the component as a result of the presence of the thermal bridge. As illustrated in Fig. 3.1, q_{TB} describes how much heat has been lost through the actual thermal bridge itself and through the adjacent plain part of the component that is influenced by thermal bridge. In other words, q_{TB} is the difference between the total heat flow rate q_{tot} and the uniform heat flow rate q_u that would take place if thermal bridge is replaced with a uniform component. This value of q_{TB}, can be used to calculate the Ψ-value, which is the value of q_{TB} per unit temperature difference between the internal and external environments.

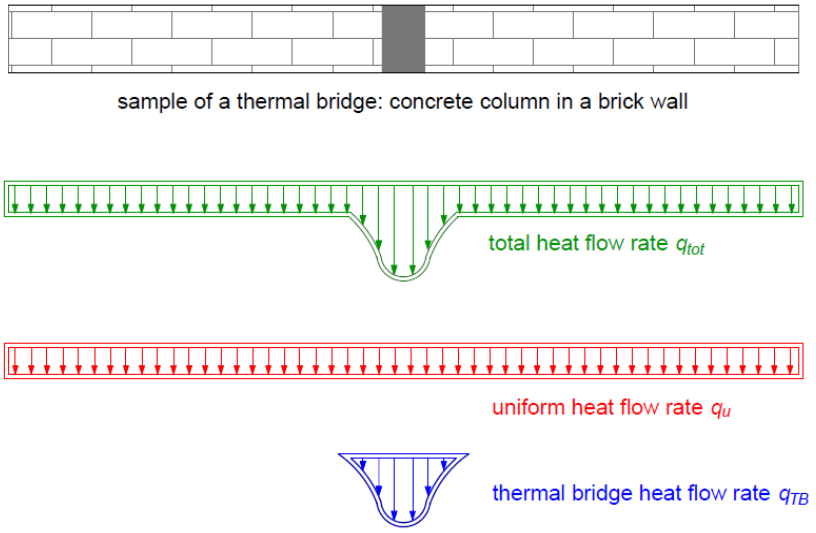

Fig.3.1. Heat flow rate through a sample wall with thermal bridge.

On homogeneous building external elements, the surface temperatures are practically uniform. The thermal bridge disturbs this uniformity by reducing the surface temperatures on the indoor surface and increasing the surface temperatures on the outdoor surface. Those temperature changes can be easily located and recorded on an infrared (IR) image. According to the surface energy balance, the rate at which energy is transferred to the surface is equal to the rate at which it is transferred from the surface in steady state conditions. This means that the conductive heat transfer rate is equal to the sum of the convective and radiative heat transfer rates. The convective and radiative heat transfer rates can be calculated from the surface temperatures. As mentioned in the introduction, researchers have applied the surface energy balance principle to calculate the *U*-value of homogeneous building elements by means of the ITT. The current methodology adapts this principle to quantify q_{TB} and the Ψ-value. The current methodology allows full quantification of the heat loss associated with thermal bridging presence by means of the ITT only. Accurate quantification of q_{TB} and the Ψ-value must account for the variation in the surface temperatures due to presence of the thermal bridge. As the IR image provides the surface temperatures for each pixel, the heat flow rate for each individual pixel may be determined. Because the convective and radiative heat transfer coefficients correlate with the surface temperature distribution, they can be evaluated for each pixel with its unique

temperature. Summation of the heat flow rate in each pixel, based on precisely evaluated heat transfer coefficients, leads to the total heat flow rate through the building element. Further calculations result in q_{TB} and the Ψ-value that fully reflect the impact of the thermal bridge. The procedure starts by taking an IR image of the indoor surface of a building envelope component containing a linear thermal bridge similar to that shown in Fig. 2. The methodology described here was developed for an indoor environment with natural convection but can be adapted for the outdoor ITT. The surface temperatures on the external face of the building envelope are strongly influenced by meteorological conditions such as sun radiation, wind velocity and precipitation. All those climatic parameters together with their impact on the ITT are described by Lehman at al. [37] where the ideal weather conditions for performing ITT are defined. All those findings should be taken into account while adapting the methodology for the outdoor ITT as they significantly affect the radiative and the convective coefficients. Taking the images on the indoor surface can be expected to give a higher degree of accuracy as the environment is controlled to a greater extent. However, indoor thermography also has limitations, such as access to the inhabited dwelling or furniture located on the external walls. Taking the above into consideration, the methodology is validated under indoor conditions with further plans of adapting it to the outdoor conditions. The procedure presented in this paper is applied to the case of a vertical thermal bridge; however, the methodology may be applied, with some adjustments, to a linear thermal bridge in any position. The IR image of a vertical thermal bridge (Fig. 3.2) shows that the surface temperatures vary only in the horizontal direction from the region where they are disrupted by the thermal bridge to the region where the thermal bridge has no influence and the surface temperature becomes uniform.

During the IR image post processing, three rows of pixels from the mid-height of the IR image are selected. From these rows, a horizontal line (IR line) is created. Each pixel on this line represents the mean surface temperature of the centreline pixel and its eight neighbouring pixels. The averaging of pixel temperatures enables smoothing of the transition of surface temperatures from one pixel on the IR line to the next one. Then the pixel length l_x is defined, which depends on the IR camera resolution and the distance between the object and the camera. From the surface

energy balance, the heat flow rate for each pixel (q_x) on the IR line is found by quantifying the convective and radiative heat transfer rates on the indoor face of the building envelope component using Equation (3.7)

$$q_x = l_x[h_{cx}(T_i - T_{sx}) + h_{rx}(T_{sur} - T_{sx})] \quad (3.7)$$

where q_x is the heat flow rate for pixel x per unit height.

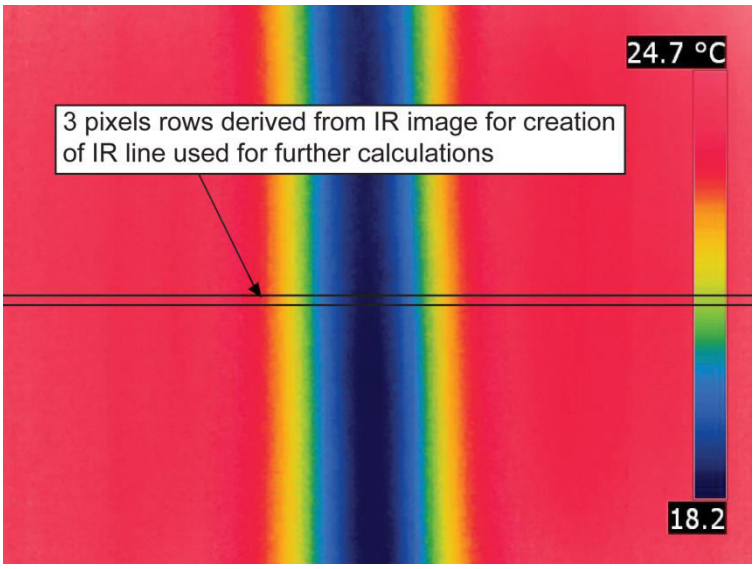

Fig. 3.2. Sample IR image of component with linear thermal bridge.

The indoor air temperature T_i in buildings is, in many cases, very similar to the surrounding temperature T_{sur}, especially when the measured external wall component is surrounded by internal walls, well insulated floor or intermediate floor and well insulated ceiling or an intermediate ceiling. In that case, q_x can be expressed as

$$q_x = l_x[(h_{cx}+h_{rx})(T_i - T_{sx})] \quad (3.8)$$

However, in some cases the surrounding temperature T_{sur} can significantly vary from the air temperature T_i, for example when the ceiling or floor or one of the walls that surround the measured external wall component is a part of an external

building envelope especially when is poorly insulated or glazed. In that case, q_x should be calculated using Equation (3.7), where T_{sur} is the area weighted average surrounding temperature. If in doubt, the surface temperature of all surrounding components can be measured and its weighted average compared to the air temperature.

Because of the heterogeneous nature of the temperature distribution of a building component containing a thermal bridge, the methodology addresses precise calculation of the convective heat transfer coefficient h_{cx} by calculating it from the Nusselt number Nu_x (Equation 3.9) for each pixel on the IR line.

$$h_{cx} = \frac{Nu_x\, k_x}{l_{ch}} \tag{3.9}$$

where l_{ch} is the characteristic length in vertical direction over which h_{cx} applied.

For the case of the internal side of a building wall component, the Nusselt number can be found from the Churchill-Chu correlation for a vertical plate, with a uniform surface temperature, under natural convection as in Equation (3.10). It is assumed that this correlation is applicable in this methodology where the Nusselt number is evaluated for each pixel characterized by a uniform surface temperature.

$$Nu_x = \left\{ 0.825 + \frac{0.387 Ra_x{}^{1/6}}{\left[1+\left(\frac{0.492}{Pr_x}\right)^{9/16}\right]^{8/27}} \right\}^2 \tag{3.10}$$

The Prandtl number represents the ratio of kinematic viscosity to thermal diffusivity. The Rayleigh number is defined as ratio of buoyancy to viscous forces and is calculated for each pixel using Equation (3.11):

$$Ra_x = \frac{g\beta_x(T_i - T_{sx})l_{ch}^3}{\nu_x\, \alpha_x} \tag{3.11}$$

All air properties used in Equations 3.9 - 3.11 are evaluated at a film temperature which is the arithmetic mean of the surface temperature of the pixel and the air temperature.

Also the radiative heat transfer coefficient h_{rx} is calculated for each pixel on the IR line using Equation (3.12)

$$h_{rx} = \varepsilon\sigma(T_{sx} + T_i)(T_{sx}^2 + T_i^2) \quad (3.12)$$

When the surrounding temperature T_{sur} varies significantly from the air temperature T_i, and q_x is calculated using Equation 3.7, h_{rx} should be obtained using Equation 3.13, where the surrounding temperature has been taken into account.

$$h_{rx} = \varepsilon\sigma(T_{sx} + T_{sur})(T_{sx}^2 + T_{sur}^2) \quad (3.13)$$

The emissivity of the surface is measured using the IR camera as described in Section 3.6.

The IR image shown in Fig. 2 was taken with a FLIR T335 IR camera with a resolution 320 x 240. From that IR image, three rows of pixels from mid-height of the IR image are selected. From these rows, an IR line is built which coincides with the central row of pixels. For each pixel on the IR line, q_x is calculated using Equation (3.7) and is plotted in Fig. 3 as the green line. The total heat flow rate of the whole length of the component captured on the IR image per unit height can be obtained from Equation (3.14):

$$q_{tot} = \sum q_x \quad (3.14)$$

Using the heat flow rate calculated for pixels with no thermal bridge influence q_{xu}, the heat flow rate through an identical building component with no thermal bridge can be predicted. This uniform heat flow rate q_{xu} is shown in Fig. 3.3 as a red line.

The thermal bridge heat flow rate for each pixel q_{xTB} is the difference between the heat flow rate q_x and the $q_{xu.}$which is presented in Fig. 3.3 as a blue line.

$$q_{xTB} = q_x - q_{xu} \tag{3.15}$$

By summing up the q_{xTB} , the thermal bridge heat flow rate q_{TB} can be found:

$$q_{TB} = \sum q_{xTB} \tag{3.16}$$

As q_{TB} is the heat flow rate per meter height of the thermal bridge, it can be used directly to determine the linear thermal transmittance Ψ-value using Equation (3.17).

$$\Psi = \frac{q_{TB}}{(T_i - T_e)} \tag{3.17}$$

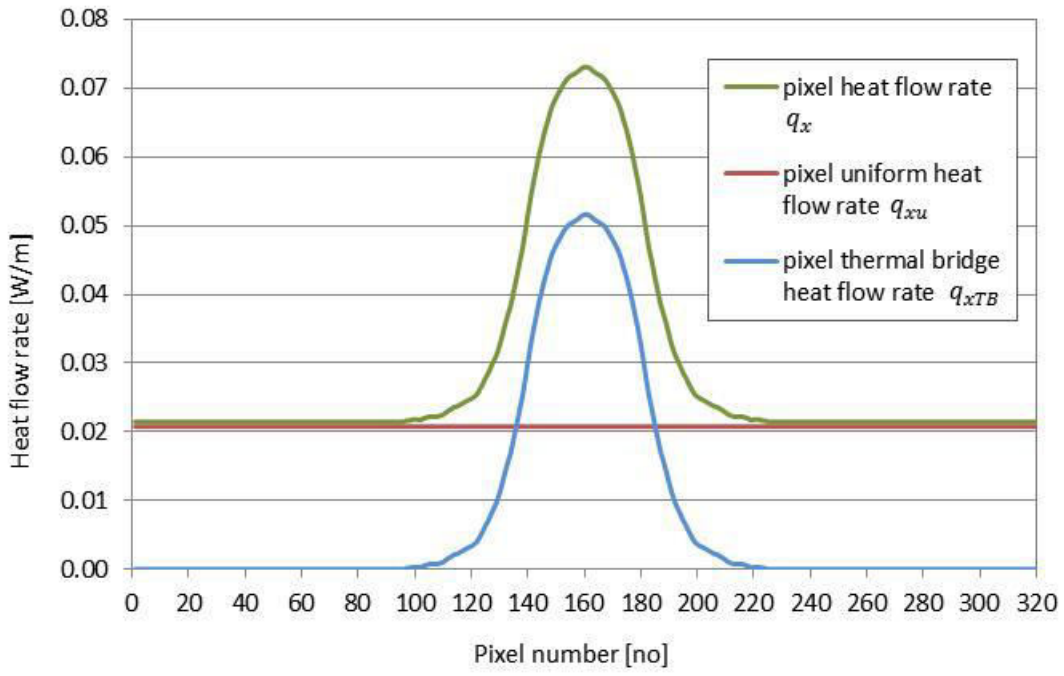

Fig. 3.3. Heat flow rates of sample building component shown in Fig.3.2.

3.5. Testing and validation of the methodology

In order to validate the methodology proposed in the previous section, an experimental programme was designed in which a number of test specimens containing thermal bridges were tested under controlled conditions in a calibrated hot box. The experimental programme was developed in consultation with industry to ensure that the test specimens represent typical building thermal bridging scenarios. The thermal performance of the specimens was also assessed using the ITT and the results of the two approaches were compared. The hot box device allowed the ambient conditions to be accurately controlled and guaranteed a steady state for the thermographic survey. The hot box used for this experiment is in Cracow University of Technology, Faculty of Environmental Engineering, Poland.

3.5.1. Experimental set up

Fig. 3.4 shows the experimental set up. The hot box test was performed first and this is described in detail in Section 3.5.3. After the hot box measurements were completed, the thermographic survey was carried out. Both the hot box test and the thermography were carried out under the same controlled conditions. In general, the conditions under which the tests were carried out were: air temperature on the cold side was kept at around -5°C and around +25°C on the hot side. Any sources of natural or artificial light were eliminated and the relative humidity was kept at a level of around 40% in the cold chamber and at around 45% in the hot chamber.

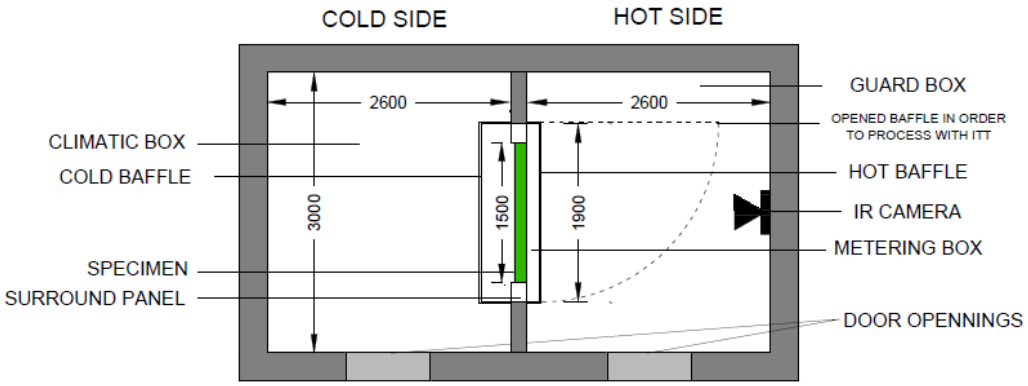

Fig. 3.4. Experimental set up.

3.5.2. Geometries and description of the specimens

Three specimens, with the length *L* of to 1.5m and the height *H* of to 1.5m, each containing a single vertical thermal bridge were tested. The specimens were made of structural insulated panels (SIP) with different thickness. The SIP panels were made of low conductivity XPS boards 100 mm or 125 mm thick with 15 mm thick oriented strandboard sheathing on each side. Any thermal bridge in a SIP panel creates a strong and easily visible surface temperature disturbance. Different types of thermal bridge were introduced into these panels during manufacture, as shown in Figs. 3.5-3.7.

Specimen 1, presented in Fig. 3.5, comprises a 130 mm thick SIP panel with a steel square hollow section (SHS) of dimensions100x100x5mm. This specimen represents a thermal bridge that is created by a steel column that is often used as a structural member of a building external envelope. This type of thermal bridge causes strong surface temperature disturbances and is easily detectable by ITT, which makes it an ideal sample to verify the methodology.

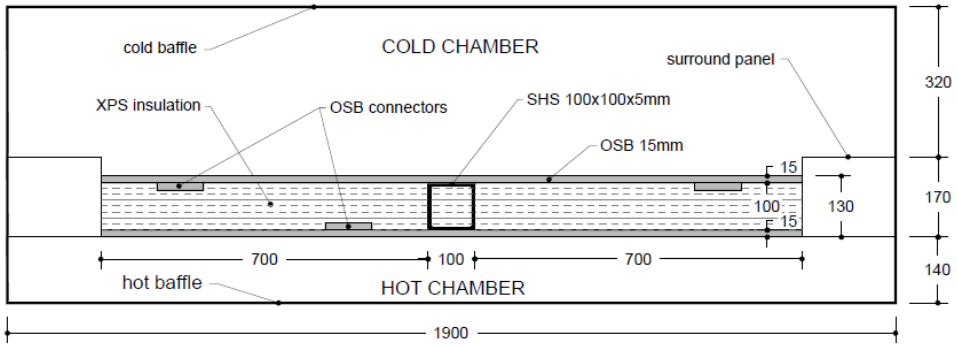

Fig. 3.5. Cross-section of Specimen 1 inserted in hot box.

Specimen 2 is a 155 mm thick SIP panel with a steel 100x100x5mm SHS (Fig. 3.6). The thermal bridge of this specimen consists of the same type of steel post as Specimen 1. In order to lower the heat loss through the thermal bridge, the thickness of the specimen was increased by 25 mm.

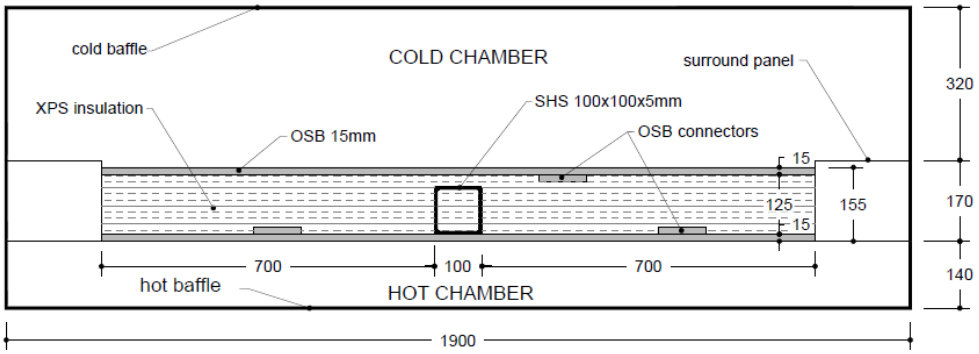

Fig. 3.6. Cross-section of Specimen 2 inserted in hot box.

Specimen 3 comprises a 155 mm thick SIP panel with 125x40mm timber stud and is shown in Fig. 3.7. As the thermal conductivity of timber is much lower than the conductivity of steel, the heat loss though this thermal bridge is not severe.

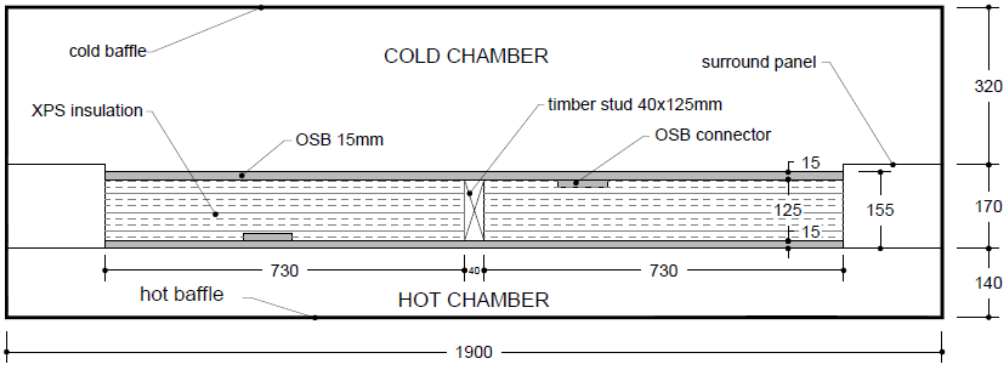

Fig. 3.7. Cross-section of Specimen 3 inserted in hot box.

3.5.3. Calorimetric Hot box device, tests and results

The hot box device, also called a calorimetric hot box (CHB) system, has been used with the test method in compliance with the EN ISO 8990 [17] standard. Fig. 3.8 shows a schematic cross-section of the hot box in thermal transmittance measurement mode [38-40]. Fig. 3.9 gives a general view of the hot box.

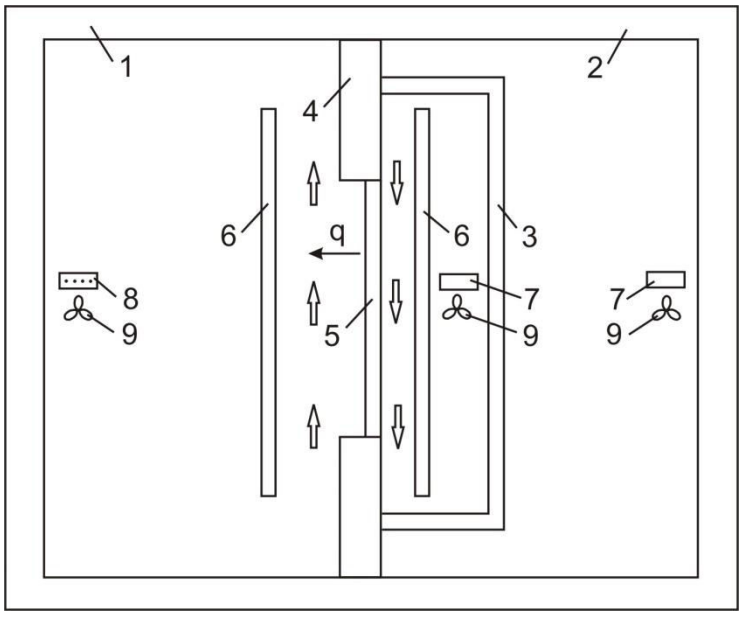

Fig. 3.8. Hot box scheme; 1 – climate box (outdoor side), 2 – guarding box (indoor side), 3 – metering box, 4 – surrounding panel, 5 – tested specimen, 6 – isothermal baffle, 7 – heater, 8 – cooling element, 9 – fan.

Fig. 3.9. General view of calorimetric hot box.

The hot box system consists of a metering box, simulating the indoor environmental conditions (hot side), and a climate box, simulating the outdoor environmental conditions (cold side). The metering box is surrounded by a guarding box in order to minimize the heat flow rate through the metering box walls. Specimens were inserted into a surrounding panel, which is made of low conductivity insulation to minimize the flanking side losses. Then a metering box was attached to the side of the specimen. To mirror the indoor environment, a free convection with a wind velocity of 0.1 m/s in the metering box was created. In the climatic box, an isothermal baffle was attached to the cold side of the specimen. That side of the device was to simulate the outdoor environment, and a wind velocity of approximately 1.50 m/s was created and kept steady along the whole specimen, during the whole test.

The measurements are taken after a few hours of steady state conditions when the heating element in the metering box distributes the necessary amount of heat to maintain the temperature difference on metering box walls equal to zero. All distributed heat is transferred through the specimen and surrounding panel when no heat is transferred through the metering box walls. The hot box was equipped with an AMR Ahlborn Wincontrol system that programs, adjusts and records measured data during the testing such as temperature, wind velocity, humidity, power provided to the hot box. On the hot surface of each specimen, surface thermocouples were attached,

one in the middle of thermal bridge (S2) and one 0.40m away from the middle of the thermal bridge (S1).

Before the actual testing, the hot box was calibrated to account for any heat flow through the surrounding panel and for any interactions between the specimen's edges and the edges of the surrounding panel. The calibration process was performed in accordance with EN ISO 8990 [17] and EN ISO 12567-1 [40]. Table 3.1 summarizes the hot box measurements for Specimens 1, 2 and 3

Table 3.1. Hot box measurements for Specimens 1, 2 and 3.

Parameter	Unit	Specimen 1	Specimen 2	Specimen 3
T_e	°C	-4.90	-4.96	-5.01
$T_{se,b}$	°C	-4.94	-5.05	-5.09
T_i	°C	24.73	24.82	24.81
$T_{si,b}$	°C	24.24	24.50	24.52
Φ_{in}	W	36.05	25.63	22.70
$\dot{q}_{sp}$	W/m²	12.92	8.31	7.01
w_i	m/s	0.1	0.1	0.1
w_e	m/s	1.43	1.55	1.57

The environmental temperatures, T_{ni} and $T_{ne,}$ express the mean of the convective and the radiative temperatures using the following relation from EN ISO 12567-1 [40]:

$$T_n = F_c T_c + (1 - F_c) T_r \qquad (3.18)$$

where T_c is a convective temperature (measured air temperature), T_r is a radiative temperature (mean value of baffle and reveal temperatures) and F_c is the fraction of convective heat transfer calculated during the calibration process [40]:

$$F_{c,i} = 0.3138 - 0.0001\dot{q}_{sp} \quad (3.19)$$

$$F_{c,i} = 0.3338 - 0.0182\dot{q}_{sp} \quad (3.20)$$

and $\dot{q}_{sp}$ is the surface heat flux through the specimen calculated according to the EN ISO 12567-1 [40] procedure:

$$\dot{q}_{sp} = \frac{\Phi_{in} - \Phi_{sur,p} - \Phi_{edge}}{A} \quad (3.21)$$

The calculated environmental temperatures for each test specimen are given in Table 3.2.

Table 3.2. Environmental temperatures for Specimens 1, 2 and 3.

Parameter	Unit	Specimen 1	Specimen 2	Specimen 3
T_{ni}	°C	24.39	24.60	24.61
T_{ne}	°C	-4.92	-5.01	-5.05

Based on measurements from Table 3.1, the heat flux $\dot{Q}_{sp}$ through each specimen and the overall U_{sp} were calculated from Equations (3.22) and (3.23):

$$\dot{Q}_{sp} = \dot{q}_{sp} A \quad (3.22)$$

$$U_{sp} = \frac{\dot{Q}_{sp}}{A(T_{ni} - T_{ne})} \quad (3.23)$$

In order to determine the q_{TB} and the Ψ-value, two additional specimens without thermal bridging were tested in the hot box, a plain panel 130mm thick (Specimen 4) and plain panel 155mm thick (Specimen 5) with the results presented in the Table 3.3.

Table 3.3. Hot box results for plain Specimens 4 and 5.

Parameter	Unit	Specimen 4	Specimen 5
$\dot{Q}_{sp\ plain}$	W	17.95	14.65

Having those results, q_{TB} and Ψ can be obtained as the difference between the heat flow rates of specimens with thermal bridges and the heat flow rates of the plain specimens, using the Equations (3.24) and (3.25), respectively. Because of different specimen thicknesses, Specimen 1 is examined with Specimen 4 whereas Specimens 2 and 3 are compared with Specimen 5:

$$q_{TB} = \frac{(\dot{Q}_{sp} - \dot{Q}_{sp\ plain})}{H} \quad (3.24)$$

$$\Psi = \frac{q_{TB}}{(T_{ni} - T_{ne})} \quad (3.25)$$

With the hot box device, the heat flow rate through the specimen can be obtained with a certain degree of accuracy. The accuracy in each separate measurement depends upon the complexity of the construction being measured, but also depends on the heat exchange with the surroundings, errors of temperature and input power measurements etc. The measurement error is not constant from specimen to specimen [41]

The uncertainty of the calculated overall heat transfer coefficient in each performed measurement was estimated according to the error propagation rule [39,42,43]. The *U*-value, $\dot{Q}_{sp}$, Ψ and q_{TB} uncertainties are connected with the measurement errors of

air temperatures, surface temperatures, specimen dimensions, input power in the hot box, which were 0.3 K, 0.3 K, 0.001 m, 0.3 W, respectively.

3.6. Thermographic survey

The thermographic survey was undertaken after the hot box measurements were completed, using the procedure described in Section 3.5. This was carried out in the steady state, and under the same environmental conditions as the hot box testing and they are summarized in Table 3.1. Air temperatures and the air velocity were measured and recorded by the hot box sensors. To obtain more accurate thermographic results, for each specimen a series of IR images were taken.

The IR camera is a very sensitive tool and survey accuracy is influenced by the camera settings and the way the camera is operated. Using an IR camera, the surface temperature of the object is measured, which is a function of the reflected ambient temperature, the thermal emissivity of the surface, and the distance between the camera and the target. The reflected ambient temperature is necessary to get the correct surface temperature readings. In this study, a direct method of measuring the reflected ambient temperature, approved by the ISO Standard 18434 [44] and used by researchers in previous studies [26,35] is followed. According to this standard a crumpled piece of aluminium foil that has high reflectivity and disperses equally in all directions is placed on the measured object. Then, with the IR camera set for black body emissivity, the average surface temperature of the aluminium foil, which is the reflected ambient temperature, is captured. To measure the temperatures using an infrared camera correctly, it is also very important that the value of emissivity of the surface element is measured on site instead of taking the emissivity value from the literature. Many factors influence the emissivity value such as age, pollution or humidity, therefore only correctly measured emissivity on site reflects the real surface conditions [22]. In order to set up the emissivity correctly in the current study, following the ISO Standard 18434 [44] , the contact method was used. Using the IR camera, a spot temperature of the object was measured. Independently from IR camera reading, the temperature of nearly the same position was measured by a surface

thermocouple. Without moving the camera, the emissivity was adjusted until the surface temperature on the IR camera was the same as the temperature shown by the thermocouple. However, the current methodology does not exclude other methods of assessing the emissivity, such as the reference emissivity material method [44], especially useful on site, or an innovative method developed by Albatici at al. [45] using an infrared thermovision technique emissometer.

Then a series of IR images of each of the specimens was taken. For calculation of the q_{TB} and Ψ-value, five sequential IR images were chosen for post processing. On each of them, a horizontal line (IR line) of pixels at mid-height was created. This IR line is sufficient to show the surface temperatures distribution caused by the vertical thermal bridge. Because of symmetry, the post processing includes one half of the specimen only. The lowest surface temperature T_{smin} indicated the middle of thermal bridge and of the specimen. From the five IR lines, a mean IR line was derived. This was used to calculate q_{tot} for the whole length of the specimen L, q_{TB} and the Ψ-value in accordance with the procedure described in Section 3.4. Also the heat flow rate through the specimen $\dot{Q}_{sp}$ (Equation 3.26) and the overall thermal transmittance coefficient U-value of the specimen were calculated (Equation 3.27):

$$\dot{Q}_{sp} = q_{tot}\, H \qquad (3.26)$$

$$U_{sp} = \frac{q_{tot}}{L(T_i - T_e)} \qquad (3.27)$$

3.7. Measurement results

In this section, the results from the ITT survey and the hot box measurements are presented and discussed. First the surface temperature distributions from the IR images of the specimens are compared with surface temperatures measured by thermocouples. Then the heat flow rate through the specimens $\dot{Q}_{sp}$ and the overall thermal transmittance U-values calculated based on the thermographic survey are compared with those obtained in the hot box device. Finally, the key results, that are the object

of this publication, q_{TB} and Ψ obtained by the ITT, are shown together with the hot box measurement.

3.7.1. Surface temperatures

During the hot box testing, the surface temperatures were measured in two spots S1 and S2. T_{S1} represents the uniform surface temperature and T_{S2} the minimum surface temperature in the middle of thermal bridge. Figs. 3.10 – 3.12 present the temperatures on these two spots measured during the hot box testing and their comparison to temperatures distributions obtained by the ITT for Specimens 1 - 3. For Specimens 1 and 2 the temperature distributions from five and for the Specimen 3 from two thermograms are presented. Only two thermograms were available for Specimen 3.

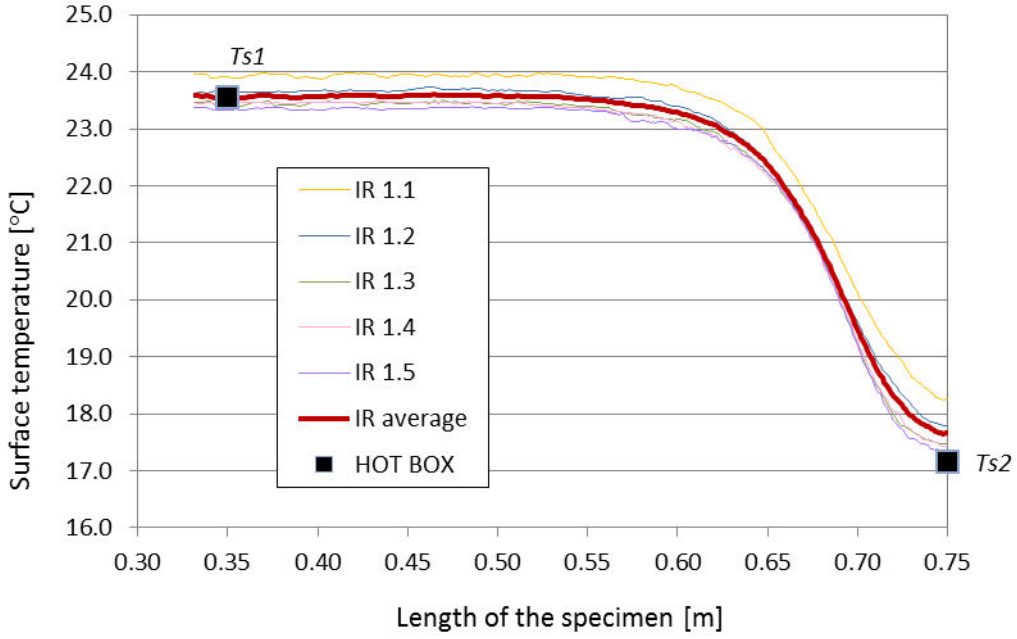

Fig. 3.10. Surface temperature of Specimen 1.

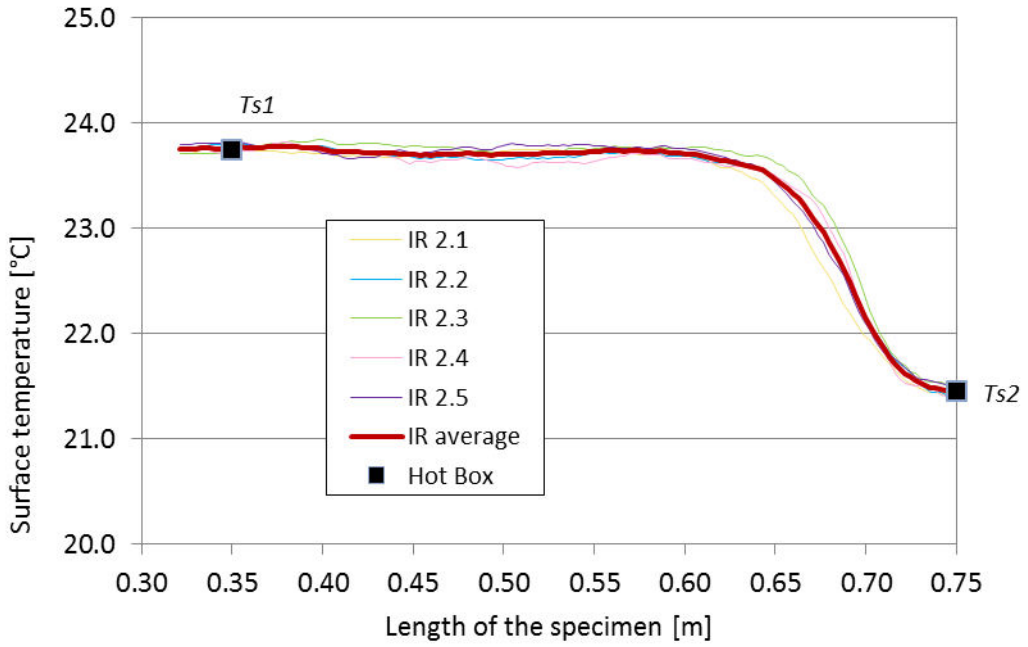

Fig. 3.11. Surface temperature of Specimen 2.

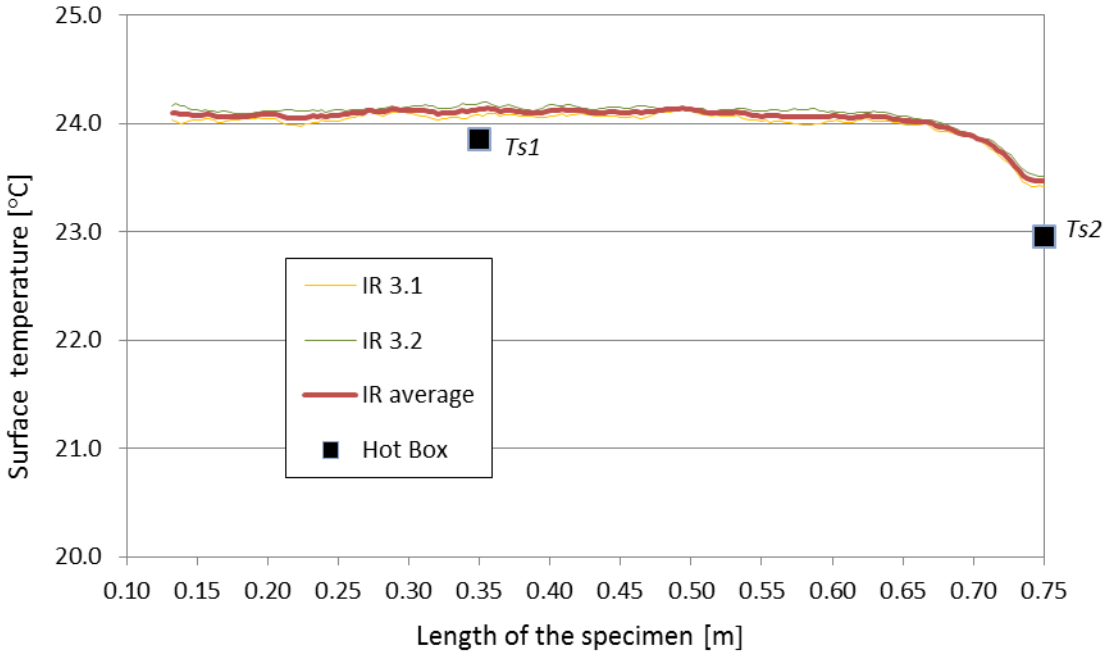

Fig. 3.12. Surface temperatures of Specimen 3.

Figs. 3.10 - 3.12 together with Tables 3.4 and 3.5 below show the maximum difference of 0.5 °C between surface temperatures measured by thermocouples during the hot box tests and recorded by the ITT.

The thermal bridge of Specimen 1 lowers the surface temperatures quite significantly, by around 6°C. The uniform surface temperature T_{S1} of this specimen measured by the ITT and the hot box device are in excellent agreement. The minimum surface temperature T_{S2} obtained by the ITT is slightly higher than the temperature measured at the hot box device, but the difference is only 0.5°C. The surface temperatures of Specimen 2 reflect the influence of its thermal bridge by dropping by about 2°C. The temperatures recorded by the ITT for this specimen co-incide with the temperatures measured during the hot box testing at positions S1 and S2 and no deviation between the measurements was noticed. The thermal bridge of the Specimen 3 causes very slight drop in the temperature distribution, less than 1°C. For this specimen the ITT show slightly higher surface temperatures than those recorded in the hot box. However, the differences between those temperatures are very low, around 0.2°C for T_{S1} and around 0.5°C for T_{S2}. A maximum standard deviation (SD) of less than 2% for the ITT and less than 1% for the hot box results was obtained. Using the contact method of setting up the emissivity [44] contributed to the very small percentage deviation in surface temperatures. Figs. 3.10 – 3.12 show the importance of processing a series of IR images for each thermal bridge case. For the Specimen 3, only two IR images were available and the temperatures recorded on those IR images show higher readings that the readings from the hot box. This discrepancy could be reduced by processing additional IR images.

Table 3.4. Uniform surface temperatures T_{S1}.

	hot box		*ITT*		*hot box/ITT*
	T_{S1} °C	*SD* %	T_{S1} °C	*SD* %	*Difference* °C
Specimen 1	23.55	0.64	23.57	0.88	0.02
Specimen 2	23.75	0.63	23.74	0.12	-0.01
Specimen 3	23.85	0.62	24.09	0.21	0.24

Table 3.5. Minimum surface temperatures T_{S2}.

	hot box		*ITT*		*hot box/ITT*
	T_{S2}	*SD*	T_{S2}	*SD*	*Difference*
	°C	*%*	*°C*	*%*	*°C*
Specimen 1	17.15	0.87	17.66	1.93	0.51
Specimen 2	21.45	0.70	21.43	0.26	-0.02
Specimen 3	22.95	0.65	23.47	0.23	0.52

3.7.2. Comparison of the heat flow rate through the specimen $\dot{Q}_{sp}$ and the overall heat transfer coefficient *U*-value

The heat flow rate through the whole specimen $\dot{Q}_{sp}$ and the overall thermal transmittance *U*-values obtained from the thermographic survey and from the hot box device are presented in Tables 3.6 and 3.7. Looking at the percentage relative deviations (RD) of the $\dot{Q}_{sp}$ obtained by means of the ITT, it can be seen that the accuracy of $\dot{Q}_{sp}$ reduces as the heat flow rate through the specimen reduces. The highest heat flow rate $\dot{Q}_{sp}$ was measured for Specimen 1, which shows a relative deviation of less than 1%. Higher relative deviations of around 12% and 24% have been found for Specimen 2 and 3, respectively. However, observing the actual difference between $\dot{Q}_{sp}$ measured by the ITT and by the hot box, almost no difference can be seen for Specimen 1 while, for Specimens 2 and 3, small differences of approximately 2 W and 4 W, respectively, were found.

A similar trend and level of relative deviation can be observed for the *U*-values obtained by two methods. The relative deviations of Specimen 1, 2 and 3 are around 1%, 11% and 24%, respectively. Despite these figures, the differences between the *U*-values obtained from the ITT measurements and those from the hot box for Specimens 1, 2 and 3 are only 0.005 W/m^{2}K, 0.03 W/m^{2}K and 0.06 W/m^{2}K, respectively. It must be underlined again that the results for Specimen 3 are based on two thermograms only and its precision could be higher with additional thermograms.

Table 3.6. Total heat flow rate through the specimen $\dot{Q}_{sp}$.

	hot box		*ITT*		*hot box/ITT*
	$\dot{Q}_{sp}$	*SD*	$\dot{Q}_{sp}$	*SD*	*RD*
	W	*%*	*W*	*%*	*%*
Specimen 1	29.07	0.63	29.09	13.46	0.07
Specimen 2	18.7	0.97	20.93	3.33	11.93
Specimen 3	15.77	1.15	12.02	6.57	-23.78

Table 3.7. Overall thermal transmittance *U*-value.

	hot box		*ITT*		*hot box/ITT*
	U_{sp}	*SD*	U_{sp}	*SD*	*RD*
	$W/(m^2K)$	*%*	$W/(m^2K)$	*%*	*%*
Specimen 1	0.441	1.33	0.436	13.23	-1.13
Specimen 2	0.281	1.41	0.312	3.33	11.03
Specimen 3	0.236	1.36	0.179	6.70	-24.15

3.7.3. Comparison of thermal bridge heat flow rate q_{TB} and linear thermal transmittance Ψ-value

The object of the paper was to validate the new methodology for obtaining thermal bridge heat flow rate q_{TB} and Ψ-value by means of the ITT. The results obtained with this method and its comparison to the hot box results are presented in the Tables 3.8 and 3.9 and they show excellent agreement. Taking into account the relative deviation calculated for q_{TB} and the Ψ-value, the results obtained by means of the ITT shows a similar trend to the $\dot{Q}_{sp}$ and *U*-value. The smallest discrepancy (about 5% for q_{TB} and about 6% for the Ψ-value) has been determined for Specimen 1. The heat flow rate caused by the thermal bridge in this specimen provides approximately 36% of the heat flow rate of the whole specimen. A higher discrepancy in the q_{TB} and the Ψ-value (10%) has been determined for Specimen 2 where 17.5% of the overall heat flow rate

is caused by its thermal bridge. In Specimen 3, the heat flow rate caused by the thermal bridge contributes only 6%. For this last specimen, the relative deviation is equal to 36%. This trend shows that the methodology works more accurately for assessing the heat loss caused by thermal bridges that have a strong impact on the overall heat flow rate. Simultaneously, these types of thermal bridges cause a significant surface temperature disturbance and thus can easily be identified by the ITT. The timber post in Specimen 3 shows an example of a thermal bridge causing only slight change in the surface temperature which could be difficult to detect by ITT. The accuracy of the hot box measurements is the same for all specimens and is described in Section 3. This results in a significantly higher standard deviation for Specimen 3, representing the low impact thermal bridge, than for Specimens 1 and 2, in hot box measurement results. Nevertheless, the actual differences in the results are very small. The q_{TB} obtained from the ITT measurements and those from the hot box for Specimens 1 differs by less than 0.4 W/m and for Specimen 2 and Specimen 3 by less than 0.3 W/m. The differences in Ψ-values are less than 0.015 W/mK for Specimen 1 and 0.009 W/mK for Specimens 2 and 3 and can be described as minor.

Table 3.8. Thermal bridge heat flow rate q_{TB}.

	hot box		*ITT*		*hot box/ITT*
	q_{TB}	*SD*	q_{TB}	*SD*	*RD*
	W/m	*%*	*W/m*	*%*	*%*
Specimen 1	7.41	1.89	7.04	4.26	-4.99
Specimen 2	2.70	5.21	2.43	13.15	-10.00
Specimen 3	0.75	18.77	0.49	4.80	-34.67

Table 3.9. Linear thermal transmittance Ψ-value.

	hot box		*ITT*		*hot box/ITT*
	Ψ	*SD*	Ψ	*SD*	*RD*
	W/(mK)	*%*	*W/(mK)*	*%*	*%*
Specimen 1	0.253	1.94	0.238	4.28	-5.93
Specimen 2	0.091	5.21	0.082	12.98	-9.89
Specimen 3	0.025	19.36	0.016	3.13	-36.00

As mentioned in the methodology section, in order to achieve a high level of accuracy in evaluating the thermal bridge heat flow rate using the ITT, the importance of calculating the convective and radiative heat transfer coefficients for each pixel on the IR line cannot be underestimated. To ascertain how this approach influences the accuracy, q_{TB} and Ψ-value of tested specimens were evaluated using constant values of h_{cx} and h_{rx} corresponding to the uniform part of the specimen. The q_{TB} and Ψ-value obtained from calculations with these undifferentiated heat transfer coefficients showed percentage relative deviations of -13% for Specimen 1, -10% for Specimen 2 and -7% for Specimen 3 when compared to the ITT results presented in Table 3.8 and 3.9, obtained by calculating h_{cx} and h_{rx} for each pixel. The following relative deviations were obtained when comparing $q_{TB,}$ evaluated using constant heat transfer coefficients, with $q_{TB,}$ obtained from the hot box: -17% for Specimen 1, -18.5% for Specimen 2 and -38.5 % for Specimen 3. Similarly, the following relative deviations were obtained when compared the Ψ-value, evaluated based on constant heat transfer coefficients, with the Ψ-value, measured using the hot box device: -18% for Specimen 1, -18.5% for Specimen 2 and -40 % for Specimen 3. These deviations are much higher than the deviations of the results presented in Table 8 and 9, obtained using the unique h_{cx} and h_{rx} for each pixel. This comparison shows the importance of the current approach to the precise calculation of h_{cx} and $h_{rx.}$ It should be noted that the heat transfer coefficient, calculated with the wind velocity of 1.50 m/s used in the hot box tests, is lower than the standard value that is recommended by EN ISO 6946 [5] for use in the absence of specific information on the boundary conditions.

3.8. Summary and conclusions

A methodology for determining the heat flow rate caused by a thermal bridge q_{TB} and the linear thermal transmittance Ψ-value by means of the ITT has been presented. The methodology developed is based solely on the ITT, without involving any other methods of measurements or tabulated values such as thermal conductivities k or overall thermal transmittance U-values. Since the surface temperature distribution around a thermal bridge is never uniform, the approach involves calculation of the heat flow rate for each pixel q_x on an IR line created from a series of thermograms. Accurate quantification of this heat flow rate includes determination of the convective and radiative heat transfer coefficients for each pixel.

This methodology has been tested, in a controlled environment, in a hot box device.The q_{TB} and the Ψ-value obtained by the ITT in that environment showed excellent agreement, with relative deviations compared to the values obtained from the hot box method for Specimen 1 and Specimen 2 of -5% and -10%, respectively. The corresponding deviation for Specimen 3 was -36%, which experienced only slight surface temperature disturbance due to the thermal bridge. The importance of precise evaluation of convective and radiative heat transfer coefficients for each pixel on the IR line has been demonstrated. The q_{TB} and the Ψ-value calculated using constant coefficients result in higher relative deviations when compared to the hot box results: -18% for Specimen 1 and Specimen 2 and -40% for Specimen 3.

It has been shown that the methodology works satisfactorily under steady state laboratory conditions. Further laboratory testing of the methodology under different wind velocities will be carried out. Testing the methodology in real buildings, under quasi-steady state is planned. It has to be borne in mind that the IR camera is a very sensitive tool and has its limitations. While working in indoor conditions, the main limitations would be issues such as the access to the inhabited house/apartment and the furniture located on or close to the external walls. The outdoor ITT on the other hand is strongly influenced by the weather conditions. The temperature difference between indoor and outdoor air cannot be expected to be about 30°C as was the case during the experiments. All these issues will challenge the accuracy of the

measurements taken by the ITT in real conditions. However, the fact that the methodology is validated with good agreement in the hot box device provides a solid basis to apply it, with possible adjustments, to the real conditions.

After testing the methodology under real conditions, it can be implemented on any linear thermal bridge. One of the main advantages of the methodology is that its application does not require any information about the composition of layers of the building external envelope, therefore it could be used in any existing building. The new methodology could be especially useful in a building post-construction stage energy efficiency assessment where the designed Ψ-values could be compared to the measured values. The methodology could also be useful for authorities that provide retrofitting grants, as a tool to assess the real improvement of thermal performance of the retrofitted building envelope.

3.9. Acknowledgments

The authors wish to thank the following

1) Cracow University of Technology for opportunity to use hot box facility with a special thanks to Head of the Institute Prof. Jacek Schnotale and to the technician Eng. Mariusz Rusiecki
2) SIP Energy Ltd., Athenry Co. Galway particularly John Moylan for providing the test specimens
3) Enterprise Ireland for financial support through Innovation Voucher IV-2014-4203

3.10. References

[1] Action Plan to Improve Energy Efficiency in the European Community, Commission of the European Communities, 2000.

[2] Delivering a sustainable energy future for Ireland, Government White Paper, Department of Communications, Marine and Natural Resources, 2007.

[3] Energy Efficiency and its contribution to energy security and the 2030 Framework for climate and energy policy, European Commission, 2014.

[4] Directive 2002/91/EC of the European Parliament and of the Council of 16 December 2002 on the energy performance of buildings, 2003.

[5] EN ISO 6946 Building components and building elements - Thermal resistance and thermal transmittance - Calculation method, 2017.

[6] EN ISO 14683 Thermal bridges in buildings construction - linear thermal transmittance - simplified methods and default values, 2007.

[7] EN ISO 10211 Thermal bridges in building construction - heat flow and surface temperatures - detailed calculations, 2017.

[8] ISO 9869 Thermal Insulation - Building elements - In-situ measurement of thermal resistance and thermal transmittance, 1994.

[9] Field investigations of the thermal performance of construction elements as built, BRE East Kilbride, 2001.

[10] F. Asdrubali, C. Buratti, F. Cotana, G. Baldinelli, M. Goretti, E. Moretti, C. Baldassarri, E. Belloni, F. Bianchi, A. Rotili, M. Vergoni, D. Palladino, and D. Bevilacqua, Evaluation of Green Buildings' Overall Performance through in Situ Monitoring and Simulations, Energies 6 (2013) 6525–6547.

[11] F. Asdrubali, F. D'Alessandro, G. Baldinelli, F. Bianchi, Evaluating in situ thermal transmittance of green buildings masonries - A case study, Case Stud.s Constr. Mater. 1 (2014) 53–59.

[12] L. Evangelisti, C. Guattari, P. Gori, R. De Lieto Vollaro, In situ thermal

transmittance measurements for investigating differences between wall models and actual building performance, Sustainability 7 (8) (2015) 10388–10398.

[13] A. Byrne, G. Byrne, A. Davies, A.J. Robinson, Transient and quasi-steady thermal behaviour of a building envelope due to retrofitted cavity wall and ceiling insulation, Energy Build. 61 (2013) 356–365.

[14] G. Desogus, S. Mura, R. Ricciu, Comparing different approaches to in situ measurement of building components thermal resistance, Energy Build. 43 (10) (2011) 2613–2620.

[15] UNI 10351 Building materials. Thermal conductivities and vapour permeabilities, 1994.

[16] UNI 10355 Walls and floors.Thermal resistance values and calculation method, 1994.

[17] EN ISO 8990 Thermal insulation - Determination of steady-state thermal transmission properties - Calibrated and guarded hot box, 1997.

[18] T. Nussbaumer, K.G. Wakili, C. Tanner, Experimental and numerical investigation of the thermal performance of a protected vacuum-insulation system applied to a concrete wall, Appl. Energy 83 (2006) 841–855.

[19] D.P. Aviram, A.N. Fried, J.J. Roberts, Thermal properties of a variable cavity wall, Build. Environ. 36 (2001) 1057–1072.

[20] A. Lechowska, J. Schnotale, M. Paszkowski, Measurement of thermal transmittance of multi-layer glazing with ultrathin internal glass partitions, Tech. Trans. Cracow Univ. Technol. 111 (3-B) (2014).

[21] EN 13187 Thermal performance of buildings-qualitative detection of thermal irregularities in building envelopes - infrared method, 1999.

[22] R. Albatici, A.M. Tonelli, Infrared thermovision technique for the assessment of thermal transmittance value of opaque building elements on site, Energy Build. 42 (11) (2010) 2177–2183.

[23] R. Albatici, A. M. Tonelli, M. Chiogna, A comprehensive experimental

approach for the validation of quantitative infrared thermography in the evaluation of building thermal transmittance, Appl. Energy 141 (2015) 218–228.

[24] I. Nardi, D. Paoletti, D. Ambrosini, T. de Rubeis, Validation of quantitative IR thermography for estimating the *U*-value by a hot box apparatus, In Proceedings of 33rd UIT Heat Transfer Conference; J. Phys.: Conf. Ser. 655 (2015)

[25] I. Nardi, D. Ambrosini, T. de Rubeis, S. Sfarra, S. Perilli, A comparison between thermographic and flow-meter methods for the evaluation of thermal transmittance of different wall constructions, In Proceedings of 33rd UIT Heat Transfer Conference, J.Phys.: Conf. Ser. 655 (2015)

[26] P.A. Fokaides, S.A. Kalogirou, Application of infrared thermography for the determination of the overall heat transfer coefficient (*U*-Value) in building envelopes, Appl. Energy 88 (2011) 4358–4365.

[27] C. Tanner, T. Frank, K.G. Wakili, W. Angaben, Vorschlag zur standardisierten Darstellung von Wärmebildern mit QualiThermo, Bauphysic 33 (2011) 345–356.

[28] L. Zalewski, S. Lassue, D. Rousse, K. Boukhalfa, Experimental and numerical characterization of thermal bridges in prefabricated building walls, Energy Convers. Manage (2010) 2869–2877.

[29] F. Ascione, N. Bianco, R.F. De Masi, G. M. Mauro, M. Musto, G. P. Vanoli, Experimental validation of a numerical code by thin film heat flux sensors for the resolution of thermal bridges in dynamic conditions, Appl. Energy 124 (2014) 213–222.

[30] F. Ascione, N. Bianco, R. Francesca, D. Masi, F. De Rossi, G. Peter, Simplified state space representation for evaluating thermal bridges in building: Modelling, application and validation of a methodology, Appl. Therm. Eng. 61 (2013) 344–354.

[31] H. Heinrich, K. Dahlem, Thermography of Low Energy Buildings, In Proceedings of International Conference on Quantitative Infrared

Thermography Qirt, Reims, France, 2000.

[32] A. Wróbel, T. Kisilewicz, Detection of thermal bridges - aims , possibilities and conditions, In Proceedings of International Conference on Quantitative Infrared Thermography Qirt, Cracow, Poland 2008.

[33] T. Taylor, J. Counsell, S. Gill, Energy efficiency is more than skin deep: Improving construction quality control in new-build housing using thermography, Energy Build. 66 (2013) 222–231.

[34] I. Benkő, Quantitative analysis of thermal bridges of structures through infrared thermograms, In Proceedings of International Conference on Quantitative Infrared Thermography Qirt, Dubrovnik, Croatia, 2002, pp. 203–208.

[35] F. Asdrubali, G. Baldinelli, F. Bianchi, A quantitative methodology to evaluate thermal bridges in buildings, Appl. Energy 97 (2012) 365-373.

[36] F. Bianchi, A. Pisello, G. Baldinelli, F. Asdrubali, Infrared Thermography Assessment of Thermal Bridges in Building Envelope: Experimental Validation in a Test Room Setup, Sustainability 6 (2014) 7107–7120.

[37] B. Lehmann, K. Ghazi Wakili, T. Frank, B. Vera Collado, C. Tanner, Effects of individual climatic parameters on the infrared thermography of buildings, Appl. Energy 110 (2013) 29–43.

[38] F. Chen, S.K. Wittkopf, Summer condition thermal transmittance measurement of fenestration systems using calorimetric hot box, Energy Build. 53 (2012) 47–56.

[39] Y. Fang, P.C. Eames, B. Norton, T.J. Hyde, Experimental validation of a numerical model for heat transfer in vacuum glazing, Sol. Energy 80 (2006) 564–577.

[40] EN ISO 12567-1 Thermal performance of windows and doors - Determination of thermal transmittance by the hot-box method - Part 1: Complete windows and doors. 2010.

[41] J. Rose, S. Svendsen, Validating numerical calculations against guarded hot box

measurements, Noric J. Build.Phys. 4 (2014) 1-9.

[42] F. Asdrubali, G. Baldinelli, Thermal transmittance measurements with the hot box method: Calibration, experimental procedures, and uncertainty analyses of three different approaches, Energy Build. 43 (2011) 1618–1626.

[43] A.H. Elmahdy, Heat transmission and R-value of fenestration systems using IRC hot box - procedure and uncertainty analysis, Trans. ASHRAE 98 (1992) 630-637.

[44] ISO 18434-1 Condition monitoring and diagnostics of machines - Thermography Part 1: General procedure, 2008.

[45] R. Albatici, F. Passerini, A.M. Tonelli, S. Gialanella, Assessment of the thermal emissivity value of building materials using an infrared thermovision technique emissometer, Energy Build. 66 (2013) 33–40.

Chapter 4

Quantification of heat losses through building envelope thermal bridges influenced by wind velocity using the outdoor infrared thermography technique

4.1. Paper overview

The application of the indoor ITT for building heat loss assessment may not be possible in cases where there are access restrictions to the building interior or where furniture or fittings are mounted on the external walls. Bearing this in mind, the next objective of this research was to adapt the methodology, proposed in Chapter 3, to outdoor conditions. Outdoor ITT is significantly more challenging than indoor ITT as it is strongly influenced by weather conditions. One of the major factors influencing the surface temperatures on the external face of the building envelope component, thus heat losses, is wind velocity. In order to quantify the impact of wind velocity on thermal bridging performance, this study includes numerical analysis and laboratory testing of the thermal bridging response while exposed to different wind velocities. The study revealed that the wind impacts thermal bridging region more significantly than the plain part of the building component. Therefore, at different velocities, different Ψ-values calculated from recorded surface temperatures were obtained. The wind impact is accounted for in the methodology via the external surface convective

coefficients. Two approaches to evaluate these coefficients were investigated, namely the Nusselt number and Jürges approximation, and the suitability of both approaches was demonstrated. As mentioned in Chapter 2, conventionally, during the design stage, outdoor convective boundary condition is assumed to correspond with wind velocity equal 4 m/s. It is important to compare the measured thermal bridging performance with the design one and/or thermal bridging performance measured before and after the building envelope retrofitting. Therefore, this project includes the development of an adjustment procedure to convert the Ψ-value measured at any wind velocity to the Ψ-value at the standard wind velocity 4 m/s. The adjustment procedure also allows comparison of Ψ-values evaluated from measurements taken at different times with different wind velocities. Extension of the methodology for use in outdoor conditions significantly increases its implementation potential to the overall thermal assessment of an existing building. A surveyor can now choose, on a case to case basis, which conditions, indoor or outdoor, are more conducive for a thermographic survey. This makes the methodology very convenient. Moreover, the adjustment procedure extends the application of the methodology at any wind condition.

The content of this chapter has been published in Applied Energy journal: *M. O'Grady, A.A. Lechowska, A.M. Harte, Quantification of heat losses through building envelope thermal bridges influenced by wind velocity using the outdoor infrared thermography technique, Applied Energy, 2017, 208:1038-1052.* In this joint publication, Małgorzata O'Grady, supervised by Dr. Annette Harte, designed the experiment, performed the testing, analysed the test results, carried out the numerical heat transfer simulations and developed the methodology for outdoor ITT assessment. Dr. Agnieszka Lechowska facilitated the testing.

4.2. Abstract

Improving the thermal performance of the existing building stock is essential to significantly reduce the overall energy consumption in the building sector. A key objective is the retrofitting of the existing building envelope. A necessary first step in the building envelope optimization process is the assessment of its actual thermal performance. This assessment should be repeated after retrofitting to clearly define the improvements that were made and the heat loss reduction that was achieved. In this study, an efficient, non-destructive, in-situ measurement method, based on an outdoor infrared thermographic survey, is developed to determine the thermal bridging performance. As wind velocity significantly influences the heat losses through the building envelope, this study includes quantification of the wind velocity impact on the Ψ-value. This was assessed by undertaking ITT of the same thermal bridge at various wind velocities, in a controlled environment, in a hot box device. The results showed that the Ψ-value is highly dependent on wind velocity so that measurement of the Ψ-value taken at different wind conditions cannot be directly compared. An adjustment procedure is proposed that can be used to convert the Ψ-value measured at any wind velocity to a standard value corresponding to a velocity of 4 m/s. From a practical point of view, this adjustment procedure makes the methodology widely applicable.

4.3. Introduction

It is estimated that energy related to buildings is responsible for 40% of total EU energy consumption. To achieve the EU 2030 energy and climate goals, it is essential to limit building-related energy. The European Union Directive 2010/31/EU on Energy Performance of Buildings (EPBD) [1] obliged the EU Member States to implement changes in national building regulations. These changes include setting strict minimum requirements on building energy performance and introducing a national building energy certification system. In November 2016, the European Commission evaluated the effectiveness and relevance of this directive [2]. They

found that combining minimum standards requirements on building energy performance and its certification works effectively particularly with respect to newly constructed buildings. However, large opportunities for savings are still not being harnessed. These concern the existing building stock which has been retrofitted but at a substantially slow pace. Based on this evaluation, a proposal for amending the EPBD [3] has been issued. Its key objective is to fast-track the retrofitting of existing buildings, particularly those with the poorest performance. The importance of this issue is further supported by the fact that about 75% of existing buildings are energy inefficient and only 0.4% - 1.2% of these buildings, depending on Member State, are retrofitted annually.

In answer to this substantial problem, a significant number of research projects have focused on optimization of the building' energy performance. These have demonstrated different approaches for achieving the most energy efficient solution when constructing a new building or renovating an existing one [4-8]. The optimisation tools developed consider a range of criteria including, inter alia, primary energy consumption, thermal comfort, investment cost and environmental impact. One of the most effective measures in optimizing building energy efficiency is upgrading the thermal performance of the building envelope. The building envelope provides a thermal barrier between the indoor and outdoor environments, and its standard determines a building's energy requirements. It is clear that the more heat that escapes via an external envelope, the more heat that has to be produced for the comfort of the users. Therefore, heat losses through the building envelope should be eliminated or at least limited [9]. Many researchers have focused on this important aspect by developing computer models for improving its design [10-13]. Variables considered in these models include thermal properties and thickness of the building envelope, external and internal shading systems, and glazing area.

To prioritise existing buildings for retrofitting and to optimise the retrofitting strategy, it is necessary to assess their current thermal performance. Heat loss via the building envelope can be considered to comprise two components: heat lost through the plain parts, described by the thermal transmittance (U-value) and heat loss via thermal bridging. A thermal bridge is a part of the building envelope which has lower thermal resistance due to a different geometry, conductivity or fabric thickness, and

this can significantly impact on the overall thermal standard of the building envelope and the energy efficiency of a building. The thermal bridging heat loss through a linear thermal bridge is usually quantified in terms of a linear thermal transmittance (Ψ-value), which is the steady state heat flow rate per unit length of bridge per unit temperature difference between the indoor and outdoor environments. Default Ψ-values for standard building details can be found in ISO 14683 [14] though their typical accuracy varies between 0% to 50% [14]. More accurate Ψ-values (±5%) can be obtained from numerical calculations [14]; however, this requires a detailed knowledge of the internal structure of the building envelope together with the properties of the component parts, which may have deteriorated with time. This requirement makes the numerical approach unsuitable for many existing buildings. In this case, the thermal bridging heat loss should be measured in-situ. This requires the development and implementation of non-destructive assessment tools.

The infrared thermography technique (ITT) may be used as a non-invasive method of measuring the building thermal performance. Thermal images provide detailed information about the internal or external surface temperature distribution, and this has been used by a number of researchers to quantify the thermal performance. Kylili et al. [15] reviewed applications of ITT for building diagnostics. To date, most of the work has focussed on the determination of the U-value of plain building components and a limited number of researchers [16-19] have applied the ITT to quantifying the Ψ-value. Benkő [16] used the outdoor ITT on site and expressed the heat loss associated with thermal bridging as a ratio that reflects the increase of heat loss in the presence of a thermal bridge. A similar approach was presented by Asdrubali et al. [17] who used indoor ITT for a laboratory-based study. To fully quantify the heat loss caused by thermal bridges, they multiplied the experimentally-determined ratio by the U-value of the plain element measured by a heat flow meter (HFM). For both studies, the surface heat transfer coefficient was treated as a constant value along the whole area of the thermogram. Bianchi et al. [18] validated the Asdrubali methodology on a full-scale building and, as the construction of the building envelope was known, they calculated the U-value, instead of measuring it with a HFM. O'Grady et al. [19] developed a methodology of quantifying the Ψ-value by means of the indoor ITT solely. This methodology considers the convective and radiative

coefficients correlated with surface temperatures. Therefore, these coefficients were evaluated for the whole range of temperatures recorded in the infrared image (IR image). This approach improved the accuracy significantly and was validated in a hot box device. It is usually easier to control the environmental conditions for ITT inside a building than outside. Additionally, as reported by Fox et al. [20], indoor ITT is more suitable to visualize building envelope defects, such as service faults, ventilation, moisture or conductivity discontinuation. However, for an occupied building, it may not be possible to undertake the indoor thermographic survey and, in that case, outdoor ITT is the only option.

The quantitative outdoor infrared thermography technique (ITT) is based on the surface energy balance principle applied to the external surface of the building envelope, and it is influenced significantly by weather conditions. Over the past number of years, researchers have aimed to define the impact that these parameters have on the outdoor ITT and to establish the most suitable weather conditions for it. Some weather factors, such as rain [21] or solar irradiation [21-22] should be always avoided during the outdoor thermography survey. Lehman et al. [23] simulated the influence of the solar irradiation on six building walls with different internal structures. Simulations revealed that the increase in wall surface temperatures depends on the thermal mass of the wall so the waiting period for the influence of solar irradiation to dissipate before performing ITT is dependent on the wall structure. In order to avoid direct sunlight, Albatici and Tonelli [24] recommended evenings and early mornings as the most suitable times for the outdoor ITT. Lehman et al. [23] and Albatici et al. [21] recommended undertaking the thermographic survey with a fully overcast sky in order to achieve a sky temperature similar to the air temperature and thus minimize radiative heat losses of the building element to the sky. Considering the difference between the indoor and outdoor air temperatures for the thermographic survey, various recommendations have been found. According to infrared camera manufacturers' FLIR manual [25] and to Fokaides et al. [26], it is important to have a minimum temperature difference of 10ºC between inside and outside. Other manufacturers [27] recommend a 15°C difference between the indoor and outdoor air temperature. Albatici et al. [21] suggest a minimum of 10°C, and preferably at least 15°C.

Many researchers have aimed to define the wind speed limit for accurate outdoor thermographic survey. Lehman et al. [23] suggested that pulsating wind up to 2 m/s has a negligible influence on the thermography and showed that surface temperature disturbance caused by the wind decay within a few hours. According to Balaras and Argiriou [28] and Albatici et al. [21], external surveys should be avoided under windy conditions, (exceeding 5 m/s). Additionally, Albatici et al. [21] recommended that the hourly average of free stream wind in the building vicinity within 24 hours should be below this limit.

This paper presents a methodology for characterizing the Ψ-value of building components using outdoor ITT. The approach is an adaptation of the methodology developed for indoor ITT described in [19] and accounts for the influence of wind velocity on the external surface temperatures. The methodology is developed using experimental and numerical approaches. The experimental study is carried out in laboratory conditions in a hot box device. This arrangement allows for isolation of the wind effect by keeping the indoor and outdoor air temperatures at the same level throughout testing and by eliminating the effect of solar irradiation. Using infrared images, the wind impact on heat loss through both thermal bridging and uniform wall components at different wind velocities is observed. To evaluate the Ψ-value, the external convective heat transfer coefficients (h_{ce}) are also required and different approaches to their evaluation are investigated. Ψ-values evaluated by means of outdoor ITT are validated against those obtained using the hot box measurement method [29].

Numerical modelling is undertaken to evaluate the standard Ψ-value in accordance with EN ISO 10211 [30] using two-dimensional heat transfer finite element models. This Ψ-value is evaluated using standard boundary conditions and specifically using external convective coefficient corresponding to a wind velocity of 4 m/s, in accordance to EN ISO 6946 [31]. To compare the in-situ thermal bridge performance to the standard value, measurements should be carried out at this exact wind speed. As it is considered very restrictive to undertake in-situ measurements only at this wind velocity, an approach is developed that can account for different wind conditions. In this work, numerical models are developed for a wide range of wind velocities and used to develop adjustment factors to convert the Ψ-value at a non-standard wind

velocity to the standard value. These adjustment factors are then validated against the experimental values.

4.4. Different approaches to accounting for wind effects on a building external surface

The external surface of a building continually interacts with the surrounding environment via thermal radiation and convection. Thermal radiation includes the energy that is emitted and absorbed by an external building surface to or from the surroundings. Convection is the interaction between the building and moving air and is dependent on the temperature difference between the surface and air, the speed and the direction of wind, and also the geometry and coarseness of the surface. It occurs in two modes at the surface, namely, free convection and forced convection. Free convection involves air flow movement that is caused by buoyancy forces as a result of changes in air density near the building surface. Forced convection describes air movement that is induced in a natural environment by wind [32,33]. This mode predominates in outdoor conditions, where wind strongly influences heat losses from building envelope surfaces.

The interaction between the outdoor environment and the building is described using the external surface heat transfer coefficient h_e that includes radiative and convective components. Evaluation of these coefficients is necessary in order to define external boundary conditions of a building envelope surface. These boundary conditions may then be implemented in heat transfer analytical and computing simulations, or in calculations from in-situ measurements, such as outdoor ITT. The radiative coefficient h_{re} is not directly influenced by the wind velocity and can be found from Equation (4.1):

$$h_{rx} = \varepsilon\sigma(T_{sx} + T_i)(T_{sx}^2 + T_i^2) \qquad (4.1)$$

where ε is the surface emissivity, σ is the Stefan-Boltzmann constant and T_s and T_e are the surface and air temperatures, respectively.

According to well-established heat transfer theory [32], several features should be taken into account when determining the value of the convective coefficient h_{ce}. Such features include the shape of the surface, the flow conditions (laminar or turbulent) and the physical properties of the air. Calculating the external heat transfer convective coefficient from Equation (4.2) takes all these aspects into account:

$$h_{ce} = \frac{Nu\, k}{l_{ch}} \qquad (4.2)$$

where Nu is the Nusselt Number, which is dependent on the type and conditions of flow, k is the thermal conductivity of air and l_{ch} is the characteristic length over which h_{ce} applies.

Thermal and hydrodynamic boundary layers are formed around building surfaces exposed to air temperatures (different to surface temperatures) and to the wind motion, respectively. A building component interacts with the air in these boundary regions. A thermal boundary layer is a region where the air temperature changes from the surface temperature into the free stream air temperature. A hydrodynamic boundary is a thin air layer in which the wind velocity changes from 0 m/s at the surface to the free stream velocity at some distance from the surface. Within this hydrodynamic boundary layer, the wind flows at a local velocity.

Different approaches to calculating the external convective coefficient have been developed. Researchers have aimed to produce accurate predictions, while simultaneously simplifying the specific calculations required. The first researchers to develop an approximation relationship between h_{ce} and the wind velocity were Nusselt and Jürges [34]. Their approximation was based on a wind tunnel experiment investigating parallel flow over a flat plate. They suggested that the convective coefficient could be calculated from linear interpolation for wind velocities lower than 5 m/s and using a power law for higher wind velocities. Those two scenarios can be

written as Equation (4.3) and Equation (4.4), respectively, and are known as Jürges' equations.

$$h_{ce} = a + bw \qquad w < 5m/s \qquad (4.3)$$

$$h_{ce} = cw^{0.78} \qquad w \geq 5m/s \qquad (4.4)$$

where w is the wind speed in m/s and constants *a*, *b* and *c* are given in Table 4.1. Cole and Sturrock [34] confirmed that Equation (4.3) includes a radiative component. This component is omitted while the approximating convective coefficient for higher wind velocities using Equation (4.4) [35].

Table 4.1. Constants *a, b* and *c* for Equations (4.3) and (4.4).

Constants	*Nusselt and Jürges* [34]	*McAdams* [36]	*Albatici et al.*[21] *Dall'O' et al.* [37]
a	5.8	5.7	0
b	4.1	3.8	3.8054
c	7.3	7.2	-

McAdams [36] published a recast of these empirical equations with slightly different constants, also given in Table 1, and since then the recast versions have been widely used. Palyvos [35] undertook a comprehensive comparison of different approaches to calculating the value of convection coefficients by surveying more than fifty correlations available in the literature. Emmel et al. [38] showed that convective coefficients strongly affect the result of thermal simulations and should, therefore, be applied precisely to fully describe the wind conditions. Sartori et al. [39] investigated the relative accuracy of the different approaches and found that the convective coefficients calculated using the Nusselt correlations tend to be the most accurate as only this approach takes into account the distinction between laminar and turbulent

flow and the characteristic length over which the convective coefficient is applied. This characteristic length corresponds to the real path of the wind over the surface and it can have a significant influence on the values of the convective coefficient for the surface considered. They showed that the coefficients calculated for turbulent and for laminar flow decrease with an increase in characteristic length, which is in agreement with the boundary layer theory.

Evaluation of the external heat transfer coefficients is an important step in the evaluation of building envelope performance using the outdoor ITT. Researchers who evaluated *U*-values of homogeneous building elements by means of the outdoor ITT evaluated surface heat transfer coefficients various ways. Albatici et al. [21] described h_{ce} using a modified Jürges' equation with the constants presented in Table 1. However, they simplified this to Equation (4.5) and applied the Stefan-Boltzmann law to express the radiative component. Their *U*-value formula, described by Equation (4.6), is valid for wind velocity lower than 5 m/s.

$$h_{ce} = 3.8054w \tag{4.5}$$

$$U = \frac{5.67\varepsilon\left[\left(\frac{T_s}{100}\right)^4 - \left(\frac{T_e}{100}\right)^4\right] + 3.8054w(T_s - T_e)}{T_i - T_e} \qquad w<5m/s \tag{4.6}$$

Albatici et al. [21] used this methodology to assess five different light-weight and heavy external walls of an experimental building. The *U*-values calculated for heavy walls using the ITT showed absolute deviations of 8 – 20% when compared to the *U*-values obtained from HFM, and around 20% in comparison to the theoretically calculated *U*-values. However, the *U*-values of light-weight walls using the ITT had absolute deviations of around 30 – 40 % compared with other methods and it was concluded that further work on developing the ITT methodology for light-weight and well-insulated walls was necessary. Similarly, Dall'O' et al. [37], used Jürges equation for evaluating the external heat transfer coefficient when evaluating the *U*-value by means of the outdoor ITT of fourteen heavy and light structure walls in existing buildings. *U*-values of these building walls, situated in suburban areas and exposed to a wind speed of 1 m/s, showed a percentage deviation of -40% to +60% between the

theoretical and the measured *U*-values using this methodology. As a much higher deviation of between -70% and +105% was found for externally insulated walls situated in the urbanized area exposed to a wind speed of 0 m/s, the method was deemed unsuitable for these types of walls.

The ISO 6946 [31] defines the standard boundary conditions that may be applied to numerical simulation, in the absence of detailed information on the boundary conditions. These conditions were evaluated for wind velocity of 4 m/s and, in practice, are widely used. The same standard provides a calculation procedure for specific boundary conditions, where the external convective coefficient h_{ce} can be obtained from Equation (4.7). This equation can be applied for any wind velocity:

$$h_{ce} = 4 + 4w \qquad (4.7)$$

In the following sections, the influence of these different approaches to evaluating the external heat transfer coefficient is considered in detail.

4.5. Experimental study

An experimental study was undertaken to assess the thermal response of building envelope components exposed to different wind velocities. To eliminate the impact of other weather factors on the thermal behaviour of the tested building components, the experimental study was conducted in a controlled laboratory environment using a guarded hot box device [29]. Hot box measurements of heat flow rate through components containing thermal bridges were carried out at three different wind velocities. IR images were then taken while the specimens were still mounted in the device immediately after completion of hot box measurements. This allowed for assessment of the suitability of a proposed external ITT methodology under variable external wind exposures.

4.5.1. Experimental set up

The experiment in the hot box device (as shown in Fig. 4.1) was designed to evaluate heat losses through thermal bridging situated in building envelope components for free stream wind velocities between 0.5m/s and 4m/s. The device comprises two chambers: the guarding box (hot side) represents indoor conditions while the climatic box (cold side) simulates the outdoor conditions. Tested specimens were placed successively into a surround panel. To control the environmental conditions close to the exposed faces of the specimen, baffles were mounted around the specimen on both sides. In order to simulate free convection conditions on the hot side and to ensure that the specimen was exposed to a uniform air temperature, the air within the baffle had a uniform velocity of 0.1 m/s. The cold baffle was fastened to the cold surface of surround panel. The heat flow rate through each specimen was measured with the metering box and the air temperature and wind velocity between the baffles and specimen were continually monitored during the tests.

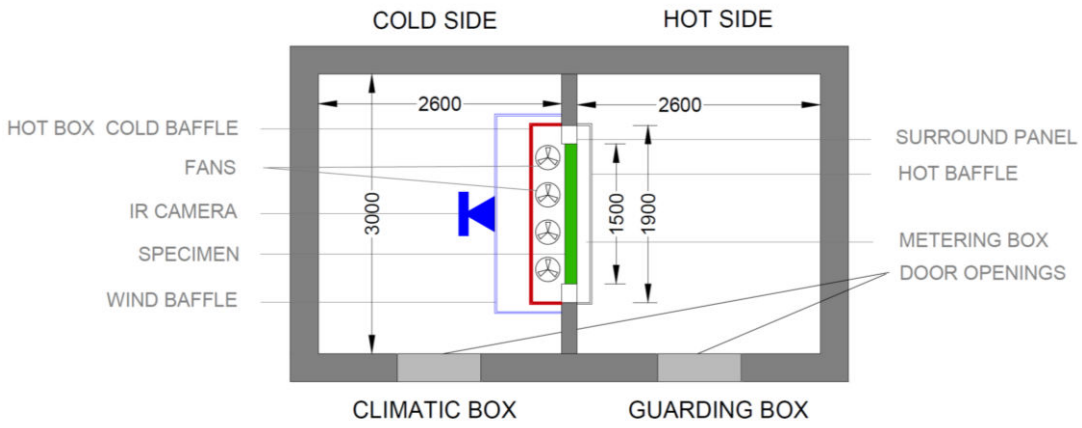

Fig.4.1.Experimental set up.

On completion of the hot box testing, the cold baffle was replaced with a new wind baffle, made of plywood, with holes to accommodate the IR camera. This was necessary because, when the original cold baffle was removed from the specimen to take the IR images, the wind changed its speed and direction. With this new baffle, it

was possible to take the images under the controlled wind conditions.

4.5.2. Geometries and description of the specimens

Two specimens containing thermal bridges and a third plain specimen were tested. The specimens were made of structural insulated panels (SIP) comprising 100 mm thick low conductivity extruded polystyrene insulation (XPS) boards and 15 mm thick oriented strandboard (OSB) sheathing on each side. All specimens were 1.5 m long, 1.5 m high and had a thickness of 130 mm. Specimen 1, presented in Fig. 4.2, is a SIP panel containing a steel square hollow section (SHS) of dimensions 100x100x5mm, filled with XPS. This specimen represents a thermal bridge created by a steel column, often used as a structural member of a building external envelope.

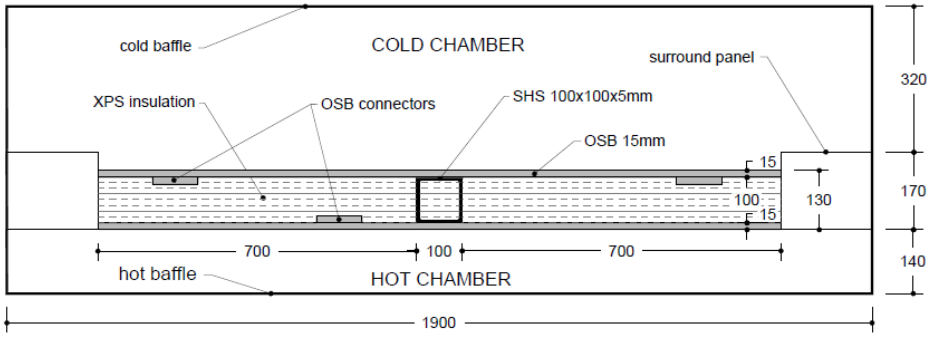

Fig. 4.2. Cross-section of Specimen 1 inserted into hot box.

Specimen 2, shown in Fig. 4.3, is a SIP panel with two steel square hollow sections (SHS) filled with XPS (dimensions 100x100x5mm). This specimen represents adjacent thermal bridges situated about 50mm apart.

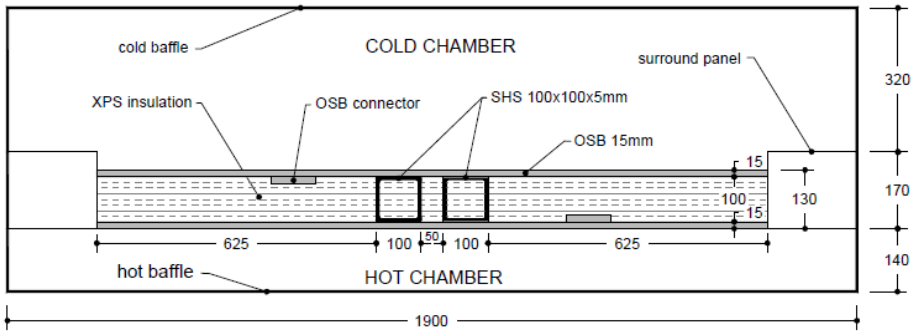

Fig. 4.3. Cross-section of Specimen 2 inserted into hot box.

Specimen 3, without thermal bridging, was tested in order to allow for the determination of the Ψ-value for Specimens 1 and 2.

4.5.3. Hot box testing

The three specimens, described in the previous section were tested in accordance to the EN ISO 8990 [29] standard. For these tests, different uniform wind velocities were induced between the cold baffle (marked in red in Fig.1) and the specimen surface. For each specimen, tests were carried out at three different wind velocities: 0.5m/s, 1.5 m/s and 4 m/s. As the wind velocities were average values measured over a period of time, it was not possible to control the wind conditions to achieve these exact values; the average values for each test are reported in Table 4.2, together with their standard deviations. The wind velocity was measured every two minutes, at mid-height and midway between the specimen surface and the cold baffle, using thermoanemometers INT 512 having a measurement range of 0.2 – 10 m/s. The air temperatures during all the tests were kept at the same level, around +25°C on hot and -5°C on the cold side.

Table 4.2. Conditions for hot box testing of Specimen 1 and Specimen 2.

		Specimen 1			*Specimen 2*		
		Case 1	*Case 2*	*Case3*	*Case 1*	*Case 2*	*Case3*
w_e	*m/s*	**0.52**	**1.43**	**4.35**	**0.52**	**1.54**	**4.35**
SD w_e	*m/s*	0.06	0.12	0.13	0.06	0.07	0.13
w_i	*m/s*	0.1	0.1	0.1	0.1	0.1	0.1
T_e	*°C*	-4.88	-4.90	-5.14	-4.66	-4.85	-5.17
T_i	*°C*	24.77	24.73	24.74	24.66	24.67	24.67
$T_{se,b}$	*°C*	-4.89	-4.94	-5.18	-4.69	24.67	-5.20
$T_{si,b}$	*°C*	24.25	24.24	24.25	24.05	24.02	24.00
T_{ne}	*°C*	-4.89	-4.92	-5.18	-4.69	-4.87	-5.20
T_{ni}	*°C*	24.41	24.39	24.40	24.24	24.23	24.21

In Table 2, environmental temperatures on the hot side (T_{ni}) were obtained as a weighting of hot air temperatures recorded during testing (T_i) and hot baffle surface temperatures ($T_{si,b}$). Similarly, the environmental temperatures on the cold side (T_{ne}) were obtained as a weighting of cold air temperatures (T_e) and a cold baffle surface temperatures ($T_{se,b}$). This was undertaken to meet requirements of EN ISO 8990 [29] and ISO 12567-1 [40]. These standards state that for calculations based on heat flow rate measured in a hot box (such as Ψ-value), an environmental temperature T_n should be used. The full procedure of obtaining the environmental temperature T_n is presented in [19].

Testing started with the insertion of Specimen 1 into the hot box device. A wind velocity of around 0.5 m/s for the first case was created by adjusting the power of the fans installed above the cold baffle. This arrangement created an upward wind. Once the desired wind velocity was achieved, the power of the vents was kept at the same level. Concurrently, the conditions in the hot chamber were set to allow for free convection with a wind velocity of 0.1 m/s directed downward. The required wind velocity and air temperatures in each chamber were kept fixed for a period of a few hours from the moment when a steady state had been reached. The measurements taken facilitated the calculation of the heat flow rate through the specimen $\dot{Q}_{sp}$. This procedure was repeated for the higher wind velocities of about 1.5 m/s and 4 m/s.

To assess the thermal bridging heat loss q_{TB} using the hot box, the heat flow rate through an identical plain specimen $\dot{Q}_{plain}$ at similar wind velocity is required. The thermal bridging heat rate q_{TB} represents the additional heat loss through the specimen caused by presence of the linear thermal bridge per unit length of the thermal bridge.

Having values of heat flow rate for all specimens, q_{TB} is obtained from Equation (4.8) and finally the Ψ-value from Equation (4.9):

$$q_{TB} = \frac{\dot{Q}_{sp} - \dot{Q}_{plain}}{H} \quad (4.8)$$

$$\Psi = \frac{q_{TB}}{T_{ni} - T_{ne}} \quad (4.9)$$

This procedure was repeated for Specimen 2. $\dot{Q}_{plain}$ for Specimen 3 was measured in the hot box device in similar conditions to Case 2. For other cases, the heat flow rates were derived from CFD simulations.

4.5.4. ITT testing

In this part of the experiment, the heat loss via thermal bridging at different wind velocities was assessed by means of the outdoor ITT. In this case, the heat loss was calculated using the surface temperatures on the cold side of the specimen recorded during a thermographic survey. The aim was to carry out all ITT tests under the same conditions as the hot box testing. However, the replacement of the original cold baffle with the new wind baffle (marked in blue in Fig. 4.1) made the control of the air temperature to -5°C not possible. The air temperature in this chamber T_e was measured during tests. The wind velocity for each of the ITT tests was kept at a comparable level to that in the hot box tests. Table 4.3 presents conditions for both specimens for the ITT testing.

Table 4.3. Conditions for the ITT testing of Specimen 1 and Specimen 2.

		Specimen 1			*Specimen 2*		
		Case 1	*Case 2*	*Case3*	*Case 1*	*Case 2*	*Case3*
w_e	*m/s*	**0.47**	**1.57**	**4.27**	**0.58**	**1.54**	**4.18**
w_i	*m/s*	0.1	0.1	0.1	0.1	0.1	0.1
T_e	*°C*	-7.2	-7.2	-7.3	-7.0	-6.5	-6.9
T_i	*°C*	24.89	24.74	25.01	24.64	24.61	24.65

Similarly to the hot box testing, the required wind velocity for each case was induced by adjusting the power of the vents installed above the cold baffle. After a steady state with the desired wind velocity and temperature established, the ITT was performed. This procedure was repeated for all test cases. Due to the fact the recorded temperatures by the IR camera oscillate even when captured under the steady conditions, a series of IR images of Specimen 1 and Specimen 2 were taken at each wind velocity. From each IR image, three horizontal rows of pixels at mid-height were extracted. The measured temperatures of these rows were used to create an IR line, which represents the temperature variation along the specimen. A typical IR image, with an IR line is shown in Fig. 4.4. To smooth the transition of surface temperatures from one pixel to the next one, each pixel on the IR line represents the mean temperature of the middle line pixel and its eight neighbouring pixels. This IR line shows fully the surface temperature disturbance caused by the vertical thermal bridge. Then from all these IR lines for each case, a mean IR line was created. As the specimens were symmetrical, it was only necessary to create IR lines for half of the specimen. Fig. 4.5 shows the IR lines from each image together with the mean IR line for one of the tests. The thermal bridge presented on this figure is caused by a steel column in a structural insulated panel (SIP) and its geometry is shown in Fig. 4.2.

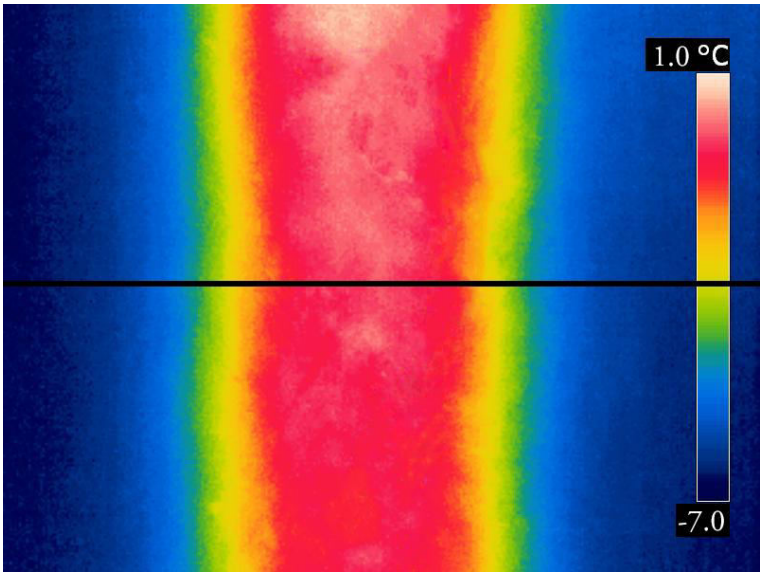

Fig. 4.4. A sample of an infrared camera image of Specimen 1, Case 2.

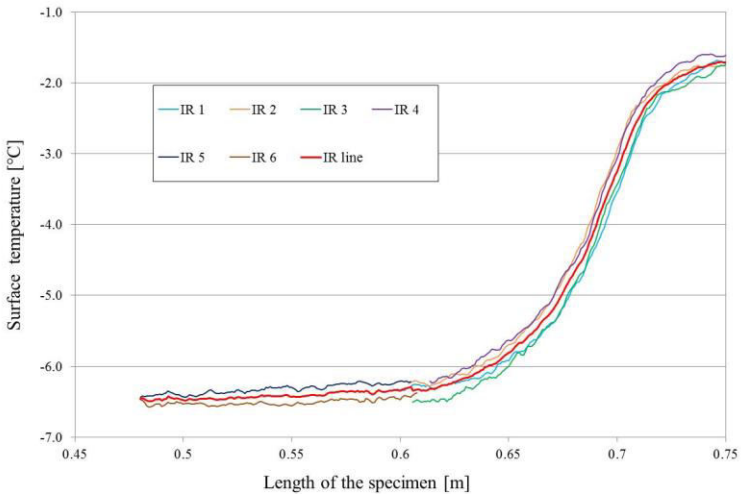

Fig. 4.5. Mean IR line created from a series of thermograms of Specimen 1, Case 2.

The horizontal field of view represents the length of the object captured by an IR camera and it depends on the camera resolution and on the distance between the camera and the surface. Throughout this experiment, the distance at which IR images were taken was dictated by the construction of the wind baffle. The IR camera used in this experiment, a FLIR T335 with resolution 320 x 480, was equipped with 25° lens. As the length of each IR image was 0.314 m. It was necessary to use more than one

image to capture the full region influenced by the thermal bridge. Merging of IR lines produced from these images was then carried out. This is seen in Fig. 4.5, were merging occurs at a specimen length of around 0.60 m.

4.6. Outdoor ITT methodology

The mean IR line was used to calculate the Ψ-value using a methodology similar to that reported by the authors for indoor ITT [19] but adapted to account for outdoor boundary conditions. It was assumed that, for a vertical thermal bridge, a horizontal line in the mid-height of the thermogram is sufficient to represent the average temperature distribution caused by the tested thermal bridge [19]. These temperatures were also the most distant from the connection with surround panel on the top and on the bottom of the specimen that may cause some additional disturbances. In reality, other factors could additionally disturb the thermogram, such as screw fixing or furniture and it is important to eliminate them while calculating Ψ-value. This is achieved by creating an IR line where thermal bridge influence can be clearly seen and where it is not perturbed by other factors. In forced convection, the wind velocity varies along the vertical direction. The IR line created at mid-height of the specimen or, in practice, of the building element, shows the temperature distribution impacted by the averaged wind conditions. Such a simplification was necessary while developing a practical method that can be implemented on site in real buildings. The methodology enables quantification of the heat loss associated with the presence of a thermal bridge using only ITT. It is based on the surface energy balance applied to the outdoor building envelope surface. According to this balance, the heat flow rate for each pixel (q_x) on the IR line is found using Equation (4.10):

$$q_x = l_x[(h_{cx}+h_{rx})(T_{sx} - T_e)] \quad (4.10)$$

Similarly, by calculating q_{xu} for a pixel outside the thermal bridge zone of influence using Equation (4.10) and multiplying it by the number of pixels on the IR line, the heat flow rate through an identical building component with no thermal bridge

can be predicted. The thermal bridge heat flow rate for each pixel q_{xTB} can then be found using Equation (4.11):

$$q_{xTB} = q_x - q_{xu} \quad (4.11)$$

By summing up q_{xTB} for all pixels on the IR line, the thermal bridge heat flow rate q_{TB} is found:

$$q_{TB} = \sum q_{xTB} \quad (4.12)$$

Finally, by dividing this thermal bridge heat flow rate q_{TB} by the temperature difference between the indoor and outdoor environments, the Ψ-value is determined.

$$\Psi = \frac{q_{TB}}{T_i - T_e} \quad (4.13)$$

In order to quantify the heat flow rate for each pixel q_x using Equation (4.10), the convective and radiative heat transfer coefficients must be determined. Since the methodology is developed for outdoor ITT use, the external convective coefficient h_{ce} for forced convection is used. Two approaches to calculating these coefficients are investigated: using heat transfer theory by means of Nusselt number and using Jürges' equation.

4.6.1. Evaluating heat transfer coefficients using heat transfer theory

The convective coefficient is determined by applying Equation (4.2) to each pixel:

$$h_{cex} = \frac{Nu_x \, k_x}{l_{ch}} \quad (4.14)$$

The Nusselt number (Nu) is a function of the Reynolds (Re) and Prandtl (Pr) numbers in forced convection.

With forced convection, two types of flow conditions can be distinguished, namely, laminar and turbulent flow. Flow induced by wind over a flat surface is first dispersed from the edge in a laminar mode and this subsequently transforms into turbulent flow. These boundary layer flows are characterized by Reynolds number, which is expressed as the ratio of the inertia to viscous forces:

$$Re_x = \frac{w\, l_{ch}}{v_x} \qquad (4.15)$$

Conventionally, the transition from laminar to turbulent flow occurs at the location for which the critical Reynolds number is 5 x 10^5. However, the transition can occur at different locations as influenced by roughness of the surface and/or disturbances of the flow. When the flow is induced artificially, by fluid machines such as fans, compressor or pumps, fully turbulent flow takes place along the entire surface [32].

As the relationship between the Nusselt number and the Reynolds (Re) and Prandtl (Pr) numbers depends on the flow conditions, it is described differently for laminar and turbulent flow. The Nusselt number correlations presented by Equations (4.16) – (4.18) were developed for parallel flow over the surface of a flat plate. However, Rowley and Eckley [39] found experimentally that there was an insignificant reduction in the convection coefficient as the angle between the surface and the wind stream was increased from 15° to 90°. Therefore, Equations (4.16) – (4.18) can be also applied to characterize flow in a direction other than parallel to external building component surface.

For laminar flow, the Nusselt number is calculated using Equation (4.16):

$$Nu_x = 0.664 Re_x^{1/2} Pr^{1/3} \qquad (4.16)$$

A correlation that accounts for mixed flow, in the transition from laminar to turbulent flow, is expressed in Equation (4.17). This equation should be used while evaluating the Nusselt number for real outdoor environments in the absence of any disturbances of the flow along the surface of the surveyed building component:

$$Nu_x = (0.037Re_x^{4/5} - 871)Pr^{1/3} \quad (4.17)$$

However, if the flow is disturbed, for example by a tree branch, an electric wire or by the surface roughness, it tends to be fully turbulent over the whole length [39]. In this case, the Nusselt number should be evaluated from the correlation expressed by Equation (4.18) that accounts for turbulent flow conditions. This equation is used in the analysis covered in this study as wind speed in the experiment was created by fans resulting in fully turbulent flow:

$$Nu_x = 0.037Re_x^{4/5}Pr^{1/3} \quad (4.18)$$

The external radiative coefficient h_{re} is calculated for each pixel on the IR line using Equation (4.19):

$$h_{rx} = \varepsilon\sigma(T_{sx} + T_e)(T_{sx}^2 + T_e^2) \quad (4.19)$$

4.6.2. Determination of heat transfer coefficients for test specimens

As seen in Equation (4.14), the convective coefficient is a function of the Nusselt number, air conductivity k, and characteristic length l_{ch}. For the tests specimens in the hot box, the characteristic length is constant and equal to the specimen height. As the Prandtl number is also constant, the changes in Nusselt number are a function of the Reynolds number, which depends on the wind velocity w and the kinematic viscosity v. Since the wind velocity can be assumed to be the same along the whole length of the specimen, it can be deduced that the air conductivity k and the kinematic viscosity v are the only factors which cause a variation in the convective coefficient calculated for each pixel of the IR line. These properties are evaluated at a film temperature, which is the arithmetic mean of the surface temperature of the pixel and the air temperature. Table 4.4 presents the average convective coefficients calculated for each

of the three cases for Specimen 1 and Specimen 2, for the turbulent flow conditions (Equation (4.17)) present during testing. Each case represents a different wind velocity induced along the specimen's cold surface. The average h_{ce} is the arithmetic mean of all convective coefficients on the IR line. The deviations between the minimum value of h_{ce} (on the thermal bridge surface) and the maximum value (on the uniform part of the specimen away from the thermal bridge) are very small and amount for Specimen 1 to 0.02 W/(m^{2}K) for Case 1, 0.04 W/(m^{2}K) for Case 2 and 0.06 W/(m^{2}K) for Case 3. It was found that the Ψ-values determined using the average values of h_{ce} and pixel specific values are equal. This finding contrasts with the case for indoor ITT where it was found that applying a convective coefficient (h_{ci}) evaluated for each pixel was necessary to accurately calculate Ψ-value by means of the indoor ITT [19], under natural convection. In natural convection, the convection coefficient is related to the difference between the surface and the air temperature. Surface temperatures of a component containing thermal bridges varied significantly, therefore variable *hci* related to these variances, improved the results accuracy. In the force convection, wind is the predominant factor in evaluating the convective coefficient, therefore does not change its value at varied surface temperatures.

The strong dependency of h_{ce} on wind velocity is seen in Table 4.4. For Specimen 1, the average value of h_{ce} increased from 3.16 W/(m^{2}K) to 18.51 W/(m^{2}K) as the wind increased from 0.47 m/s to 4.27 m/s. These coefficients are lower than coefficients calculated using the approximate procedure in accordance with EN ISO 6946 [31], Equation (4.7). As mentioned in Section 2, h_{ce} evaluated using Nusselt number tends to be the most accurate as it takes into account, for instance, flow conditions, that is not distinguished in the standard approach.

Table 4.4. Convective coefficient values calculated using Nusselt correlation (Equation 4.17) and radiative coefficient values

		Specimen 1			*Specimen 2*		
Parameter	*Unit*	*Case 1*	*Case 2*	*Case3*	*Case 1*	*Case 2*	*Case3*
aver h_{ce}	W/(m^{2}K)	3.16	8.31	18.50	3.74	8.17	18.17
aver h_{re}	W/(m^{2}K)	4.01	3.99	3.98	4.03	4.03	4.00

The average h_{re} was calculated as an arithmetic mean of all radiative coefficients on the IR line. The differences between Ψ-values calculated from average h_{re} and Ψ-values obtained from pixel values of h_{re} are very small and are the order of 1.5%. Therefore, it is reasonable used average radiative coefficients. The average values of h_{re} for each case are given in Table 4.4 and can be seen to be independent of wind speed.

4.6.3. Evaluating heat transfer coefficients using Jürges' equation

The second method used to evaluate the external heat transfer coefficient was using Jürges' equations. In this study, only wind velocities up to 5m/s are implemented; therefore, Equation (4.3), with constants provided by McAdams [36], is applied. Sartori [39] compared the relationship between wind velocities up to 5m/s and convective coefficients expressed by different approximations. He concluded that h_{ce} evaluated by Jürges' equation increases with increasing wind velocity at the same rate as that obtained using the Nusselt correlation for fully turbulent flow (Equation 4.18). Therefore, Jürges' approach is included in this study as an alternative way to characterize turbulent flow. Values of coefficients evaluated using Jürges' equation also account for radiative losses [41] and they are constant along the whole length of the specimen (see Table 4.5). Table 4.5 also shows the total average heat transfer coefficient for each case determined by adding the average h_{re} and average h_{ce} values given in Table 4.4. The maximum difference in the heat transfer coefficients calculated using the two approaches is 5.3%.

Table 4.5. External heat transfer coefficients using Jürges' equation and heat transfer approach

		Specimen 1			*Specimen 2*		
Parameter	*Unit*	*Case 1*	*Case 2*	*Case 3*	*Case 1*	*Case 2*	*Case 3*
Jürges $h_{ce}+h_{re}$	W/(m^{2}K)	7.49	11.67	21.93	7.90	11.55	21.58
Nusselt $h_{ce}+h_{re}$	W/(m^{2}K)	7.17	12.30	22.48	7.77	12.20	22.17
Difference	%	4.5	5.1	2.5	1.7	5.3	2.7

4.7. Experimental results and discussion

In this section, the results obtained from the hot box device and from the ITT survey taken at different wind velocities are presented and discussed. Surface temperature distributions measured by the outdoor ITT are presented and then the heat losses via thermal bridging expressed as linear thermal transmittance Ψ-values for each specimen tested at three different wind velocities are presented.

4.7.1. Surface temperatures measured by the outdoor ITT

Temperature distributions of each specimen were obtained at different wind velocities. In each case, several thermograms were recorded and a mean IR line representing the horizontal variation of the temperature distribution for each specimen was evaluated. In Fig. 4.5, IR lines from 6 thermograms and the mean IR line are shown.

Obviously, surface temperatures decrease when exposed to increased wind velocity. Fig. 4.6 and Fig. 4.7 present surface temperature distributions for the left

halves of Specimens 1 and 2 for all three cases. The maximum temperature occurs in the middle of the thermal bridge in both cases. This corresponds to a distance of 0.75 m for Specimen 1 and 0.626 m for Specimen 2. Figures 4.6 – 4.7 clearly demonstrate the correlation between the wind velocity and surface temperatures.

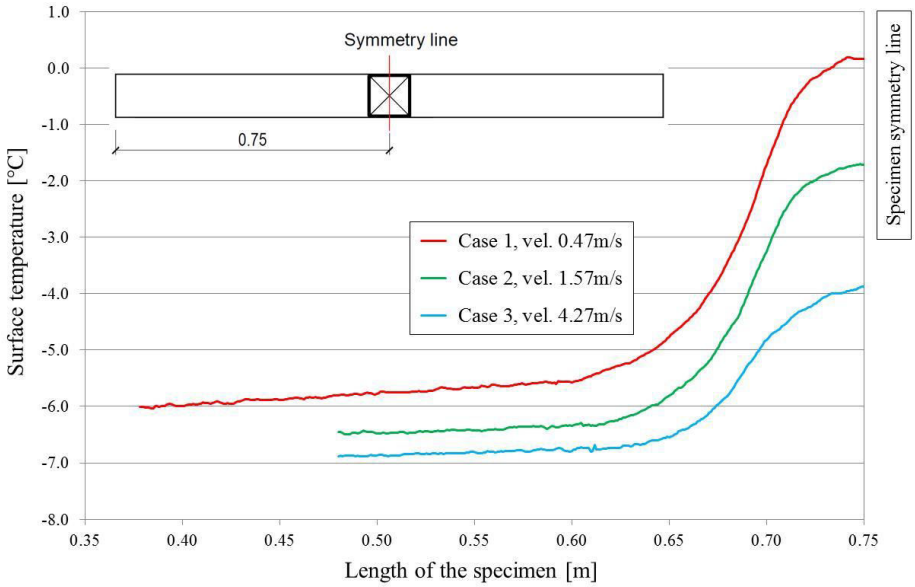

Fig. 4.6. The surface temperature distribution of Specimen 1 obtained with the ITT for three cases.

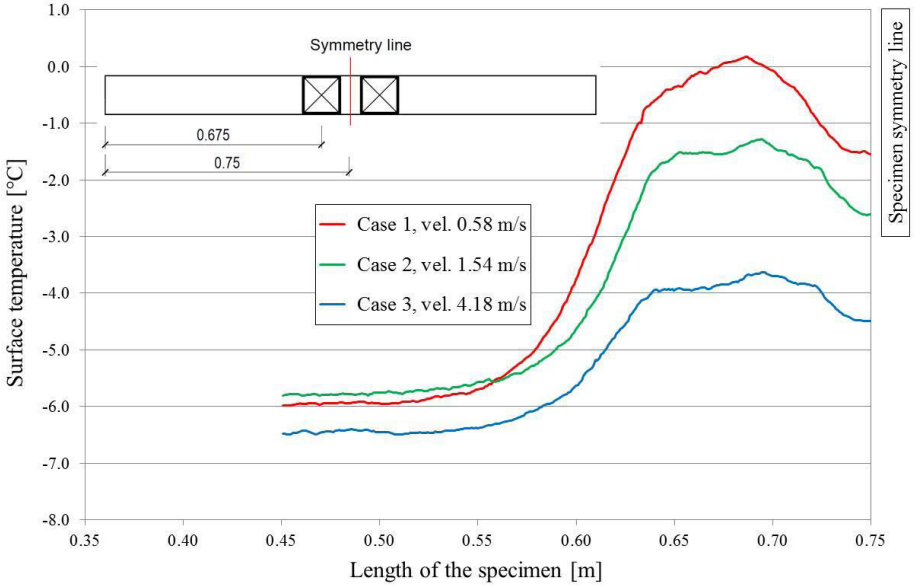

Fig. 4.7. Surface temperature distribution of Specimen 2 obtained with the ITT for three cases.

Table 6 gives a summary of the temperatures on the thermal bridge (T_{TB}) and the uniform temperature (T_u) on the plain part of the specimen for each case. The T_{TB} was measured in the middle of the thermal bridge, at distance of 0.75 m for Specimen 1 and 0.675 m for Specimen 2. Both temperatures, T_u and T_{TB}, were measured at the specimens' mid-height. In addition, the standard deviations *(SD)* for these temperatures are given. The wind velocity has a greater impact on the surface temperatures on the thermal bridge than those on the plain surface. For Specimen 1, the plain temperature, measured at a wind velocity of 1.57m/s, decreases by 0.46℃ whereas the temperature on the thermal bridge decreases by 1.90℃ when compared to the surface temperatures captured with the wind velocity of 0.47m/s. Increasing the wind velocity to 4.27m/s results in a further decrease in the plain temperature of 0.41℃, compared to 2.14℃ on the thermal bridge. As a result, the difference between the minimum and maximum surface temperatures decreases as the wind velocity increases. This difference for Specimen 1 is 6.17°C at 0.47 m/s, 4.73°C at 1.57 m/s and 3.00°C at 4.27 m/s. A similar trend is seen for Specimen 2.

Table 4.6. Surface temperatures on the plain part T_u and on the thermal bridge T_{TB} from ITT

		Specimen 1			*Specimen 2*		
Parameter	*Unit*	*Case 1*	*Case 2*	*Case3*	*Case 1*	*Case 2*	*Case3*
w_e	*m/s*	**0.47**	**1.57**	**4.27**	**0.58**	**1.54**	**4.18**
T_u	°C	-6.01	-6.47	-6.88	-5.93	-5.79	-6.49
(SD)		(0.08)	(0.06)	(0.22)	(0.10)	(0.07)	(0.08)
T_{TB}	°C	0.16	-1.74	-3.88	0.17	-1.32	-3.63
(SD)		(0.14)	(0.09)	(0.11)	(0.03)	(0.06)	(0.04)

4.7.2. Thermal bridge heat loss expressed by linear thermal transmittance Ψ-value

In this section, Ψ-values evaluated by means of outdoor ITT are compared to these measured in the hot box. For the ITT calculations, the external convection coefficient h_{ce} was calculated using the two procedures described above. The Ψ-values calculated using the Nusselt number to obtain the surface heat transfer coefficients are labelled with a subscript *Nu* and those evaluated using h_{ce} from Jürges' equation, are labelled with subscript *Ju.*

Though the aim was to perform both the hot box and the ITT testing under exactly the same conditions, the wind velocities varied slightly as they represent average values measured over a period of time. However, as can be seen in Tables 4.2 and 4.3, the maximum difference between the wind velocities in both tests is 0.17 m/s and can be described as minor. Due to the necessity to change the wind baffle for the ITT tests, the temperature in the cold chamber was different: for the hot box tests this temperature was about -5°C whereas for the ITT tests it was about -7°C. The difference in air temperatures between the hot and cold chambers are summarized in Table 4.7. However, as the Ψ-values are calculated as the quotient of q_{TB} and the

difference between the cold and hot air temperatures, values from both test methods can be compared directly.

Table 4.7. Testing conditions: the difference between air temperatures in cold and hot chambers (ΔT).

	Specimen 1			*Specimen 2*		
	Case 1	*Case 2*	*Case 3*	*Case 1*	*Case 2*	*Case 3*
	ΔT [°C]			ΔT [°C]		
Hot box	29.30	29.31	29.58	28.93	29.10	29.41
ITT	32.09	31.94	32.31	31.64	31.11	31.55
difference	2.79	2.63	2.73	2.71	2.01	2.14

Ψ-values are presented in Table 4.8 for each wind velocity. As expected, heat losses via the thermal bridging increase proportionally to the increase in wind velocity along the surface of the specimens. In Case 1 for both specimens, the ITT and the hot box measured the smallest Ψ-value compared to other cases. In this case, relative deviations (*RD*) between Ψ_{Nu}-values amounted to -9% for Specimen 1 and -6% for Specimen 2, in contrast to hot box measurements. Ψ_{Ju}-values represent *RD* of -5% for both specimens. For Case 2, representing a higher wind velocity, the Ψ-values obtained from all methods increased for both specimens. The percentage deviations of Ψ_{Nu}-values from the hot box measurements are 2% and +1% for Specimen 1 and Specimen 2, respectively. The Ψ_{Ju}-values represent slightly higher deviations, equal to -6% for the first and -4% for the second specimen. For the highest wind velocities in Case 3, the largest Ψ-values were achieved in all methods. In this case, Ψ-values obtained by means of the ITT are slightly higher than those derived from the hot box. Ψ-values based on h_{ce} calculated from the Nusselt correlation are higher by 5% for Specimen 1 and 12% for Specimen 2 than those measured by the hot box. Similarly, Ψ-values based on h_{ce} calculated from Jürges equation are higher by 3% for Specimen 1 and 9% for Specimen 2 than values obtained from the hot box. However, summarizing the results it can be stated that Ψ-values determined by all methods

maintain the same trend of increasing the heat loss via thermal bridging while increasing the wind velocity. The levels of relative deviations of the results show that the outdoor ITT method has been successfully validated against the well-established hot box experimental testing for these cases. Ψ-values obtained using two different approaches to calculating external convective coefficients, namely Nusselt and Jürges correlations, are very close to each other.

Table 4.8. Ψ-values obtained from the ITT using two approaches and hot box

		Hot box	*ITT Nu*	*ITT Ju*	*Hot box*	*ITT Nu*	*ITT Ju*	*ITT Nu/ Hot box*	*ITT Ju/ Hot box*
		Ψ [W/mK]			*SD [W/mK]*			*RD [%]*	
Case 1	*Specimen 1*	0.243	0.220	0.231	0.020	0.004	0.004	-9.47	-4.94
	Specimen 2	0.421	0.395	0.403	0.021	0.009	0.009	-6.18	-4.28
Case 2	*Specimen 1*	0.253	0.249	0.237	0.010	0.020	0.019	-1.58	-6.32
	Specimen 2	0.449	0.454	0.431	0.010	0.005	0.005	1.11	-4.01
Case 3	*Specimen 1*	0.263	0.277	0.271	0.010	0.035	0.020	5.32	3.04
	Specimen 2	0.469	0.525	0.511	0.011	0.023	0.021	11.94	8.96

Fig. 4.8 shows graphically how Ψ-values, derived from three methods, for Specimen 1 and Specimen 2 are influenced by wind velocity. A power law function (Equation 4.20), with Pearson's coefficient R^2 between 0.83 and 1.00, is the best fit to describe the correlation between Ψ-values and wind velocity.

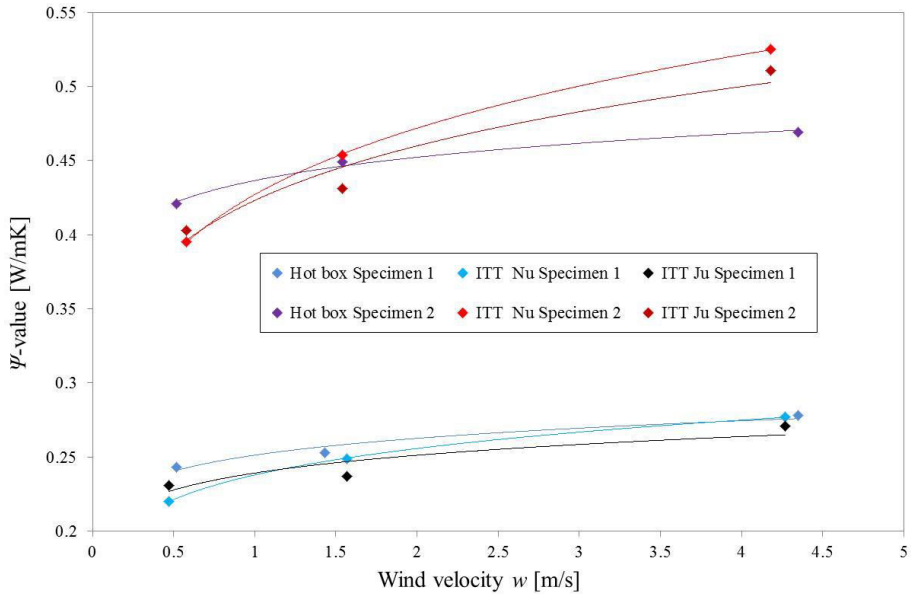

Fig. 4.8. Dependence of Ψ-values on wind velocity for Specimen 1 and Specimen 2

Coefficients d and e of the power law are given in Table 4.9 for each case.

$$\Psi = dw^e \qquad (4.20)$$

Table 4.9. Values of d and e for trend lines showed in Fig. 4.8.

	d			e		
	Hot box	*ITT Nu*	*ITT Ju*	*Hot box*	*ITT Nu*	*ITT Ju*
Specimen 1	0.2512	0.2379	0.2392	0.0637	0.1043	0.0706
Specimen 2	0.4366	0.4270	0.4231	0.0509	0.1441	0.1204

For Specimen 1, the Ψ_{Nu}-values increase more rapidly than Ψ_{Ju}-values and hot box measurements, when the wind velocity increases. As a result, the trend line describing the relation of Ψ-values obtained from the ITT using the Nusselt correlation is steeper than those obtained from the ITT using Jürges approach and from hot the box. For Specimen 2, the Ψ-values measured by the hot box increase at a significantly lower rate when wind velocity rises than the Ψ-values obtained from the ITT, using both approaches to calculating $h_{ce.}$

4.8. Comparison of measured and standard Ψ-values

The standard Ψ-value is generally predicted by means of numerical modelling, in accordance with EN ISO 10211 [30]. This standard refers to standard boundary conditions from ISO 6946 [31], that includes an external surface heat transfer coefficient calculated for a wind velocity of 4 m/s. In order to compare the as-built performance of a thermal bridge to its numerical prediction, the measurements should be taken at the standard conditions. To compare Ψ-values measured at different construction stages, for example before and after an existing building retrofitting, they also must be taken at the standard conditions. However, it is not practical to carry out in-situ measurements only at a wind velocity of 4 m/s. In this section, the Ψ-value measured by the outdoor ITT with different wind velocities is compared to the standard Ψs-value.

4.8.1. Standard Ψ-value using finite element software

In order to determine the standard Ψ-value (Ψ_S), two-dimensional heat transfer analyses were carried out for Specimens 1 and 2 using the finite element package ABAQUS. The analyses were carried out at a steady state and included the whole 1.5 m length of specimens. Material properties used for this simulation are presented in Table 4.10.

Table 4.10. Material properties applied in 2D numerical simulation

Property	*Unit*	*Symbol*	*Material*		
			OSB	*Steel*	*XPS*
Conductivity	*W/mK*	*k*	0.13 [42]	50.2 [43]	0.033 [44]
Density	*kg/m³*	*ρ*	600 [42]	7850 [45]	33 [44]
Emissivity	-	*ε*	0.93 [19]	-	-

The type of element used was a 4-noded quadrilateral linear heat transfer element (DC2D). A mesh convergence study was undertaken to establish a suitable element size. An element size of 0.005 m was selected since only a 0.25% difference between total heat flow rate q_{tot} obtained with this size element and a greater size element was recorded. Because the steel post was only 0.005m thick, a finer element size of 0.001m was used for this part. Fig. 4.9 shows a portion of the mesh for Specimen 1.

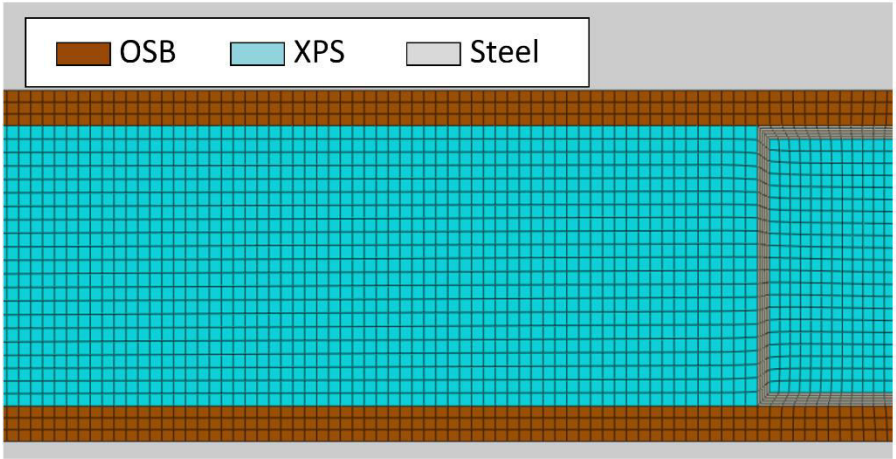

Fig. 4.9. A part of meshed Specimen 1.

The Ψ_S-values were obtained for Specimen 1 and Specimen 2 from finite numerical modelling according to the standard EN ISO 10211 [30] with standard boundary conditions recommended in ISO 6946 [31]. This standard gives different internal surface resistances R_i depending on the direction of flow in the building element considered and external surface resistance R_e calculated for wind velocity 4m/s. These surface resistances account for radiation and convection, and their reciprocals are the standard heat transfer coefficients. For these simulations, the surface heat transfer coefficient on the internal surface of a building wall h_i was 7.7 W/(m^{2}K) and the external surface coefficient h_e was 25 W/(m^{2}K). The difference between indoor and outdoor air temperatures was set at 20°C as recommended by [46]. The air temperature on the hot side was 20°C and on the cold side 0°C.

The simulations provide values for q_{tot} which is the total heat flow rate of the specimen per unit height. In order to determine the heat flow rate q_{TB} through a plain

specimen, a similar model but without a thermal bridge was created. The difference between the heat flow rate of the specimen containing thermal bridge q_{tot} and the heat flow rate of this plain specimen q_u is the thermal bridge heat flow rate q_{TB} (Equation (4.21)):

$$q_{TB} = q_{tot} - q_u \quad (4.21)$$

Then, the Ψ_S-value was calculated by dividing q_{TB} by the temperature difference between the hot and the cold sides in accordance with Equation (4.13).

4.8.2. Comparison of standard and measured Ψ-values

In this section, the Ψ-values, evaluated by means of the outdoor ITT, for the two specimens, each at three wind velocities, are compared with the standard Ψ_S-values. The Ψ-values evaluated by means of the outdoor ITT using the Nusselt number correlation to determine the convective coefficient (Ψ_{Nu}) are used for this comparison. As can be seen in Table 11, the greater the difference between the test wind velocity and the standard value of 4 m/s, the greater the difference in measured Ψ-values and the standard value. For a velocity of about 0.50 m/s, the deviation from the standard value for Specimens 1 and 2 are -23% and -24%, respectively. For a wind velocity of about 1.50 m/s, the deviation is approximately -13% for both specimens. Finally, for Case 3, with a wind velocity of 4.20 m/s, the experimental Ψ_{Nu}-values show excellent agreement, with a maximum deviation of only -2% from the Ψ_S-value. Results presented in Table 4.11 clearly demonstrate that the thermal bridging heat losses evaluated from the ITT performed under a wind velocity lower than 4m/s are underestimated. On the other hand, the Ψ-value obtained from the measurement taken at wind velocity in a region of 4 m/s is comparable with the standard value.

Table 4.11. Comparison of Ψ-value from ITT at different wind velocities to Ψ_S-value.

	standard Ψ-value	*Ψ_{Nu}-value [W/mK] obtained from:*			*relative deviation (RD) from*		
		ITT Case 1	*ITT Case 2*	*ITT Case 3*	*Case 1/ standard*	*Case 2/ standard*	*Case3/ standard*
Specimen 1	0.284	0.220	0.249	0.277	-22.5%	-12.5%	-2.4%
Specimen 2	0.520	0.395	0.454	0.525	-24%	-12.7%	1.0%

4.9. Adjustment of Ψ-values measured at different wind velocities to the standard values.

It is not always possible to undertake a thermographic survey at the standard 4 m/s wind velocity. This section investigates how the Ψ-value obtained from the ITT undertaken at any wind velocity may be adjusted to one obtained at the standard wind velocity of 4m/s. To examine this problem, two-dimensional heat transfer numerical simulations were performed. For this analysis, the range of wind velocities was extended up to 10 m/s.

The geometry of Specimen 1 was chosen for the simulations. To investigate the influence of the thermal conductivity of the main plain component surrounding thermal bridge on the Ψ-value, six different models were created where the original XPS insulation with the thermal conductivity k equal 0.033 W/(mK) for was replaced with fabric with conductivities varying between 0.05 W/(mK) and 1.00 W/(mK) as detailed in Table 4.12. The same steel box section used in Specimen 1 (SHS 100x100x5mm) was the thermal bridge used in all models and the OBS facing remained unchanged.

Table 4.12. Thermal conductivity of insulation material in wall configurations A-F.

Sample	A	B	C	D	E	F
k [W/mK]	0.033	0.050	0.150	0.320	0.650	1.000

The boundary conditions applied to finite element models were evaluated in accordance with the ISO 6946 [31]. In all cases, on the hot side, the air temperature T_i was equal to 20°C and the sum of convective and radiative coefficient equal to 7.7 W/m²K. The air temperature on the cold side T_e was kept at 0°C, and the convective coefficient h_{ce} was calculated for each different wind velocity using Equation (4.7) in accordance to Annex A of ISO 6946 [31].

To observe the influence of the wind on the Ψ-values, all configurations (A – F) were simulated under five wind velocities: 1m/s, 2.5m/s, 4m/s, 7m/s, and 10m/s. The results are presented in Fig. 4.10. The relationship between wind velocity and Ψ-value of all analyzed samples, similarly to the experimental Ψ-values shown in Fig. 4.8, can be described by a power law (Equation (20)).

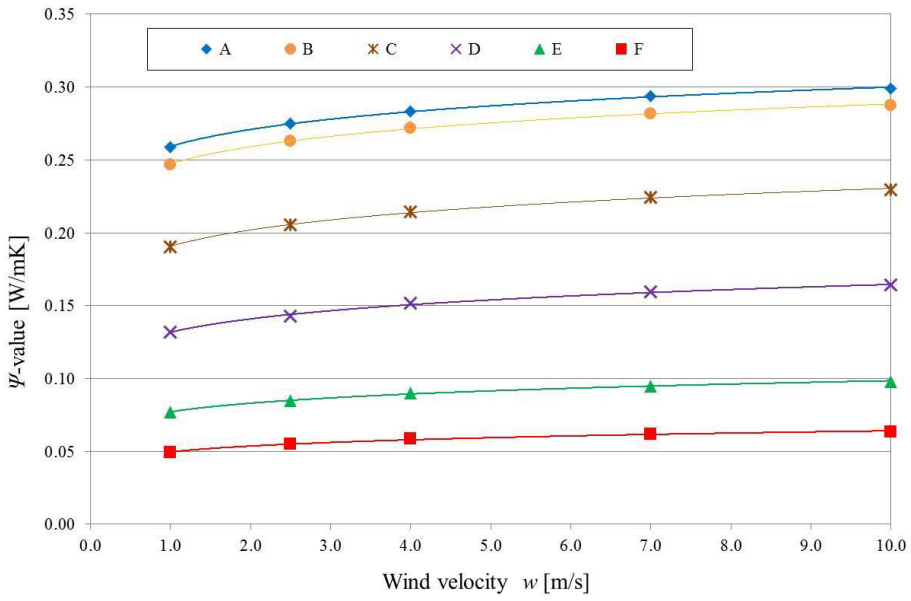

Fig. 4.10. Dependence of Ψ-values on wind velocity for six wall samples.

The power law coefficients c and b for each configuration are presented in Table 4.13.

Table 4.3. Values of *d* and *e* for configurations A-F.

	A	B	C	D	E	F
d	0.2599	0.2480	0.1913	0.1323	0.0775	0.0499
e	0.0603	0.0636	0.0789	0.0920	0.1016	0.1068

In order to develop a method of adjusting the measured Ψ-value to the value evaluated at standard wind conditions, two ratios are introduced. The Ψ_{ratio} is the ratio of Ψ-value calculated for a wind velocity of 4 m/s and Ψ calculated at wind velocities other than 4m/s. The wind ratio w_{ratio} is equal to the standard wind velocity of 4m/s divided by the actual wind velocity at which Ψ-value was evaluated. Fig. 4.11 shows the relationship between Ψ_{ratio} and w_{ratio} for the six wall configurations. Fitting a power law to the data, the relationship can be written as Equation (4.22) with the coefficient for each wall configuration given in Table 4.14:

$$\Psi_{ratio} = f w_{ratio}^{g} \qquad (4.22)$$

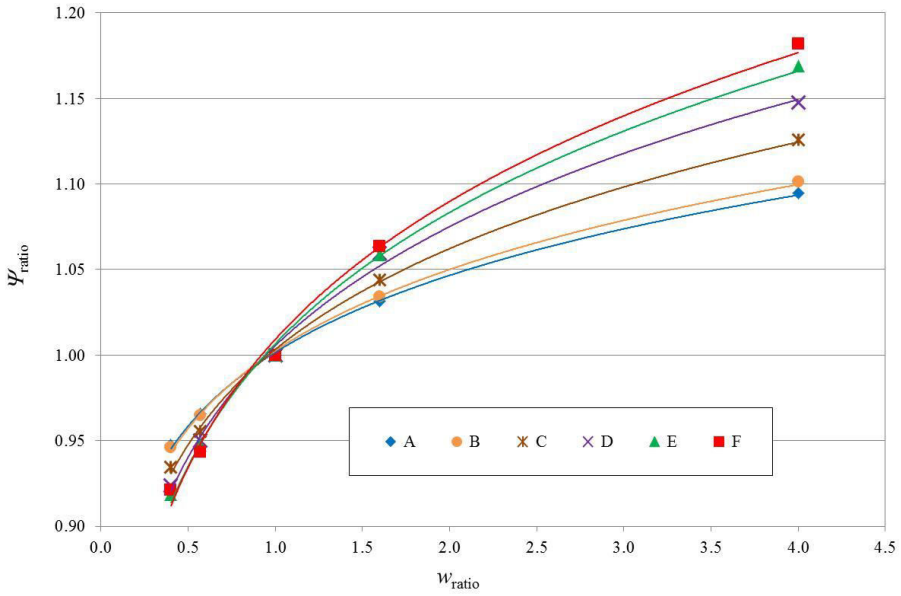

Fig. 4.11. Dependence of Ψ-ratio on wind ratio for six wall samples.

Table 4.14. Coefficients *f* and *g* for Equation (4.22) and uniform surface heat fluxes $\dot{q_u}$ for wall samples.

	A	B	C	D	E	F
f	1.0039	1.0043	1.0058	1.008	1.0091	1.0115
g	0.061	0.0636	0.0778	0.0920	0.1016	0.1068
$\dot{q_u}$	5.80	8.29	21.63	28.39	36.92	41.16

As the value of coefficient *f* is approximately 1 for all samples, the expression for Ψ_{ratio} can be approximated as:

$$\Psi_{ratio} = w_{ratio}^{g} \qquad (4.23)$$

Coefficient *g* in Equation (4.23) is linearly dependent on the surface heat flux of the uniform part of the component $\dot{q_u}$ as seen in Fig. 4.12.

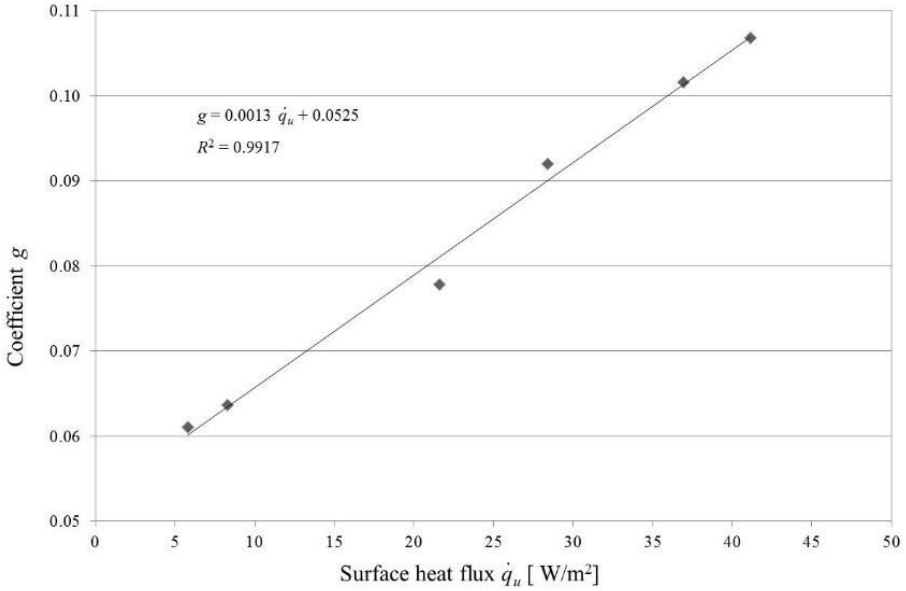

Fig. 4.12. Dependence of coefficient g on surface heat flux $\dot{q_u}$.

Now the Ψ_{ratio} can be expressed by Equation (4.24):

$$\Psi_{ratio} = w_{ratio}^{0.0013\dot{q_u}+0.0525} \qquad (4.24)$$

Knowing the wind velocity at which the Ψ-value was measured and the surface heat flux of the uniform part of the specimen, the Ψ_{ratio} can be calculated. This can then be used to adjust the measured Ψ-value to obtain the Ψ adjusted (Ψ_{adj}) to a wind velocity of 4 m/s using Equation (4.25). This Ψ_{adj} can be then compared to the Ψ_S – value.

$$\Psi_{adj} = \Psi_{ratio}\,\Psi_{meas} \qquad (4.25)$$

The adjustment factors are applied to the experimentally measured Ψ-values of specimens tested at different velocities to make them comparable to the standard value. To calculate the Ψ_{ratio}, the uniform surface heat flux $\dot{q_u}$ of the component surrounding the thermal bridge is first calculated. The value of $\dot{q_u}$ is calculated using

Equation (4.26), where N is the number of pixels on the IR line, and q_{xu} is calculated using Equation (4.10) applied to the uniform part of the specimen away from the thermal bridge:

$$\dot{q}_u = (N * q_{xu})/L \qquad (4.26)$$

Values of $\dot{q_u}$ of tested specimens for each case are given in Table 4.15.

Table 4.15. Uniform surface heat flux $\dot{q_u}$ of tested specimens.

	Unit	*Uniform surface heat flux $\dot{q}_u$ for:*		
		Case 1	*Case 2*	*Case 3*
Specimen 1	W/m²	8.54	8.93	9.56
Specimen 2	W/m²	8.29	8.62	9.18

Using first Equation (4.24), the Ψ_{ratio} was calculated for each case and all experimental Ψ-values (Ψ_{meas}) were multiplied by these ratios. Table 4.16 presents the Ψ-values obtained from the ITT at different wind velocities adjusted to the Ψ-value obtained at 4m/s and their comparison to the standardized Ψ_S-value. As can be seen, the relative deviation between these values is significantly lower than those of non-adjusted values presented in Table 4.11. The relative deviation of Ψ-values measured at the lowest wind velocity around 0.5m/s reduced from -23% and -24% before adjustment to -11% and -14% after adjustment for Specimens 1 and 2, respectively. In the next case, when the wind velocity was around 1.5m/s the relative deviations reduced from -13% before adjustment to -7% after adjustment for both specimens. In the last case, the differences between the measured and the standard results are very small and changed insignificantly after the adjustment procedure. This occurred because Case 3 represented a wind velocity around 4m/s and the adjustment is not necessary. The analysis also shows that the adjustment procedure is more effective when applied to Case 2 (1.5m/s) rather than to Case 1 (0.5m/s).

Table 4.16. Comparison of adjusted Ψ-value to the standard Ψ-value.

	standard Ψ-value	*Ψ-value adjusted [W/mK]:*			*Relative deviation*		
		ITT Case 1	*ITT Case 2*	*ITT Case 3*	*Case 1*	*Case 2*	*Case 3*
Specimen 1	0.284	0.252	0.264	0.276	-11.2%	-6.9%	-2.9%
Specimen 2	0.520	0.446	0.482	0.524	-14.2%	-7.3%	0.8%

4.10. Conclusions

A non-destructive measurement methodology for determining the linear thermal bridge performance, using infrared thermography applied to the exterior building surface, is presented. A method of accounting for different wind velocities is proposed, which allows for measurements under different wind conditions to be adjusted to standard values. The methodology is evaluated by comparison with experimental measurements in a hot box device and numerical modelling of the tested components.

Key conclusions from the work are as follows:

- Heat loss from a building surface is significantly influenced by wind velocity with Ψ-values increasing with increasing velocity. Measurement of Ψ-value at a wind velocity below 4.0 m/s underestimates the standard Ψ-value. For specimens tested at ~0.5 m/s, the relative deviation is ~23%.
- Wind impacts on the heat loss through thermal bridges are significantly greater than through the plain parts of the component. For the tested components, increasing the wind velocity from ~0.5 m/s to ~4 m/s resulted in a temperature drop at the thermal bridge of 3.8 °C (Specimen 2) and 4.0 °C (Specimen 1) while the corresponding drop on the plain part of the component were only 0.6 °C and 0.9 °C.
- For the Ψ-value calculation, the external convective coefficient h_{ce} was determined using Jürges approximation and the Nusselt number. The results of

this study demonstrated the suitability of both approaches for Ψ-value calculation, while Jürges approximation is less time-consuming.

- ITT is an effective tool for determination of the Ψ-value. For specimens with single and multiple thermal bridges, tested at wind speeds between 0.5 m/s and 4.0 m/s, the relative deviation between the Ψ-value determined using the proposed methodology and that from hot box measurements varied between -5% and + 9%.
- Based on a numerical study, where a wide range of wall thermal conductivity values were investigated, a power law relationship was established between the Ψ-ratio (the ratio of the Ψ-value under standard wind conditions to that at other wind velocities) and the wind ratio (the ratio of the standard wind velocity of 4 m/s to the other wind velocity). The exponent of the power law is expressed as a function of the surface heat flux of the uniform part of the specimen.
- To date, the methodology has been validated under laboratory conditions in a hot box device for a range of wind speeds up to 4.0 m/s. The test specimens were manufactured from high thermal efficiency SIP panels, which provide a very severe test of the ITT approach. The accuracy levels achieved indicate that there is great potential for widespread adoption for in-situ use on existing buildings. The adjustment procedure makes the methodology practical for application in wind conditions up to 4.0 m/s. The approach could be implemented at different stages of a thermal retrofitting project:
    - project planning phase: to identify those building envelopes most in need of retrofitting;
    - project design phase: to determine the existing thermal performance so that an optimum retrofit strategy for each building envelope can be established;
    - project evaluation phase: to undertake a post-retrofit thermal condition survey and demonstrate the effectiveness of the measures used and inform future design approaches.

4.11. Acknowledgments

The authors wish to thank the following

1) Cracow University of Technology CUT, in particular Head of the Institute Prof. Jacek Schnotale and to the technician Eng. Mariusz Rusiecki for allowing us the opportunity to use hot box facility and for providing assistance during the experimental process
2) SIP Energy Ltd., Athenry Co. Galway and in particular Mr. John Moylan for providing the test specimens for experimental purposes
3) Enterprise Ireland for the provision of financial support for this study through Innovation Voucher IV-2014-4203

4.12. References

[1] Directive 2010/31/EU of the European Parliament and of the Council on the energy performance of buildings, 2010.

[2] Evaluation of Directive 2010/31/EU on the energy performance of buildings, European Commission, 2017.

[3] Proposal for a Directive of the European Parliament and of the Council amending Directive 2010/31/EU on the energy performance of buildings, 2016.

[4] A.L. Pisello, M. Goretti, F. Cotana, A method for assessing buildings' energy efficiency by dynamic simulation and experimental activity, Appl. Energy 97 (2012) 419–429.

[5] J. Yao, Energy optimization of building design for different housing units in apartment buildings. Appl. Energy 94 (2012) 330–337.

[6] F.P. Chantrelle, H. Lahmidi, W. Keilholz, M.E. Mankibi, P. Michel, Development of a multicriteria tool for optimizing the renovation of buildings, Appl. Energy 88 (2011) 1386–1394.

[7] M. Karmellos, A. Kiprakis, G. Mavrotas, A multi-objective approach for optimal prioritization of energy efficiency measures in buildings: Model, software and case studies, Appl. Energy 138 (2015) 131–150.

[8] T. Niemelä, R. Kosonen, J. Jokisalo, Cost-optimal energy performance renovation measures of educational buildings in cold climate, Appl. Energy 183 (2016) 1005–1020.

[9] J. Goggins, P. Moran, A. Armstrong, M. Hajdukiewicz, Lifecycle environmental and economic performance of nearly zero energy buildings (NZEB) in Ireland, Energy Build 111 (2016) 622–637.

[10] F. Ascione, R.F. De Masi, F. de Rossi, S. Ruggiero, G.P. Vanoli, Optimization of building envelope design for nZEBs in Mediterranean climate: Performance analysis of residential case study, Appl. Energy 183 (2016) 938–957.

[11] J. Berger, N. Mendes, An innovative method for the design of high energy performance building envelopes, Appl. Energy 190 (2017) 266–277.

[12] Y.H. Lin, K.T. Tsai, M.D. Lin, M.D. Yang, Design optimization of office building envelope configurations for energy conservation, Appl. Energy 2016;171:336–346.

[13] Y. Fan, X. Xia, A multi-objective optimization model for energy-efficiency building envelope retrofitting plan with rooftop PV system installation and maintenance, Appl. Energy 189 (2017) 327–335.

[14] EN ISO 14683 Thermal bridges in buildings construction - linear thermal transmittance - simplified methods and default values, 2007.

[15] A. Kylil, P.A. Fokaides, P. Christou, S.A. Kalogirou, Infrared thermography (IRT) applications for building diagnostics: A review, Appl. Energy 134 (2014) 531–549.

[16] I. Benkő, Quantitative analysis of thermal bridges of structures through infrared thermograms, In Proceedings of International Conference on Quantitative Infrared Thermography Qirt 2002, Dubrovnik, Croatia, pp. 203–208.

[17] F. Asdrubali, G. Baldinelli, F. Bianchi, A quantitative methodology to evaluate thermal bridges in buildings, Appl. Energy 97 (2012) 365-373.

[18] F. Bianchi, A. Pisello, G. Baldinelli, F. Asdrubali, Infrared Thermography Assessment of Thermal Bridges in Building Envelope: Experimental Validation in a Test Room Setup, Sustainability 6 (2014) 7107–7120.

[19] M. O'Grady, A.A. Lechowska, A.M. Harte, Infrared Thermography Technique as an in-situ method of assessing the heat loss through thermal bridging, Energy Build. 135 (2017) 20–32.

[20] M. Fox, S. Goodhew, P. De Wilde, Building defect detection: External versus internal thermography. Build. Environ. 105 (2016) 317–331.

[21] R. Albatici, A.M. Tonelli, M. Chiogna, A comprehensive experimental approach for the validation of quantitative infrared thermography in the evaluation of building thermal transmittance, Appl. Energy 141 (2015) 218–228.

[22] EN 13187 Thermal performance of buildings-qualitative detection of thermal irregularities in building envelopes - infrared method, 1999.

[23] B. Lehmann, K. Ghazi Wakili, Th. Frank, B. Vera Collado, Ch.Tanner, Effects of individual climatic parameters on the infrared thermography of buildings, Appl. Energy 110 (2013) 29–43.

[24] R. Albatici, A.M. Tonelli, Infrared thermovision technique for the assessment of thermal transmittance value of opaque building elements on site. Energy Build. 42 (2010) 2177–2183.

[25] Flir Systems, User's manual FLIR Bxxx series FLIR Txxx series, 2011.

[26] P.A. Fokaides, S.A. Kalogirou, Application of infrared thermography for the determination of the overall heat transfer coefficient (*U*-Value) in building envelopes, Appl. Energ*y* 88 (2011) 4358–4365.

[27] Kieszonkowy przewodnik Termografa,Tesco, 2009.

[28] C.A. Balaras, A.A. Argiriou, Infrared thermography for building diagnostics.

Energy Build. 34 (2002) 171–183.

[29] EN ISO 8990 Thermal insulation - Determination of steady-state thermal transmission properties - Calibrated and guarded hot box, 1997.

[30] EN ISO 10211 Thermal bridges in building construction - heat flow and surface temperatures - detailed calculations, 2017.

[31] EN ISO 6946 Building components and building elements - Thermal resistance and thermal transmittance - Calculation method, 2017.

[32] M.J. Moran, H.N. Shapiro, B.R. Munson, D.P. Dewitt, Introduction to Thermal Systems Engineering : Thermodynamics, Fluid Mechanics and Heat Transfer. John Wiley & Sons, Inc. 2003.

[33] H. Hens, Building Physics - heat, air and moisture. Ernst &Sohn, Wiley Company, Berlin, 2007.

[34] R.J. Cole, N.S. Sturrock, The convective heat exchange at the external surface of buildings. Build. Environ. 12 (1977) 207–214.

[35] J.A. Palyvos, A survey of wind convection coefficient correlations for building envelope energy systems' modeling, Appl. Therm. Eng. 28 (2018) 801–808.

[36] W. McAdams, Heat Transmission, Third edition, McGraw-Hill International Book Company, 1958.

[37] G. Dall'O' , L. Sarto, A. Panza, Infrared screening of Residential Buildings for Energy Audit Purposes: Results of a Field Test, Energies 6 (2013) 3859–3878.

[38] M.G. Emmel, M.O. Abadie, N. Mendes, New external convective heat transfer coefficient correlations for isolated low-rise buildings. Energy Build. 39 (2007) 335–342.

[39] E. Sartori, Convection coefficient equations for forced air flow over flat surfaces. Sol. Energy 80 (2016) 1063–1071.

[40] EN ISO 12567-1 Thermal performance of windows and doors - Determination of thermal transmittance by the hot-box method - Part 1: Complete windows and doors, 2010.

[41] J.H. Watmuff, W.W.S. Charters, D. Proctor, Solar and wind induced external coefficients-solar collectors. Comples Rev. Int. d'Heliotechnique 2 (1977) 56.

[42] Product Data Sheet of Eurostrand OSB 3, E EGGER, 2009.

[43] http://hyperphysics.phy-astr.gsu.edu/hbase/Tables/, accessed on the 16.01.2017.

[44] Product Data Sheet of Styrofoam LBH-X, Dow Chemical Company Limited, 2014.

[45] www.engineeringtoolbox.com/metal-alloys-densities-d_50.html, accessed on the 16.01.2017.

[46] T. Ward, C. Sanders, Conventions for calculating linear thermal transmittance and temperature factor, IHS BRE Press, 2007.

Chapter 5

Application of infrared thermography technique to the thermal assessment of multiple thermal bridges and windows

5.1. Paper overview

This article describes the application of the ITT for heat loss evaluation in the case of multiple thermal bridging. Multiple thermal bridges occur frequently in a building envelope and the distance between them is correlated with the degree of thermal interaction that takes place. The testing carried out as part of this study has revealed that this relationship must be taken into account while evaluating thermal bridging performance, otherwise the evaluation is overestimated. The methodology for indoor ITT, presented in Chapter 3, is shown to be suitable for evaluation of the heat loss associated with multiple thermal bridges and accounting for interaction effects. Application of this methodology does not require knowledge of thermal bridges structure or their precise location. In the post-processing of the thermogram with two or more thermal bridges, the zone of influence of each thermal bridge is defined. Unless a uniform surface temperature is reached between them, they interact with each other. In this case, their heat loss must be evaluated from the same thermogram. Within this research, the application of the methodology for complex multiple thermal bridging assessments, such windows, is investigated. An important feature of this approach is taking into account heat losses due not only to a window itself but also to its installation into a building wall. Moreover, this approach does not require

knowledge of the window and surrounding wall properties. A window thermal transmittance *M*-value is introduced to quantify the total additional heat losses through building element due to the presence of a window.

The research also includes an evaluation of two numerical approaches, FE steady-state heat transfer, and CFD, to multiple thermal bridges assessment. Detailed information on the internal structure material properties of tested specimens is required to generate these numerical models. Where this information is available, the more suitable numerical approach is defined.

The content of this chapter has been published in Energy and Building journal: *M. O'Grady, A.A. Lechowska, A.M. Harte, Application of infrared thermography technique to the thermal assessment of multiple thermal bridges and windows, Energy and Buildings, 2018, 168: 347-362.* In this joint publication, Małgorzata O'Grady, supervised by Dr. Annette Harte, designed the experiment, performed the testing, analysed the test results, carried out the numerical heat transfer simulations and developed the methodology. Dr. Agnieszka Lechowska facilitated the testing and carried out computational fluid dynamic analysis.

5.2. Abstract

A major contribution to the global trend in reducing energy consumption can be made by improving the thermal performance of buildings. Minimization of heat loss via the building envelope is key to maximizing building energy efficiency. The building envelope contains different types of thermal bridging that must be accounted for while assessing the overall building envelope thermal performance. Multiple thermal bridges commonly occur and the distance between them determines the degree to which they interact thermally. To avoid overestimation of the linear thermal transmittance, it is important to account for interaction effects. Complex multiple thermal bridging occurs in window systems. The thermal performance of windows depends not only on the window performance itself but also on its installation into the wall. This study demonstrates an application of the quantitative infrared thermography technique to evaluate the heat lost via multiple thermal bridging. It is shown that using this methodology, the heat loss via multiple thermal bridges can be easily estimated in an

existing building envelope, without any knowledge of its internal structure or material properties. For windows, it is demonstrated that jointly assessing the additional heat loss through the window and due to the installation of the window into the wall is a practical way to determine the actual heat loss caused by the presence of a window. A window thermal transmittance or *M*-value is introduced to quantify the total additional heat loss through the building element due to the presence of the window. The methodology was validated against experimental measurements taken on different specimens in a hot box device. Results from the thermographic analysis also co-related well with results from finite element heat transfer and computational fluid dynamics simulations.

5.3. Introduction

Buildings are associated with approximately one-third of global primary energy consumption and one-third of total energy-related greenhouse gas emissions [1]. In order to limit energy consumption related to buildings at a European level, the European Union Directive 2010/31/EU on Energy Performance of Buildings (EPBD 2010) [2] defined minimum targets for EU Member States in relation to national building regulations. Consequently, building regulations within EU countries became stricter on building energy performance. Evaluation of EPBD 2010 [3] revealed that these changes have had a particularly positive impact on energy performance improvement of newly constructed buildings. Nevertheless, a large portion of the existing buildings still needs deep retrofitting to meet the minimum thermal performance requirements. This provides opportunities for significant energy savings but is, at the same time, a major challenge due to the large number of buildings involved.

When considering building energy efficiency, several factors should be taken into account; however, the role of the building envelope in providing a barrier between the indoor and outdoor environments cannot be underestimated. The thermal standard of a building envelope is one of the major factors to be considered in ensuring that a building is energy efficient [4]. The building envelope consists of plain components of uniform thermal resistance together with regions of thermal bridging. Because a

thermal bridge represents part of a building envelope with higher thermal conductivity or different geometry, it is associated with significantly higher heat losses than the plain component surrounding the thermal bridge. It is crucial to account for this additional heat loss while assessing the building envelope thermal performance. Two types of thermal bridging can be distinguished: a point thermal bridge, which appears at the connection of three building components and a linear thermal bridge, characterized by a uniform cross-section along one of the three orthogonal axes [5]. The heat loss related to linear thermal bridges may be described by the linear thermal transmittance (Ψ-value). According to standard ISO 14683 [5], it expresses the heat flow rate in a steady state per unit length and per degree of difference in the indoor and outdoor air temperatures on each side of a thermal bridge. There are several ways of obtaining the linear thermal transmittance. The simplified way is to use default values given in this standard. However, they only apply to standard building details and their typical accuracy varies between 0% and 50%. A more sophisticated and widely-used approach to evaluate the Ψ-value is through numerical calculation. Detailed instructions about how a Ψ-value can be derived from a numerical model are given in EN ISO 10211 [6]. To build a model, the construction of the thermal bridge and of the plain components must be known. Therefore, this approach is suitable at the design stage.

The numerical and analytical approaches have been widely used by researchers to predict thermal bridging performance. Capozzoli et al. [7] used finite element (FE) modelling to carry out a sensitivity analysis of the factors influencing heat flow through thirty six common thermal bridges in masonry structures. For cases where internal or external insulation continues over the thermal bridge, they identified the thickness of the insulation layer as the most significant variable that influences the Ψ-value. In cases with non-continuous insulation, variables such as the thermal conductivity of the masonry and floor, roof and wall thickness are also important. However, masonry thermal conductivity has a greater impact on the Ψ-value than its thickness. Viot et al. [8] suggested that the most accurate way of thermal bridging heat loss evaluation is using an unsteady 3D heat transfer model. Hassid developed an analytical approach to evaluate thermal bridging heat loss located in both, homogeneous [9] and multilayer walls [10] that showed good agreement with

numerical results. Using this approach, the effect of different parameters such as thermal bridge and plain component thicknesses and their conductivities can be also assessed.

Considering the thermal bridges located in an existing building, their structure is very often unknown. In this case, a measurement method must be used to evaluate their heat loss. The Irish Building Regulations [11] allow determination of the Ψ-value from measurement. However, there is no standardized measurement method. To experimentally measure heat loss via thermal bridges some researchers [12-14] have used heat flow meters (HFMs) that were placed on the thermal bridge and at the significant distance away from the thermal bridge. The qualitative infrared thermography technique (ITT) was used as a supplementary technique to locate the thermal bridge and correctly position HFMs.

A quantitative ITT approach was used by Heinrich and Dahlem [15] to find the distribution of the indoor surface temperature of a lightweight wall containing an I-beam, and this was then compared with numerical simulations. They reported that the thermal bridge zone of influence in the numerical model was smaller than that recorded by the ITT. Wróbel and Kisielewicz [16] used a quantitative ITT to define the lowest surface temperature on the thermal bridge. To extend evaluation to other environmental conditions, they used numerical simulation. Fox et al. [17] compared the effectiveness of indoor and outdoor qualitative thermographic surveys in building defect identification. They found that, in almost 60% of all tested dwellings, the defects could be detected from both sides, but the indoor ITT presented the defects more clearly. In 40% of cases, the defects were located using the indoor thermography and they were not visible while taking the external survey. In only 2% of dwellings, detection of anomalies was possible externally and not internally.

Benkő [18] was one of the first researchers to assess the heat loss associated with thermal bridging by means of the outdoor quantitative ITT. On an IR image of a building wall, two surface temperatures were identified: one on the thermal bridge and the other on the plain part of the building envelope not affected by the thermal bridge. Based on these temperatures, Benkő defined an energy saving factor that expressed the proportion of the heat losses of a building component including and excluding

thermal bridging influence. Similarly, Asdrubali et al. [19] described the heat loss via thermal bridging as a factor showing how the heat loss through a building component increases due to the presence of the thermal bridge, using the indoor ITT. Their approach is more precise than the Benkő method as it accounts for the temperature in each pixel. Asdrubali et al. [19] validated the methodology under laboratory conditions on a thermal bridge between a window frame and glazing. To fully quantify the thermal bridging heat loss, they multiplied the factor by the *U*-value of the plain component measured by a heat flow meter (HFM). Their methodology has been validated on a test room by Bianchi et al. [20]. O'Grady et al. [21] expanded the last approach and introduced a methodology that allows quantification of the thermal bridge heat flow rate q_{TB} and the linear thermal transmittance Ψ-value by means of the ITT alone. Their methodology was adapted for outdoor ITT where weather conditions, especially wind, significantly influence the building surface temperatures [22].

The literature shows that various approaches to evaluate the heat loss through a single linear thermal bridge have been developed. In the building envelope, thermal bridges rarely occur in isolation and multiple thermal bridges must often be accounted for in assessment of the thermal performance of the building envelope. The distance between the thermal bridges determinates the degree of interaction between them. If they are located close to each other, the heat flow rate through one thermal bridge affects the heat flow rate of the other. Ward and Sanders [23] give some guidelines of how to account for this interaction in numerical modelling. According to [23], two adjacent thermal bridges that are located less than the thickness of the building component apart, should be included in the same numerical model. This prevents an overestimation of their Ψ-values. Thermal bridges located at a greater distance apart are assumed not to interact and independent numerical models can be created.

All buildings have installed windows, which may be considered as complex multiple thermal bridging systems. The total heat loss through the window consists of heat losses via window glazing, window frame and the connection between them. According to ISO 10077-1 [24], all these heat losses, expressed by *U*-value of the frame, *U*-value of glazing and Ψ-value of the window frame and glazing connection are to be included in the window *U*-value. This *U*-value is specified for a range of

windows available on the market by numerical evaluation, according to [24] or hot box method in accordance with EN ISO 12567-1 [25].

Once the window is fixed into the building wall, additional thermal bridging, as a result of junctions between the window and the wall, occurs. According to BRE Scotland [26], this Ψ-value around windows is to be determined numerically. In the model, only the building wall is included, and adiabatic boundary conditions are assumed where the window frame connects to the wall. The Ψ-value around windows calculated this way depends only on the dimensions of the frame and on its location in the jamb. A more rigorous approach to the installation Ψ-value is presented by the Passive House Institute [27]. According to their procedure, this heat loss is also evaluated numerically; however, their model includes the window and therefore accounts for the interaction between the window and the wall. Cappelletti et al. [28] proposed to express heat losses associated with an installed window by an overall, two-dimensional U_{2D}-value.

Summarizing, in a building envelope in addition to single thermal bridges more complex multiple thermal bridges often occur. In the literature, guidelines on how to numerically predict heat losses due to single thermal bridging, multiple thermal bridging and thermal bridging associated with windows and their installation can be found. However, they apply to the building design stage where information about the structure is available. At this stage, no construction/installation errors are considered so the thermal bridges are designed for their perfect performance. However, once a building is constructed, the performance may vary from that predicted and ideally should be evaluated based on field measurements. Such measurements would reveal construction/installation errors and deterioration of materials over time. Also, commonly for older buildings, the building envelope structure is unknown making them unsuitable for numerical simulations.

As pointed out earlier, to achieve overall energy savings in the building sector, the industry should put particular emphasis on retrofitting the existing building stock. In-situ measurements of the existing building thermal performance before and after retrofitting are necessary to define the actual thermal improvement. Quantitative ITT has been shown to be an accurate and efficient approach for quantifying the heat loss

through linear thermal bridges [21]. However, the methodology has been only validated on regular single thermal bridges with gentle temperature gradients. This study investigates the applicability of the ITT methodology to more realistic situations occurring in buildings. The response of thermal bridges located in close proximity to each other, often with steep gradients in the surface temperature distribution, is investigated. The testing includes complex scenarios, such as multiple linear thermal bridges and window installations. The latter is multifaceted heat loss system, comprising heat losses via glazing, frame, the connection between frame and glazing and heat losses around the window due to installation. In the methodology presented in this paper, the whole installed window is treated as a unit and the additional heat loss through the building component due to the window system is quantified. To do this a new window thermal transmittance or *M*-value is introduced.

Indoor thermography is used in this study, as it has been shown [16,17] that the indoor ITT is more suitable for thermal bridge detection than the outdoor ITT. The proposed methodology is applied to test specimens containing multiple thermal bridges, which were tested in controlled conditions in a hot box device [29]. Initially, specimens containing parallel thermal bridges are investigated to determine the interaction effects. More complex multiple bridging is then examined using specimens containing window elements to demonstrate the applicability of the approach to these situations. In addition, two different numerical approaches, heat transfer finite element (FE) and computational fluid dynamics (CFD) analysis that are validated against the hot box measurements, are used to model the thermal performance. The numerical predictions serve as additional checks on the validity of the ITT approach.

5.4. Experimental study

To investigate the suitability of the quantitative ITT approach for multiple thermal bridging heat loss assessment, testing of a number of specimens was carried out. First, the thermal performance of specimens, with multiple parallel thermal bridges at different spacings, was examined. This was followed by testing of specimens containing different window elements displaying more complex thermal bridging behaviour. Tests were performed in a hot box under steady-state conditions. The hot

box device is located in Cracow University of Technology, Faculty of Environmental Engineering, Poland.

5.4.1. Experimental procedure

The experiment was performed in the hot box, consisting of two climatic chambers, simulating indoor and outdoor conditions. Fig. 5.1 shows the experimental arrangement. First, the hot box testing was completed, as described in Section 5.4.3. Afterward, the thermographic survey was performed, as described in Section 5.4.4. Both types of testing were accomplished under the same controlled, environmental conditions. Generally, the air temperature in the hot chamber was kept at about 25°C and in the cold chamber at about -5°C.

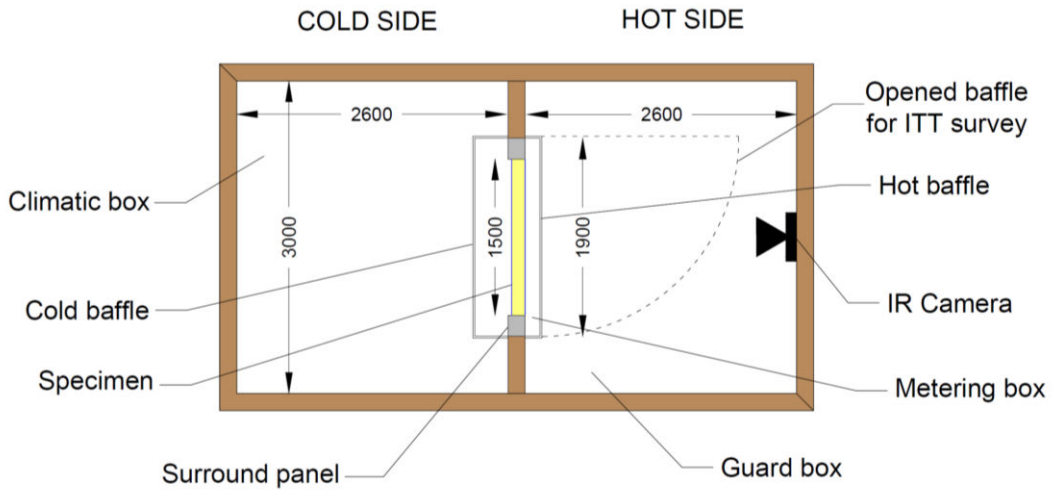

Fig. 5.1. Geometry of hot box.

5.4.2. Test specimen description

Four specimens, 1.5m long and 1.5m high, containing thermal bridges were tested. Geometries of the specimens are presented in Table 5.1. All specimens consist of structural insulated panels (SIPs) with total thicknesses of 130 mm. Each SIP panel consists of 100 mm thick low conductivity extruded polystyrene insulation (XPS)

boards with 15 mm thick oriented strandboard (OSB) sheathing on both sides. Specimens 1 - 2 contain parallel thermal bridges created by steel square hollow (SHS) sections 100mm x 100mm x 5mm running from the top to bottom of the specimens. Specimen 1 contains two parallel thermal bridges positioned 50 mm apart which is less than the specimen thickness. Specimen 2 contains two steel square hollow sections (SHS) situated 300mm apart from each other, which is greater than the thickness of the component. Specimens 3 and 4 contain window elements. Specimen 3 has a window with a timber frame whereas Specimen 4 has a window with a PVC frame. For experimental purposes, the window glazing has been replaced with polystyrene, in accordance with the standard EN ISO 12412-2 [30] for testing the thermal performance of window frames. The 30 mm thick polystyrene sheet has a *U*-value of approximately 1 W/m^{2}K and is thermally-similar to double glazing. However, it has to be underlined that the thermal bridging between the frame and the polystyrene is different to the one between the frame and real glazing. This is due the presence of spacers used to limit the thermal bridging heat loss. Fig. 5.2. shows Specimen 3 mounted into the hot box surround panel. Additionally, a plain Specimen 5, with the same structure but without any thermal bridge was tested to enable the evaluation of the thermal bridging heat loss for Specimens 1 – 4.

Table 5.1. Geometries of test specimens

Specimen number	Geometries
1	
2	
3	
4	
Legend:	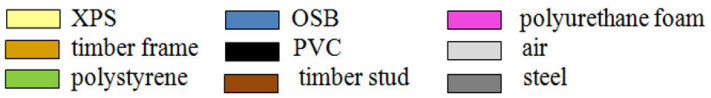

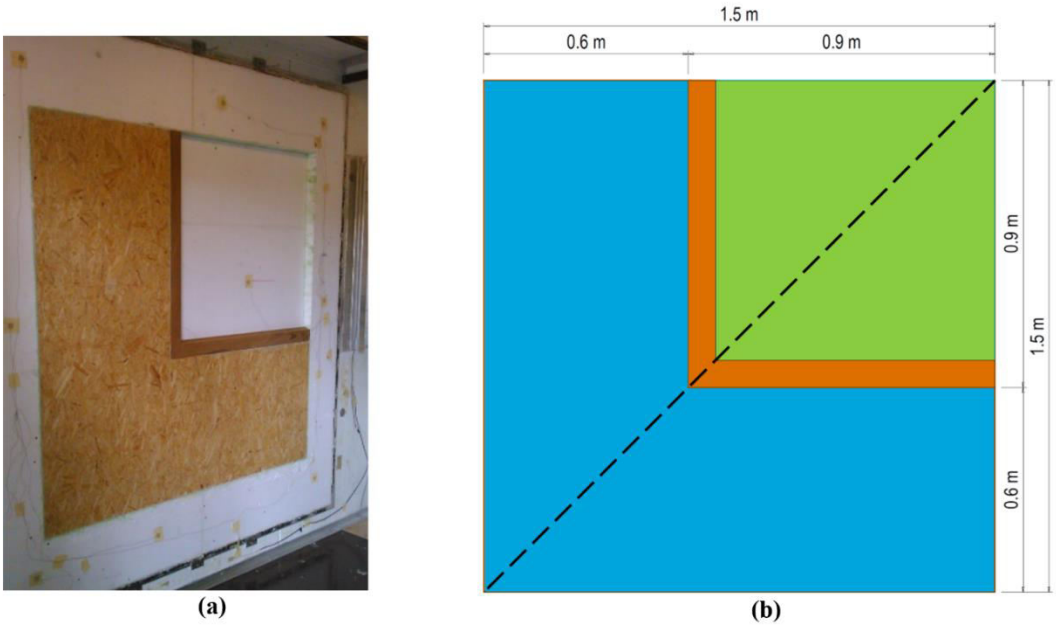

Fig.5.2. Specimen 3 mounted into the hot box surround panel (a); Specimen dimensions (b).

5.4.3. Hot Box measurements

The hot box testing has been carried out in accordance with the EN ISO 8990 [29] standard. The hot side of the system simulates indoor environmental conditions and the cold side simulates outdoor environmental conditions. The construction of the hot box includes baffles to keep the air temperature and the air velocity uniform along the specimen surfaces. Specimens 1 – 5 were placed in sequence into a surround panel. To ensure that there was no air infiltration, silicone sealant and polystyrene foam insulation with low thermal conductivity (0.030 W/mK) were used to seal the junction between the surround panel and the specimen. The joints were checked using the IR camera to ensure that sealing was correctly carried out. Then a metering box was fastened to the hot side of the surround panel and covered the whole area of the specimen (Fig 5.3). The aim of metering box is to ensure that the air temperature along the whole specimen is uniform. To obtain this, an air stream with very low velocity of 0.1 m/s is directed downward (inverted convection) between the hot baffle and the hot surface of the specimen throughout the test. The metering box is equipped with apparatus to measure the heat loss through the specimen. Fig. 5.1 shows the metering

box situated in the guard box on the hot side. This arrangement minimizes the heat flow rate through the metering box walls.

Fig. 5.3. Metering box fastened to the surround panel.

On the cold side of the specimen, an isothermal cold baffle was attached where a wind velocity of approximately 1.50 m/s was induced. Two thermocouples were attached to the hot surface. On specimens with parallel thermal bridges (Specimen 1-2) they were placed in the mid-height of a specimen, one outside the thermal bridge zone of influence (S1) and one in the middle of one of the thermal bridges (S2). On specimens containing a window element (Specimen 3 – 4) the thermocouples were placed on the area not affected by thermal bridges, S1 on the SIP panel and S2 on the polystyrene. After a few hours, steady state conditions were achieved, and they were maintained throughout testing. At this stage, the hot box measurements were taken. Based on these measurements, the heat transferred through the specimen and surround panel was defined. A more detailed description of the hot box measurement procedure can be found in [21].

During the testing, data such as air temperatures, surface temperatures provided by thermocouples S1 and S2, air velocities, heat power input to the hot box were measured and recorded by the AMR Ahlborn Wincontrol system. These are summarized in Table 5.2.

Table 5.2. Hot box measurements

Parameter	*Unit*	*Specimen 1*	*Specimen 2*	*Specimen 3*	*Specimen 4*	*Specimen 5*
T_e	°C	-4.85	-4.84	-4.88	-4.89	-4.91
T_i	°C	24.67	24.57	24.51	24.51	24.81
$T_{se,b}$	°C	-4.91	-4.91	-4.93	-4.89	-4.94
$T_{si,b}$	°C	24.02	23.98	23.94	23.91	24.53
T_{ni}	°C	24.23	24.16	24.12	24.09	24.62
T_{ne}	°C	-4.87	-4.86	-4.90	-4.89	-4.93
w_e	m/s	1.54	1.49	1.51	1.48	1.47
w_i	m/s	0.1	0.1	0.1	0.1	0.1
T_{S1}	°C	23.59	23.44	23.74	23.74	23.60
T_{S2}	°C	16.94	17.24	20.6	20.58	23.68
Φ	W	44.51	45.53	44.97	45.58	24.63

In Table 5.2, environmental temperatures on the cold and on the hot sides (T_{ne} and T_{ni}, respectively) were obtained as a weighting of air temperatures recorded during testing (T_e and T_i) and baffle surface temperatures ($T_{se,b}$ and $T_{si,b}$). This was necessary as, according to EN ISO 8990 [29] and ISO 12567-1 [25], for calculations based on the heat flow rate measured in a hot box, an environmental temperature T_n should be used. The full procedure for obtaining the environmental temperature T_n is described in [21].

Before commencement of hot box testing, the device was calibrated in accordance with EN ISO 8990 [29] as described in [21]. The calibration process enables the quantification of how much heat has been transmitted via the surround panel, the specimen edges and via the specimen itself. The surface heat flux, $\dot{q}_{sp}$, and the heat flow rate through the whole specimen, $\dot{Q}_{sp}$, of each tested specimen was calculated using Equations (5.1) and (5.2), respectively.

$$\dot{q}_{sp} = \frac{\Phi_{in} - \Phi_{sur,p} - \Phi_{edge}}{A} \quad (5.1)$$

$$\dot{Q}_{sp} = \dot{q}_{sp} A \quad (5.2)$$

After testing the plain specimen, the thermal bridge heat loss was obtained. The heat loss via parallel thermal bridges (Specimens 1 – 2) is expressed by thermal bridging heat flow rate q_{TB} and was obtained using Equation (5.3). This heat loss is the difference between the heat flow rate for specimens containing thermal bridges, $\dot{Q}_{sp}$, and the uniform heat flow rate for the plain Specimen 5, $\dot{Q}_{plain}$, divided by the specimen height H_{sp}. By dividing q_{TB} by the environmental temperature difference on each side of the specimen, the Ψ-value is obtained (Equation (5.4)). For Specimens 3 and 4, the heat loss associated with the presence of the window is expressed by the thermal bridging heat flow rate $\dot{Q}_{TB}$ and was calculated using Equation (5.5), as the difference between the heat flow rate for specimens containing thermal bridges, $\dot{Q}_{sp}$, and the uniform heat flow rate for Specimen 5, $\dot{Q}_{plain}$. A window thermal transmittance or M-value is introduced to describe the total additional heat lost from the building element due to the window element per unit temperature difference on each side of the element and is expressed in W/K. The M-value for the test specimens is found by dividing $\dot{Q}_{TB}$ by the environmental temperature difference between the hot and cold chambers (Equation (5.6)).

$$q_{TB} = \frac{(\dot{Q}_{sp} - \dot{Q}_{plain})}{H_{sp}} \quad (5.3)$$

$$\Psi = \frac{q_{TB}}{(T_{ni} - T_{ne})} \quad (5.4)$$

$$\dot{Q}_{TB} = \dot{Q}_{sp} - \dot{Q}_{plain} \quad (5.5)$$

$$M = \frac{\dot{Q}_{TB}}{(T_{ni} - T_{ne})} \quad (5.6)$$

The uncertainty of the calculated results arising due to measurement errors is estimated using the error propagation rule [31-33]. The q_{TB}, Ψ-value, $\dot{Q}_{TB}$ and M-value

uncertainties are linked to the measurement errors of air temperatures, surface temperatures, heat power input to the hot box, and specimen dimensions, which were 0.3 K, 0.3 K, 0.3 W and 0.001 m, respectively. The uncertainty (u) of q_{TB}, Ψ-value, $\dot{Q}_{TB}$ and M-value obtained from hot box tests are given in the Results and discussion section.

5.4.4. Thermographic survey

The ITT measurements were taken on the hot surfaces immediately after the hot box experiment and after removing the baffle from the hot side of the specimen. The infrared images (IR images) were taken with a Flir T335 IR camera with a 25° lens, 320 x 240 resolution and a spectral range 7.5 – 13 μm. The survey environmental conditions were the same as for the hot box testing given in Table 5.2. Fig. 5.4 presents examples of thermograms for Specimens 1 and 2. This figure demonstrates that the two thermal bridges in Specimen 1 interact so strongly with each other that they practically act as a single thermal bridge. Fig. 5.5 shows a sample IR image taken on Specimen 3 containing a timber frame window. The surface temperatures are disturbed by the window components and junctions including the window frame, the polystyrene glazing replacement, and the connections between the window frame and the wall and between the frame and polystyrene. A sequence of IR images of each tested specimen has been taken. Using each image, an IR line was created using the temperature data from three adjacent horizontal rows of pixels. Each temperature on the IR line represents the average of the temperatures of the middle pixel and the eight surrounding pixels. This temperature averaging resulted in smooth transition of temperature values from one pixel to another. From all IR lines for each specimen, a mean IR line was formed. For parallel multiple thermal bridges (Specimens 1-2), IR lines were created using rows of pixels at mid-height of the IR image. The mean IR line shows satisfactorily the full temperature distribution across the specimen and, since the specimens were symmetrical, it was created only for one-half of the specimen. The location of the IR lines is shown in red in Fig. 5.4. Considering specimens with window elements (Specimens 3-4), the IR line was created using rows of pixels at the mid-height of the vertical window frame, as indicated in Fig. 5.6. The methodology described in the next section is applied to the mean IR line.

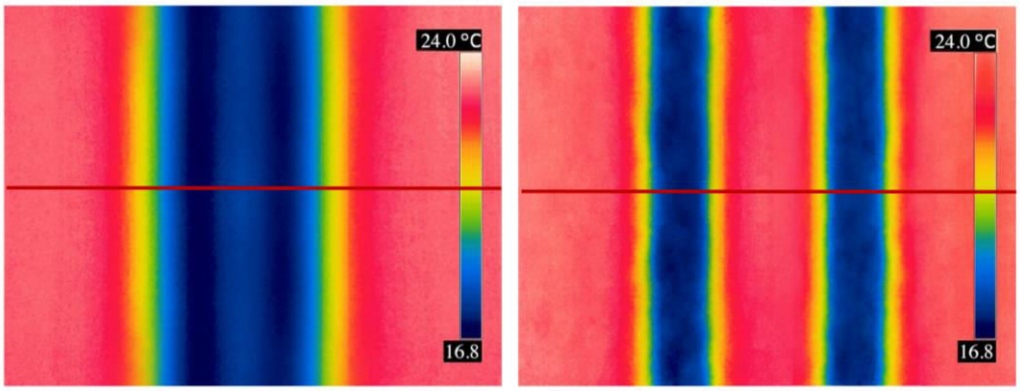

Fig. 5.4. Sample IR images for Specimen 1 (left) and of Specimen 2 (right).

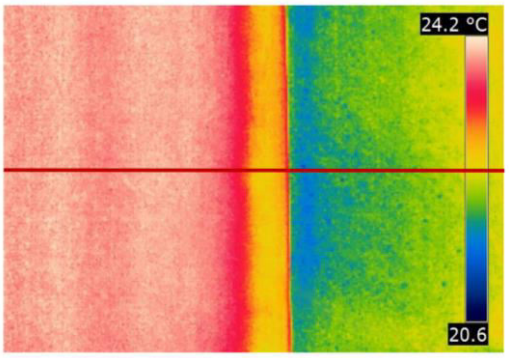

Fig. 5.5. IR image of Specimen 3 with a timber frame window.

5.5. Application of ITT methodology to quantifying the heat loss through multiple thermal bridges and through window elements.

In the current study, the methodology, originally developed for single thermal bridge assessment [21], is applied to evaluate the heat flow rate through multiple linear thermal bridges and through complex thermal bridges such as window elements. The methodology is based on the surface energy balance applied to the internal face of the building envelope component containing the thermal bridge. Using this balance rule,

the heat flow rate for each pixel (q_x) on the IR line can be obtained using Equation (5.7).

$$q_x = l_x[(h_{cx}+h_{rx})(T_i - T_{sx})] \quad (5.7)$$

Surface temperatures on the IR line, located at a significant distance from the thermal bridge are not impacted by the thermal bridge. The temperature of any pixel in this region is used to calculate the uniform heat flow rate q_{xu}, using also Equation (5.7). This is used to predict the heat flow rate of the same building component but without a thermal bridge.

The thermal bridge heat flow rate for each pixel q_{xTB} is then found using Equation (5.8).

$$q_{xTB} = q_x - q_{xu} \quad (5.8)$$

The thermal performance of multiple thermal bridges is described by the thermal bridge heat flow rate q_{TB} and the Ψ-value. These values describe heat loss in Watts per unit height. The q_{TB} is obtained by summing the q_{xTB} for all pixels on the IR line.

$$q_{TB} = \sum q_{xTB} \quad (5.9)$$

Finally, the Ψ-value is obtained by dividing this thermal bridge heat flow rate q_{TB} by the difference in indoor and outdoor air temperatures.

$$\Psi = \frac{q_{TB}}{(T_i - T_e)} \quad (5.10)$$

In the current methodology, the heat loss due to the installed window is expressed as an additional heat loss through the building envelope and described by the thermal bridging heat flow rate $\dot{Q}_{TB}$. $\dot{Q}_{TB}$ describes the complex additional heat loss through the zone affected by the presence of the window and is expressed in Watts. This complex heat loss accounts also for heat losses around the window due to

installation that can, especially in older buildings, significantly impact the window thermal performance. The other reason for including the installation Ψ-value in $\dot{Q}_{TB}$ is the infeasibility of separating the thermal bridges located close to each other while performing the ITT assessment.

Due to the window geometry, the surface temperatures at the corners of the window frame are slightly different to those along the rest of the frame. To investigate how this influences the $\dot{Q}_{TB}$, numerical analyses were carried out. They included windows with: (i) polystyrene 'glazing' and glass double glazing, (ii) two types of frames, timber and PVC and (iii) three different types of spacers, namely, steel, aluminium and polypropylene. The window thermal bridging heat flow rate $\dot{Q}_{TB}$ was then calculated using two approaches. First, it was derived from the entire window/wall surface. In the second approach, an assumption was made that the surface temperatures are the same along the perimeter of the window frame and $\dot{Q}_{TB}$ was determined from a line of temperatures across the frame. For the models of windows with polystyrene 'glazing', the maximum deviation of $\dot{Q}_{TB}$ calculated using this assumption from that derived using the entire surface accounted to +1.8%. This simplification had a smaller impact on the $\dot{Q}_{TB}$ of the double-glazed windows, where the maximum deviation between $\dot{Q}_{TB}$ calculated using this assumption from that derived from the entire surface was +1.0 %. In the all analyzed cases, the surface temperatures were higher in the corner of the frames due to change of the geometry. Therefore, using the assumption that they are the same along the whole frame perimeter results in a slight overestimation of $\dot{Q}_{TB}$. To make the methodology practical and quick, it was decided to introduce the approximation that the surface temperatures are the same along the frame perimeter. With this simplification, the heat loss via the window frame and glazing together with connections between the frame and wall and between the frame and glazing may be determined from a single IR line.

In a similar manner, the heat flow rate for each pixel q_x and the thermal bridge heat flow rate for each pixel q_{xTB} on an IR line containing the wall unit and all window components are calculated using Equations (5.7) and (5.8), respectively. For the tested window specimens, due to diagonal symmetry, it is only necessary to carry out the analysis on half of the specimen as outlined in blue in Fig. 5.6. The IR line for half of

the specimen is shown in red on Fig. 5.6. To determine the $\dot{Q}_{TB}$ associated with the installed window, each q_{xTB} is multiplied by an associated height H_x (Equation (5.11)). Fig. 6 shows H_x corresponding pixel x. By summing the $\dot{Q}_{xTB}$ over all pixels on the IR line (Equation (5.12)) and multiplying by 2, the thermal bridging heat loss via the window element for the full specimen is calculated. By dividing the $\dot{Q}_{xTB}$ by the air temperature difference on each side of the specimen, window thermal transmittance *M*-value is obtained, using Equation (5.13).

$$\dot{Q}_{xTB} = q_{xTB} * H_x \tag{5.11}$$

$$\dot{Q}_{TB} = \sum \dot{Q}_{xTB} * 2 \tag{5.12}$$

$$M = \frac{\dot{Q}_{TB}}{(T_i - T_e)} \tag{5.13}$$

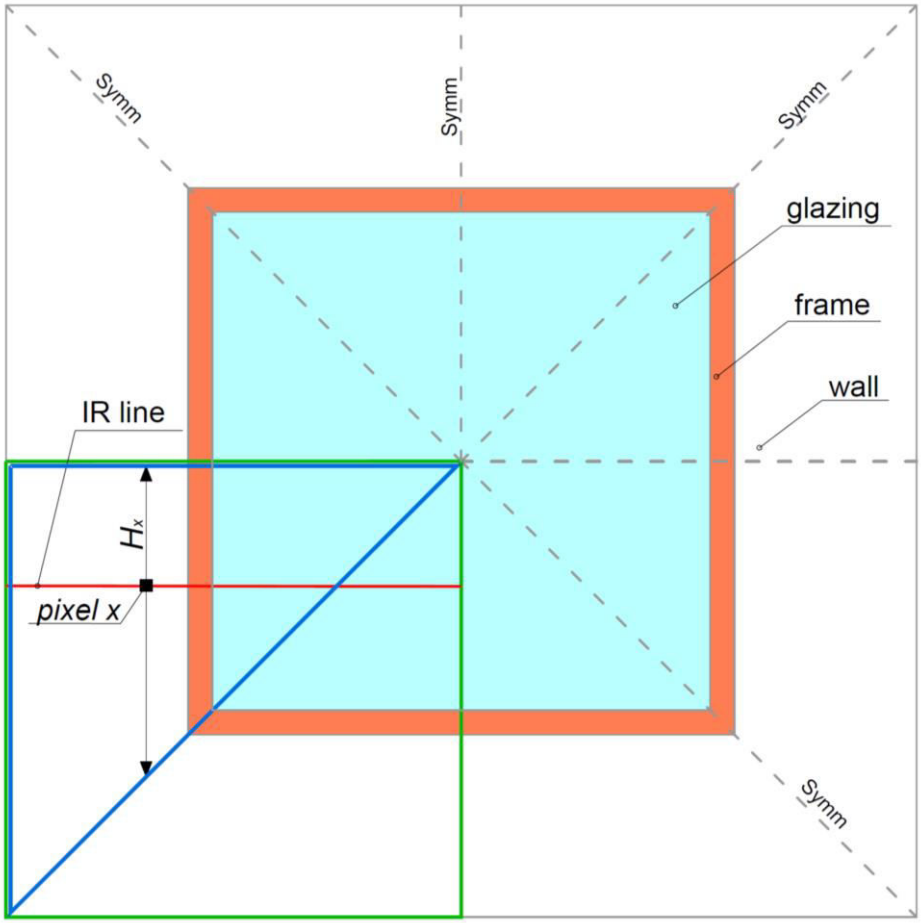

Fig. 5.6. Geometry of a window installed into a wall. Tested section outlined in green, section for calculation outlined in blue.

The determination of heat flow rate for each pixel using Equation (5.7) requires accurate calculation of the heat transfer coefficients. It was shown by O'Grady et al. [21] that this approach contributed to improved accuracy when compared with results obtained with a uniform convective coefficient. Therefore, in the current methodology, precise calculation of the convective heat transfer coefficients h_c for each pixel x is carried out using the Nusselt number Nu (Equation (5.14)).

$$h_{cx} = \frac{Nu_x\, k_x}{l_{ch}} \tag{5.14}$$

where l_{ch} is the characteristic length over which h_c applies and k is the thermal conductivity of the air. Nu is the Nusselt number which is a dimensionless surface temperature gradient [34]. In the indoor environment, it can be evaluated using the Churchill-Chu correlation (Equation (5.15)) that was originally developed for a vertical plate.

$$Nu_x = \left\{ 0.825 + \frac{0.387 Ra_x{}^{1/6}}{\left[1+\left(\frac{0.492}{Pr_x}\right)^{9/16}\right]^{8/27}} \right\}^2 \tag{5.15}$$

The Prandtl number (Pr) is the ratio of kinematic viscosity to thermal diffusivity of the air. The Rayleigh number (Ra) characterizes free convection flow by describing the relationship between buoyancy and viscosity of air and is obtained for each pixel using Equation (5.16):

$$Ra_x = \frac{g\beta_x(T_i - T_{sx})l_{ch}^3}{\nu_x\, \alpha_x} \tag{5.16}$$

The radiative heat transfer coefficient h_r is also evaluated for each pixel on the IR line using Equation (5.17)

$$h_{rx} = \varepsilon\sigma(T_{sx} + T_i)(T_{sx}^2 + T_i^2) \quad (5.17)$$

The surface emissivity ε used in Equation (5.17) was measured in-situ with the ITT, using the contact method, in accordance to ISO 18434-1 [35]. This emissivity was used for both the experimental calculation and the numerical simulations and is given in Table 5.3.

Equations (5.7) and (5.17) are used under the assumption that the building indoor air temperature T_i is constant and very similar to the surrounding temperature T_{sur} which is very often the case. The equations that are appropriate for other cases can be found in [21].

5.6. Numerical studies

Numerical studies of the tested specimens were undertaken to allow for comparison of the ITT surface temperature distributions with the simulated ones. As only two thermocouples were used during the hot box testing, a comparison with the experimental temperatures was limited to two spot temperatures. In addition, since the numerical approach is commonly used in practice to assess thermal bridging where the wall construction details are known, it is useful to compare this approach with the ITT results.

The thermal bridge heat flow rate q_{TB}, Ψ-value of the linear thermal bridges and $\dot{Q}_{TB}$ and M-value of window elements are also determined. For specimens with linear thermal bridges two types of simulations are investigated: finite element (FE) steady-state heat transfer analysis using the ABAQUS package [36] and computational fluid dynamic (CFD) analyses using Ansys Fluent. The results derived from these two types of simulations suggest that FE steady-state heat transfer analysis is sufficiently accurate for thermal bridging heat loss evaluation. Therefore, for window thermal bridging evaluation, only this type of simulation is carried out.

5.6.1. Two-dimensional heat transfer finite element models in Abaqus Standard

Two-dimensional (2D) steady-state FE heat transfer numerical simulations were carried out for Specimens 1 – 2 containing linear parallel thermal bridges and for plain Specimen 5, under the tested environmental conditions. The analyses were carried out with air temperatures and wind velocities mirroring the conditions of the hot box experiment presented in Table 5.2. Simulations included the whole 1.50 m specimen length. Material properties used for the models are presented in Table 5.3.

Table 5.3. Material properties applied to numerical simulations

Property	*Unit*	*Symbol*	*Material*				
			OSB/ timber	*Steel*	*XPS*	*Polystyrene*	*Polyurethane foam*
Conductivity	*W/(mK)*	k	0.13 [37]	50.2 [38]	0.033[39]	0.037[21]	0.030[40]
Density	kg/m^3	ρ	600 [37]	7850 [41]	33 [39]	24 [42]	30 [43]
Emissivity	-	ε	0.93	-	-	-	

The type of element used was a 4-node linear heat transfer quadrilateral (DC2D). A mesh convergence study resulted in an element size of 0.005 m being selected. With this element size, the total heat flow rate q_{tot} varied by only 0.25% from that with a coarser mesh. A finer element size of 0.001 m was used for the steel post, as the post was only 0.005 m thick. Fig. 5.7 shows part of the meshed Specimen 1 in the vicinity of the steel posts.

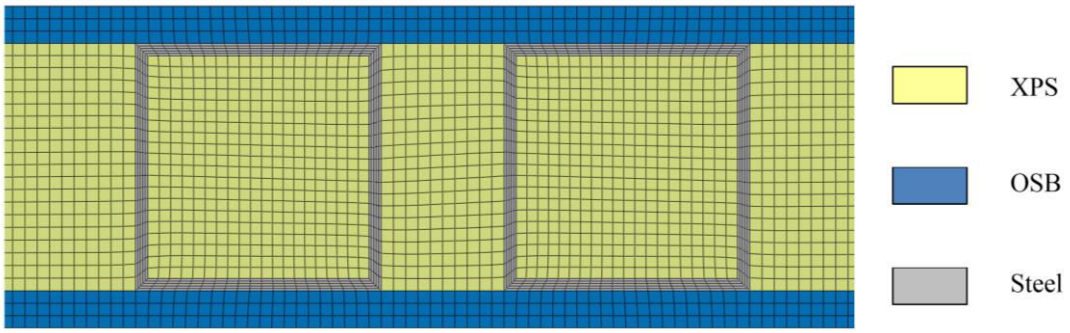

Fig. 5.7. A part of meshed Specimen 1.

Variable indoor convective boundary conditions were implemented in the simulations. These coefficients were evaluated using Equation (5.14), initially from nodal temperatures on the hot surface obtained in a simulation with constant h_{ci}. Based on the predicted temperatures the convective coefficients were updated, and the analysis was repeated. After a further iteration convergence was achieved. Fig. 8 shows the calculated surface convective coefficients for each specimen. As can be seen in this figure, h_{ci} is constant in the plain part of the specimens, outside the thermal bridge zone of influence, but increases significantly by about 1.3 W/m^{2}K for all specimens at the thermal bridge location. Local disturbance in the h_{ci} values, between 1.05 – 1.15 m for Specimen 1, corresponds to the location of OSB connectors used to join two sheets of external OSB in the SIP manufacturing process. The external convective coefficient h_{ce} was calculated for the wind velocities presented in Table 5.2, using Equation (5.18), given by standard EN ISO 6946 [44].

$$h_{ce} = 4 + 4w \qquad (5.18)$$

The FE software used in this study calculates surface radiation using the Stefan-Boltzmann law using the input value of surface emissivity given in Table 5.3, which was derived from measurements as described above.

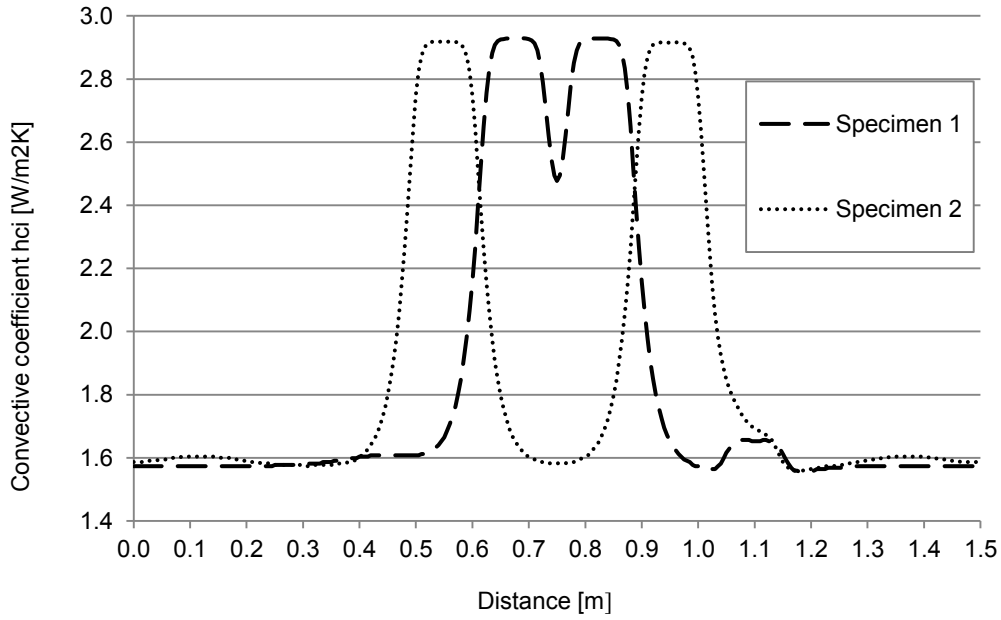

Fig. 5.8. Indoor convective coefficients.

The total heat flow rate for the specimen per unit height, $q_{tot,}$ is obtained directly as an output from the simulation. To obtain the thermal bridge heat flow rate $q_{TB,}$ the uniform heat flow rate q_u of plain Specimen 5 was simulated. The q_{TB} was obtained from Equation (5.19).

$$q_{TB} = q_{tot} - q_u \tag{5.19}$$

The Ψ-value was then calculated in accordance with Equation (5.10).

5.6.2. Three-dimensional numerical simulations in Ansys Fluent

The Ansys Fluent numerical tool was used for the CFD calculations. Using this program, the behaviour of systems, processes and equipment involving the flow of gases and liquids, heat and mass transfer can be simulated. It can also be used for simulating energy efficient building systems and components including building partition's thermal performance [45]. The program implements the finite volume method.

In this section, geometrical 3D models of tested Specimens 1 – 2 with linear thermal bridges and of a plain Specimen 5 are introduced. The specimens' geometries are shown in Table 1. The 3D simulations mirror the hot box tests and take into account not only the specimens themselves but also the supporting panel (into which the specimens are mounted), the air flowing along the specimens on both sides and the baffles around both sides of the specimens forming the air channel. A 3D view of the model for Specimen 1 mounted into the surrounding Styrofoam panel with an air inlet and outlet and baffles is given in Fig. 5.9. The cold baffle is shown in green and warm baffle in red.

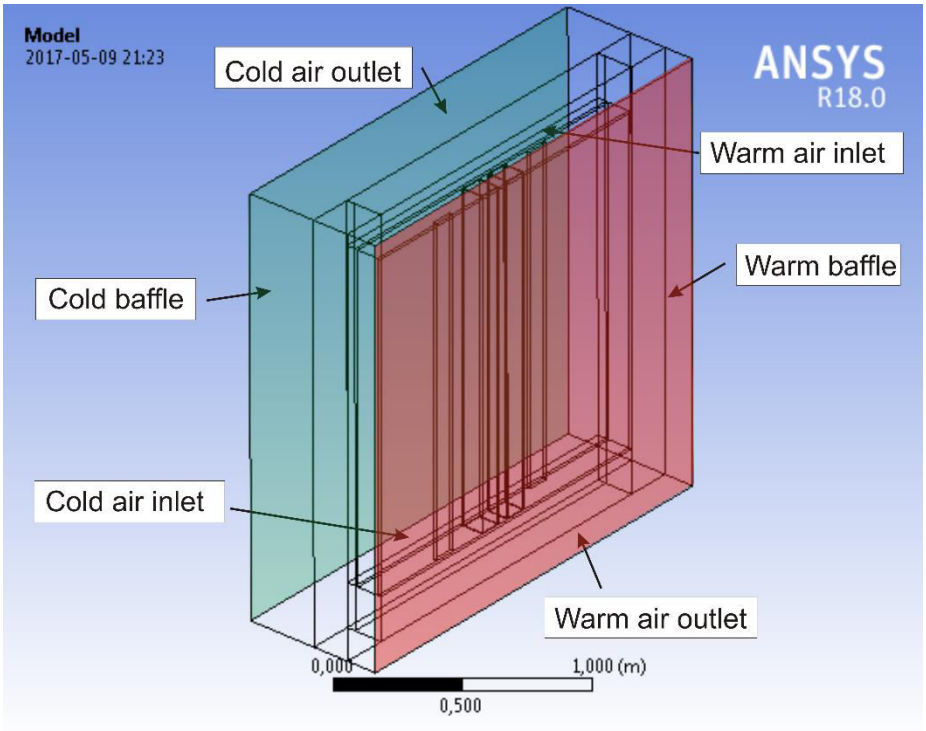

Fig. 5.9. The 3D view of Specimen 1 with surrounding elements.

The same material properties, listed in Table 5.3, were applied as for 2D FE simulations. Additionally, the thermal conductivity of the surround panel made of Styrofoam was assumed to be 0.033 W/(mK) and its surface emissivity 0.92. For the hot and cold baffles, a surface emissivity is 0.95 was used. Air thermal properties were assumed to be piecewise linear between the values presented in Table 4.

Table 5.4. Air thermal properties applied for the calculations

T [°C]	ρ [kg/m^3]	λ [W/(mK)]	c_p [J/(kgK)]	μ [kg/(ms)]
-10	1.342	0.0236	1005.0	$1.67 \cdot 10^{-5}$
0	1.293	0.0244	1005.0	$1.72 \cdot 10^{-5}$
10	1.247	0.0251	1005.0	$1.76 \cdot 10^{-5}$
20	1.205	0.0259	1005.0	$1.81 \cdot 10^{-5}$
30	1.165	0.0267	1005.0	$1.86 \cdot 10^{-5}$

A mass flow inlet of warm air at a uniform temperature at the top of the model and warm air outlet at the bottom of the model simulates the inverted convection in the hot box during the testing. The cold baffle surface was assumed to be isothermal with the mean surface temperature known from measurements. The warm baffle surface was defined as adiabatic because the baffle was the hot box wall; hence no heat was transferred through the hot box walls during the measurements. Boundary conditions for all three specimens are given in Table 5.5. The warm air inlet and the cold air inlet temperatures $T_{inlet,i}$ and $T_{inlet,e}$, respectively, were measured during the experiment using three thermocouples for each case. The inlet temperatures were the average values from these three thermocouples.

Table 5.5. Boundary conditions

Specimen	$T_{se,b}$ [°C]	$\dot{m}_e$ [kg/s]	$T_{inlet,e}$ [°C]	$\dot{m}_e$ [kg/s]	$T_{inlet,i}$ [°C]
1	-4.91	1.337	-7.05	0.0346	26.05
2	-4.91	1.298	-7.35	0.0346	26.15
5	-4.95	1.239	-5.15	0.0346	24.78

5.6.2.1. Mesh and model settings

All calculations were performed with a mesh of about 4.5 million elements. The mesh qualities were checked for: aspect ratio (max. 1:27) and skewness (max. 0.94). Their values should not exceed the limiting values of 1:35 and 0.95, respectively [45].
The settings for the finite volume CFD model for the convective and radiative heat transfer are listed in Table 5.6.

Table 5.6. CFD model settings

Solver	Stationary	
Viscous model	k-ε	
Air thermal properties	Density, conductivity and dynamic viscosity	Piecewise-linear
	Specific heat	Constant
Discretization schemes	Gradient	Least squares cell based
	Pressure	Standard
	Momentum	Second order upwind
	Turbulent kinetic energy	Second order upwind
	Turbulent dissipation rate	Second order upwind
	Energy	Second order upwind
Radiation model	Discrete Transfer Radiation Model	

The heat flow rate through specimens containing thermal bridges 1 – 2 ($\dot{Q}_{sp}$) and heat flow rate through the plain Specimen 5 ($\dot{Q}_{plain}$) was derived from the models. Then, using Equations (5.3) and (5.10), q_{TB} and Ψ-value were calculated, respectively.

5.6.3. Three-dimensional heat transfer finite element models in Abaqus Standard

Results of the modelling of Specimens 1 and 2, presented in Section 5.7, show that it is sufficient to perform steady-state heat transfer FE simulation for multiple thermal bridging assessment. Therefore, for Specimens 3 and 4 containing window thermal bridging only this type of simulation was undertaken. Because of the complexity of the window geometry, a 3D model was created. The analyses were carried out with the same air temperatures and wind velocities as the hot box experiment (Table 5.2). Material and air properties used for the models are presented in Table 5.3 and Table 5.4, respectively. For Specimen 4, the thermal properties of the PVC frame were calculated as the area-averaged values for PVC and air. As the window specimen had diagonal symmetry, only one half of the specimen was modelled.

The type of element used was a 20-node quadratic heat transfer brick (DC3D20), with an element size 0.01m. With this size, mesh convergence was found, as the heat flow rate of the whole specimen $\dot{Q}_{sp}$ differed by only 0.15% from that with a coarser mesh. Fig. 5.10 shows the FE meshes for Specimen 3 (a) and Specimen 4 (b).

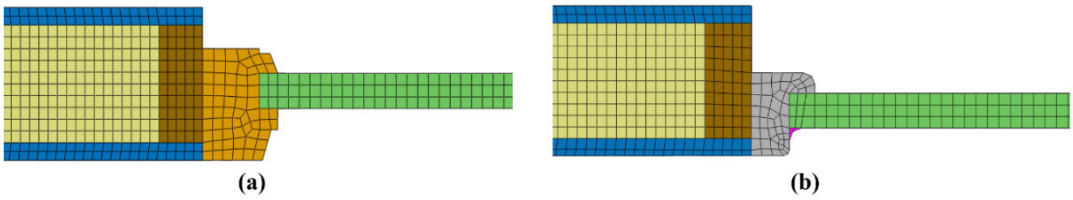

Fig. 5.10. Part of mesh of model for Specimen 3 (a) and Specimen 4 (b). (For colour legend, refer to Table 1)

From the 3D FE simulations, the thermal bridging heat flow rate $\dot{Q}_{TB}$ was calculated using Equation (5.5), as the difference between the heat flow rate for specimens containing thermal bridges, $\dot{Q}_{sp}$, and the uniform heat flow rate for

Specimen 5, $\dot{Q}_{plain}$. Then the thermal transmittance associated with window system *M*-value was calculated using Equation (5.13).

5.7. Results and discussion

In this section, the results from the thermographic survey and from 3D CFD, 2D FE and 3D FE simulations are presented and compared with the hot box measurements. All experimental results are given together with their uncertainties *(u)*. The uncertainty of the ITT results is expressed in terms of the experimental standard deviation (*SD*). The *SD* is calculated from series of five ITT measurements to characterize the dispersion from the mean value, according to Guide 98-3 [46]. As only one set of measurements for each specimen was taken using the hot box and thermocouples, the uncertainties are calculated, as described in Section 5.4.3, for the hot box and taken as the measurement accuracy provided by the manufacturer for the thermocouples.

5.7.1. Linear parallel thermal bridges

Results obtained from measurements and from numerical simulations of Specimens 1 and 2 containing parallel linear thermal bridges are presented and discussed. The results include surface temperatures, thermal bridge heat flow rate q_{TB} and linear thermal transmittance Ψ-value.

5.7.1.1. Surface temperature distributions

Figs. 5.11 – 5.12 show the temperature distributions along a horizontal line at the specimens' mid-height on the hot surface. On these lines, two spot temperatures measured by thermocouples (TC) S1 and S2 during the hot box testing are marked. The temperature T_{S1} denotes the uniform surface temperature outside the thermal bridge zone of influence and temperature T_{S2} the surface temperature measured in the middle of thermal bridge. Table 5.7 presents these temperatures obtained from four different methods. Temperatures obtained by means of the ITT and from numerical simulations are compared to the temperatures measured by thermocouples. As can be

seen in Figs. 5.11 – 5.12 and in Table 5.7, the uniform surface temperatures T_{S1} measured by the ITT and the thermocouples and obtained from numerical simulations are in excellent agreement. The maximum difference for T_{S1} between the thermocouple and ITT measurements was -0.29°C for Specimen 1. The maximum difference between minimum surface temperatures in the middle of the thermal bridge T_{S2} was +0.60°C and relates to the temperature obtained in CFD model for Specimen 1. These maximum differences between these values indicate a good agreement between all methods.

While considering the surface temperature at the symmetry line between the two thermal bridges in Specimen 1, an increase of around 3°C from the temperature on the thermal bridge, T_{S2}, can be seen in all simulated temperatures. At the same point, the temperature recorded by the ITT increased by only 1 °C. While comparing the temperatures at the specimen symmetry line of Specimen 2, it can be seen that the temperatures obtained from FE simulations came back to the uniform temperature. This thermal behaviour is in agreement with [23], which stated that thermal bridges situated further apart than the component thickness, do not influence each other. The temperature obtained by the ITT at the same point shows a value 0.34°C lower than the uniform temperature T_{S1}. The fact that the uniform temperature has not been reached between the two thermal bridges indicates that the ITT recording shows a greater level of interaction between the thermal bridges. The thermal bridge zone of influence recorded by the ITT is in all cases greater than that simulated numerically, as it can be seen in Figs. 5.11 – 15.2. This difference was previously identified by Heinrich and Dahlem [15].

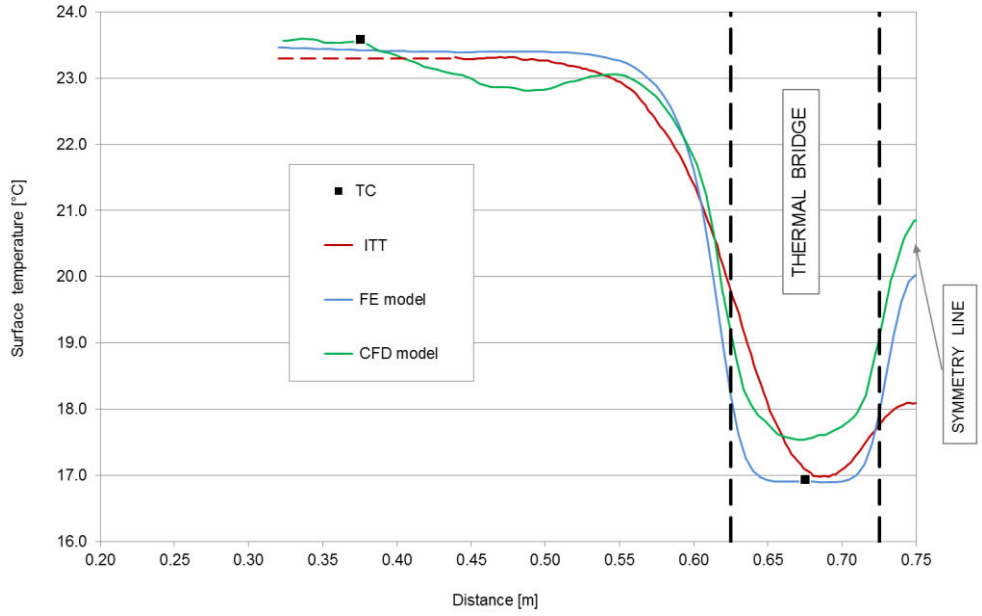

Fig. 5.11. Surface temperature on the warm side of Specimen 1 obtained from thermocouples, the ITT, 2D FE and 3D CFD models.

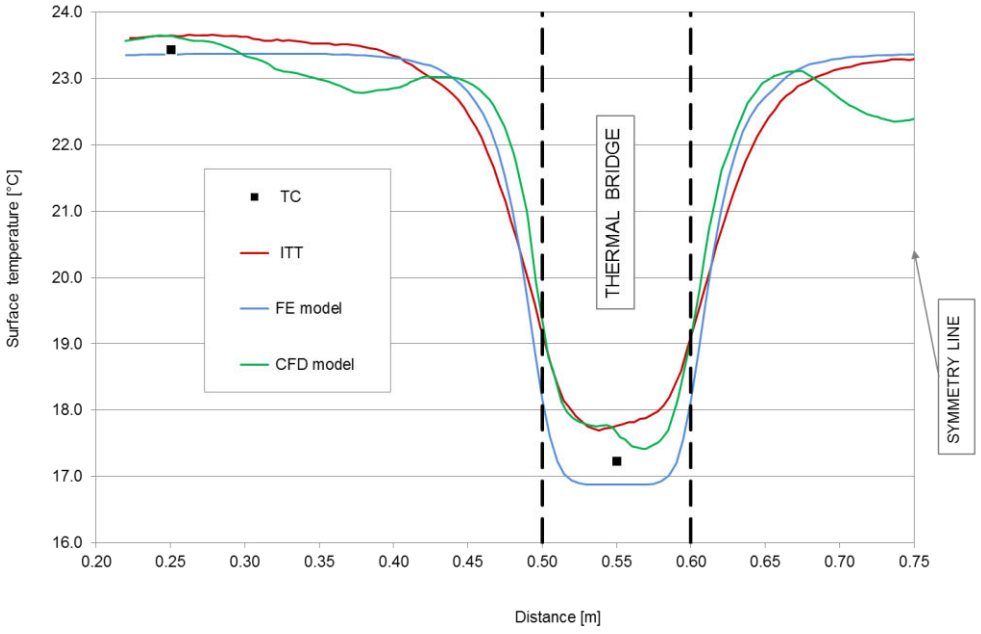

Fig. 5.12. Surface temperature on the warm side of Specimen 2 obtained from thermocouples, the ITT, 2D FE and 3D CFD models.

The differences in surface temperature distribution provided from numerical simulations can be explained in part by the different approaches used to account for

convective boundary conditions along the hot specimen surface. In the 2D FE simulations, the indoor convective boundary conditions were applied using variable indoor convective coefficients correlated with surface temperatures. On the other hand, the 3D CFD simulations included the baffles surrounding the specimen in the model and the boundary conditions were applied by specifying the air inlet and outlet properties, hence they account for convective movements along the specimen surfaces. This was done to reflect the test conditions in the hot box as closely as possible. The CFD simulations revealed that, due to the thermal bridge presence, the conditions between the specimen and the hot baffle did not stay uniform as shown in Fig. 5.13 for Specimen 2. The dark green line represents the surface temperatures whereas the other lines represent air temperatures at different distances from the specimen. This figure demonstrates the non-uniformity of the air while testing a specimen containing thermal bridges in the hot box and explains the presence of irregularities in the temperature profiles seen in Figs. 5.11 – 5.12. It should be pointed out that the ITT was performed after the hot box testing was completed and after the hot baffle was removed so the downstream flow along the specimen was no longer present. This may explain the difference between temperature distributions measured by the ITT and simulated in CFD models. Other factors influencing the accuracy of the numerically-predicted temperature distributions are errors in the assumed material properties and homogeneity, which may not fully reflect the actual conditions.

As can be seen in Figs. 5.11-5.12, the simulated thermal bridge zones of influence are smaller than those recorded by the ITT. As mentioned previously, this was also reported in a study by Heinrich and Dahlem [15] who attributed the difference to the boundary conditions assumed in the simulations. Using ITT or other in-situ measurements of temperatures such as thermocouples does not have this drawback. However, to obtain a complex surface temperature distribution of a component affected by thermal bridging, a significant number of thermocouples would be needed. For this purpose, the ITT is a much more suitable tool as it allows the full surface temperature distribution impacted by thermal bridging to be measured.

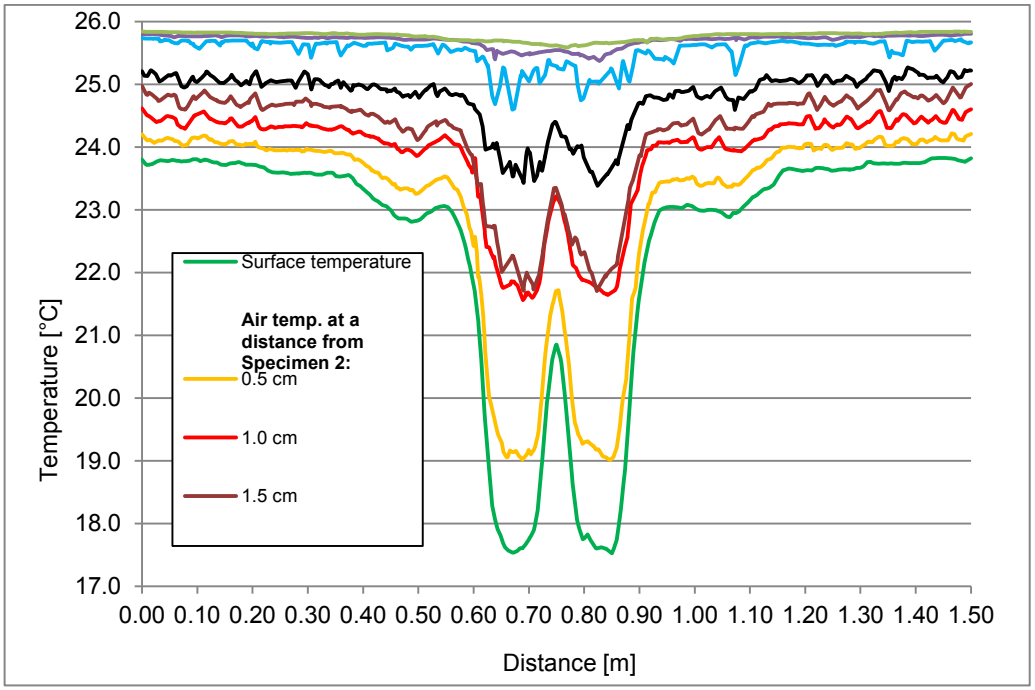

Fig. 5.13. Surface and air temperatures distribution along the Specimen 2 at mid-height.

Table 5.7. Surface temperatures comparison

		Surface temperatures [°C]						*Differences from TC [°C]*		
		TC	*u TC*	*ITT*	*SD ITT*	*FE model*	*CFD model*	*ITT*	*FE model*	*CFD model*
T_{S1}	Specimen 1	23.59	0.30	23.30	0.21	23.43	23.55	-0.29	-0.16	-0.04
	Specimen 2	23.44	0.30	23.64	0.11	23.37	23.64	0.20	-0.07	0.20
T_{S2}	Specimen 1	16.94	0.30	16.98	0.06	16.91	17.54	0.04	-0.03	0.60
	Specimen 2	17.24	0.30	17.77	0.16	16.9	17.67	0.53	-0.34	0.43

5.7.1.2. Thermal bridge heat flow rate q_{TB} and linear thermal transmittance Ψ-value

The thermal bridge heat flow rate q_{TB} and the linear thermal transmittance Ψ obtained from the hot box measurements and from the ITT, as well as those obtained from numerical simulations, are presented in Table 5.8. The results from the ITT and from simulations

are compared to the results from hot box, as reference values. The ITT results are calculated using variable convective coefficients, as described in Section 3.

Comparison of the results (Table 5.8) obtained according to proposed methodology using the ITT with those measured by the hot box shows good agreement. The percentage deviations between -5.0 % and +2.5 % for q_{TB} and between +1.0 % and +7.0 % for Ψ-values have been recorded. Considering the thermal bridge heat flow rate q_{TB} derived from numerical simulations for Specimen 1, the greatest deviation was +12.5 % for CFD model. For Specimen 2, the q_{TB} derived from FE model had the highest deviation at +10.0 %. When comparing the Ψ-values for Specimen 1, the greatest deviation was +8.5 % for the FE model. The maximum deviation was -13.0 % in the Ψ-value obtained from the CFD model for Specimen 2. In general, the maximum deviation of results derived from numerical simulations from the hot box measurements is greater than for the ITT results. This may be due to the boundary conditions input and the assumed thermal properties input to the simulations being different from the actual values. Also, in the numerical analysis, possible workmanship mistakes or inhomogeneities in the construction are not taken into account. On the other hand, the ITT method represents the results based on measurements thus represents the actual thermal performance of the specimen.

To define how the accuracy of ITT results is impacted by the pixel-based approach to determining the h_{ci} value, the Ψ-value of the tested specimens was also calculated using a constant value of h_{ci} equal to 2.5 W/m^{2}K, in accordance with EN ISO 6946 [40]. Using the constant h_{ci} approach, the calculated Ψ-values deviate by 2.5% and 8.5% more that the values obtained using the variable approach for Specimens 1 and 2, respectively. This comparison confirms the correctness of approach presented in [21], where it was demonstrated that evaluation of surface coefficients for each pixel on the IR line improves the results accuracy.

Table 5.8. Thermal bridge heat flow rate q_{TB} and linear thermal transmittance Ψ-value.

		q_{TB} and Ψ results						*Deviation from hot box [%]*		
		hot box	*u hot box*	*ITT*	*SD ITT*	*FE model*	*CFD model*	*ITT*	*FE model*	*CFD model*
q_{TB} [W/m]	Specimen 1	7.41	0.28	7.04	1.61	7.54	8.33	-4.99	1.75	12.42
	Specimen 2	13.09	0.28	13.42	2.63	14.41	13.61	2.52	10.08	3.97
ψ [W/mK]	Specimen 1	0.450	0.010	0.455	0.017	0.488	0.418	1.11	8.44	-7.11
	Specimen 2	0.474	0.010	0.507	0.090	0.496	0.412	6.96	4.64	-13.08

5.7.1.3. Influence of the distance between parallel thermal bridges on Ψ-values.

In this section, the influence of thermal bridges' positioning on the Ψ-value is presented and discussed. To observe the increase of heat loss caused by two thermal bridges located at different distances from each other, test results from a specimen containing a single thermal bridge (Specimen S), included in a study published in [21], are used as reference values. The first row of Table 5.9 presents Ψ-values for this specimen, multiplied by two to represent the influence of two independent non-interacting thermal bridges. The remaining rows give the differences between this Ψ-value and the Ψ-values evaluated for Specimens 1 and 2. The differences between Ψ-values are very small; however, some trends can be noticed. The Ψ-values for Specimen 1, situated 0.05m apart, are lower than the Ψ-value of two single thermal bridges. In general, the heat loss increases when the distance between thermal bridges increases. However, the simulated values showing negligible differences between results predicted for thermal bridges located 0.05 m and 0.30 m apart. The Ψ-value measured by the ITT shows the greatest increase (11.5 %) while extending the distance between the thermal bridges. The Ψ-value provided by the hot box measurement for

Specimen 2 is 5% greater than the Ψ-value of Specimen 1. As demonstrated previously in Section 5.7.1.1, the ITT recorded stronger interaction between the thermal bridges at 0.05 m spacing than the simulation methods. Also, as can be seen in the temperature distribution of Specimen 2 in Fig. 5.12, the ITT still shows some degree of interaction between the thermal bridges at 0.30 m spacing whereas simulation methods do not reflect any interaction. This explains the greater increase of Ψ-values measured by the ITT than from the simulations.

When undertaking an assessment of thermal bridging using the ITT, adjacent bridges can be assumed to interact if the temperature between the bridges remains lower than the uniform surface temperature. In this case, the assessment of the two bridges should be included in the same analysis.

Table 5.9. Ψ-values in [W/mK] for thermal bridges at different spacing.

	hot box	*ITT*	*FE model*	*CFD model*
Specimen S x 2	0.506	0.476	0.514	0.510
Specimen S x 2 – Specimen 1	0.056	0.021	0.022	0.092
Specimen S x 2 – Specimen 2	0.032	-0.031	0.014	0.098

5.7.2. Window system thermal bridges

Experimental and numerical results for Specimens 3 and 4 containing window elements are presented and discussed. The temperatures, heat flow rates and window thermal transmittance results obtained from ITT measurement and from numerical simulations are compared with those obtained in the hot box device.

5.7.2.1. Surface temperature distributions on specimens with windows

Figs. 5.14 – 5.15 show the temperature distributions along horizontal lines across Specimen 3 and 4 at the mid-height of the vertical window frame on the hot surface. During testing, two uniform surface temperatures were measured by thermocouples (*TC*). The temperature T_{S1} recorded the uniform temperature on the wall surface (at a distance of 0.3 m from the left edge of the specimen) and T_{S2} on the polystyrene 'glazing' (at a distance of 0.9 m from the left edge of the specimen). The ITT temperature profile is the mean temperature determined from five individual thermograms (Lines IR 1 – IR 5). In addition, the temperature distribution derived from the numerical simulations (FE model) is presented. These lines show how the presence of an installed window disturbs the uniform wall surface temperatures. As can be seen in these figures and in Tables 5.10 – 5.11, the surface temperature distribution measured by the ITT and the thermocouples and obtained from numerical simulations are in good agreement.

Considering the temperatures of points *S1* and *S2*, it can be seen that the steady state temperature on the wall component from both the ITT and the FE simulation are in excellent agreement with the *TC* measurements with a deviation of +/- 0.30 ℃ for both methods. For point S2 on the polystyrene 'glazing', the temperature obtained from the ITT deviates by 1.20 ℃ for Specimen 3 and 1.00 ℃ for Specimen 4 from the *TC* measurements while the corresponding deviations for the FE model are 0.30 ℃.

To facilitate discussion of the temperature disturbance at window frame and its connection to the wall unit and glazing, three points where peaks in the temperature distribution occur (Figs. 5.14 and 5.15) are considered. At point *A*, a temperature drop occurs as a result of thermal bridging at the wall and window frame connection at a distance of 0.6m from the left edge of the specimen. Point *B* is the location of a temperature peak at the edge of the window frame and at point *C* the temperature drops again at the window frame and polystyrene connection. For Specimen 3 with the timber frame window, excellent correlation is found between the ITT and FE temperatures at these three points shows good agreement with differences between the measured and simulated temperatures lower than 0.5 ℃ in all cases. For Specimen 4

with a PVC window, the temperatures provided by the ITT and derived from FE model for points *A* and *B* agreed to within +/-0.5 ℃ while, for point *C*, a slightly higher difference of +1.0 ℃ was recorded. It can be noted from Figs. 5.14 and 5.15 that the zone of influence of the windows is greater in the ITT temperature profiles than for the FE predictions as was the case with the parallel thermal bridges. The differences in surface temperature distribution derived from the ITT and from the FE model are due in part to boundary conditions implemented in the FE model, as explained further in Section 5.7.1.1. Other reasons for the differences in surface distribution obtained from these two methods may be the assumed thermal properties input and the homogeneities of materials in the numerical analysis.

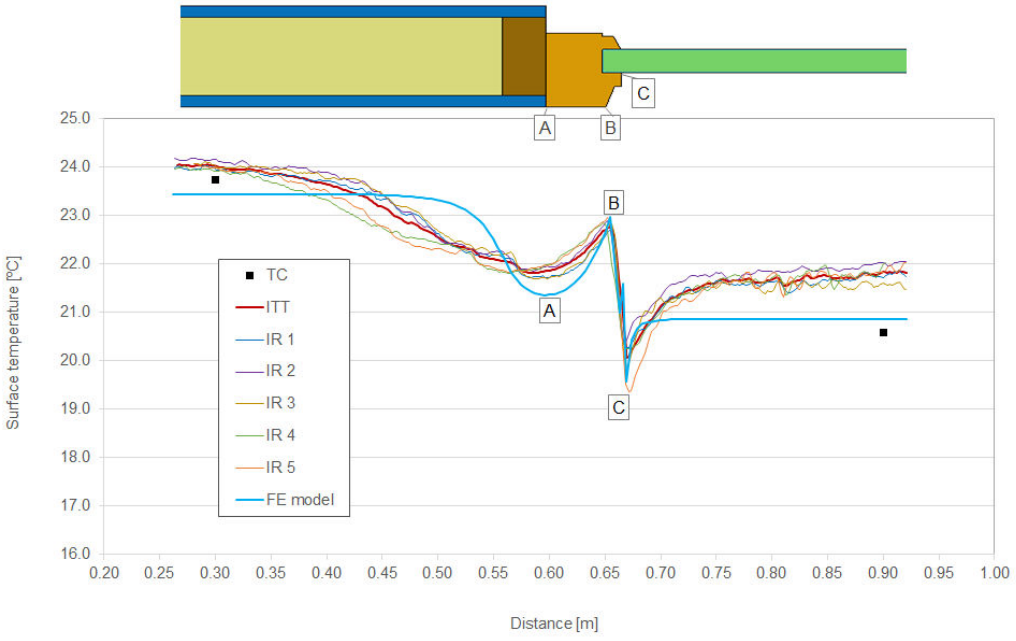

Fig. 5.14. Temperature distribution for Specimen 3 with timber frame window.

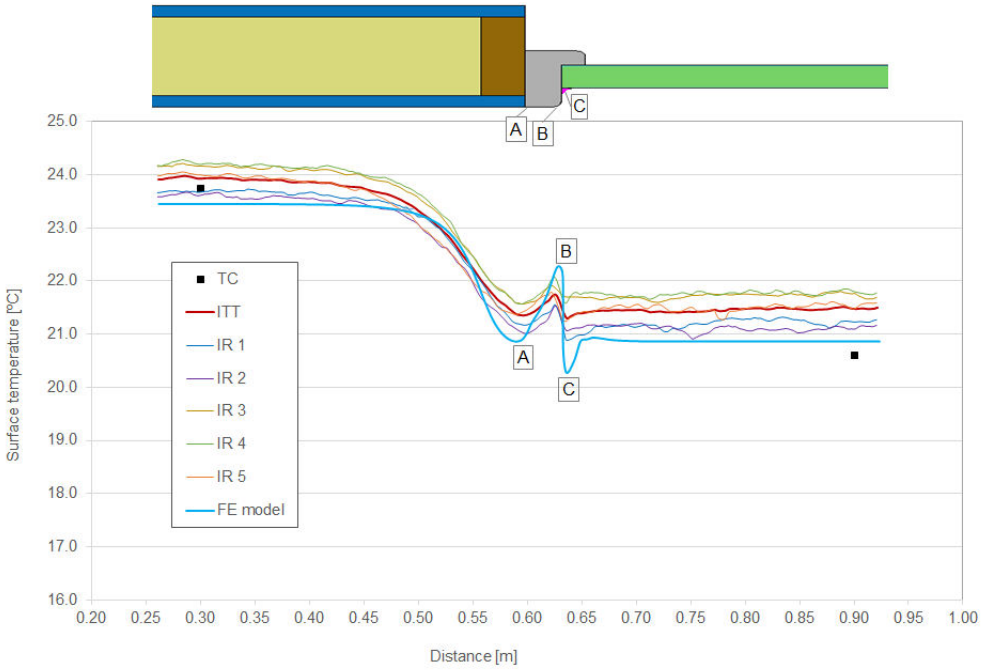

Fig. 5.15. Temperature distribution for Specimen 4 with PVC frame window

Table 5.10. Uniform surface temperatures T_{S1} and T_{S2} comparison

		T_{S1} and T_{S2} [°C]					Differences from TC [°C]	
		TC	*u TC*	*ITT*	*SD ITT*	*FE*	*ITT*	*FE*
T_{S1}	Specimen 3	23.74	0.30	24.04	0.07	23.45	0.30	-0.29
	Specimen 4	23.74	0.30	23.95	0.24	23.45	0.21	-0.29
T_{S2}	Specimen 3	20.60	0.30	21.81	0.18	20.86	1.21	0.26
	Specimen 4	20.58	0.30	21.59	0.28	20.86	1.01	0.28

Table 5.11. Temperature distribution obtained from ITT and FE model

	Point A [°C]				Point B [°C]				Point C [°C]			
	ITT	*SD ITT*	*FE*	*difference*	*ITT*	*SD ITT*	*FE*	*difference*	*ITT*	*SD ITT*	*FE*	*difference*
Specimen 3	21.82	0.08	21.36	0.46	22.78	0.12	22.97	-0.19	20.05	0.32	19.58	0.47
Specimen 4	21.35	0.22	20.86	0.49	21.74	0.21	22.27	-0.53	21.30	0.30	20.28	1.02

5.7.2.2. Comparison of window thermal bridging heat flow rate $\dot{Q}_{TB}$ and window thermal transmittance *M*-value

The thermal bridging heat flow rate $\dot{Q}_{TB}$ and thermal transmittance *M*-value of window specimens are presented in Table 5.12. In general, the results obtained from the ITT and from numerical simulations are in good agreement showing similar deviations from the hot box results. Considering $\dot{Q}_{TB}$ for Specimen 3, percentage deviations of +1.9 % and -6.48 % for the ITT and for FE model were recorded, respectively. For Specimen 4 both ITT and the FE model results show a deviation of about -8.0 % compared to the $\dot{Q}_{TB}$ measured by the hot box. While considering the window thermal transmittance *M*-values for Specimen 3, the ITT value is within 0.61 % and the FE value within -7.66 % of the hot box measurements. For Specimen 4, the *M*-value measured by the ITT and simulated numerically deviates from the hot box measurement by about -9.5 %. Considering the ITT results, a high level of accuracy with the hot box measurements was found for Specimen 3. For Specimen 4, the accuracy is less; however, as the error is less than 10 %, it is a reasonable alternative to existing thermal bridging assessment methods. In regard to the FE results, their deviations from the hot box measurements may be explained by the assumed boundary conditions, thermal properties and the lack of accounting for workmanship mistakes and for material inhomogeneity, as previously mentioned in Section 5.7.1.2. An additional source of error could be the use of an area-averaged thermal conductivity for the PVC window frame in modelling Specimen 4. A sensitivity analysis revealed that increasing thermal conductivity of this PVC frame by 20 % results in a 2 % higher thermal bridging heat flow rate. This demonstrates the significant influence of the thermal properties on the simulated $\dot{Q}_{TB}$ results.

Table 5.12. Window thermal bridging heat flow rate $\dot{Q}_{TB}$ and window thermal transmittance *M*-value.

		$\dot{Q}_{TB}$ *and M results*					*Deviation from hot box [%]*	
		hot box	*u hot box*	*ITT*	*SD ITT*	*FE*	*ITT*	*FE*
$\dot{Q}_{TB}$ *[W]*	Specimen 3	20.05	0.30	20.43	3.72	18.75	1.90	-6.48
	Specimen 4	20.66	0.30	19.00	0.38	18.93	-8.03	-8.37
M [W/K]	Specimen 3	0.691	0.011	0.695	0.118	0.638	0.61	-7.66
	Specimen 4	0.713	0.011	0.646	0.013	0.644	-9.35	-9.68

5.8. Summary and conclusions

This paper has demonstrated the suitability of the indoor quantitative ITT for the heat loss assessment of multiple thermal bridges and windows in building components. A significant advantage of this methodology is that the actual heat loss associated with multiple thermal bridges and with windows installed into a building envelope can be determined without knowing the building envelope structure. As the actual heat loss is measured, factors that influence the thermal efficiency of a building such as interaction effects, material degradation over time or poor workmanship are automatically accounted for.

The developed methodology has been validated in the case of multiple parallel thermal bridges, such as occurs when steel columns form part of the building envelope. For these situations, the additional heat loss is expressed by thermal bridging heat losses q_{TB} and Ψ-values. Comparing the multiple thermal bridging heat losses q_{TB} and Ψ-values obtained from the ITT with those measured in calibrated hot box tests, the differences varied between -5.0 % and +2.5 % and between +1.0 % and +7.0 % for these two measures, respectively. The good agreement between these two measurements approaches points to the suitability of the proposed ITT method for parallel thermal bridging assessment. The distance between adjacent thermal bridges determines the degree of interaction between them; however, it was concluded that,

when using the ITT methodology, it is not necessary to know the critical distance in advance. In the post-processing of IR images with two or more thermal bridges, the thermal bridge zone of influence of each thermal bridge is defined and the IR line is created. If the uniform surface temperature of the building envelope is not reached between the thermal bridges, it means they interact with each other. Therefore, the assessment of their heat loss should be evaluated from the same thermogram.

In the proposed methodology, the additional heat being dissipated because of the presence of a window is described by the thermal bridging heat flow rate $\dot{Q}_{TB}$. Using this measure, both the window thermal quality and the window installation, which may contribute significant additional heat loss, are assessed. A new window thermal transmittance or *M*-value is introduced, which is defined as the thermal bridging heat flow rate $\dot{Q}_{TB}$ per unit temperature difference between the indoor and outdoor environments. In tests on specimens containing timber- and PVC-framed windows, the $\dot{Q}_{TB}$ and *M*-values evaluated using the ITT deviated from the hot box measurements by between -8.0 % and +1.9 % and between -9.4 % and +0.6 %. As the deviation in all measured cases are less than 10 %, this suggests that this approach gives reasonable estimation of the actual thermal bridging performance.

The paper has demonstrated two different numerical approaches to multiple thermal bridges assessment, validated against the hot box measurements. These are FE steady-state heat transfer simulation and CFD analysis. The study revealed that time-consuming CFD modelling, where the convective air movements along the specimen were modelled explicitly, did not improve the results accuracy. The results show that the relatively more straightforward FE heat transfer modelling approach is sufficient for predicting the thermal bridging heat losses. The thermography results were found to be in good agreement with the simulated results. It was possible to create these numerical models as the internal structure of tested specimens was known. However, in the case of existing buildings, this information may not be available, and so it is not possible to develop accurate numerical models. In these cases, in-situ measurement is the only way to evaluate thermal bridging performance. This study has shown that the indoor quantitative ITT can be applied in these cases.

The application of the indoor ITT methodology for evaluating heat loss through multiple parallel linear thermal bridges and through installed windows has been validated in laboratory conditions, using a hot box device. Testing the suitability of this method in the real conditions, on real buildings, under quasi-steady state conditions is required where some limitations and challenges are to be expected. The quasi-steady state needs to be maintained before and while performing the ITT survey. This may be challenging since outdoor conditions, such air temperature, solar radiation and wind, cannot be controlled. Some recommendations on choosing the optimum outdoor conditions can be found in Albatici at el. [47], who suggested that a deviation of up to 6 ℃ in the outdoor air temperature within 12 hours before testing is acceptable. Solar radiation should be always avoided by carrying out the survey in the early morning before sunrise. With regard to the influence of wind, O'Grady at el. [22] showed how to adjust the Ψ-value obtained from ITT surveys carried out at different wind speeds to that at standard wind conditions. To achieve the recommended minimum difference of 10 ℃ [48] between the indoor and outdoor air temperatures for the ITT survey, it is often necessary to raise the indoor air temperature significantly. This can be created and controlled by the thermographer using a space heating system.

A practical application of this methodology would be for building thermal assessments before and after retrofitting of existing buildings, so that the actual improvement in thermal performance can be quantified. It could also be useful to building owners in planning their thermal retrofit strategy as priority could be given to those buildings where the need is greatest.

5.9. Acknowledgments

The authors wish to thank the following:

1) College of Engineering and Informatics, National University of Ireland Galway for providing a Postgraduate Scholarship for the first author.
2) Cracow University of Technology CUT, especially the Head of the Institute, Prof. Jacek Schnotale, and the technician, Eng. Mariusz Rusiecki, for access to the hot box facility and constant assistance during the testing.
3) SIP Energy Ltd., Athenry Co. Galway, in particular John Moylan, for supplying the test specimens.
4) Enterprise Ireland for Innovation Voucher IV-2014-4203.

5.10. References

[1] International Energy Agency, Transition to Sustainable Buildings: Strategies and Opportunities to 2050, Paris 2013.

[2] Directive 2010/31/EU of the European Parliament and of the Council on the energy performance of buildings 2010.

[3] Evaluation of Directive 2010/31/EU of the European Parliament and of the Council on the Energy Performance of Buildings, European Commission, 2016.

[4] J. Goggins, P. Moran, A. Armstrong, M. Hajdukiewicz, Lifecycle environmental and economic performance of nearly zero energy buildings (NZEB) in Ireland, Energy Build. 116 (2016) 622–637.

[5] EN ISO 14683 Thermal bridges in buildings construction - linear thermal transmittance - simplified methods and default values, 2007.

[6] EN ISO 10211 Thermal bridges in building construction - heat flow and surface temperatures - detailed calculations, 2017.

[7] A. Capozzoli, A. Gorrino, V. Corrado, A building thermal bridges sensitivity analysis, Appl. Energy, 107 (2013) 229–243.

[8] H. Viot, A. Sempey, M. Pauly, L. Mora, Comparison of different methods for calculating thermal bridges: Application to wood-frame buildings, Build. Environ. 93 (2015) 339–348.

[9] S. Hassid, Thermal bridges in homogeneous walls: A simplified approach, Build. Environ. 24 (1989) 259–264.

[10] S. Hassid, Thermal bridges across multilayer walls: An integral approach, Build. Environ. 25 (1990) 143–150.

[11] Building Regulation Conservation of Fuel and Energy Technical, Guidance Document Part L 2017.

[12] L. Zalewski, S. Lassue, D. Rousse, K. Boukhalfa, Experimental and numerical characterization of thermal bridges in prefabricated building walls, Energy Convers. Manag. 51 (2010) 2869–2877.

[13] F. Ascione, N. Bianco, R. F. De Masi, G. M. Mauro, M. Musto, G. P. Vanoli, Experimental validation of a numerical code by thin film heat flux sensors for the resolution of thermal bridges in dynamic conditions, Appl. Energy 124 (2014) 213–222.

[14] F. Ascione, N. Bianco, R. Francesca, D. Masi, F. De Rossi, G. Peter, Simplified state space representation for evaluating thermal bridges in building: Modelling, application and validation of a methodology, Appl. Therm. Eng. 61 (2013) 344–354.

[15] H. Heinrich, K. Dahlem, Thermography of Low Energy Buildings, In Proceedings of International Conference on Quantitative Infrared Thermography Qirt 2000, Reims, France.

[16] A. Wróbel, T. Kisilewicz, Detection of thermal bridges - aims, possibilities and conditions, In Proceedings of International Conference on Quantitative Infrared Thermography Qirt 2008, Cracow, Poland.

[17] M. Fox, S. Goodhew, P. De Wilde, Building defect detection: External versus internal thermography, Build. Environ. 105 (2016) 317–331.

[18] I. Benkő, Quantitative analysis of thermal bridges of structures through infrared

thermograms, In Proceedings of International Conference on Quantitative Infrared Thermography Qirt 2002, Dubrovnik, Croatia, 203–208.

[19] F. Asdrubali, G. Baldinelli, F. Bianchi, A quantitative methodology to evaluate thermal bridges in buildings, Appl. Energy 97 (2012) 365-373.

[20] F. Bianchi, A. Pisello, G. Baldinelli, F. Asdrubali, Infrared Thermography Assessment of Thermal Bridges in Building Envelope: Experimental Validation in a Test Room Setup, Sustainability 6 (2014) 7107–7120.

[21] M. O'Grady, A.A. Lechowska, A.M. Harte, Infrared Thermography Technique as an in-situ method of assessing the heat loss through thermal bridging, Energy Build. 135, (2017) 20–32.

[22] M. O'Grady, A.A. Lechowska, and A.M. Harte, Quantification of heat losses through building envelope thermal bridges influenced by wind velocity using the outdoor infrared thermography technique, Appl. Energy 208 (2017) 1032-1052.

[23] T. Ward and C. Sanders, Conventions for calculating linear thermal transmittance and temperature factors, IHS BRE Press.

[24] ISO 10077-1:2006 Thermal performance of windows, doors and shutters - Calculation of thermal transmittance - Part 1: General, 2017.

[25] ISO 12567-1 Thermal performance of windows and doors - Determination of thermal transmittance by the hot-box method - Part 1: Complete windows and doors, 2010.

[26] IP 1/06 Assessing the effects of thermal bridging at junctions and around openings, BRE Scotland, 2006.

[27] G.S. Wright, Calculating Window Performance Parameters for Passive House Energy Modeling, Passive House Institute US Tech Corner 1 (4) (2012)

[28] F. Cappelletti, A. Gasparella, P. Romagnoni, P. Baggio, Analysis of the influence of installation thermal bridges on windows performance: The case of clay block walls, Energy Build. 43 (2011) 1435–1442.

[29] EN ISO 8990 Thermal insulation - Determination of steady-state thermal

transmission properties - Calibrated and guarded hot box, 1997.

[30] EN ISO 12412-2 Thermal performance of windows, doors and shutters - determination of thermal transmittance by hot box method - Part 2: Frames, 2003.

[31] Y. Fang, P.C. Eames, B. Norton, T.J. Hyde, Experimental validation of a numerical model for heat transfer in vacuum glazing, Sol. Energy 80 (2006) 564–577.

[32] F. Asdrubali and G. Baldinelli, Thermal transmittance measurements with the hot box method: Calibration, experimental procedures, and uncertainty analyses of three different approaches, Energy Build. 43 (2011) 1618–1626.

[33] A.H. Elmahdy, Heat transmission and R-value of fenestration systems using IRC hot box - procedure and uncertainty analysis, Trans. ASHRAE 98 (1992) 630-637.

[34] M.J. Moran, H.N. Shapiro, B.R. Munson, and D.P. Dewitt, Introduction to Thermal Systems Engineering: Thermodynamics, Fluid Mechanics and Heat Transfer. Hohn Wiley & Sons, Inc., 2003.

[35] ISO 18434-1 Condition monitoring and diagnostics of machines - Thermography - Part 1: General procedure, 2008.

[36] Abaqus 6.13 User's manual, 2015.

[37] Product Data Sheet of Eurostrand OSB 3, E EGGER.

[38] http://hyperphysics.phy-astr.gsu.edu/hbase/Tables/, accessed on the 16.01.2017.

[39] Product Data Sheet of Styrofoam LBH-X, Dow Chemical Company Limited.

[40] https://www.engineeringtoolbox.com/thermal-conductivity-d_429.html, accessed on the 27.10.2017

[41] www.engineeringtoolbox.com/metal-alloys-densities-d_50.html, accessed on the 16.01.2017.

[42] https://www.engineeringtoolbox.com/density-materials-d_1652.html, accessed

on the 27.10.2017

[43] http://www.greenspec.co.uk/building-design/insulation-materials-thermal-properties/, accessed on the 27.10.2017.

[44] EN ISO 6946 Building components and building elements - Thermal resistance and thermal transmittance - Calculation method, 2017.

[45] Ansys Fluent User's manual, 2011.

[46] ISO/IEC Guide 98-3 Uncertainty of measurement - Part 3: Guide to the expression of uncertainty in measurement, 2008.

[47] R. Albatici, A.M. Tonelli, M. Chiogna, A comprehensive experimental approach for the validation of quantitative infrared thermography in the evaluation of building thermal transmittance, Appl. Energy, 141 (2015) 218–228.

[48] Flir User's manual for IR cameras Flir Bxxx series and Flir Txxx series, 2011.

Chapter 6

Application of the infrared thermography technique to thermal bridging heat loss assessment in an existing building

6.1. Introduction

The methodology for thermal bridging heat loss assessment was developed and validated in a hot box device where the environmental conditions were controlled to ensure that a steady state was maintained throughout. But steady state conditions cannot realistically be obtained on site. In that case, the performance of the ITT survey under the quasi-steady state is recommended. The aim of the experiment presented in this chapter is to test the performance of the quantitative ITT for evaluation of thermal bridging in a real building under real environmental conditions. The thermal bridge chosen for the experiment was an external wall/wall junction located in a residential building built in 1956 and retrofitted in 2011. This type of thermal bridge is an example of a thermal bridge arising from a change in geometry. During the retrofitting, internal insulation boards were fixed to timber battens on the internal wall surface. The type of insulation board used included insulation and gypsum plasterboard. The thermographic survey was performed after the retrofitting. The linear thermal transmittance of the junction was also derived from numerical simulations. The simulations were carried for the junction before and after retrofitting, using the finite element software, Abaqus.

6.2. Experimental set up

The experiment took place under real environmental conditions, where a quasi-steady state was created according to recommendations of Albatici et al.[1]. The indoor ITT survey took place in January 2018, in the early morning between 5:10 am and 6:40 am, more than 2 hours before the sunrise, to minimize the effects of (or amount of) solar irradiation. The sky was overcast over 12 hours before the survey. The indoor and the outdoor air temperatures were monitored during 12-hour period prior to the survey. The average outdoor air temperature during this time was 7.72 ℃ and deviated by +/- 2.31 ℃ from this mean value. According to [1], the maximum variation in this temperature during 12 hours prior to the survey must be lower than 6 ℃. The indoor air temperature was kept at an average level of 22.97 ℃ for 12 hours before the testing, with a deviation of +/- 0.89 ℃. This was achieved by having an electric heater, fitted with a thermostat, switched on for 15 hours before the testing. Using a velocimeter, the outdoor free wind stream velocity was measured and its average value for the 24 hours prior the survey was 1.55 m/s. Indoors, free convection took place for the 24 hours prior to and during the survey itself. The average difference between the indoor and outdoor air temperatures for the survey was 13.94 ℃. The IR camera was positioned at a distance of 1.40 m from the junction wall. The average relative humidity during 12 hours prior the survey was 85.46 % outdoor and 46.76 % indoor.

6.3. In situ measurements

The outdoor and indoor air temperatures were measured and recorded every minute with a Hobo U12 data loggers with built-in air temperature sensors. Their accuracy for air temperatures in the range 0°C to 50°C is ±0.35°C. The wall surface temperatures were measured with two thermocouples (TC), manufactured by Onset, type TMC6-HE, connected to the Hobo U12 data logger, with an accuracy of ±0.25°C. The first thermocouple was placed on the wall junction to measure the minimum surface temperature caused by the thermal bridge and the other one 0.4 m away from the corner where the thermal bridge has no influence on the surface temperature distribution. (Figure 6.1). The surface temperatures measured by the TCs are

compared with the temperatures recorded by the IR camera in the Results and Discussion Section 6.5.

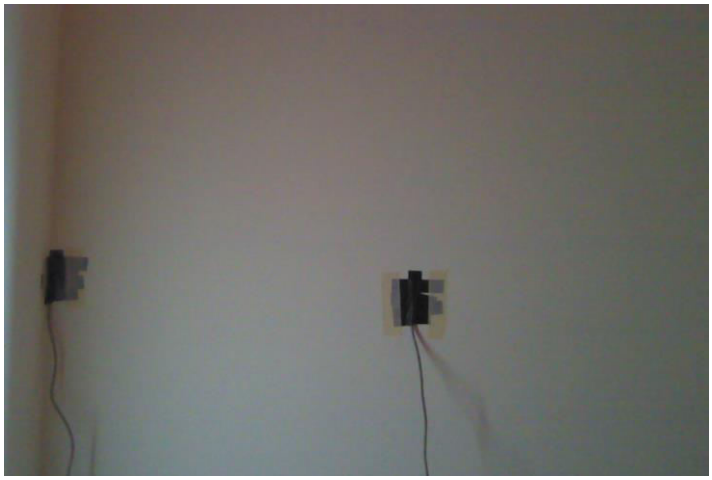

Fig. 6.1. Thermocouples placed on the tested corner

To prepare the IR camera for the testing, the reflected ambient temperature and the surface emissivity were first determined. The reflected ambient temperature was measured using a direct method, approved by the ISO Standard 18434 [2]. According to this standard, the reflective temperature can be determined by measuring the temperature of a surface covered by crumpled aluminum foil, measured with the IR camera set for black body emissivity. This approach was also used by researchers in [3-5]. To measure the emissivity of the surface, a piece of black tape with known emissivity was placed on the surface. With the emissivity setting on IR camera set to black tape, the surface temperature of the tape was measured. Then the temperature of the surface near the tape was measured and the emissivity was adjusted to give the same temperature reading as for the black tape [6].

The thermographic survey took place between 5:10 am and 6:40 am. Every 10 minutes five IR images of the corner were recorded. As the corner was symmetrical, only one half of the corner was considered. Table 6.1 presents the environmental conditions for each survey.

Table 6.1. Air temperatures at thermographic surveys measured by thermocouples TMC6-HE with the uncertainty u ±0.25°C.

Time	*Ti [°C]*	*Te[°C]*	*Ti and Te difference [°C]*
05:10 am	23.30	9.76	13.54
05:20 am	23.47	9.76	13.71
05:30 am	23.40	9.71	13.69
05:40 am	23.51	9.71	13.80
05:50 am	23.69	9.73	13.96
06:00 am	23.76	9.71	14.05
06:10 am	23.83	9.71	14.12
06:20 am	23.83	9.61	14.22
06:30 am	23.69	9.56	14.13
06:40 am	23.69	9.56	14.13
average	**23.62**	**9.68**	**13.94**

Figure 6.2 (a) shows a sample IR image taken at 5:10 am, used for q_{TB} and Ψ-value evaluation. As seen in this figure, the surface temperatures of the upper part of the wall are higher than those of the lower part of the wall. This is due to convection movements of the air in the room that was heated for the previous 12 hours in order to obtain the quasi-steady state. For comparison, Figure 6.2 (b) presents an IR image taken at 8:40 am, two hours after the space heating was switched off. By 8:40 the indoor air temperature decreased by 3.10 °C and the quasi-steady state required for a thermographic survey was not met.

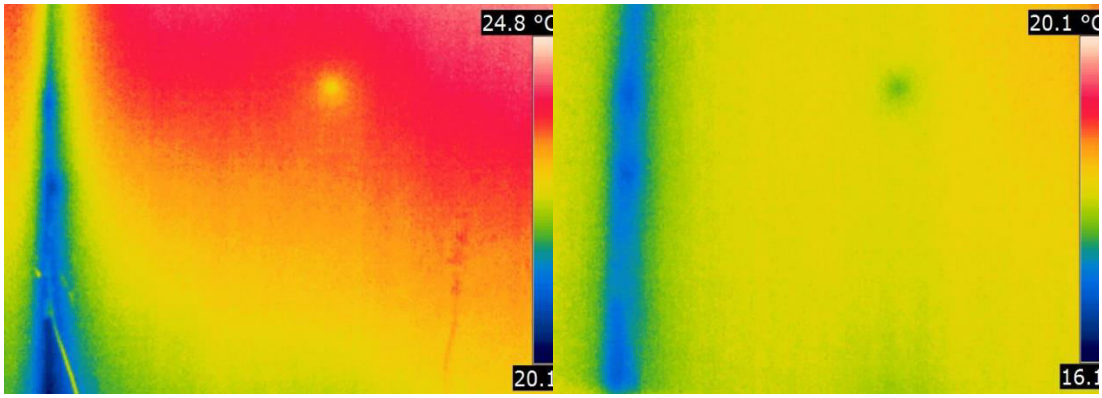

(a) **(b)**

Figure 6.2. IR images of the corner taken (a) during the testing and (b) 2 hours after switching off the space heating.

On each IR image, at the mid-height of the thermogram, an IR line was created, as described in Chapter 3. The thermal bridging heat flow rate q_{TB} and the linear thermal transmittance Ψ were calculated for each test at 10 minutes intervals. For each test, an IT line was created from five thermograms. The final results are the average values calculated from q_{TB} and Ψ obtained in ten tests.

6.4. Numerical simulations

Analysis of the corner thermal bridge is also carried using a steady-state two-dimensional heat transfer finite element model created using the Abaqus package [7]. The q_{TB} and Ψ-values were simulated for two scenarios: first for the corner before the retrofitting and, second for the same corner but after retrofitting. Table 6.2 summarizes the material properties used for the models and also presents information on the assumed internal structure of the wall/wall junction before and after retrofitting. The information about the structure was obtained from the owner of the house and from the building contractor who carried out the retrofitting. The model length was 1.00 m on the internal side, as recommended in EN ISO 10211 [8]. The surface emissivity of the corner wall surface was measured on site. The material properties given in Table 6.2 were obtained from the Irish Building Regulations Part L 2011 with Amendment

2017 [9] unless otherwise stated. The air properties used in the simulations are summarized in Table 6.3.

Table 6.2. Material properties

	Material	Thickness [m]	Thermal conductivity k [W/(mK)]	Density ρ [kg/m^3]	Emissivity ε [-]
Before retrofitting	External render	0.025	1.00	1800	-
	Concrete blocks	0.215	1.33	2000	-
	Internal plaster	0.010	1.00	1800	0.94
Added after retrofitting	Air cavity	0.025	See Table 3		-
	Timber battens 25x47mm	0.025	0.13	500	-
	Insulation board Kingspan Kooltherm	0.050	0.02 [10]	40 [11]	-
	Gypsum plasterboard	0.010	0.17	900	-
	Gypsum plaster	0.003	0.18	600	0.94

Table 6.3. Air thermal properties

T[^{o}C]	ρ[kg/m^3]	k [W/(mK)]
-10	1.342	0.0236
0	1.293	0.0244
10	1.247	0.0251
20	1.205	0.0259
30	1.165	0.0267

In the simulations, 4-noded linear heat transfer quadrilateral (DC2D) elements were used. The mesh size selected for the study was 0.05 m as with this element size, the total heat flow rate (q_{tot}) through the model varied by only 0.05% from that obtained using a model with a coarser mesh. The layers with a thickness smaller than 0.05 m were subdivided into two elements that resulted in a finer element size in these layers. Figure 6.3 shows the meshed geometry of the wall corner (a) before and (b) after retrofitting.

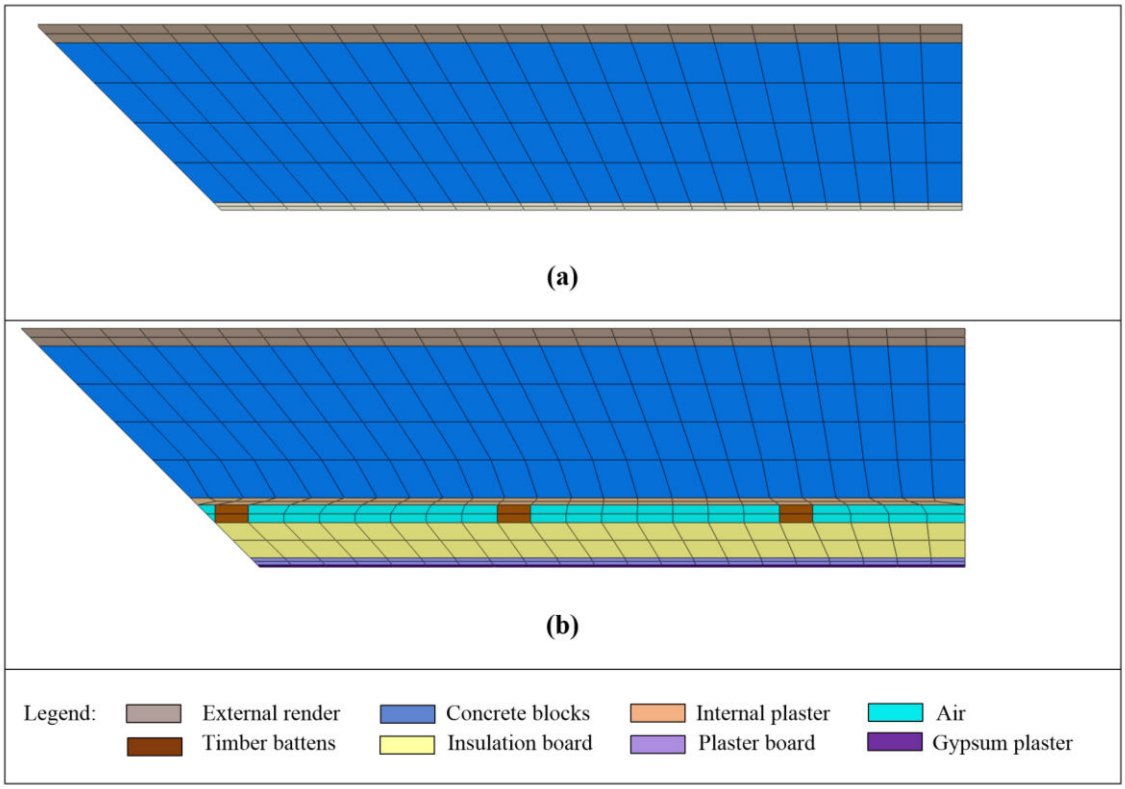

Figure 6.3. Meshed geometry of a corner wall (a) before and (b) after retrofitting.

The boundary conditions in the simulations before (FE before) and after retrofitting (FE after) were defined using the standard surface heat transfer coefficients, in accordance with EN ISO 6946 [12] and include both radiative and convective effects. According to this standard, the surface coefficients are equal to 7.7 W/m^{2}K and 25.0 W/m^{2}K, for the indoor and outdoor environment, respectively. As recommended by [13], the difference between indoor and outdoor air temperatures

was set at 20°C with the indoor air temperature 20°C and the outdoor air temperature 0°C. These two models are compared to each other to observe the improvement in thermal standard of the junction after the retrofitting. Additionally, the model of the junction after retrofitting was simulated under the average environmental conditions (FE real) measured during the thermographic survey. For this case, the air temperature on the hot side was set for 23.62 ℃ and on the cold side for 9.68 ℃. On the internal surface, an average indoor convective coefficient h_{ci}, calculated from surface temperatures obtained during the thermographic survey, according to the methodology presented in Section 3.4, was applied. The value of this coefficient is relatively low and equals 1.18 W/m^{2}K. This is due to the fact that the zone of influence of the wall/wall junction thermal bridge is narrow, thus the average h_{ci} value is determined by h_{ci} related to plain surface component. The external surface convective coefficient was calculated using Jürges approximation (Equation 6.1.) for the average wind velocity during the thermographic survey. The measured surface emissivity given in Table 6.2 was inputted and the surface radiation was calculated by Abaqus using the Stefan-Boltzmann law. The simulated results from the model with measured boundary conditions are compared to the results measured with *TC* and with the ITT.

$$h_{ce} = 5.7 + 3.8w \qquad (6.1.)$$

The simulations provide the total heat flow rate through the wall corner q_{tot}. The thermal bridging heat flow rate q_{TB} can be calculated from the difference between q_{tot} and the uniform heat flow rate q_u of a wall with identical structure but without the junction geometry (Equation (6.2)).

$$q_{TB} = q_{tot} - q_u \qquad (6.2)$$

Then, the Ψ-value was calculated by dividing q_{TB} by the temperature difference between the indoor and outdoor environments.

6.5. Results and discussion

In this section, the simulation and the measured results are presented. Firstly, the results derived from numerical models of the wall/wall junction with standard boundary conditions simulated before and after retrofitting are presented. This is followed with comparison of the retrofitted junction results, measured with the ITT and simulated with the boundary conditions measured during the thermographic survey. The surface temperatures are compared with these measured with thermocouples at the thermal bridging and on the uniform surface. All experimental results are given together with their uncertainties *(u)*. The *u* for the thermocouples is given as the accuracy provided by the manufacturer. The uncertainty of the ITT results is given as the experimental standard deviation (*SD*) calculated from a series of five ITT measurements from each test, according to Guide 98-3 [14].

6.5.1. Numerical results with standard boundary conditions

In this section, the results obtained from a numerical model of a junction before and after retrofitting are presented and discussed. Both cases were simulated with the same standard boundary conditions. This allows the level of improvement in thermal standard of the wall/wall junction to be clearly demonstrated. Table 6.4 presents the thermal bridge heat flow rate q_{TB}, Ψ-value, the minimum surface temperatures on the thermal bridge T_{TB} and the uniform surface temperature T_u for each case. As presented in this table, the retrofitting significantly improved the thermal bridging performance. The q_{TB} decreased by 4.56 W/m and Ψ-value by 0.228 W/mK. These decreases expressed in percentage account to as much as 91.20 %. The difference between T_{TB} and T_u before the retrofitting was 3.00 ℃. As after retrofitting T_{TB} increased by 2.16 ℃ more than T_u, the difference reduced to 0.84 ℃. This demonstrated that the retrofitting, involving continuous internal insulation over the thermal bridge, successfully limited improved its thermal performance.

Table 6.4. Simulation results of junction before and after retrofitting

	FE model before	*FE model after*	*Difference*
q_{TB} *[W/m]*	5.00	0.44	-4.56
Ψ *[W/mK]*	0.250	0.022	-0.228
T_{TB} *[°C]*	9.91	18.51	8.60
T_u *[°C]*	12.91	19.35	6.44

6.5.2. Comparison of measured and numerical results

The results presented in this section refer to the retrofitted junction. The surface temperatures T_{TB} and T_u were measured with TCs and the IR camera and simulated with the same boundary conditions as for the measurements (FE real). The thermal bridge heat flow rate, $q_{TB,}$ and the Ψ-value are calculated using the methodology for thermal bridging assessment using the ITT presented in Chapter 3 and derived from simulations.

6.5.2.1. Surface temperatures

The surface temperatures recorded by the IR camera and simulated with the real boundary conditions are compared to the surface temperatures measured by TCs on the thermal bridge T_{TB} and on the uniform part of the wall $T_{u.}$ As presented in Table 6.5, good agreement was found between them. It can be seen that the maximum deviation from temperatures measured by TCs accounts to 1.04 °C for the FE model. For the uniform surface temperature, the maximum difference of only 0.33 °C and was recorded for the ITT measurement.

Table 6.5. Comparison of surface temperatures measured by IR camera and TCs.

	TC	*u TC*	*ITT*	*SD ITT*	*FE real*	*Difference TC/ITT*	*Difference TC/FE*
T_{TB} [℃]	21.42	0.25	21.20	0.07	22.46	-0.22	1.04
T_u [℃]	22.84	0.25	23.17	0.07	23.10	0.33	0.26

6.5.2.2. Thermal bridge heat flow rate q_{TB} and Ψ-value comparison.

As mentioned earlier, the experimental q_{TB} and Ψ-value were obtained applying the ITT method of assessing the heat loss through thermal bridging, described in detail in Chapter 3. The simulated values are derived from an FE model with boundary conditions representing the environmental conditions during the thermographic survey. As presented in Table 6.6, the simulated values varied by 10.00 % from the measured values. It should be pointed out that information about the internal structure of the simulated corner wall was assumed based on the information provided by the owner and building contractor. In general, for the simulations, the material properties of the internal structure of the wall corner were not measured (except the emissivity) but derived from Building Regulations, manufacture spreadsheet or engineering tables. They may not reflect the actual properties. It should also be borne in mind that the ITT methodology was originally developed under steady state conditions and in this case, is applied under the quasi-steady state conditions that may impact its accuracy. When comparing simulated q_{TB} and Ψ-value to those obtained from ITT measurements, for a building component with known structure tested under steady-state conditions in the laboratory (Specimen 1 and 2 described in Chapter 5), the maximum RD of 7.25 % was recorded. Considering this, the 10.00 % discrepancy in the in-situ results may be considered acceptable.

Table 6.6. The q_{TB} and Ψ-value obtained from the ITT and from FE simulations

	ITT	*SD ITT*	*FE real*	*RD ITT/FE [%]*
q_{TB} *[W/m]*	1.40	0.02	1.54	10.00
Ψ *[W/mK]*	0.100	0.001	0.110	10.00

6.6. Summary and conclusions

The experiment successfully demonstrated the application of the methodology for thermal bridging heat loss assessment by means of the quantitative ITT in real environmental conditions. The methodology was developed and validated in laboratory conditions in a hot box device, as described in Chapter 3. In real buildings, it is not feasible to take the measurements under steady state conditions and a quasi-steady state has to be created. For this experiment, the quasi-steady state was successfully generated, following the recommendations of Albatici et al. [1]. Within the 12 hours prior to the survey, the average outdoor air temperature deviated by only +/- 2.31 ℃ and the indoor air temperature with only +/- 0.89 ℃. Also, the recommended difference between the indoor and outdoor air temperatures for the survey was achieved (13.94 ℃). The q_{TB} and Ψ-value were calculated from ten measurements sessions to guarantee their accuracy. The measured values varied from values simulated with the same boundary conditions as for the thermographic survey by 10.00 % for the q_{TB} and Ψ-value. This level of discrepancy may be caused by material approximations inputted to the model that may not reflect the actual properties. Also, performing the ITT under the quasi-steady state conditions may impact on its accuracy. In conclusion, this study demonstrated that the methodology for thermal bridging assessment using ITT developed in steady state conditions is suitable for application in real buildings.

During this project, numerical analyses of the wall/wall junction before and after retrofitting were undertaken also to observe the expected improvement in its

thermal performance. The results clearly demonstrated that the retrofitting has a significant impact on the thermal bridging heat loss, reducing it by 91.20 %.

6.7. References

[1] R. Albatici, A.M. Tonelli, M. Chiogna, A comprehensive experimental approach for the validation of quantitative infrared thermography in the evaluation of building thermal transmittance, Appl. Energy 141 (2015) 218–228.

[2] ISO 18434-1 Condition monitoring and diagnostics of machines, Thermography Part 1: General procedure, 2008.

[3] P.A. Fokaides, S.A. Kalogirou, Application of infrared thermography for the determination of the overall heat transfer coefficient (*U*-value) in building envelopes, Appl. Energy 88 (12) (2011) 4358–4365.

[4] F. Asdrubali, G. Baldinelli, F. Bianchi, A quantitative methodology to evaluate thermal bridges in buildings, Appl. Energy 97 (2012) 365-373.

[5] M. O'Grady, A.A. Lechowska, A.M. Harte Infrared Thermography Technique as an in-situ method of assessing the heat loss through thermal bridging, Energy Build. 135 (2017) 20–32.

[6] Flir User's Manual for IR cameras Flir Bxxx series and Flir Txxx series, 2011.

[7] Abaqus 6.13 User's manual, 2015.

[8] EN ISO 10211, Thermal bridges in building construction — Heat flows and surface temperatures — Detailed calculations, 2017.

[9] Building Regulations Conservation of Fuel and Energy - Dwellings, Technical Guidance Document Part L 2011 with Amendment 2017.

[10] Kingspan Koohlterm K17 Insulated Plasterboard, Typical Constructions and Total R-values, 2017.

[11] https://www.engineeringtoolbox.com/density-materials-d_1652.html, density of insulated plasterboard, accessed on the 15.12.2017.

[12] EN ISO 6946 Building Components and Building Elements - Thermal Resistance and Thermal Transmittance - Calculation Method, 2017.

[13] T. Ward and C. Sanders, Conventions for calculating linear thermal transmittance and temperature factors, IHS BRE Press.

[14] ISO/IEC Guide 98-3 Uncertainty of measurement Part 3: Guide to the expression of uncertainty in measurement, 2008.

Chapter 7

Conclusions and recommendations

7.1. Conclusions

As the existing European building stock is relatively old and in general energy inefficient, acceleration of retrofitting of existing buildings is a key priority in European energy policy [1]. The primary aim of this work is to support the implementation of this policy by developing an effective and efficient method to assess the thermal bridging performance. This can be used for the pre- and post-retrofitting thermal assessment of existing buildings.

To achieve this aim, a methodology for quantifying heat loss via thermal bridging in the external building envelope based on the infrared thermography technique has been developed. The methodology is based on the surface energy balance principle, applied to the internal or external face of a building component containing a thermal bridge. According to this principle, the amount of energy transferred to the surface is identical to the amount of energy leaving the surface. The latter can be determined using the temperatures recorded by an IR camera on either the indoor or outdoor surface. The development of the methodology included the establishment of procedures for undertaking the thermographic survey of the building envelope to enhance the accuracy of the method. The analysis of the data from the thermographic survey was implemented in a Microsoft Excel-based tool. This tool can be used for convenient and relatively quick thermal bridging evaluation, expressed by q_{TB} and Ψ-value. Details of the underlying building physics principles implemented in the tool and the analysis procedures are presented in detail in Chapter 3 for indoor

conditions and in Chapter 4 for outdoor conditions. Examples of the tool output for indoor and outdoor ITT are given in Appendices A – C.

Up to now, different methods for thermal bridging evaluation have been used. The most common, the numerical approach, including FE [2,3], CFD [4,5], and FD [6], is especially suitable for building design stage, where the internal building envelope structure is known. As for existing buildings, this condition is very often not met and experimental assessment methods are an alternative. The only standardized experimental method, the HFM, covers a small areas of building surface, therefore it is conventionally used for *U*-values evaluation [7-9]. It has also been applied for thermal bridging evaluation [10,11]; however, a large number of HFMs are necessary to cover the whole are affected by thermal bridging. The minimum time of 72 hours for HFM measurements makes this approach time consuming which is its main disadvantage. Another tool used for building envelope assessment is an IR camera. Application of IR technology is not new and it is widely used qualitatively to identify building anomalies such a thermal bridging. The use of ITT to quantitatively assess building envelope performance is still evolving. It has been used successfully to determine the *U*-values of plain components where the surface temperature is uniform, using indoor [12,13] and outdoor [14-16] ITT. In the case of thermal bridging, the increase in heat transfer not only through the thermal bridge itself but also in a zone surrounding the thermal bridge is distinctly non-uniform and a more sophisticated approach is required to accurately characterise the behaviour. For thermal bridging assessment, Benkő [17] developed a highly simplified approach based on only two temperature measurements, namely, one at the centre of the thermal bridge and one on the plain part of the specimen. Asdrubali et al. [4] used a more refined approach that used the recorded temperature at each pixel in the IR image to determine the heat flow via the thermal bridge. The current work includes a further development and refinement of the Asdrubali approach and the unique features are outlined below. In addition, a novel approach to Ψ-value assessment that accounts for measurements at different wind speeds and a proposal for window thermal bridging impact assessment (*M*-value) are proposed.

As part of the development and validation of the methodology, an experimental program was designed in consultation with an industrial partner to ensure that realistic

cases of thermal bridging in buildings were considered. The test specimens contained linear thermal bridges with different structure and material properties and window elements representing frames with different geometries and materials. The methodology for both the indoor and the outdoor ITT was validated in a hot box device where environmental conditions were strictly monitored. Furthermore, numerical modelling of the heat transfer through the test specimens was undertaken. Both the hot box testing and the complementary numerical studies confirmed that both the indoor and outdoor ITT methodologies could predict the thermal bridging heat loss with a high degree of accuracy.

The following research objectives were addressed by the project:

- Objective 1

  The first objective of the research was to develop a stand-alone methodology based only on ITT measurements for indoor thermal bridging assessment. This has been achieved with the characterisation of the heat transfer via the thermal bridging and plain components through extending the analysis of pixel temperature data to both components. In other studies, the plain component assessment was performed either analytically or via heat flux meters. A sub-objective of this work involved investigation of different approaches to determining surface heat transfer coefficient on the accuracy of the methodology. For indoor conditions, an approach, in line with well-established heat transfer theory involving the Nusselt number, is used for temperature dependent convective coefficients evaluation. The radiative coefficients are calculated using Stefan Boltzmann law. Determination of unique coefficients for each pixel is based on using the recorded pixel temperature. The findings show that the use of temperature dependent coefficients for q_{TB} and Ψ-value calculation resulted in improved accuracy when compared to values obtained using constant coefficients related to the plain part of a building component. Temperature-dependent surface heat transfer coefficients for thermal bridging heat loss evaluation, implemented in the current approach, have not been previously employed.

- Objective 2

  As the application of the ITT under outdoor conditions is influenced by weather conditions, especially wind velocity, the next objective of the research was the development of an ITT methodology that would account for wind effects. The first step in this was the quantification of the wind impact on thermal bridging performance. This was achieved using numerical analysis, laboratory testing and analytical evaluation of convective coefficients. As the wind velocity at the time of measurement resulted in different velocity-dependent Ψ-values, a methodology to adjust the calculated Ψ-values to that at a reference wind velocity was developed. As outlined in Chapter 2, conventionally at the building design stage, standard boundary conditions consistent with a wind velocity of 4 m/s are used. Therefore, in the current study an adjustment procedure to convert the Ψ-value measured at any wind velocity to the Ψ-value at the standard wind velocity 4 m/s was developed. The proposed procedure also allows for comparison of Ψ-values evaluated from measurements taken at different times with different wind velocities. Details of this study and the proposed adjustment procedure are presented in Chapter 4. The quantification of the correlation between wind velocity and Ψ-value and the development of this adjustment procedure is a novel feature of the current work. It provides the opportunity to the building assessor to undertake a thermographic study under a range of different external wind conditions.

  For outdoor conditions with forced convection, two approaches to evaluating convective coefficients were investigated. The first one uses Nusselt number and the second one uses Jürges approximation. It was found that both approaches are suitable for q_{TB} and Ψ-value calculation. The analysis shows that for outdoor conditions, the use of variable radiative coefficients has a negligible impact on the accuracy q_{TB} and Ψ-value.

- Objective 3

  In a building envelope, the occurrence of multiple thermal bridges is commonplace. The presence of adjacent thermal bridges has an impact on the heat transfer regime. This interaction must be accounted for in the building envelope assessment to avoid overestimation of the heat loss. To satisfy the

third objective of this study, the ability of the ITT methodology to account for interaction effects in heat loss assessments associated with multiple thermal bridges was clearly demonstrated. Every building envelope contains complex multiple bridging in the form of window elements. Thermal bridging between the wall element and the frame, via the frame, between the frame and the glazing and via the glazing interact and, for practical reasons, their combined effect must be measured together during the ITT assessment. It is proposed, therefore, that the impact of a window and its installation in the building wall is treated together. This is done by introducing a window thermal transmittance *M*-value as described in Chapter 5. The ability of the ITT methodology to accurately quantify the heat flow via window elements was validated through comparisons with the hot box measurements and numerical modelling of the test component. Higher levels of accuracy were achieved when testing timber framed windows that PVC framed windows.

- Objective 4

  The methodology for thermal bridging heat loss assessment was developed and validated in a hot box device under a steady state in a laboratory. The final objective of this research was to carry out some initial testing of the methodology under site conditions. For this purpose, the indoor ITT methodology was applied to a real building with the measurements taken under quasi-steady state conditions. The quasi-steady state conditions for the study were created in accordance with the recommendations of Albatici et al. [18] for determining the *U*-value using the outdoor ITT. Using the ITT methodology under these conditions, the Ψ-value of a building corner agreed with numerical predictions to within 10%, which is a very satisfactory result.

To summarise, a methodology has been developed which permits evaluation of the thermal bridging heat flow rate q_{TB} and Ψ-value through external building envelopes without the need for information about the internal structure of the building envelope. This approach has significant advantages for assessment of older buildings as details of the structure and material quality of these buildings are often unavailable and, therefore, numerical assessment methods cannot be used. For these cases, in-situ

assessment methods must be used to evaluate their thermal performance. The fact that the methodology can be used in indoor and outdoor conditions provides significant flexibility. Now a surveyor can take a decision on which conditions, indoor or outdoor, are more suitable for a thermographic survey. It should be borne in mind that the methodology for indoor ITT assumed free convection, therefore, prior to survey, it should be assured that equipment such fan or air-conditioning causing forced convection are switched off. When carrying out a survey in a presence of artificially induced forced convection, the outdoor ITT methodology should be used, as this was developed for forced convection which usually takes place in outdoor conditions. However, in absence of wind, the indoor ITT methodology should be used.

Implementation of the methodology for thermal bridging evaluation to a real building the verified its potential for in-situ use, as a part of the overall thermal assessment of existing buildings. As mentioned in the previous chapters, such assessment is necessary to facilitate upgrading of the thermal standard of existing building envelopes. Development of the adjustment procedure for Ψ-value evaluation extends the application of the methodology to any wind conditions. For windows, a new practical procedure is proposed where all additional heat losses associated with the installed window are quantified. Based on a thermal assessment involving in-situ measurements such as proposed in this project, a building retrofit strategy can be planned. Repeating the assessment after building retrofitting will quantify the actual improvement in thermal performance.

7.2. Recommendations for further study

Further studies with the potential to enhance and validate of the methodology for thermal bridging heat loss assessment by means of ITT developed in this project should be considered. These include the following:

- Wind velocity effects

  In Chapter 4, an adjustment factor allowing conversion of the Ψ-value measured under any wind velocity to the Ψ-value measured at the standard

velocity has been introduced. Within this study, the wind velocity impact on thermal bridges created by steel posts in SIP-panels was tested. It is suggested that the response of other types of thermal bridges when exposed to different wind velocities be investigated.

- Establishment of quasi-steady state conditions

  Considering the application of the ITT methodology in real buildings, the establishment of the quasi-steady state for the experiment presented in Chapter 6 was quite time-consuming taking 12 hours. This may be challenging while undertaking a building thermal assessment. A study assessing the correlation between accuracy of the methodology and the time required for a quasi-steady state preparation is suggested. Such a study may result in a less time-consuming survey preparation. Within this study, during 12-hour period prior to the survey small deviations in air temperatures were recorded. The outdoor and indoor air temperatures deviated by only 2.31 ℃ and 0.89 ℃, respectively, from the averages values. An investigation of the methodology accuracy, with greater air temperature deviation before the survey, is suggested.

- In-situ testing and validation of outdoor ITT methodology

  In Chapter 4 of this work, development of a methodology for thermal bridging assessment in an existing building envelope by means of outdoor ITT is presented. The appliance of this methodology is significantly influenced by weather conditions, especially wind velocity. This methodology was validated in laboratory conditions with hot box measurements. Further testing of the methodology in real outdoor conditions is recommended.

- Extension of the methodology to thermal bridging with irregular geometry

  Within this study, the methodology was first developed for a single linear thermal bridge. This was followed by the implementation of the methodology for multiple thermal bridges and windows. Additional applications of the methodology are to consider for further research. An example of possible use of the methodology is a quantification of additional heat losses via building

envelope component area with missing insulation. Also, heat losses due to the presence of ducts in a building may be quantified using the methodology.

- Enhancement of the data analysis tool

  In this project, the analysis of the data from the thermographic survey was implemented in a Microsoft Excel-based tool to calculate the heat losses due to the presence of thermal bridging. Usability of the tool would be greatly enhanced via the development of a graphical user interface to guide the user through the data input and analysis.

7.3. References

[1] Proposal for a Directive of the European Parliament and of the Council amending Directive 2010/31/EU on the energy performance of buildings 2016.

[2] E. Troppová, J. Klepárník, J. Tippner, Thermal bridges in a prefabricated wooden house: comparison between evaluation methods, Wood Mater. Sci. Eng. 11 (5) (2016) 305–311.

[3] H. Viot, A. Sempey, M. Pauly, L. Mora, Comparison of different methods for calculating thermal bridges: Application to wood-frame buildings, Build. Environ. 93 (2015) 339–348.

[4] F. Asdrubali, G. Baldinelli, F. Bianchi, A quantitative methodology to evaluate thermal bridges in buildings, Appl. Energy 97 (2012) 365-373.

[5] K. Martin, A. Campos-Celador, C. Escudero, I. Gómez, J.M. Sala, Analysis of a thermal bridge in a guarded hot box testing facility, Energy Build. 50 (2012) 139–149.

[6] A. Capozzoli, A. Gorrino, V. Corrado, A building thermal bridges sensitivity analysis, Appl. Energy 107 (2013) 229–243.

[7] A. Byrne, G. Byrne, A. Davies, A.J. Robinson, Transient and quasi-steady thermal behaviour of a building envelope due to retrofitted cavity wall and

ceiling insulation, Energy Build. 61 (2013) 356–365.

[8] F. Asdrubali, C. Buratti, F. Cotana, G. Baldinelli, M. Goretti, E. Moretti, C. Baldassarri, E. Belloni, F. Bianchi, A. Rotili, M. Vergoni, D. Palladino, D. Bevilacqua, Evaluation of Green Buildings' Overall Performance through in Situ Monitoring and Simulations, Energies 6 (2013) 6525–6547.

[9] L. Evangelisti, C. Guattari, P. Gori, R. De Lieto Vollaro, In situ thermal transmittance measurements for investigating differences between wall models and actual building performance, Sustainability 7 (8) (2015) 10388–10398, 2015.

[10] F. Ascione, N. Bianco, R.F. De Masi, G.M. Mauro, M. Musto, G.P. Vanoli, Experimental validation of a numerical code by thin film heat flux sensors for the resolution of thermal bridges in dynamic conditions, Appl. Energy 124 (2014) 213–222.

[11] L. Zalewski, S. Lassue, D. Rousse, K. Boukhalfa, Experimental and numerical characterization of thermal bridges in prefabricated building walls, Energy Convers. Manag. 51 (12) (2010) 2869–2877.

[12] P.A. Fokaides, S.A. Kalogirou, Application of infrared thermography for the determination of the overall heat transfer coefficient (*U*-Value) in building envelopes, Appl. Energy 88 (12) (2011) 4358–4365.

[13] B. Tejedor, M. Casals, M. Gangolells, X. Roca, Quantitative internal infrared thermography for determining in-situ thermal behaviour of façades, Energy Build. 151 (2017) 187–197.

[14] R. Albatici, A.M. Tonelli, Infrared thermovision technique for the assessment of thermal transmittance value of opaque building elements on site, Energy Build. 42 (11) (2010) 2177–2183.

[15] R. Albatici, A.M. Tonelli, M. Chiogna, A comprehensive experimental approach for the validation of quantitative infrared thermography in the evaluation of building thermal transmittance, Appl. Energy 141 (2015) 218–228.

[16] G. Dall'O', L. Sarto, A. Panza, Infrared screening of Residential Buildings for Energy Audit Purposes: Results of a Field Test, Energies 6 (2013) 3859–3878.

[17] I. Benkő, Quantitative analysis of thermal bridges of structures through infrared thermograms, In Proceedings of International Conference on Quantitative Infrared Thermography Qirt, Dubrovnik, Croatia, 2002, pp. 203–208.

[18] R. Albatici, F. Passerini, A.M. Tonelli, S. Gialanella, Assessment of the thermal emissivity value of building materials using an infrared thermovision technique emissometer, Energy Build. 66 (2013) 33–40.

Appendices

Appendix A

Excerpt from thermal bridging analysis using indoor ITT of Specimen 1, Chapter 3

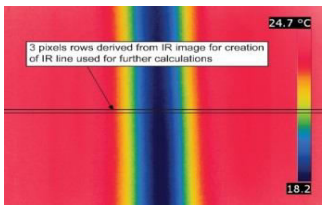

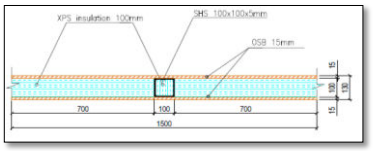

IR image information								
Number of pixel in horizontal direction			320					
Length of the component captured in IR image	*lIR*	m	0.74					
length of a pixel	*lx*	m	0.00232					
Environmental/surface information								
Indoor air temperature	*Ti*	℃	24.73					
Outdoor air temperature	*Te*	℃	-4.90					
Surface emissivity	*ε*		0.93					
Stefan-Bolzman constant	*σ*		5.67E-08					
Gravity	*g*	m/s²	9.8					
specimen height	*H*	m/s²	1.50					
Calculation data								
Pixel width	*pixw*	m	0.484	0.00232	0.00232	0.00232	0.00232	0.00232
Ruler		m	0.000	0.484	0.486	0.488	0.491	0.493
Pixels numbers		no.	EXTRA	1	2	3	4	5
Surface temperature of each pixel on the IR line	*Tsx*	℃	23.57	23.57	23.57	23.57	23.57	23.57
		K	296.72	296.72	296.72	296.72	296.72	296.72
Plain surface temperature	*Tsu*	℃	23.57	23.57	23.57	23.57	23.57	23.57
Pixel surface and plain surface temperature differenc	Δ *Tsx Tsu*	℃	0.00	0.00	0.00	0.00	0.00	0.00
Internal air temp	*Ti*	℃	24.73	24.73	24.73	24.73	24.73	24.73
		K	297.88	297.88	297.88	297.88	297.88	297.88
Surface and Indoor air temperature difference	Δ *Tsx Ti*	K/°C	1.16	1.16	1.16	1.16	1.16	1.16
Film temp.	*Tf*	℃	24.15	24.15	24.15	24.15	24.15	24.15
External temp.	*Te*	℃	-4.90	-4.90	-4.90	-4.90	-4.90	-4.90
Indoor and outdoor air temperature difference	Δ*Ti Te*	K or °C	29.63	29.63	29.63	29.63	29.63	29.63
Air properties								
Characteristic length	*lch*	m	1.5	1.5	1.5	1.5	1.5	1.5
Kinematic viscosity	*v*	m²/s	1.57E-05	1.57E-05	1.57E-05	1.57E-05	1.57E-05	1.57E-05
Diffusivity	*α*	m²/s	2.17E-05	2.17E-05	2.17E-05	2.17E-05	2.17E-05	2.17E-05
Air conductivity	*k*	W/mK	2.56E-02	2.56E-02	2.56E-02	2.56E-02	2.56E-02	2.56E-02
Prandtl number	*Pr*	n/a	0.712	0.712	0.712	0.712	0.712	0.712
Expansion coefficient	*β*	1/K	3.33E-03	3.33E-03	3.33E-03	3.33E-03	3.33E-03	3.33E-03
Surface coefficients calculation								
$Ra_x = \frac{g\beta_x(T_i - T_{sx})l_{ch}^3}{\nu_x\,\alpha_x}$								
Rayleigh number	*Ra*		3.75E+08	3.75E+08	3.75E+08	3.75E+08	3.75E+08	3.75E+08
$Nu_x = \left\{0.825 + \frac{0.387Ra_x^{1/6}}{\left[1+\left(\frac{0.492}{Pr_x}\right)^{9/16}\right]^{8/27}}\right\}^2$								
Nusselt number	*Nu*		9.10E+01	9.10E+01	9.10E+01	9.10E+01	9.10E+01	9.10E+01
$h_{cx} = \frac{Nu_x\,k_x}{l_{ch}}$								
Convective coefficient	*hci*	W/m²K	1.55	1.55	1.55	1.55	1.55	1.55
$h_{rx} = \varepsilon\sigma(T_{sx} + T_i)(T_{sx}^2 + T_i^2)$								
Radiative coefficient	*hri*	W/m²K	5.54	5.54	5.54	5.54	5.54	5.54
Heat loss calculation								
$q_x = l_x[(h_{cx}+h_{rx})(T_i - T_{sx})]$								
Heat flow rate of each pixel	*qx*	W/m	3.97	0.02	0.02	0.02	0.02	0.02
$q_{tot} = \sum q_x$								
Total heat flow rate per unit length	*qtot*	W/m	19.39					
$\dot{Q}_{sp} = q_{tot} * H$								
Total heat flow rate through specimen	$\dot{Q}_{sp}$	W	29.09					
$U_{sp} = \frac{q_{tot}}{L(T_i - T_e)}$								
Overal thermal transmittance U-value	*U*	W/m²K	0.436					
Heat flow rate of plain pixel	*qxu*	W/m	3.97E+00	1.90E-02	1.90E-02	1.90E-02	1.90E-02	1.90E-02
$q_{xTB} = q_x - q_{xu}$								
Thermal bridge heat flow rate of a each pixel	*qxtb*	W/m	0.00E+00	0.00E+00	0.00E+00	0.00E+00	0.00E+00	0.00E+00
$q_{TB} = \sum q_{xTB}$								
Thermal bridge heat flow rate of a each pixel	*qtb*	W/m	7.04					
$\Psi = \frac{q_{TB}}{(T_i - T_e)}$								
Linear thermal transmittance	*Ψ*	W/mK	0.238					

Appendix B

Excerpt from thermal bridging analysis using outdoor ITT and Nusselt number of Specimen 1, Chapter 4

Appendix B: Excerpt from thermal bridging analysis using outdoor ITT and Nusselt number of Specimen 1, Chapter 4

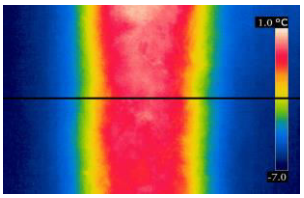

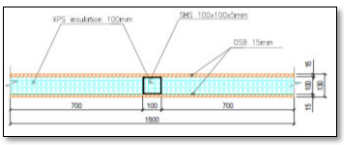

IR image information

Number of pixel in horizontal direction			320					
Length of the component captured in IR image	l_{IR}	m	0.31					
length of a pixel	lx	m	0.00098					
Environmental/surface infortmation								
Indoor air temperature	Ti	℃	24.74					
Outdoor air temperature	Te	℃	-7.20					
Surface emissivity	ε		0.93					
Stefan-Bolzman constant	σ		5.67E-08					
Gravity	g	m/s²	9.8					
specimen height	H	m/s²	1.50					
Calculation data								
Pixel length	lx	m	0.48024	0.00098	0.00098	0.00098	0.00098	0.00098
ruler			0.00	0.48	0.48	0.48	0.48	0.48
pix number			EXTRA	1.00	2.00	3.00	4.00	5.00
Surface temperature of each pixel on the IR line	Tsx	°C	-6.47	-6.47	-6.47	-6.47	-6.47	-6.47
		K	266.68	266.68	266.68	266.68	266.68	266.68
Plain surface temperature			-6.47	-6.47	-6.47	-6.47	-6.47	-6.47
Pixel surface and plain surface temperature differenc	$\Delta\ Tsx\ \ Tsu$	°C	0.00	0.00	0.00	0.00	0.00	0.00
External air temp	Te	°C	-7.20	-7.20	-7.20	-7.20	-7.20	-7.20
		K	265.95	265.95	265.95	265.95	265.95	265.95
Surface and Outdoor air temperature diffrence	$\Delta\ Tsx\ \ Te$	K/°C	0.73	0.73	0.73	0.73	0.73	0.73
Film temp temperature	Tf	°C	-6.837	-6.84	-6.84	-6.84	-6.84	-6.84
Indoor air temperature	Ti	°C	24.74	24.74	24.74	24.74	24.74	24.74
Indoor and outdoor air tempemperature difference	$\Delta Ti\ \ Te$	K or °C	31.94	31.94	31.94	31.94	31.94	31.94
Air properties								
Wind velocity	w	m/s	1.57	1.57	1.57	1.57	1.57	1.57
Characteristic length	lch	m	1.5	1.5	1.5	1.5	1.5	1.5
Kinematic viscosity	v	m²/s	1.30E-05	1.30E-05	1.30E-05	1.30E-05	1.30E-05	1.30E-05
Diffusivity	α	m²/s	1.77E-05	1.77E-05	1.77E-05	1.77E-05	1.77E-05	1.77E-05
Air conductivity	k	W/mK	2.33E-02	2.33E-02	2.33E-02	2.33E-02	2.33E-02	2.33E-02
Prandtl number	Pr	n/a	0.718	0.718	0.718	0.718	0.718	0.718
Expansion coefficient	β	1/K	3.81E-03	3.81E-03	3.81E-03	3.81E-03	3.81E-03	3.81E-03
Surface coefficients calculation								
$Re_x = \frac{w\ l_{ch}}{v_x}$								
Reynolds number	Re		1.82E+05	1.82E+05	1.82E+05	1.82E+05	1.82E+05	1.82E+05
$Nu_x = 0.037 Re_x^{4/5} Pr^{1/3}$								
Nusselt number (for fully turbulent flow)	Nu		5.34E+02	5.34E+02	5.34E+02	5.34E+02	5.34E+02	5.34E+02
$h_{cex} = \frac{Nu_x\ k_x}{l_{ch}}$								
Convective coefficient	hce	W/m²K	8.31	8.31	8.31	8.31	8.31	8.31
$h_{rx} = \varepsilon\sigma(T_{sx} + T_e)(T_{sx}^2 + T_e^2)$								
Radiative coefficient	hre	W/m²K	3.98	3.98	3.98	3.98	3.98	3.98
Average radiative coefficient			3.99					
Heat loss calculation								
$q_x = l_x[(h_{cx}+h_{rx})(T_{sx} - T_e)]$								
Heat flow rate of each pixel	qx	W/m	4.28	0.01	0.01	0.01	0.01	0.01
$q_{tot} = \sum q_x$								
Total heat flow rate per unit length	$qtot$	W/m	21.35					
$\dot{Q}_{sp} = q_{tot} * H$								
Total heat flow rate through specimen	$\dot{Q}_{sp}$	W	32.03					
$U_{sp} = \frac{q_{tot}}{L(T_i - T_e)}$								
Overal thermal transmittance U-value	U	W/m²K	0.446					
heat flow rate of plain pixel	qxu	W/m	4.28E+00	8.75E-03	8.75E-03	8.75E-03	8.75E-03	8.75E-03
$q_{xTB} = q_x - q_{xu}$								
Thermal bridge heat flow rate of a each pixel	$qxtb$	W/m	0.00E+00	0.00E+00	0.00E+00	0.00E+00	0.00E+00	0.00E+00
$q_{TB} = \sum q_{xTB}$								
sum of qxtb	qtb	W/m	7.96					
$\Psi = \frac{q_{TB}}{(T_i - T_e)}$								
Linear thermal transmittance	Ψ	W/mK	0.249					

Appendix C

Excerpt from thermal bridging analysis using outdoor ITT and Jürges approximation of Specimen 1, Chapter 4

Appendix C: Excerpt from thermal bridging analysis using outdoor ITT and Jürges approximation of Specimen 1, Chapter 4

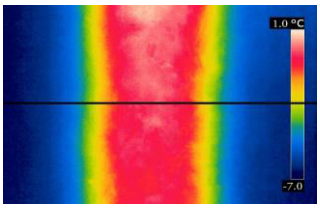

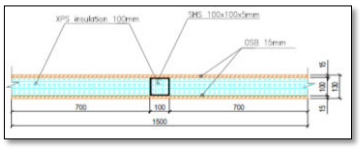

IR image information

Number of pixel in horizontal direction			320
Length of the component captured in IR image	l_{IR}	m	0.31
length of a pixel	lx	m	0.00098

Environmental/surface infortmation

Indoor air temperature	Ti	℃	24.74
Outdoor air temperature	Te	℃	-7.20
Surface emissivity	ε		0.93
Stefan-Bolzman constant	σ		5.67E-08
Gravity	g	m/s²	9.8
specimen height	H	m/s²	1.50
Wind velocity	w	m/s	1.57

Calculation data

Pixel length	lx	m	0.48024	0.00098	0.00098	0.00098	0.00098	0.00098
ruler			0.00	0.48	0.48	0.48	0.48	0.48
pixel number			EXTRA	1.00	2.00	3.00	4.00	5.00
Surface temperature of each pixel on the IR line	Tsx	°C	-6.47	-6.47	-6.47	-6.47	-6.47	-6.47
		K	266.68	266.68	266.68	266.68	266.68	266.68
Plain surface temperature			-6.47	-6.47	-6.47	-6.47	-6.47	-6.47
Pixel surface and plain surface temperature difference	$\Delta\ Tsx\ \ Tsu$	°C	0.00	0.00	0.00	0.00	0.00	0.00
External air temp	Te	°C	-7.20	-7.20	-7.20	-7.20	-7.20	-7.20
		K	265.95	265.95	265.95	265.95	265.95	265.95
Surface and Outdoor air temperature diffrence	$\Delta\ Tsx\ \ Te$	K/°C	0.73	0.73	0.73	0.73	0.73	0.73
Film temp temperature	Tf	°C	-6.837	-6.84	-6.84	-6.84	-6.84	-6.84
Indoor air temperature	Ti	°C	24.74	24.74	24.74	24.74	24.74	24.74
Indoor and outdoor air temperature difference	$\Delta Ti\ \ Te$	K or °C	31.94	31.94	31.94	31.94	31.94	31.94

Surface coefficients according to Jurges approximation

$$h_e = 5.7 + 3.8w$$

Convective and Radiative coefficient	he	W/m²K	11.67

Heat loss calculation

$$q_x = l_x[(h_{cx}+h_{rx})(T_{sx} - T_e)]$$

Heat flow rate of each pixel	qx	W/m	4.06	0.01	0.01	0.01	0.01	0.01

$$q_{tot} = \sum q_x$$

Total heat flow rate per unit length	$qtot$	W/m	20.27

$$\dot{Q}_{sp} = q_{tot} * H$$

Total heat flow rate through specimen	$\dot{Q}_{sp}$	W	30.41

$$U_{sp} = \frac{q_{tot}}{L(T_i - T_e)}$$

Overal thermal transmittance U-value	U	W/m²K	0.423

heat flow rate of plain pixel	qxu	W/m	4.06E+00	8.30E-03	8.30E-03	8.30E-03	8.30E-03	8.30E-03

$$q_{xTB} = q_x - q_{xu}$$

Thermal bridge heat flow rate of a each pixel	$qxtb$	W/m	0.00E+00	0.00E+00	0.00E+00	0.00E+00	0.00E+00	0.00E+00

$$q_{TB} = \sum q_{xTB}$$

sum of qxtb	qtb	W/m	7.57

$$\Psi = \frac{q_{TB}}{(T_i - T_e)}$$

Linear thermal transmittance	Ψ	W/mK	0.237